

# Light-Activated Antimicrobial Surfaces Containing Quantum Dots for the Prevention of Hospital- Acquired Infections

Ethel G. A. Owusu

2020

Supervised by: Professor Alexander J. MacRobert, Professor Ivan P. Parkin, Dr  
Elaine Allan and Dr Elnaz Yaghini

This thesis is presented to UCL in partial fulfilment of the requirements for the Degree of Doctor of  
Philosophy (Division of Surgery & Interventional Science)

## **Declaration**

I, Ethel G. A. Owusu, confirm that the work presented in this thesis is my own. Where information has been derived from other sources, I confirm that this has been indicated in the thesis.

## Abstract

This thesis details the development of effective light-activated antimicrobial polymers for use in healthcare environments, with the aim of reducing hospital-acquired infections (HAIs). The overuse and misuse of antibiotics is the most important factor that has led to increased incidence of multi-drug resistant HAIs. In the hospital setting where there is an abundance of immunosuppressed patients and often hygiene protocols are not strictly followed, HAIs can spread quickly, leading to increased length of hospital stay, morbidity and mortality and high healthcare costs. Self-disinfecting surfaces can reduce the incidence of HAIs by reducing the levels of bacteria on frequently touched hospital surfaces that serve as bacterial reservoirs, thus reducing the risk of HAI transmission.

Quantum dots (QDs), extremely small nanoparticles that exhibit unique size-dependent properties, combined with photosensitisers display potent strong bactericidal activity upon incorporation into polymer surfaces. When irradiated under ambient white light, polymer surfaces induce the lethal photosensitisation of a range of Gram-positive and Gram-negative bacteria through the production of reactive oxygen species (ROS). ROS cause irreversible damage leading to cell apoptosis and death by attacking bacterial cells in a non-specific fashion thus making the development of resistance unlikely. Polyurethane substrates were impregnated with QDs and photosensitiser dye (crystal violet) using a modified version of the simple and easily scalable dipping procedure known as the “swell-encapsulation-shrink” technique. Solely cadmium-free, indium-based QDs were used in this study, thereby circumventing issues regarding toxicity arising from the release of cadmium ions from traditional, commonly prepared QDs such as CdTe, CdSe and CdS. Materials were characterised using techniques such as UV-Vis absorbance spectroscopy, fluorescence spectroscopy and transmission electron microscopy. The prepared polymer substrates were activated under white light conditions mimicking those used in the hospital (~500 – 6000 lux). In order to deduce the photochemical pathway responsible for light-activated antibacterial activity, whether Type I, Type II or both, the antimicrobial surfaces were tested in a series of microbiological assays using specific ROS inhibitors and quenchers.

The surfaces were tested against a range of nosocomial pathogens including *Escherichia coli*, *Staphylococcus aureus*, epidemic methicillin-resistant *Staphylococcus aureus* and *Pseudomonas aeruginosa*. The novel materials described in this thesis demonstrate very strong self-disinfecting properties even under low light levels, demonstrating their potential for use in hospitals to reduce HAIs without the use of antibiotics.

## Impact Statement

One approach to tackling the rising incidence of resistance to antibiotics is the use of antibacterial surfaces. Light-activated antibacterial surfaces, based on antimicrobial photodynamic therapy (aPDT), are attractive as bactericidal activity is reliant on the generation of reactive oxygen species (ROS). Since ROS operate by oxidising multiple intracellular sites of the microorganism, development of resistance is highly unlikely, which is crucial to the long-term effectiveness of these materials.

The incorporation of quantum dot (QD) and photosensitiser crystal violet (CV) into polymers via the dipping procedure known as swell-encapsulation-shrink provides a reproducible and easy means to fabricate light-activated antibacterial surfaces. This process has been shown to be feasible in this and other studies and can continue to be utilised in academia to embed a range of nanoparticles and photosensitisers into different flexible polymers. In this work, a simple approach to nanoparticle quantification in the polymeric bulk is outlined that can be applied to future academic studies in tandem with other analytical methods. Also, the successful application of cadmium-free QDs in antibacterial surface applications for the first time opens the way for further investigation and attention to these low toxicity alternatives to cadmium-containing QDs, which are more studied but highly unlikely to see clinical application due to Cd's low permissible exposure limits and restrictions placed on its use in medical applications.

Outside academia, the single-step swell-encapsulation-shrink process allows for easy scale-up and implementation to polymer production lines, making surfaces produced by this method very attractive commercially. Further, the potent antibacterial activity of QD and CV embedded (QD + CV) polymers offers an alternative to reducing the incidence of hospital-acquired infections by reducing the bacterial load on surfaces. Due to the flexibility, ease of modification, low cost and durability of polymers, high-touch surfaces such as overbed tables, rails, doorknobs, supply carts and intravenous pumps can be easily coated with the QD + CV materials in a cost-effective manner. The antibacterial surfaces are also economical as they do not require specialised lighting because they are effective at both low (ambient levels) and high light intensities, allowing use under general lighting conditions. Finally, the installation of antibacterial QD + CV PU surfaces in areas such as hospitals, nursing homes, farms and food processing plants could reduce or even prevent bacterial colonisation of surfaces, helping to prevent bacterial infections thus protecting hospitalised patients, care residents, medical personnel and consumers.

## Acknowledgements

The work for this thesis was the result of a collaborative partnership of the UCL Division of Surgery and Interventional Science, the UCL Department of Chemistry, UCL Eastman Microbial Diseases Division with the UK-based nanotechnology company Nanoco Technologies Ltd. I am deeply appreciative of the unique privilege I have had to undertake a truly multi-disciplinary PhD.

I would like to thank my primary supervisor Prof. Sandy MacRobert for his expert knowledge and guidance. Thank you to my secondary supervisors: Dr. Elaine Allan for teaching a novice like me microbiology from scratch and giving me confidence in my skills; Prof Ivan Parkin, without whom I wouldn't have even been involved in this project; and Dr. Elnaz Yaghini, my 'research big sister' who has always believed in me more than I ever did, pushed me to achieve more and been a listening ear when I needed it. Thank you Dr. Imad Naasani and Dr. Lesley Smith from Nanoco Technologies for your insightful feedback and enthusiastic support of this project.

Thank you to Dr. Sandeep Sehmi for being my first point of contact in the early days. Your patience and approachableness has been a model I have endeavoured to follow as I have supervised others. Thank you to all my friends and colleagues whose generosity and friendliness created a positive atmosphere to do science.

The biggest thanks goes to my family, who have supported my education and without whom, I could not be where I am today. Finally, a special thanks to my husband who has been my champion and never let me give up. Your encouragement, enthusiasm, wisdom and understanding through my successes and failures has pushed me further than I thought I could go.

# Table of Contents

Declaration.....	i
Abstract.....	ii
Impact Statement.....	iii
Acknowledgements.....	iv
Table of Contents.....	v
List of Figures.....	xii
List of Tables.....	xxiii
List of Abbreviations.....	xxv
INTRODUCTION.....	1
CHAPTER 1. LITERATURE REVIEW.....	4
1.1. QUANTUM DOTS.....	4
1.1.1. Introduction.....	4
1.1.2. Bulk Semiconductor Physics and Quantum Confinement.....	5
1.1.3. Properties of Quantum Dots.....	8
1.1.3.1. Potential Drawbacks.....	10
1.1.4. Synthesis of Quantum Dots.....	12
1.1.4.1. Hot Injection Colloidal Synthesis of Quantum Dots.....	13
1.1.4.2. One Pot Organic Synthesis of Colloidal Quantum Dots.....	15
1.1.4.3. Solubilisation of Quantum Dots.....	16
1.1.4.3.1. Ligand Exchange.....	17
1.1.4.3.2. Addition of Secondary Hydrophilic Shell.....	18
1.1.4.4. Aqueous Synthesis of Quantum Dots.....	18
1.1.4.5. Hydrothermal Synthesis.....	19
1.1.4.6. Microwave Synthesis.....	19
1.1.4.7. Molecular Seeding.....	19
1.1.5. Optical and Electronic Applications of Quantum Dots.....	21
1.1.5.1. Displays.....	21
1.1.5.2. Solid State Lighting.....	24
1.1.5.3. Energy Storage.....	25

1.1.6. Biomedical Applications .....	27
1.1.6.1. Imaging.....	27
1.1.6.2. Drug Delivery.....	28
1.1.6.3. Sensors .....	29
1.1.7. Toxicity of Quantum Dots .....	30
1.1.7.1. Type and Composition.....	31
1.1.7.2. Surface Modifications .....	32
1.1.7.3. Size and Charge.....	34
1.2. PHOTODYNAMIC THERAPY.....	36
1.2.1. Introduction & History.....	36
1.2.2. PDT Mechanisms.....	40
1.2.3. Photodynamic Therapy by Quantum Dots.....	43
1.2.4. Förster resonance energy transfer (FRET).....	45
1.2.4.1. QDs as Donors .....	47
1.2.4.1.1. Biosensing .....	48
1.2.4.1.2. pH and ion Sensing.....	49
1.2.4.1.3. Probes for Enzymatic Activity .....	49
1.2.4.1.4. Photodynamic Therapy .....	50
1.2.4.1.5. DNA Replication.....	51
1.2.4.2. QDs as Acceptors.....	51
1.2.5. Charge Transfer.....	52
1.3. HOSPITAL ACQUIRED INFECTIONS.....	54
1.3.1. Introduction .....	54
1.3.2. Transmission of Hospital-Acquired Infections.....	54
1.3.3. Antimicrobial Resistance .....	56
1.3.4. Resistance in Common Nosocomial Pathogens .....	58
1.3.5. Prevention Strategies .....	59
1.3.5.1. Hand Hygiene.....	59
1.3.5.2. Cleaning .....	59
1.3.5.3. Disinfection.....	60

1.3.5.4. Sterilization .....	61
1.3.5.5. Behaviours and Practices Affecting Cleaning and HAIs .....	61
1.4. ANTIMICROBIAL MATERIALS & SURFACES .....	63
1.4.1. Antimicrobial Action of Metal Nanoparticles.....	63
1.4.1.1. Silver Nanoparticles .....	63
1.4.1.2. Zinc Oxide Nanoparticles.....	64
1.4.1.3. Titanium Dioxide Nanoparticles .....	64
1.4.1.4. Copper Nanoparticles .....	64
1.4.1.5. Other Metal Nanoparticles .....	65
1.4.2. Antimicrobial Action of Semiconductor Nanoparticles.....	67
1.4.2.1. Combinatorial Antimicrobial Treatments with Quantum Dots .....	67
1.4.3. Antibacterial Surfaces .....	68
1.4.3.1. Photosensitiser-Based Light-Activated Antibacterial Surfaces .....	68
1.4.3.2. Light-Activated Antibacterial Surfaces – Photosensitisers Combined with Other Materials.....	69
CHAPTER 2. SOLUTION PHASE STUDIES OF MECHANISMS OF REACTIVE OXYGEN SPECIES (ROS) GENERATION OF QUANTUM DOTS-PHOTOSENSITISER COMPLEXES .....	72
2.1. Introduction.....	72
2.2. Methods & Materials .....	74
2.2.1. Synthesis of CFQD <sup>®</sup> nanoparticles.....	74
2.2.2. Material Characterisation .....	75
2.2.2.1. Transmission electron microscopy (TEM) of quantum dots.....	75
2.2.2.2. Spectroscopic measurements.....	76
2.2.3. Electron Paramagnetic Resonance Spectroscopy.....	76
2.2.4. Time-Resolved Fluorescence Lifetime Measurements .....	76
2.2.4.1. Derivation of Fluorescence Lifetimes .....	77
2.2.5. Singlet Oxygen Phosphorescence .....	78
2.3. Results & Discussion.....	80
2.3.1. QD Nanoparticle Synthesis and Characterisation.....	80
2.3.2. Complex formation between QD and PS.....	82
2.3.3. Spectral Overlap .....	84

2.3.4. Steady-state Fluorescence Measurements .....	86
2.3.5. Time-Resolved Fluorescence Lifetime Measurements .....	89
2.3.6. Stern-Volmer Relationship .....	93
2.3.7. Singlet Oxygen Phosphorescence Measurements .....	95
2.3.8. Electron Transfer Interactions .....	97
2.4. Conclusion.....	101
<b>CHAPTER 3. QUANTUM DOTS IN POLYMER AS LIGHT-ACTIVATED ANTIMICROBIAL AGENTS.....</b>	<b>102</b>
3.1. Introduction.....	102
3.2. Materials & Methods .....	103
3.2.1. Synthesis of Indium-based Nanoparticles.....	103
3.2.2. Polymer Samples Preparation.....	103
3.2.3. Optimisation of QD Uptake into Polymer from Solvent .....	103
3.2.4. Polymer Samples for Antibacterial Testing .....	103
3.2.5. Characterisation of Modified Polymer Samples .....	104
3.2.6. Antibacterial Activity .....	104
3.2.6.1. Bacterial Strains .....	104
3.2.6.2. Microbiology Assay.....	105
3.2.6.3. Log and Percentage Reductions in Antimicrobial Studies .....	105
3.2.6.4. Statistical Analysis .....	106
3.3. Results & Discussion.....	107
3.3.1. Optimisation of Polymer Swelling .....	107
3.3.2. Characterisation of QD-Incorporated Polyurethane .....	109
3.3.3. Antibacterial Activity .....	111
3.3.4. Effect of Increasing QD Concentration .....	114
3.3.5. Estimation of Quantum Dot Uptake by Polymer.....	117
3.4. Conclusion.....	119
<b>CHAPTER 4. LIGHT-ACTIVATED ANTIMICROBIAL SURFACES: QUANTUM-DOT – PHOTOSENSITISER COMBINATIONS IN POLYURETHANE .....</b>	<b>121</b>

4.1. Introduction.....	121
4.2. Materials & Methods.....	123
4.2.1. Quantum Dot Nanoparticles.....	123
4.2.2. Nanoparticle Characterisation.....	123
4.2.3. Polymer Samples.....	123
4.2.3.1. Chemicals and Reagents.....	123
4.2.3.2. Polymer Samples for Antibacterial Testing.....	123
4.2.4. Material Characterisation.....	124
4.2.4.1. Spectroscopic measurements.....	124
4.2.4.2. Water Contact Angle.....	125
4.2.5. Antibacterial Activity.....	125
4.2.5.1. Bacterial Strains.....	125
4.2.5.2. Microbiology Assay – Nosocomial Bacteria.....	125
4.2.5.3. Microbiology Assay – Food-Borne Bacteria.....	126
4.2.5.4. Log and Percentage Reductions in Antimicrobial Studies.....	127
4.2.5.5. Statistical Significance.....	127
4.3. Results & Discussion.....	128
4.3.1. Characterisation.....	128
4.3.1.1. Quantum Dots.....	128
4.3.1.2. Crystal Violet.....	128
4.3.2. Incorporation of QDs and CV into Polyurethane.....	130
4.3.3. Antibacterial Activity.....	133
4.3.3.1. Low QD Content.....	133
4.3.3.2. Effect of Increasing QD Content in Polymer on Antimicrobial Activity.....	135
4.3.4. Improving Antibacterial Activity of QD-CV Polymer Substrates.....	138
4.3.4.1. Red QD-CV Polymer Substrates.....	138
4.3.4.2. Red QD-CV Substrates by 1-Step Encapsulation against Clinical Strains of Bacteria.....	145
4.3.4.3. Green QD-CV Substrates by 1-Step Encapsulation.....	148
4.3.4.4. Green QD-CV Substrates by 1-Step Encapsulation against Clinical Strains.....	150
4.3.5. Foodborne Pathogens.....	152
4.3.5.1. Salmonella.....	153

4.3.5.2. Listeria.....	155
4.3.6. Evaluation of Synergistic Effects .....	157
4.4. Conclusion.....	159
CHAPTER 5. LOW LIGHT INTENSITY ANTIBACTERIAL ACTIVITY OF QD + CV PU SURFACES .....	161
5.1. Introduction.....	161
5.2. Materials & Methods.....	163
5.2.1. Quantum dot nanoparticles .....	163
5.2.2. Incorporation of nanoparticles and dye into polymer .....	163
5.2.3. Material Characterisation .....	164
5.2.3.1. Transmission Electron Microscopy .....	164
5.2.3.2. Fluorescence Microscopy .....	164
5.2.4. Bacterial strains.....	164
5.2.5. Antibacterial Activity .....	165
5.2.5.1. Log and Percentage Reductions in Antimicrobial Studies .....	165
5.2.6. Detection of Superoxide.....	165
5.2.7. Statistical Analysis .....	166
5.3. Results & Discussion.....	167
5.3.1. Material Characterisation .....	167
5.3.2. Antimicrobial Testing.....	169
5.3.3. Photophysics.....	173
5.3.4. Preliminary Type I Mechanism Investigations.....	174
5.4. Conclusion.....	176
CHAPTER 6. EVALUATION OF MECHANISMS OF REACTIVE OXYGEN SPECIES (ROS) GENERATION OF QUANTUM DOTS-PHOTOSENSITISER COMPLEXES .....	177
6.1. Introduction.....	177
6.2. Materials and Methods .....	178
6.2.1. Materials .....	178
6.2.2. Steady-state Emission.....	178

6.2.3. Time-Resolved Lifetime Measurements .....	178
6.2.4. Singlet Oxygen Phosphorescence .....	178
6.2.5. Detection of Superoxide by XTT Reduction.....	179
6.2.6. Reactive Oxygen Species Generated by Materials.....	179
6.3. Results & Discussion .....	180
6.3.1. Steady-State and Time-Resolved Emission Studies of QD-CV Polymer Surfaces .....	180
6.3.2. Singlet Oxygen Phosphorescence Studies of QD-CV Polymer Surfaces.....	185
6.3.3. Superoxide Generation by QD-CV Substrates .....	188
6.3.4. Chemical Detection of Superoxide Release by Polymer Substrates: XTT Assay .....	189
6.3.5. ROS Detection with ROS Scavengers.....	194
6.4. Conclusion.....	200
CHAPTER 7. CONCLUSIONS AND FUTURE WORK .....	202
7.1. Summary of Thesis.....	202
7.2. Implications & Importance of Findings .....	210
7.3. Future Work.....	211
Publications & Presentations.....	213
References .....	215

# List of Figures

Figure 1.1 Basic structure of quantum dots. ....	5
Figure 1.2 Band structure of bulk insulators, semiconductors and conductors.....	6
Figure 1.3 Quantisation of energy bands in bulk semiconductors to discrete energy levels in semiconductors nanoparticles due to quantum confinement .....	8
Figure 1.4 <b>(A)</b> Absorption and <b>(B)</b> emission spectra of CdSe/ZnS core/shell QDs: from left to right. QDs with peak emission at: 525,545, 565, 585, 605, 625, 655, 705, and 800 nm. Reproduced with permission from Ishikawa <i>et al.</i> , 2011. <sup>4</sup> .....	9
Figure 1.5 Fluorescence decay behaviour of to a typical QD (CdSe/ZnS, multi-exponential, mean lifetime of 10.3 ns) compared to typical organic dyes (mono-exponential, lifetimes of 1.5 ns (Cy5) and 3.6 ns (Nile Red)). Reproduced with permission from Resch-Genger <i>et al.</i> , 2008. <sup>32</sup> .....	10
Figure 1.6 Models depicting blinking. <b>(A)</b> Blinking resulting from an Auger-assisted ionisation process. Here, ON and OFF periods correspond to a neutral nanocrystal ( $X^0$ ) and a charged nanocrystal ( $X^-$ ), respectively. <b>(B)</b> Blinking resulting from the charging and discharging of surface electron traps. Surface traps can act as reactive sites. The OFF state is due to the activation of surface traps (R) that capture hot electrons at a rate that is higher than the intraband relaxation rate, preventing relaxation to ground state via photon emission. (The ground and the excited electron states are shown as $^1S_e$ and $^1P_e$ , respectively; $^1S_h$ is the band-edge hole state). The position of the Fermi level, $E_F$ , relative to the trap energy, $E_R$ , is determined by the electrochemical potential and controls the occupancy of the surface trap R. Reproduced with permission from Galland <i>et al.</i> , Nature 2011. <sup>46</sup> .....	12
Figure 1.7 Synthesis of CdSe/ZnS core/shell quantum dots by high temperature colloid synthesis. Reproduced with permission from Bailey <i>et al.</i> , Physica E, 2004. <sup>62</sup> .....	14
Figure 1.8 QD solubilisation and functionalisation. QDs stabilised by organic surfactants can be solubilised into aqueous solution by formation of a 2nd shell with molecules that possess both hydrophilic (w-) and hydrophobic (w-) moieties. Examples include cross-linked polymers, amphiphilic copolymers and phospholipids ((a) – (c) respectively). Solubilisation may also be achieved through exchange of organic surfactants with molecules that are able to coordinate to the QD surface on one end and react with biomolecules on the other end. Examples are mercaptoacetic acid (MAA), dithiothreitol (DTT), dihydrolipoic acid (DHLLA), oligomeric	

phosphines, cross-linked dendrons and peptides ((d) – (i) respectively). The curved arrow indicates sites available for further functionalisation.. Adapted with permission from Michalet *et al.*, Science, 2005.<sup>83</sup> ..... 17

Figure 1.9 Molecular seeding synthesis of a cadmium selenide quantum dot using  $[M_{10}Se_4(SPh)_{16}][X]_4$  ( $X = Li^+$  or  $(CH_3)_3NH^+$ ) as the molecular seed and dropwise addition of cadmium acetate ( $Cd(OAc)_2$ ) and tri-n-octylphosphine selenide (TOP-Se) as the cadmium and selenium element-source precursors, with hexadecylamine (HDA) used as the capping agent. Reproduced from O'Brien *et al.* Preparation of Nanoparticle Materials, 2011.<sup>116</sup> ..... 20

Figure 1.10 Schematic illustration of three different device geometries in QD-based displays. (a) on-chip: QDs are placed within an LED package. (b) on-edge: QDs are placed between LED and light guide plate. (c) on-surface: QDs are embedded in a film and placed on the top surface of light guide plate. (LGP: light guide plate, red dots: red-emitting QDs; green dots: green-emitting QDs). Reproduced with permission from Haiwei *et al.*, IEEE Journal of Selected Topics in Quantum Electronics, 2017.<sup>119</sup> Copyright © 2017, IEEE..... 22

Figure 1.11 Typical emission spectra for green and red quantum dots using CdSe (solid line) and InP (dashed line). Blue LED with emission peak  $\lambda = 450$  nm is also displayed. Reproduced with permission from Haiwei *et al.*, IEEE Journal of Selected Topics in Quantum Electronics, 2017. <sup>119</sup> Copyright © 2017, IEEE. .... 23

Figure 1.12 Schematic representation and QDSCs, comprising a photoanode, QD (sensitizer), electrolyte containing a redox couple, and a counter electrode. Reproduced with permission from Pan *et al.*, Chem. Soc. Rev. 2018. <sup>137</sup> ..... 26

Figure 1.13 Spectrally resolved in vivo fluorescence images of live mouse models bearing human prostate tumours of similar sizes (0.5 – 1.0 cm in diameter) using QD probes with three different surface modifications: carboxylic acid groups (left), PEG groups (middle) and PEG-PSMA antibody conjugates (right). The site of QD injection was observed as a red spot on the mouse tail. Reproduced with permission from Xiaohu *et al.*, Nat Biotechnol 2004. <sup>140</sup> ..... 27

Figure 1.14 Schematic of doxorubicin-loaded hyaluronic acid PEG-encapsulated ZnO quantum dots (HA-ZnO-PEG) drug delivery system and mechanism of action. Reproduced with permission from Cai,*et al.*, ACS Appl Mater Inter 2016. <sup>143</sup> Copyright © 2016, American Chemical Society ..... 29

Figure 1.15 Factors affecting QD toxicity with respect to the QD core, QD shell/capping agents and the QD nanoparticle as a whole. .... 30

Figure 1.16 Examples of tetrapyrrole photosensitisers used in PDT.....	37
Figure 1.17 Examples of non-tetrapyrrole photosensitisers used in PDT.....	38
Figure 1.18 Simplified Jablonksi diagram showing the processes involved in PDT when a photosensitiser undergoes energetic transitions upon light absorption. The photosensitiser in its excited singlet state can undergo radiative decay (fluorescence) or non-radiative decay via internal conversion. It may also convert to the excited triplet state via intersystem crossing. The triplet state molecule may decay radiatively by phosphorescence, non-radiatively via internal conversion, or interact with molecular oxygen via resonant energy transfer (Type II reaction). The triplet state molecule may also interact with molecular oxygen and/or other substrate molecules via electron transfer (Type I reactions).....	40
Figure 1.19 Common Type I photochemical reactions during photodynamic therapy. <b>(A)</b> Reactions of the photosensitiser upon activation to form superoxide <b>(B)</b> Dismutation of superoxide. <b>(C)</b> Fenton reaction. PS*: excited state photosensitiser, PS <sup>•-</sup> : photosensitiser radical anion, Subs: substrate, Subs <sup>•+</sup> : substrate radical cation, O <sub>2</sub> <sup>•-</sup> : superoxide radical anion, <sup>1</sup> O <sub>2</sub> : singlet oxygen, H <sub>2</sub> O <sub>2</sub> : hydrogen peroxide, HO <sup>•</sup> : hydroxyl radical, HO <sup>-</sup> : hydroxide, Fe <sup>3+</sup> : oxidised iron cation, Fe <sup>2+</sup> : reduced iron cation.....	41
Figure 1.20 Type II photochemical reactions during photodynamic therapy. 3PS*: excited triplet state photosensitiser, 1PS: ground state photosensitiser, <sup>3</sup> O <sub>2</sub> : ground state molecular oxygen, <sup>1</sup> O <sub>2</sub> : excited state singlet oxygen, Subs: substrate .....	41
Figure 1.21 Schematic representation of a QD-protein-dye donor/acceptor pair for biosensing. Reproduced with permission from Medintz <i>et al.</i> , Nat. Mater., 2003. <sup>227</sup> .....	48
Figure 1.22 <b>(A)</b> Schematic of a pH sensor constructed from CdSe/ZnS QDs coupled to a pH-sensitive squaraine dye. <b>(B)</b> The emission profile of the QD–squaraine dye conjugate changes as a function of pH (red solid, 6.0; orange dotted, 7.0; yellow dotted, 8.0; green dotted, 9.0; and blue solid, 10) with λ <sub>ex</sub> = 380 nm. Adapted from Snee <i>et al.</i> , J. Am. Chem. Soc., 2006. <sup>233</sup> Copyright © 2006, American Chemical Society .....	49
Figure 1.23 Schematic presentation of the design of the QD-based nanosensors for detecting Bla (β- lactamases). The Bla substrate is labelled with the FRET acceptor carbocyanine dye; (Cy5), and immobilized to QDs via the biotin and streptavidin binding. Bla activity cleaves the lactam ring and releases Cy5 to restore the QD fluorescence emission. Reproced with permission from Xu <i>et al.</i> , Biochem. Biophys. Res. Commun., 2006. <sup>238</sup> .....	50

Figure 1.24 Mechanisms of resistance. Adapted from Per Nordberg *et al.*, Priority Medicines for Europe and the World. ‘A Public Health Approach to Innovation – Antibacterial Drug Resistance, 2004.<sup>294</sup> ..... 57

Figure 1.25 Mechanisms of metal toxicity to microbial cells. **A)** Metals can lead to protein dysfunction. **B)** They can also catalyse the generation of reactive oxygen species (ROS) and depletion of antioxidants. **C)** Certain metals have been shown to impair membrane function. **D)** Some can interfere with nutrient assimilation. **E)** Metals can also be genotoxic. Solid arrows represent pathways in which the underlying biochemistry has been elucidated, whereas dashed arrows represent a route of toxicity for which the underlying biochemical mechanism is unclear. [ALAD:  $\delta$ -aminolevulinic acid dehydratase, FbaA: fructose-1,6-bisphosphate aldolase, NQR: NADH:quinone oxidoreductase, PDF: peptide deformylase, PvdS: a  $\sigma$ -factor ( $\sigma^{24}$ ) from *P. aeruginosa*.] Reproduced with permission from Lemire *et al.*, Nat Rev Microbiol, 2013.<sup>323</sup> ..... 66

Figure 2.1 Set up for the experimental detection of singlet oxygen phosphorescence. Phosphorescence was detected at right angles to the laser excitation and collected via a series of lenses. A variable attenuator was placed in front of the laser beam to vary the incident power on the quartz cuvette. NIR: near-infrared, PMT: photomultiplier tube..... 79

Figure 2.2 **(A)** High resolution TEM images of red-emitting QDs **(B)** red QD size distribution determined by HR-TEM. .... 80

Figure 2.3 **(A)** High resolution TEM images of green-emitting QDs **(B)** green QD size distribution determined by HR-TEM ..... 81

Figure 2.4 Absorption spectra for the formation of QD-PS complexes in 1:1 cyclohexane/dichloromethane solutions. **(A)** Absorption of 0.02mg/mL red QDs (red line), 5  $\mu$ M CV (blue line) and 0.02mg/mL red QDs combined with 5  $\mu$ M CV (black line). Inset: zoomed section of absorption profile to clearly show red QD absorption features. QDs **(B)** Absorption of 0.02mg/mL green QDs (red line), 1  $\mu$ M CV (blue line) and 0.02mg/mL red QDs combined with 1  $\mu$ M CV (black line). .... 82

Figure 2.5 **(A)** Spectral overlap between the emission spectrum of the FRET donor (red QDs) and the absorption spectrum of the FRET acceptor (CV). Emission spectrum of red-emitting QDs (red line) and absorption spectrum of CV (blue line) and overlap region (shaded area). **(B)** Spectral overlap between the emission spectrum of the FRET donor (green QDs) and the

absorption spectrum of the FRET acceptor (CV). Emission spectrum of green-emitting QDs (green line) and absorption spectrum of CV (blue line) and overlap region (shaded area) .. 85

Figure 2.6 Fluorescence spectral changes in solution with fixed QDs concentration and increasing CV concentration. **(A)** Steady-state fluorescence emission spectra (400 nm excitation) of pure red QDs (red line) and QD-PS complexes with increasing CV concentration (2  $\mu\text{M}$  – 10  $\mu\text{M}$ ). **(B)** Steady-state fluorescence emission spectra (400 nm excitation) of pure green QDs (green line) and QD-PS complexes with increasing CV concentration (0.5  $\mu\text{M}$  – 5  $\mu\text{M}$ ). ..... 88

Figure 2.7 Logarithmic plots of time-resolved fluorescence intensities using the time correlated single photon counting method, recorded after pulsed excitation at 400 nm. **(A)** Red-emitting QDs and QD-CV mixtures with increasing CV concentrations (10  $\mu\text{M}$  – 30  $\mu\text{M}$ ). **(B)** Green-emitting QDs and QD-CV mixtures with increasing CV concentrations (0.5  $\mu\text{M}$  – 5  $\mu\text{M}$ ). .... 90

Figure 2.8 Stern-Volmer (S-V) relationships. **(A)** S-V relationship of QD quenching vs. CV concentration in solution at 620 nm. ( $\lambda_{ex}$  at 400 nm). **(B)** S-V relationship of QD quenching vs. CV concentration in solution at 500 nm ( $\lambda_{ex}$  at 400 nm). ..... 93

Figure 2.9 Time-resolved  $^1\text{O}_2$  phosphorescence at 1270 nm after pulsed laser irradiation of 1:1 cyclohexane/DCM solutions containing QDs only and QDs combined with CV. (A) Red QDs and red QD combined with CV. (B) Green QDs and green QDs combined with CV. .... 96

Figure 2.10 **(A)** EPR spectra for QDs with/without CV with controls. **(B)** EPR spectrum of irradiated green QDs and computer simulation for DMPO/hydroxyl adduct (red trace). **(C)** EPR spectrum of irradiated red QDs mixed with CV and computer simulations of oxygen-centred DMPO adducts (purple and blue traces) and a carbon-centred DMPO adduct (red trace). Final concentrations – DMPO: 250 mM; red QD – 12.5 mg/mL; green QD – 40 mg/mL; CV – 0.4 mM. .... 99

Figure 3.1 Schematic diagram illustrating the preparation of QD-encapsulated polyurethane from QD solution via swell-encapsulation-shrink for antimicrobial testing ..... 104

Figure 3.2 Plot showing normalised emission spectra of polyurethane solvent-treated (black line), encapsulated with green QDs (green line) and polyurethane encapsulated with red QDs (red line). ..... 109

Figure 3.3 **(A)** In (3d) region XPS spectra for red QD-incorporated polyurethane at the surface, sputtered 0 s (black line) and red QD-incorporated polyurethane in the bulk, sputtered 500 s

(red line). **(B)** Zn (2p) region XPS spectra for red QD-incorporated polyurethane at the surface, sputtered 0 s (black line) and red QD-incorporated polyurethane in the bulk, sputtered 500 s (red line)..... 110

Figure 3.4 XPS analysis. (A) In (3d) region XPS spectra for green QD-incorporated polyurethane at the surface, sputtered 0 s (black line) and green QD-incorporated polyurethane in the bulk, sputtered 500 s (green line). (B) Zn (2p) region XPS spectra for green QD- incorporated polyurethane at the surface, sputtered 0 s (black line) and green QD-incorporated polyurethane in the bulk, sputtered 500 s (green line). ..... 110

Figure 3.5 Testing of red QD-encapsulated polyurethane against Gram-positive and Gram-negative bacteria. **(A)** Counts of MRSA after incubation on solvent-treated polyurethane (blue bar) and incubation on polyurethane incorporated with red QDs (red bar) after 1 h white light illumination ( $6600 \pm 900$  lux). **(B)** Counts of *E. coli* after incubation on solvent-treated polyurethane (blue bar) and incubation on polyurethane incorporated with red QDs (red bar) after 2 h white light illumination ( $6600 \pm 900$  lux). The grey bar indicates the starting inoculum. (QD concentration used in swelling solution: 1mg/mL) ..... 112

Figure 3.6 Testing of green QD-encapsulated polyurethane against Gram-positive and Gram-negative bacteria. **(A)** Counts of EMRSA after incubation on solvent-treated polyurethane (blue bar) and incubation on polyurethane incorporated with green QDs (green bar) after 1 h white light illumination ( $6600 \pm 900$  lux). **(B)** Counts of *E. coli* after incubation on solvent-treated polyurethane (blue bar) and incubation on polyurethane incorporated with green QDs (green bar) after 2 h white light illumination ( $6600 \pm 900$  lux). The grey bar - starting inoculum. (QD concentration used in swelling solution: 1mg/mL) ..... 113

Figure 3.7 Effect of QD concentration and illumination time on antibacterial activity of QD-encapsulated polyurethane. **(A)** Counts of *E. coli* after incubation on solvent-treated polyurethane (blue bar) and on polyurethane swell-encapsulated in 3 mg/mL red QDs suspension (red bar) after 6 h white light illumination ( $6600 \pm 900$  lux). **(B)** Counts of *E. coli* after incubation on solvent-treated polyurethane (blue bar) and incubation on polyurethane swell-encapsulated in 7 mg/mL red QDs suspension (red bar) after 6 h white light illumination ( $6600 \pm 900$  lux). \* indicates  $p < 0.05$ . ..... 115

Figure 3.8 Typical plot of near detector absorbance of solvent-treated polyurethane absorbance (black line) alongside QD-encapsulated polyurethane (blue line)..... 117

Figure 4.1 Schematic illustrating the activation of a nearby photosensitiser molecule (PS) via energy transfer (FRET) after excitation of QDs, leading to generation of reactive oxygen species (ROS). Excitation of QDs may also enable generation of ROS via electron transfer processes (PET). .....	122
Figure 4.2 Graph showing absorption spectra of red QDs (red line), green QDs (green line), crystal violet (purple line); and emission spectra following excitation at 400 nm for red QDs (red dotted line) and green QDs (green dotted).....	128
Figure 4.3 Molecular structure of crystal violet, a photosensitiser with extensive history of use as an antiseptic. ....	129
Figure 4.4 Scheme showing two-step 'swell-encapsulation-shrink' technique used to produce polyurethane substrates containing both QDs and CV. ....	131
Figure 4.5 Characterisation of modified polymers. <b>(A)</b> Normalised emission spectra of red QD-encapsulated polyurethane (red line), CV-coated polyurethane (violet line), red QD-encapsulated and CV-coated polyurethane (pink line). <b>(B)</b> Normalised emission spectra of green QD-encapsulated polyurethane (green line), CV-coated polyurethane (violet line), green QD-encapsulated and CV-coated polyurethane (dark green line).....	132
Figure 4.6 Antibacterial action of modified polyurethane substrates. Viable counts of <i>E. coli</i> ATCC 25922 bacteria after 3 h incubation at 20°C in the dark and under white light (6600 ± 990 lux) on <b>(A)</b> red QD-encapsulated and CV-coated polyurethane and <b>(B)</b> green QD-encapsulated and CV-coated polyurethane. (Concentrations of swelling solutions used to modify PU: QDs – 0.1 mgmL <sup>-1</sup> ; CV – 1 mM).....	134
Figure 4.7 Antibacterial action of modified polyurethane substrates. Viable counts of <i>E. coli</i> ATCC 25922 bacteria after 3 h incubation at 20°C in the dark and under white light (6600 ± 990 lux) on <b>(A)</b> red QD-encapsulated and CV-coated polyurethane and <b>(B)</b> green QD-encapsulated and CV-coated polyurethane. (Concentrations of swelling solutions used to modify PU: QDs – 0.5 mgmL <sup>-1</sup> ; CV – 1 mM).....	135
Figure 4.8 Förster resonance energy transfer (FRET) considerations. <b>(A)</b> Absorption spectrum of CV dye superimposed with emission spectra of green and red QDs in solution, normalised. <b>(B)</b> The size-dependent colour of quantum dots (not drawn to scale). Red-emitting QDs are characteristically larger than their green counterparts. ....	138

Figure 4.9 Scheme illustrating the modified swell-encapsulation-shrink technique used to prepare the new quantum dot and CV-encapsulated polyurethane substrates. Polyurethane squares were dipped in a 1:1 cyclohexane/DCM solvent mixture containing QDs (1 mgmL<sup>-1</sup>) and CV dye (0.5 mM) for 24h. .... 141

Figure 4.10 Confirmation of nanomaterial and photosensitiser uptake. **(A)** Image showing polymer substrate after modification. From left to right: Appearance of polymer after treatment with plain solvent (control PU), with CV solution only (CV PU), with red QD QD solution only (rQD PU) and red QD combined with CV solution (rQD + CV PU). **(B)** Emission of polymer after preparation using new swell-encapsulation-shrink technique. .... 142

Figure 4.11 Antibacterial action of polyurethane substrates produced using the 1-step swell-encapsulation-shrink method. Viable counts of *E. coli* ATCC 25922 bacteria after 2 h incubation at 20°C in the dark and under white light (6600 ± 990 lux) on red QD and CV-encapsulated polyurethane. (Concentrations of swelling solutions used to modify PU: red QDs – 1 mgmL<sup>-1</sup>; CV – 0.5 mM) ..... 143

Figure 4.12 **(A)** Viable counts of MRSA NCTC 13143 on unmodified and modified polyurethane substrates incubated at 20°C under dark conditions and under white light (6000 lux ± 990 lux) for 1 h; **(B)** Viable counts of clinical strain EMRSA 4742 on unmodified and modified polyurethane substrates incubated at 20°C under dark conditions and under white light (6000 lux ± 990 lux) for 1 h. Concentrations of swelling solutions (made in 1:1 Cy/DCM solvent) used to modify PU: QDs – 1 mgmL<sup>-1</sup>; CV – 0.5 mM. .... 147

Figure 4.13 Antibacterial action of red QD + CV polymer made by the 1-step swell-encapsulation-shrink method. Viable counts of *E. coli* 1030 on unmodified and modified polyurethane substrates incubated at 20°C under dark conditions and under white light (6000 lux ± 990 lux) for 4 h. Concentrations of swelling solutions used to modify PU: red QDs – 1 mgmL<sup>-1</sup>; CV – 0.5 mM ..... 148

Figure 4.14 Antibacterial action of polymer embedded with green QDs and CV using the 1-step swell-encapsulation-shrink method. Viable counts of lab strain *E. coli* ATCC 25922 bacteria after 2 h incubation at 20°C in the dark and under white light (6600 ± 990 lux) on green QD and CV-encapsulated polyurethane. (Concentrations of swelling solutions used to modify PU: green QDs – 1 mgmL<sup>-1</sup>; CV – 0.5 mM) ..... 149

Figure 4.15 Antibacterial action of gQD + CV polymers against **(A)** clinical strain of EMRSA 4742 (1 h, 6600lux white light irradiation, 20°C incubation) and **(B)** clinical strain of *E. coli* (*E.*

*coli* 1030, 6600lux white light irradiation for 4 h, 20°C incubation). Concentrations of swelling solutions used to modify PU: green QDs – 1 mgmL<sup>-1</sup>; CV – 0.5 mM..... 151

Figure 4.16 Antibacterial action of gQD + CV polymer made by the 1-step swell-encapsulation-shrink method. Viable counts of lab strain *S. typhimurium* ATCC 14028 after 4 h incubation at 20°C in the dark and under white light (6600 ± 990 lux). Concentrations of swelling solutions used to modify PU: green QDs – 1 mgmL<sup>-1</sup>; CV – 0.5 mM ..... 154

Figure 4.17 Antibacterial action of gQD + CV polymer made by the 1-step swell-encapsulation-shrink method. Viable counts of *L. monocytogenes* NCTC 7973 after 1.5 h incubation at 20°C in the dark and under white light (6600 ± 990 lux). Concentrations of swelling solutions used to modify PU: green QDs – 1 mgmL<sup>-1</sup>; CV – 0.5 mM. ♦ indicates bacteria numbers are below the detection limit of 100. .... 156

Figure 5.1 **(A)** HR-TEM image of green-emitting indium-based quantum dots. **(B)** Histogram of size distribution of green-emitting QDs. **(C)** and **(D)** CCD false coloured fluorescence microscope images of 15 micron thick sections of modified polyurethane sections (control subtracted). The polymer is shown from the right hand side of the images. Colour intensity (top) ranges from black (no fluorescence or background) to red/white (corresponding to maximum fluorescence). Image resolution: 512 x 512 pixels (557 x 557 microns). Scale: 100 microns. **(C)** Polymer prepared via swell-encapsulation-shrink in 1mgml-1 green QD suspension (1:1 cy/DCM); **(D)** Polymer prepared via swell-encapsulation-shrink in a suspension of 1mgml-1 green QD and 20 µM crystal violet (1:1 cy/DCM). **(E)** and **(F)** The distribution of the fluorescence, for both polymer substrates in C and D respectively..... 168

Figure 5.2 Low light intensity antibacterial activity of gQD + CV substrates. Viable counts of **(A)** environmental *P. aeruginosa* P12 on modified polyurethane surfaces after 24 h irradiation at 500 lux, **(B)** clinical *P. aeruginosa* P1068 on modified polyurethane surfaces after 24 h irradiation at 500 lux. (Concentrations of swelling solutions used to modify PU: green QDs – 1 mgmL<sup>-1</sup>; CV – 0.5 mM) ..... 170

Figure 5.3 Low light intensity antibacterial activity of gQD + CV substrates. Viable counts of multi-drug resistant *E. coli* 1030 on modified polyurethane surfaces after 18 h irradiation at 500 lux. (Concentrations of swelling solutions used to modify PU: green QDs – 1 mgmL<sup>-1</sup>; CV – 0.5 mM)..... 171

Figure 5.4 **(A)** Steady-state emission of green QD with increasing CV concentration in **solution** (1:1 cyclohexane/DCM) at 400 nm excitation. **(B)** Time-resolved emission of green

QD alone or in combination with increasing concentrations of CV in **polyurethane**. The concentrations represent those used to swell the polyurethane. QD concentration in all swelling solutions:  $1 \text{ mg mL}^{-1}$ . ..... 174

Figure 5.5 Viable counts of EMRSA 4742 on unmodified and modified polyurethane polymers tested under standard conditions ( $20^\circ\text{C}$ , 1 h white light treatment at 6000 lux) without SOD (left) and in the presence of 50 U/mL SOD (same temperature and lighting conditions as standard test) (right). Concentrations of swelling solutions (made in 1:1 Cy/DCM solvent) used to modify PU: QDs – 1 mg/mL; CV – 500  $\mu\text{M}$ . (\*\* indicates significance of  $p < 0.01$  compared to CV PU)..... 175

Figure 6.1 Emission spectra of polyurethane substrates when incorporated with  $1 \text{ mg mL}^{-1}$  QD only or in combination with increasing concentrations of CV (excitation at 400 nm). **(A)** shows the spectra for red-emitting QDs and **(B)** for green-emitting QDs..... 181

Figure 6.2 Logarithmic plots of time-resolved photoluminescence measurements of pure QDs and QD-CV combinations embedded in polyurethane via swell-encapsulation-shrink. (A) Time-resolved emission lifetimes of red QDs and red green QD-CV combinations at 620 nm. (B) Time-resolved emission lifetimes of green QDs and green QD-CV combinations at 520 nm. In all cases, final QD concentration in swelling solutions was kept constant at  $1 \text{ mg mL}^{-1}$ . ..... 182

Figure 6.3 Logarithmic time-resolved singlet oxygen phosphorescence recorded at 1270 nm following pulsed laser irradiation of modified polyurethane. (A) Singlet oxygen phosphorescence signals for polymer containing red QDs (bright red), containing CV only (black), and a combination of red QD and CV (dark red). (Concentrations: QDs – 1 mg/mL; CV – 50  $\mu\text{M}$  CV). (B) Singlet oxygen phosphorescence signals for polymer containing green QDs (bright green), containing CV only (black), and a combination of green QD and CV (dark green). (Concentrations: QDs – 1 mg/mL; CV – 20  $\mu\text{M}$  CV). Insets for (A) and (B): Linear scale plot over the same time range. All signals have been subtracted from the control (untreated polyurethane)..... 186

Figure 6.4 XTT reduction to formazan by superoxide ..... 190

Figure 6.5 Experimental setup of polymer samples used for superoxide anion ( $\text{O}_2^{\bullet-}$ ) detection with XTT reagent. Release of  $\text{O}_2^{\bullet-}$  from QD and/or CV-incorporated polyurethane leads to reduction of XTT solution lying in direct contact with the polymer surface to form the orange formazan product which produces a detectable optical signal at 470 nm. .... 191

Figure 6.6 Measurement of XTT formazan formation as a result of superoxide generation. Absorbance of 470nm. Representative results when CV PU, rQD PU and rQD + CV PU are exposed to XTT and irradiated with 455 nm light at shorter time intervals **(A)** and longer time intervals **(B)**. Respectively, **(C)** and **(D)** show representative results when CV PU, rQD PU and rQD + CV PU are exposed to XTT and irradiated with 595 nm light at shorter time intervals and longer time intervals. The control (well with only XTT) has been subtracted for each point. .... 192

Figure 6.7 Viable counts of EMRSA 4742 on unmodified and modified polyurethane polymers tested under standard conditions (20°C, 1 h white light treatment at 6000 lux) without SOD (left) and in the presence of 50 U/mL SOD (same temperature and lighting conditions as standard test) (right). Concentrations of swelling solutions (made in 1:1 Cy/DCM solvent) used to modify PU: QDs – 1 mg/mL; CV – 500 µM. (\*\* indicates significance of  $p < 0.01$  compared to CV PU)..... 195

Figure 6.8 Photo-bactericidal activity of control PU, CV PU and QD + CV PU against EMRSA in the absence of ROS scavengers ('no scavenger') and in the presence of catalase (H<sub>2</sub>O<sub>2</sub> scavenger), mannitol (hydroxyl scavenger) and L-histidine (<sup>1</sup>O<sub>2</sub> scavenger). \*\* indicates that QD + CV PU has  $p \leq 0.01$  compared to CV PU. The experiment labelled "no scavenger" was the control, where no ROS quencher was added. The subsequent experiments labelled "catalase", "mannitol" and "L-histidine" are the results when that quencher was present... 196

## List of Tables

Table 2.1 Overlap integral ( $J\lambda$ ) and Förster distances ( $R_0$ ) for the QD-PS donor-acceptor pairs .....	86
Table 2.2 Donor/acceptor lifetime analysis data for red QD and red QD-CV complexes. Pre-exponential components ( $A_1$ and $A_2$ ), emission lifetimes ( $\tau_1$ and $\tau_2$ ) and amplitude weighted lifetime ( $\tau_0$ ) of the QDs with increasing CV concentration are shown. ....	91
Table 2.3 Donor/acceptor lifetime analysis data for green QD and green QD-CV complexes showing pre-exponential components ( $A_1$ and $A_2$ ), emission lifetimes ( $\tau_1$ and $\tau_2$ ) and amplitude weighted lifetime ( $\tau_0$ ) of the QDs with increasing CV concentration. ....	91
Table 2.4 Amplitude weighted lifetimes ( $\tau_0$ ) and corresponding FRET efficiencies ( $E$ ) for red QD-CV complexes .....	92
Table 2.5 Amplitude weighted lifetimes lifetimes ( $\tau_0$ ) and corresponding FRET efficiencies ( $E$ ) for green QD-CV complexes. ....	92
Table 2.6 Stern-Volmer quenching constants ( $K_{SV}$ ), amplitude weighted lifetimes of QDs in the absence of quencher ( $\tau_0$ ) and bimolecular quenching constants ( $k_q$ ) of QDs upon addition of quencher in solution phase. ....	93
Table 3.1 Percentage polymer swelling of 1 cm <sup>2</sup> polyurethane samples after submersion in in different ratios of cyclohexane and dichloromethane for 24 h.....	108
Table 3.2 QD Uptake by Polymer. Data utilised in the analysis of QD material uptake by polymer. ....	118
Table 4.1 Resulting antibacterial effectiveness of surfaces against laboratory strain of <i>E. coli</i> according to nanoparticle and photosensitiser concentrations used to make them.....	136
Table 4.2 Comparison of the antibacterial activities of rQD + CV substrates prepared by either the original 2-step dipping process or the novel single-step dipping procedure .....	144
Table 4.3 Comparison of the antibacterial activities of gQD + CV substrates prepared by either the original 2-step dipping process or the novel single-step dipping procedure .....	150

Table 4.4 Test for synergy between red QDs and CV for each strain: tabulated fractional viabilities and derived values for  $\alpha$ . The values are greater than unity in each case which demonstrates a synergistic interaction. .... 157

Table 4.5 Test for synergy between green QDs and CV for each strain: tabulated fractional viabilities and derived values for  $\alpha$ . The values are greater than unity in each case which demonstrates a synergistic interaction. \*  $\alpha = \infty$  at the detection limit of the test..... 158

Table 6.1 Mean fractional amplitude weighted red QD emission lifetimes and calculated FRET efficiencies of pure QD and QD-CV complexes with increasing CV concentrations (in the swell-encapsulation medium) when incorporated into polyurethane via swell- encapsulation-shrink ..... 183

Table 6.2 Mean fractional amplitude weighted green QD emission lifetimes and calculated FRET efficiencies of pure QD and QD-CV complexes with increasing CV concentrations (in the swell-encapsulation medium) when incorporated into polyurethane via swell-encapsulation-shrink ..... 184

## List of Abbreviations

aPDT	antimicrobial Photodynamic therapy
A.U.	Arbitrary units
BHI	Brain heart infusion
CFU	Colony forming unit
CRE	Carbapenem-resistant Enterobacteriaceae
CV	Crystal violet
Cy	Cyclohexane
DCM	Dichloromethane
DNA	Deoxyribonucleic acid
E <sub>g</sub>	Band gap energy
EMRSA	Epidemic methicillin-resistant <i>Staphylococcus aureus</i>
EPR	Electronic paramagnetic resonance
eV	Electron volts
FRET	Förster resonance energy transfer
FWHM	Full width half maximum
HAI	Hospital-acquired infection
HR-TEM	High-resolution transmission electron microscopy
IC	Internal conversion
IR	Infra-red
ISC	Intersystem crossing
LED	Light emitting diode
MAC	MacConkey agar
MB	Methylene blue
MDR	Multidrug resistant
MRSA	Methicillin-resistant <i>Staphylococcus aureus</i>
nm	nanometre
NIR	Near infra-red
NP	Nanoparticle
<sup>1</sup> O <sub>2</sub>	Singlet oxygen
O <sub>2</sub> <sup>•-</sup>	Superoxide
•OH	Hydroxyl radical
PBS	Phosphate buffer solution

PDT	Photodynamic therapy
PEG	Polyethylene glycol
PET	Photo-induced electron transfer
PHE	Public Health England
PL	Photoluminescence
PS	Photosensitiser
PU	Polyurethane
PVC	Polyvinyl chloride
ROS	Reactive oxygen species
QD	Quantum dot
SOD	Superoxide dismutase
TBO	Toluidine blue O
TCSP	Time correlated single photon counting
TEM	Transmission electron microscopy
TICT	Twisted intramolecular charge transfer
TOP	Tri-n-octylphosphine
TOPO	Tri-n-octylphosphine oxide
UV	Ultraviolet
UV-vis	Ultraviolet-visible
VRE	Vancomycin-resistant enterococci
XPS	X-ray photoelectron spectroscopy
ZnS	Zinc sulphide

# INTRODUCTION

The overall aim of this thesis was to investigate the potential of quantum dots (QDs) and photosensitisers (PS) as effective light-activated antimicrobial agents in self-disinfecting surfaces. It has been reported that nanoparticle-photosensitiser combinations show enhanced photo-activity compared to nanoparticle or dye alone for photodynamic therapy (PDT). Exploiting the concept of PDT, this thesis details the development of potent light-activated antibacterial polymers that act against bacteria by generating reactive oxygen species (ROS) through photo-induced energy transfer (to produce singlet oxygen  $^1\text{O}_2$ ) and electron transfer (to produce radicals such as superoxide anion  $\text{O}_2^{\bullet-}$  and hydroxyl radical  $\bullet\text{OH}$ ). These surfaces were initially intended to address the increasing problem of hospital acquired infections (HAIs) by reducing the bacterial load on frequently touched surfaces in healthcare facilities. In view of this, indium-based QDs were selected over the more common but intrinsically more toxic cadmium-based QDs. Also, a clinically approved photosensitiser, crystal violet was employed. A literature review outlining the background and theory behind QD nanoparticles, PDT and HAIs follows in CHAPTER 1.

The first objective of this thesis was to study the properties of the selected indium-based quantum dots when combined with the selected photosensitiser in solution phase (CHAPTER 2). To investigate the potential of the QD-PS complexes to act as donor/acceptor pairs based on Förster resonance energy transfer (FRET) and photo-induced electron transfer (PET) processes, the indium-based QDs were combined with crystal violet (CV) in suspension and examined using steady state and time-resolved photoluminescence measurements. The formation of  $^1\text{O}_2$  was examined using near-infrared detection of  $^1\text{O}_2$  phosphorescence.

The second objective was to examine the effectiveness of surfaces containing QDs alone as light-activated antibacterial surfaces (CHAPTER 3). A simple, easily scalable technique, swell-encapsulation-shrink, was used to incorporate indium-based red-emitting QDs as well as green-emitting QDs into medical-grade polyurethane. Antibacterial tests using laboratory strain *Escherichia coli* and a white light source similar to that used in hospitals, emitting at 6000 lux with polyurethane surfaces containing increasing QD concentrations. The QD polymers were found to show poor photo-antibacterial activity. Quantification studies using UV-vis absorbance measurements showed that QD uptake by polyurethane was suboptimal

and thus poor antibacterial activity was attributed to insufficient ROS generation due to low levels of nanoparticles in the polymer.

The third objective of this work was to investigate the photo-antibacterial action of polymer encapsulated with a combination of indium-based QDs and CV (CHAPTER 4). Incorporation of QDs and CV into the polymers using a two-step swell-encapsulation-shrink process result in little to no improvement on the light-activated antibacterial action observed by CV alone, in contrast to what has been reported previously. Thus, conditions required for efficient energy transfer interactions were considered and a modified one-step swell-encapsulation-shrink process was developed. Controlling conditions in this manner to encourage better FRET resulted in a synergistic enhancement of the surfaces' photo-antibacterial activity for both red QD-CV surfaces and green QD-CV surfaces. The QD-CV surfaces displayed excellent potency against both Gram-negative and Gram-positive bacteria, achieving  $> 3 \log_{10}$  kill within 4 h of 6000 lux white light illumination.

Photodynamic therapies ideally require light sources with strong light output or special light such as lasers because the light source employed must emit enough energy at the right wavelength to activate the photosensitiser to generate ROS. Most hospital and healthcare facilities use less than optimal lighting conditions for PDT, with recommended lighting levels for many areas in the hospitals set at less than 1000 lux. To mimic hospital conditions more realistically, the light intensity was reduced from 6000 lux to 500 lux. CHAPTER 5 details the investigation of antibacterial effectiveness of green QD-CV surfaces at low light intensities against Gram-negative bacteria. At ambient levels, the QD-CV surfaces were effective against multi-drug resistant *E. coli* and *Pseudomonas aeruginosa*, inducing  $> 3 \log_{10}$  kill within 24 h. The potency of the photo-bactericidal response of the QD-CV surfaces at both low and high light intensities as well as their easy production makes these materials exciting candidates for commercial production.

The final objective of this thesis was to probe the mechanisms involved in generation of ROS in the QD-CV antibacterial surfaces (CHAPTER 6). A wide range of methods – steady state photoluminescence measurements, and time-resolved photoluminescence lifetime measurements,  $^1\text{O}_2$  phosphorescence measurements, chemical detection assay for  $\text{O}_2^{\bullet-}$ , redox potential analyses of the QDs, CV and oxygen, electron paramagnetic resonance

measurements and microbiological assays to detect various ROS – were employed. To an extent, these methods allowed the distinguishing of Type I and Type II photochemical mechanism that generate ROS and to evaluate which processes contributed more greatly to the photo-bactericidal activity of the QD-CV materials.

# CHAPTER 1. LITERATURE REVIEW

## 1.1. QUANTUM DOTS

### 1.1.1. Introduction

Nanomaterials are state-of-the-art tools for modern scientific and technological advances. As the size of inorganic and organic materials is reduced to the nanometre scale, optical and electronic properties change and largely vary from the bulk form, becoming size- and shape-dependent. These properties open up new and promising applications from solar energy conversion to biomedicine. Quantum dots (QDs) are among the most interesting nanomaterials to have emerged over the last 20 years due to their novel optical and electronic properties, including tuneable emission wavelength, extreme signal brightness, resistance to photobleaching and the simultaneous excitation of multiple fluorescence colours.<sup>1-4</sup>

Quantum dots are zero-dimensional systems where electrons and holes are confined in all three dimensions.<sup>5</sup> QDs typically range from 1 to 10 nm in diameter with emission wavelengths that can be tuned from the ultraviolet through visible to the near-IR region by changing QD composition, size, and shape. Typically, QDs are spherical in shape with an inorganic semiconductor core (consisting of group II and VI elements such as CdSe and CdTe) enclosed within a shell of another semiconductor that has a larger bandgap such as ZnS (Figure 1.1). Generally, the composition of the semiconductor nanoparticle (NP) determines the range of accessible wavelengths because quantum confinement can only produce a blue shift in the emission relative to the band gap energy of the bulk material. For a particular composition, the degree to which the photoluminescence (PL) emission peak can be tuned depends upon the Bohr radius of the material and the range of sizes that can be produced in practice. Manipulating the composition and shape of the QDs requires control of the chemistry of QD synthesis and capping.<sup>6</sup> To date, the most synthesised and studied QDs are cadmium containing NPs of the II-VI periodic groups e.g. CdTe, CdSe, CdS, due to their superior optical properties as well as established synthetic methods.<sup>7-9</sup> However, many other non-cadmium containing QDs have been synthesised including InP, InAs, PbS, PbSe, ZnS and ZnSe QDs.<sup>10-</sup>

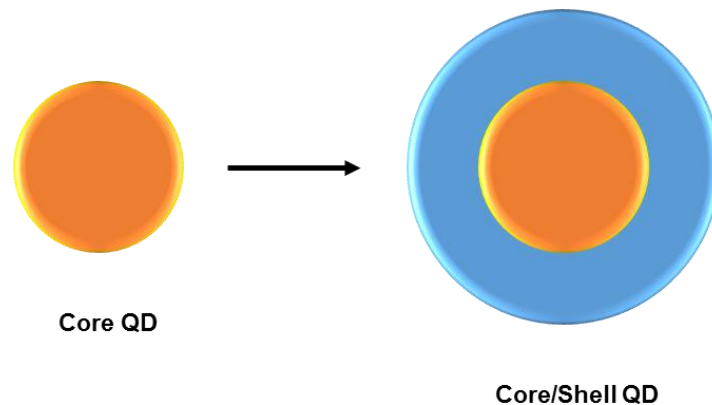


Figure 1.1 Basic structure of quantum dots.

Brus *et al.* reported the first colloidal QDs in 1983, deriving a close relationship between size and band gap for semiconductor NPs by applying a sphere model approximation to the wave function for bulk semiconductors and employing a bottom-up chemical synthesis rather than a top-down epitaxial approach to obtain semiconductor NPs.<sup>15-17</sup> Then in the mid-1990s, Murray, Guyot-Sionnest, Bawendi, and others pioneered refined synthetic methods that yielded nearly monodisperse, crystalline QDs.<sup>9, 18, 19</sup> For example, Murray *et al.* successfully synthesised colloidal CdS, CdSe, and CdTe QDs with size-tuneable band-gap emission and absorption.<sup>18</sup> A breakthrough in biological applications of QDs was made in 1998 when Alivisatos *et al.* and Chan and Nie reported the synthesis of water-soluble QDs and the conjugation of QDs to biomolecules enabling the use of QDs as biological agents.<sup>20, 21</sup> Since then, rapid progress has been made in the systematic refinement of QD synthesis to produce monodispersed and high stable NPs with diverse properties, surface chemistries and applications.

### 1.1.2. Bulk Semiconductor Physics and Quantum Confinement

The electrical properties of bulk conductors (metals), bulk semiconductors, and insulators can be understood in terms of energy bands and energy band gaps (Figure 1.2). The highest energy band that is occupied at room temperature is known as a valence band and the next available band in the energy structure is known as a conduction band. The difference in the energy level between the valence and conduction band (band gap), typically expressed in

electron volts (eV) determines the conductivity of the solid materials. In metals, the valence band overlaps with the conduction band, forming a continuous band, meaning that electrons are free to move with little or no additional electric field applied. Insulators are characterised by a large energy band gap between the valence and conduction bands such that when an electric field is applied, electrons cannot acquire enough kinetic energy to overcome the band gap and occupy the conduction band. Materials known as semiconductors have a narrow band gap between the valence and conduction bands. At low temperatures, there is little thermal energy available to push valence electrons across this gap, and the semiconductor behaves as an insulator. At higher temperatures, though, the ambient thermal energy becomes enough to force electrons across the gap, increasing the conductivity.<sup>22</sup>

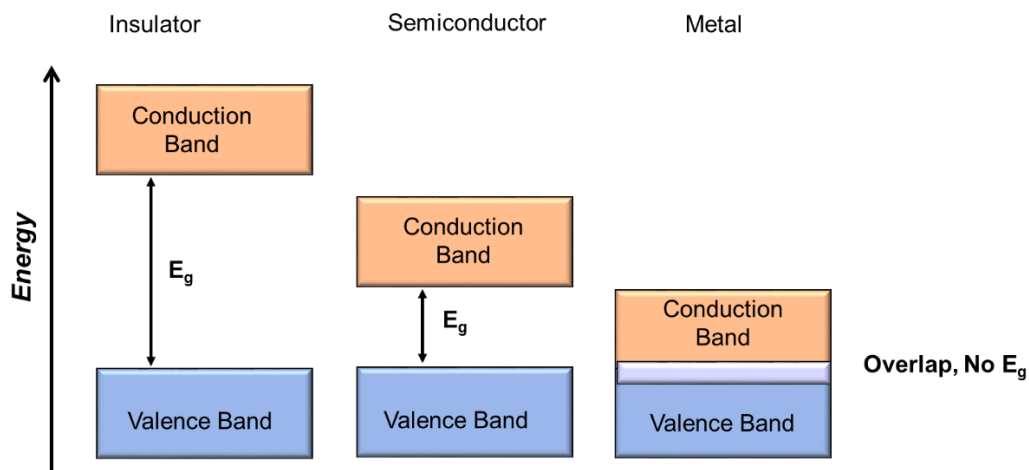


Figure 1.2 Band structure of bulk insulators, semiconductors and conductors

When a valence band electron is excited across the band gap into the conduction band by the absorption of a photon equal to or greater than the energy band gap, it leaves behind a positively charged vacancy or 'hole' in the valence band. In the presence of an electric field, the negatively charged electron and positively charged hole may be mobilized to yield a current, but their lowest energy state is an electrostatically bound electron-hole pair, known as the exciton. The excited electron may relax back to its ground state in the valence band, annihilating the exciton. This process is known as radiative recombination and is accompanied by the emission of a photon. Alternatively, the exciton may undergo charge transfer interactions and recombine non-radiatively.

The exciton has a finite size within the crystal defined by the Bohr exciton radius which can vary from 1 nm to more than 100 nm depending on the material. In analogy to the Bohr model of the hydrogen atom, the Bohr exciton radius ( $a_B$ ) can be written as:

$$a_B = \frac{\hbar^2 \varepsilon}{e^2} \left( \frac{1}{m_e} + \frac{1}{m_h} \right)$$

Equation 1.1

where  $\hbar$  is the reduced Planck constant,  $\varepsilon$  is the dielectric constant of the semiconductor,  $e$  is the charge of the electron,  $m_e$  the effective mass of the electron and  $m_h$  the effective mass of the hole. When the radius of the semiconductor NP is smaller than the Bohr exciton radius, the motions of the electron-hole pair become spatially confined to dimensions smaller than in the bulk.<sup>6</sup> Due to this *quantum confinement* effect, the electronic structure and optical properties of QDs significantly differ from their bulk counterparts. The confinement induces quantisation of the bulk energy bands into discrete electronic levels and the increase in band gap energy (Figure 1.3). As the size of the semiconductor nanocrystal decreases, the band gap increases, producing a blue shift (shorter wavelengths) of both absorbance and PL. This quantum confinement effect is analogous to the quantum mechanical model known as “particle in a box”, in which the energy of the particle increases as the size of the box decreases. In bulk materials, numerous energy levels are available and subsequent transitions between these states gives rise to a broad emission peak. In QDs, only a few states are allowed, thus the energy transitions are discrete and yield a narrower emission peak compared to the bulk material. Because of these atom-like discrete electronic states under strong quantum confinement, QDs are sometimes described as artificial atoms. The discrete electronic states bring about many new size-dependent properties that are both physically interesting and useful in many different applications.<sup>23, 24</sup>

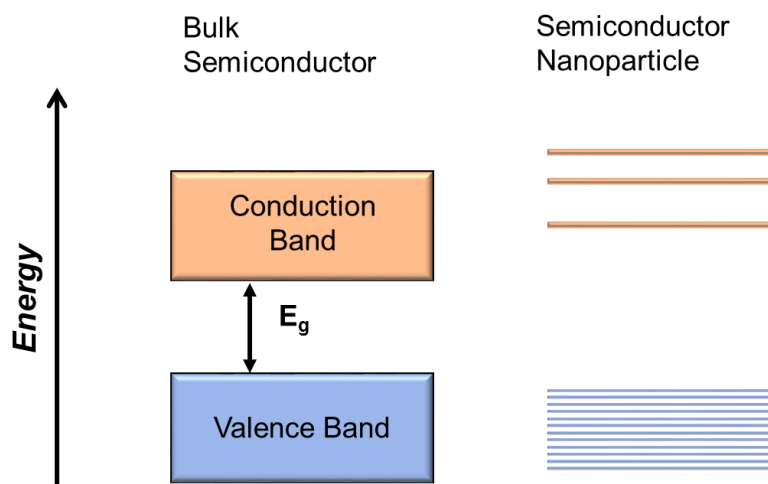


Figure 1.3 Quantisation of energy bands in bulk semiconductors to discrete energy levels in semiconductors nanoparticles due to quantum confinement

### 1.1.3. Properties of Quantum Dots

QDs have large excitation (absorption) bandwidths extending, and generally increasing in intensity at wavelengths shorter than the size-tuned band gap energy. This allows efficient excitation of several different colour probes with a single light source, a feat that is impossible with organic dyes which tend to show high absorptions over very narrow ranges. Broad absorption spectra also allow the freedom to select any excitation wavelength below the band gap energy. It also potentiates a large effective Stokes shift between the excitation wavelength and QD PL emission typically on the order of many tens of nanometres, and can potentially exceed 100–200 nm. Fluorescent dyes, on the other hand, experience small Stokes shifts typically ~10-20 nm.<sup>4, 25</sup>

Using optimised synthetic methods, a high level of control over QD PL emission maxima may be achieved (Figure 1.4). This allows the development of probes with tuneable emission wavelength that span the entire visible electromagnetic spectrum. Progress in QD synthesis enables excellent control over particle size and size distribution. The wavelength range covered by different sizes of the same QD is much broader than the one obtained with different dye molecules, from the blue to the near infrared region. As a result, it is possible to select a wavelength that is especially suited to a particular application and subsequently synthesise a QD-based probe by selecting the appropriate semiconductor materials and nanocrystal size. QDs exhibit narrow and symmetric emission peaks (FWHM ~15-50 nm) compared to organic

dyes which often have broader and asymmetric emission profiles. For simultaneous multicolour staining, labelling or detection procedures, narrow emission linewidths are important to avoid cross talk.<sup>26</sup>

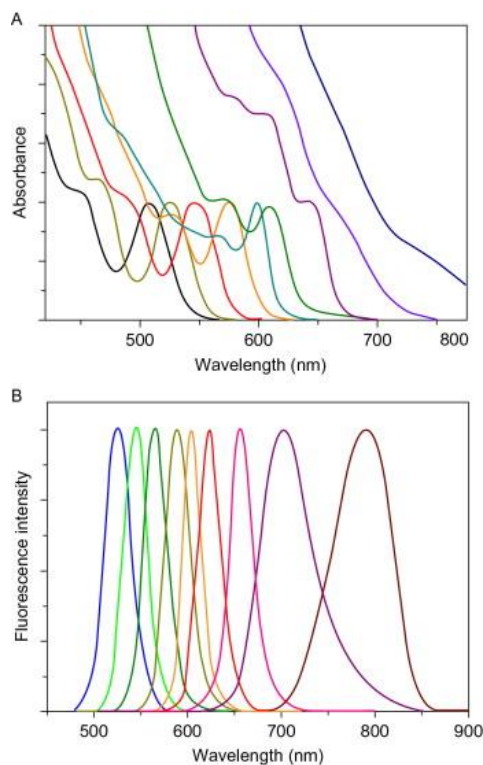


Figure 1.4 **(A)** Absorption and **(B)** emission spectra of CdSe/ZnS core/shell QDs: from left to right. QDs with peak emission at: 525, 545, 565, 585, 605, 625, 655, 705, and 800 nm. Reproduced with permission from Ishikawa *et al.*, 2011.<sup>4</sup>

Properly passivated QDs display a strong resistance to photobleaching and superior thermal stability, making continuous or long-term monitoring of slow biological processes as well as the use of intense laser excitation possible.<sup>27, 28</sup> On the other hand, organic fluorescent dyes can begin to photobleach immediately upon exposure to light<sup>29</sup> and despite improvements, organic dyes and particularly NIR fluorophores generally suffer from poor photostability.<sup>30, 31</sup>

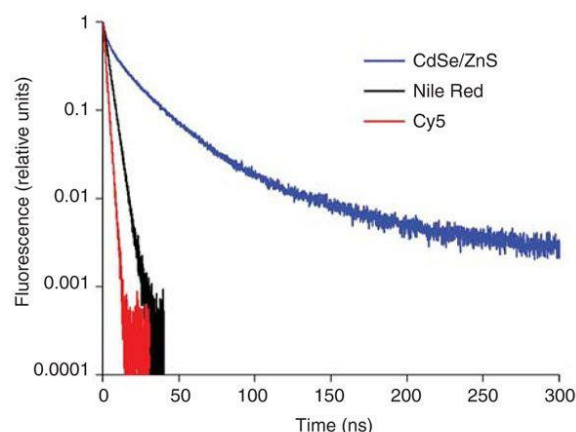


Figure 1.5 Fluorescence decay behaviour of to a typical QD (CdSe/ZnS, multi-exponential, mean lifetime of 10.3 ns) compared to typical organic dyes (mono-exponential, lifetimes of 1.5 ns (Cy5) and 3.6 ns (Nile Red)). Reproduced with permission from Resch-Genger *et al.*, 2008.<sup>32</sup>

High brightness of QDs resulting from the combination of high quantum yields (QY) and large molar absorption coefficients is very advantageous for imaging applications, with studies reporting QDs to be 20 times brightness than conventional organic dyes.<sup>33</sup> The fluorescence lifetime of typical organic dyes ranges from 1–5 ns while QDs fluorescence lifetimes can be of order of 10 to a few hundred ns (Figure 1.5). The long PL lifetimes of QDs are advantageous for distinguishing QD signals from background fluorescence using fluorescence lifetime imaging (FLIM) and for achieving high-sensitivity detection.<sup>20, 34, 35</sup>

#### 1.1.3.1. Potential Drawbacks

Though QDs exhibit superior optical properties, they also bear some drawbacks. On their own, core QDs are unstable, prone to oxidation and often suffer from low QY and so a shell is needed – this increases the NP size, particularly if water-soluble functionalisation is required, which is disadvantageous since the properties of the QD change with size.<sup>36</sup> In addition, due to less than optimal surface chemistry, QDs can aggregate, reducing their stability.<sup>37</sup> Further, the large sizes of QDs (compared to conventional PS) could sterically hamper access to cellular targets.<sup>32</sup> Furthermore, the cytotoxicity of QDs, particularly relevant for imaging cells and in vivo applications, is a major issue. Often, cytotoxicity is determined by NP compositions and the preparation of the surface layers. Studies have ascribed QD cytotoxicity to factors such as release of toxic ions e.g. Cd<sup>2+</sup> and Se<sup>2+</sup>, reactive oxygen species (ROS) generation

upon illumination and photo-oxidation,<sup>38, 39</sup> cytotoxic surface ligands<sup>40</sup> and NP aggregation; while others observed no cytotoxicity of QDs.<sup>41-43</sup>

Another limitation of QDs is the phenomenon known as blinking, where the continuously illuminated QDs emit detected luminescence for limited times, interrupted by dark periods during which no emission occurs similar to effects that have also been observed for fluorescent dyes and proteins.<sup>32, 44, 45</sup> Although this phenomenon can also be observed with molecular fluorophores, it is more prominently associated with QDs. Blinking is thought to be caused by two processes: from an Auger-assisted ionisation process or from trapping of one of the charge carriers at or near the particle surface (Figure 1.6). In the former process, when a neutral QD is excited upon irradiation, it may relax back to the ground state by emitting photons, which makes the NPs appear bright. However, charged particles may appear dark when they relax by ejecting electrons in an Auger electron emission (instead of releasing energy in the form of an emitted photon, the energy is transferred to another electron, which is ejected from the QD, resulting in the re-ionisation of the QD). The latter process is based on charging and discharging of surface electron traps. If these traps are unoccupied, they can intercept energetic or “hot” electrons, thereby preventing the electrons from relaxing to a state that would otherwise lead to photon emission.<sup>46</sup> The fluorescence blinking phenomenon, universal to all QDs, adversely affects applications in photovoltaic and energy storage devices as well as certain bioimaging and tracking applications, however, researchers have exploited this intrinsic property to develop super-resolution microscopy. Because fluorescence intermittency is only observed for single QDs (in a QD ensemble, the probability that different QDs all blink simultaneously is very low therefore blinking is not observed), it can be used to resolve closely spaced QDs and thereby achieve resolution several times greater than the resolution limit of the microscope.<sup>47-51</sup> Nevertheless, structural modifications of QDs that reduce blinking have been developed.<sup>52, 53</sup> For example, Ren *et al.* recently synthesised a completely non-blinking core/shell (Zn)CuInS/ZnS QDs by synthesising core CuInS then eliminating interior traps by forming graded (Zn)CuInS alloyed QDs and subsequently modifying the surface traps of QDs by introducing ZnS shells onto (Zn)CuInS QDs.<sup>54</sup>

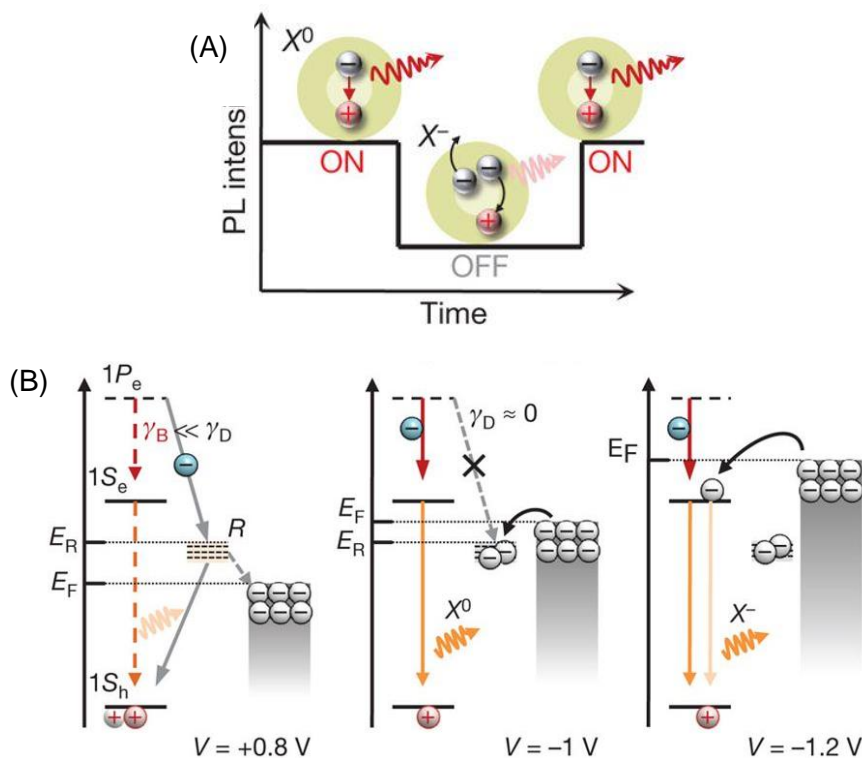


Figure 1.6 Models depicting blinking. **(A)** Blinking resulting from an Auger-assisted ionisation process. Here, ON and OFF periods correspond to a neutral nanocrystal ( $X^0$ ) and a charged nanocrystal ( $X^-$ ), respectively. **(B)** Blinking resulting from the charging and discharging of surface electron traps. Surface traps can act as reactive sites. The OFF state is due to the activation of surface traps (R) that capture hot electrons at a rate that is higher than the intraband relaxation rate, preventing relaxation to ground state via photon emission. (The ground and the excited electron states are shown as  $1S_e$  and  $1P_e$ , respectively;  $1S_h$  is the band-edge hole state). The position of the Fermi level,  $E_F$ , relative to the trap energy,  $E_R$ , is determined by the electrochemical potential and controls the occupancy of the surface trap R. Reproduced with permission from Galland *et al.*, Nature 2011.<sup>46</sup>

#### 1.1.4. Synthesis of Quantum Dots

Historically, the synthesis of small semiconductors was developed using techniques similar to those used to produce colloidal gold NPs. However, early procedures yielded nanocrystals with large size distributions, low fluorescence QY and the poly-dispersity within these samples made the resolution of size-dependent properties difficult.<sup>55, 56</sup> A major breakthrough towards the synthesis of monodisperse, high quality QDs was made by Murray *et al.* in 1993 and since then rapid development has led to excellent control of QD synthetic chemistry.<sup>57</sup>

#### 1.1.4.1. Hot Injection Colloidal Synthesis of Quantum Dots

The traditional approach for the synthesis of QDs, which was pioneered by Murray *et al.* in 1993, is called high-temperature colloidal synthesis or hot injection synthesis.<sup>57</sup> This process relies on the heating of specific organic solvents and injection of semiconductor precursors. For instance, to prepare CdSe QDs, typically a room temperature mixture of the Cd precursor (dimethylcadmium,  $\text{Cd}(\text{CH}_3)_2$ ) and Se precursor (tri-n-octylphosphine selenide, TOP-Se) is rapidly injected into hot (300 °C) trioctylphosphine oxide (TOPO) solution under an inert atmosphere (nitrogen or argon flow) in a three-neck round-bottom flask. Alternatively, a cadmium precursor is dissolved in the TOPO solvent in an inert atmosphere and heated to 300 °C. Under continuous vigorous stirring, the selenium precursor dissolved in TOP (room temperature) is swiftly injected into the vessel. TOPO simultaneously serves as the metal precursor and solvent which allows the reaction mixture to reach high temperatures of up to 320 °C. These conditions lead to rapid particle nucleation followed by particle growth and annealing at lower temperatures. During the growth period, the QD size can be monitored by measuring aliquots taken at various intervals or by means of a spectroscopic probe fitted within the reaction vessel. Once the preferred size has been obtained, growth is quenched by cooling the solution down. After preparation, the NPs are coated with a monolayer of TOPO surfactant, ensuring solubility in non-polar solvents and acting as a stabilising agent to prevent particle aggregation.<sup>58</sup> QDs with different sizes can be obtained over a period of a few hours by controlling the growth temperature. The maximum particle size and rate of growth may also be controlled to a degree by adjusting the initial precursor concentration and the length of growth time. During the growth period, extra precursor material can also be added to the reaction mixture to improve size distributions and increase QD size.

High temperature colloidal synthesis has been employed to produce CdSe, CdTe and CdS QDs with relatively high fluorescence QY and narrow size distribution and bright tunable luminescence. The discovery of new precursors and ligands in subsequent years has led to further progress in this approach. This includes the use of naturally occurring, inexpensive and lower toxicity cadmium precursor cadmium oxide ( $\text{CdO}$ ) in place of  $\text{Cd}(\text{CH}_3)_2$ , which is extremely toxic, pyrophoric and expensive. Other environmentally more benign precursors that have been proposed as alternatives to  $\text{Cd}(\text{CH}_3)_2$  include cadmium acetate and cadmium carbonate.<sup>59, 60</sup> Yu *et al.* also demonstrated that the use of non-coordinating solvent octadecane

(ODE) instead of coordinating solvent TOPO has not only feasible but offered advantages in size-tunability and dispersity.<sup>61</sup>

Formation of a ZnS shell causes a considerable increase in the QY of luminescence. To coat the QD cores, capping material precursor can be added slowly to the raw reaction mixture following the annealing step (Figure 1.7). Dropwise addition of shell precursor at lower temperature (than the nucleation temperature) promotes epitaxial deposition of the material rather than nucleation of new NPs. Aliquots can be analysed to determine when the shell has reached its optimal thickness by observing the resulting fluorescence yield from the particles. The core/shell QDs obtained from these procedures are highly fluorescent, photostable, and sufficiently monodisperse for use as labels in biological studies, though further modifications are required to make QDs soluble in water and biocompatible.<sup>62</sup>

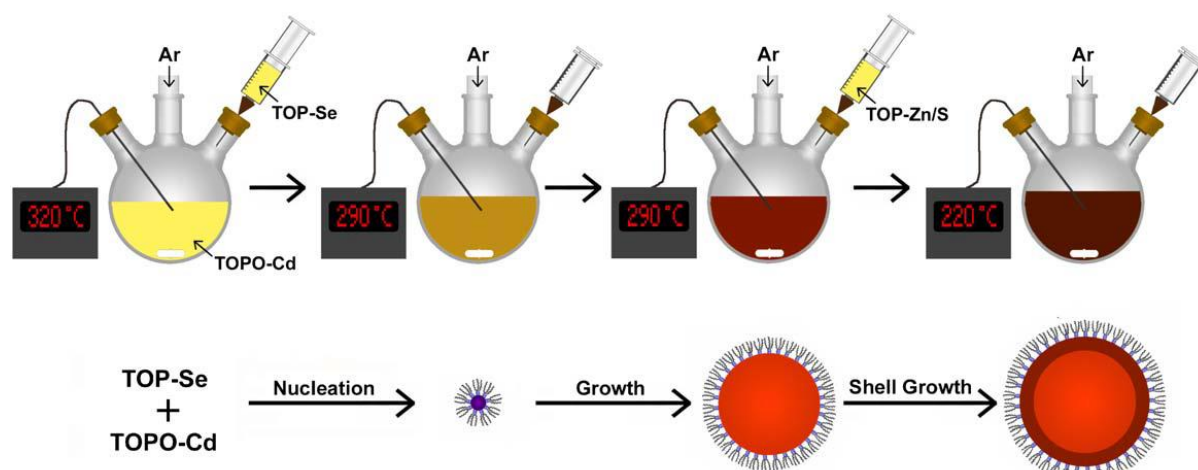


Figure 1.7 Synthesis of CdSe/ZnS core/shell quantum dots by high temperature colloid synthesis. Reproduced with permission from Bailey *et al.*, *Physica E*, 2004.<sup>62</sup>

High-temperature colloid synthesis, which has proved rather successful the production of II-VI semiconductor NPs, is attractive for the synthesis of InP QDs. However, employing the conditions, solvents, ligands and precursors used in the fabrication of CdSe QDs has yielded unsatisfactory results for III-V NPs such as InP. Nucleation and crystal growth in this system occur very slowly and the growth of NPs of a specified size requires very long periods of time (hundreds of hours).<sup>63-65</sup> In addition, the strength of covalent bonding in InP makes it difficult to separate the nucleation and growth of the NPs, complicating the acquisition of monodispersed particles and leading broad size distributions and broad photoluminescence spectra with wide FWHM of 40 – 60 nm or more, compared to less than 40 nm for CdSe.<sup>66-68</sup>

However, by careful selection of corresponding conditions and precursors, colloidal synthesis of InP QDs with a narrow particle size distribution may be achieved within practical time periods. For example, the use of safer and cheaper octadecene (ODE) instead of organophosphine solvents as the uncoordinating solvent significantly reduced the duration of synthesis, allowing the fabrication of 3 nm InP QDs, characterised by a variance of the size distribution function of 4.7%, within a few hours rather than previous several days.<sup>11</sup> Also the use of new indium carboxylate precursors such as indium(III) laurate, indium(III) myristate, and indium(III) stearate to replace indium(III) acetate and indium(III) chloride has enabled the synthesis of highly uniform InP QDs with the use of ODE alone, without the addition of coordinating solvents, ligands, or surfactants.<sup>12</sup> Unfortunately, low luminescence QY and low chemical stability is observed immediately after synthesis of InP QDs by this method. This is caused by the presence of numerous deep surface traps, such as unsaturated bonds and packing defects, on InP QDs and a higher activation barrier of escape from the traps compared with II-VI semiconductors.<sup>69, 70</sup>

The QY can be increased by epitaxial growth of shells using semiconductors with wider band gap (mainly ZnS shells)<sup>71, 72</sup> or by chemical modification of the NP surface.<sup>73, 74</sup> Post-synthetic treatment of InP QDs with HF or NH<sub>2</sub>F solutions (chemical annealing) have been reported to increase QY by more than 10 times to 30% and also impart intense band-to-band luminescence.<sup>73</sup> Photochemical annealing (UV radiation) has also been combined with chemical annealing to improve the properties of InP QDs.<sup>75</sup>

#### **1.1.4.2. One Pot Organic Synthesis of Colloidal Quantum Dots**

Hot-injection synthesis produces high-quality photo-stable QDs with low defects due to precise control of injection speed, stirring rate and precursor temperature. However, low batch reproducibility is a major problem with this approach due to difficulties controlling the reaction temperature upon injection the room temperature precursor into the hot solvent in the batch reactor, in turn, stalling progress in large-scale production. A number of one-pot, lower temperature strategies to produce QDs in larger quantities have been developed. Pradhan and Efrima described a generic method for producing high-quality metal sulfide NPs of a controllable and narrow size distribution using metal salts of alkylxanthates. Here, metal xanthtes were heated in the presence of hexadecylamine (HDA) which is an electron-donating solvent, allowing the formation of metal sulphide at temperatures as low as 70 °C without the

use of any air-sensitive techniques. By controlling the reaction temperature, control of NP size was achieved, with a lower temperature resulting in larger NP size and vice versa.<sup>76</sup>

Ouyang and co. developed a one-pot non-injection colloidal synthesis approach to multiple families of CdSe NPs of sizes ranging of 1.7 – 2.2 nm by using cadmium acetate dihydrate ( $\text{Cd}(\text{OAc})_2 \cdot 2\text{H}_2\text{O}$ ) and elemental selenium as Cd and Se sources respectively, with octadecene (ODE) as the reaction solvent and fatty acid as the surface ligand. All reagents were loaded at room temperature into a three-necked round bottom flask fitted with an air-cooled condenser and the growth of the CdSe particles was carried out at 120 – 240 °C, resulting in high-quality CdSe NPs exhibiting strong bandgap photoluminescence.<sup>77</sup> The one-pot non-injection organometallic synthesis methods have been applied to other types of QDs types including CdSe, CdTe, CuS, PbS and  $\text{Ag}_2\text{S}$ .<sup>77-81</sup>

Continuous flow processes were also developed to improve the consistency and reproducibility of QDs.<sup>82</sup>

#### **1.1.4.3. Solubilisation of Quantum Dots**

High quality colloidal QDs produced by hot injection or one pot synthesis are well soluble in non-polar solvents due to organic and hydrophobic stabilising ligands. However, they are insoluble in water and other biologically relevant media and do not possess the appropriate moieties for conjugation to biomolecules such as DNA, peptides and antibodies. Therefore, surface modification of QDs to make them water-soluble and thus enable use in biomedical applications is necessary. Generally, preparation of hydrophilic QDs can be grouped into two main categories: (i) exchange of hydrophobic ligands for hydrophilic ligands and (ii) creation of a secondary hydrophilic shell around the hydrophobic QD shell (Figure 1.8).

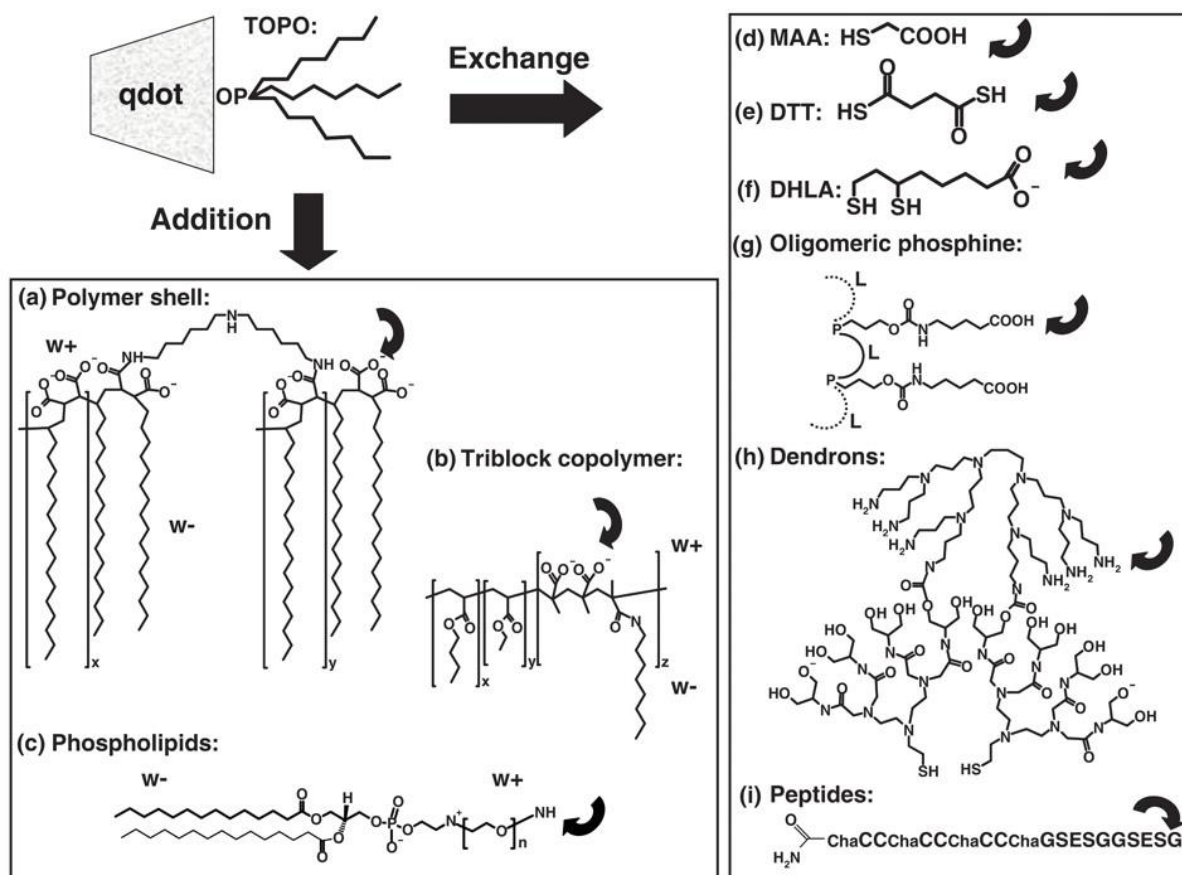


Figure 1.8 QD solubilisation and functionalisation. QDs stabilised by organic surfactants can be solubilised into aqueous solution by formation of a 2nd shell with molecules that possess both hydrophilic (w-) and hydrophobic (w-) moieties. Examples include cross-linked polymers, amphiphilic copolymers and phospholipids ((a) – (c) respectively). Solubilisation may also be achieved through exchange of organic surfactants with molecules that are able to coordinate to the QD surface on one end and react with biomolecules on the other end. Examples are mercaptoacetic acid (MAA), dithiothreitol (DTT), dihydrolipoic acid (DHLA), oligomeric phosphines, cross-linked dendrons and peptides ((d) – (i) respectively). The curved arrow indicates sites available for further functionalisation.. Adapted with permission from Michalet *et al.*, Science, 2005.<sup>83</sup>

#### 1.1.4.3.1. Ligand Exchange

Ligand exchange consists involves replacing the hydrophobic superficial ligands with new water-soluble bifunctional ligands that presenting anchoring groups to bind to the QDs surface on one end and hydrophilic solubilising groups that can react with biomolecules on the other end (Figure 1.8(d) – (i)). Examples of water-soluble bifunctional molecules used for ligand exchange method include are thiol-containing molecules, oligomeric phosphines, aminated

polymers, dihydrolipoic acid (DHLLA), PEG derivatives and peptides.<sup>83, 84</sup> QDs generated with this method are useful for biological environment, however ligand exchange is usually associated with decreased QY and a tendency to aggregate and precipitate in biological buffers.

#### 1.1.4.3.2. *Addition of Secondary Hydrophilic Shell*

Problems associated with replacement of the hydrophobic surfactants from organic QDs can be alleviated by keeping the hydrophobic ligands on the surface, and forming a secondary water-soluble shell that allows phase transfer from organic to aqueous (Figure 1.8(a) – (c)). The second shell may be fabricated through formation of a micelle-like surrounding the organic layer of QDs, encapsulation into an additional inorganic (e.g., SiO<sub>2</sub>) shell or formation of a water-soluble polymeric coating. Examples of molecules used for QDs encapsulation are phospholipid micelles, polymer beads, polymer shells and silica shells and amphiphilic copolymers such as cyclodextrins.<sup>83, 85</sup> QDs transferred to the aqueous phase via these methods usually retain high QY of luminescence. However, although encapsulation in a silicate or polymer-phospholipid shell ensures stability in a wide range of pH values, it leads to a substantial increase QD size, which adversely affects intracellular mobility and fluorescent studies based on resonance energy transfer. For example, CdSe/ZnS QDs have been reported to experience increases in diameter from 4 – 8 nm to 20 – 30 nm after phospholipid and block-copolymer shell encapsulation.<sup>3</sup> Additionally, some methods of hydrophilic encapsulation such as silinisation are complicated and cannot be done on a large scale as coating with silica shells must be carried out in dilute conditions.

#### 1.1.4.4. **Aqueous Synthesis of Quantum Dots**

In most cases, water-soluble QDs may be prepared via synthesis in aqueous solutions of thiol-substituted compounds. A number of water-soluble thiol-capped CdTe QDs have been prepared and studied. The general procedure involves the dissolution of a cadmium salt in water and the addition of a thiol-substituted capping ligands such as mercaptoacetic acid,<sup>86, 87</sup> mercaptopropionic acid,<sup>88</sup> dihydrolipoic acid,<sup>89</sup> cysteine,<sup>90</sup> 2-mercaptoethanol and 1-thioglycerol<sup>91, 92</sup> is added to the solution under vigorous stirring. NaOH is added to adjust the pH of the mixture to that suitable for the selected capping agent then oxygen is evacuated by bubbling inert gas through the mixture. Subsequently, NaHTe solution or H<sub>2</sub>Te gas is added to the reaction then refluxed to obtain water-soluble CdTe QDs.<sup>93</sup> Though improvement of QD

properties can be achieved by additional procedures such as prolonged refluxing and UV irradiation, water-soluble QDs produced in this fashion are usually characterized by a broad size distributions and very low QY.<sup>85</sup> Additionally, synthesis of QDs in aqueous media usually occurs slowly, sometimes taking days. The hydrothermal method and microwave irradiation have emerged as techniques to develop fast, controlled synthesis of high quality QDs.<sup>94, 95</sup>

#### **1.1.4.5. Hydrothermal Synthesis**

Hydrothermal synthesis involves the heating of QD precursors in an autoclave at temperatures up to 200°C over a few hours under high pressure. This method has been used to prepare CdS, ZnS and CdSe QDs with narrow size distribution, high photostability and good QY.<sup>96-98</sup>

#### **1.1.4.6. Microwave Synthesis**

Microwave irradiation accelerates the synthesis of water-soluble QDs as a result of extremely fast and uniform heating of the reaction mixture. For example, CdTe QDs emitting at ~730 nm were prepared by microwave irradiating (300 W) the CdTe precursor in a closed vessel for only 45mins at 160 °C, a process would have taken 2-3 days with conventional aqueous synthesis methods.<sup>99</sup> The microwave assisted synthesis method tends to result in higher fluorescence QYs than the hydrothermal method however weak luminescence is often observed with CdTe QDs. It can be used to prepare water-soluble core QDs such as CdTe, ZnSe, CdS and CdSe,<sup>100-103</sup> alloyed QDs,<sup>88, 104</sup> as well as core/shell QDs.<sup>105-107</sup> The microwave assisted synthesis method is also suitable for fabricating hydrophobic QDs in non-polar solvents<sup>14, 108-110</sup> and even for the synthesis of ZnSe QDs solvent-free.<sup>111</sup>

Despite advances in aqueous QD synthesis, QDs prepared by organic synthesis and capping followed by surface modification is still favoured as this procedure produces QDs with comparably narrower size distributions and higher fluorescence efficiencies.

#### **1.1.4.7. Molecular Seeding**

The above synthesis methods work well for small scale QD fabrication however batch to batch reproducibility remains a problem.<sup>112</sup> Additionally, with increasing reaction scales, control of particle sizes becomes challenging leading to wider size distributions. To make QDs useful for lighting and display applications, synthetic routes must be able to reproducibly yield pure, high-quality, monodispersed crystalline QDs. These synthetic methods must be scalable. Larger

scale synthesis using a hybrid flow reactor has also been described with a typical solution flow of  $1 \text{ mL min}^{-1}$ , though the reaction yield is not reported.<sup>113</sup> The “molecular seeding method”, illustrated in Figure 1.9, has recently been used to deliver kilogram-scale quantities of red and green QDs.<sup>114-116</sup> In this scalable method, individual molecules of a cluster compound act as “seeds” or nucleation points upon which NP growth can be initiated. Because suitable nucleation sites are already provided in the system by the molecular clusters, the need for a high temperature nucleation step to initiate NP growth is eliminated. Particle growth is maintained by the periodic addition of further precursors, facilitated by incremental temperature changes, providing high control over the emission wavelength and affording substantially monodisperse NPs.

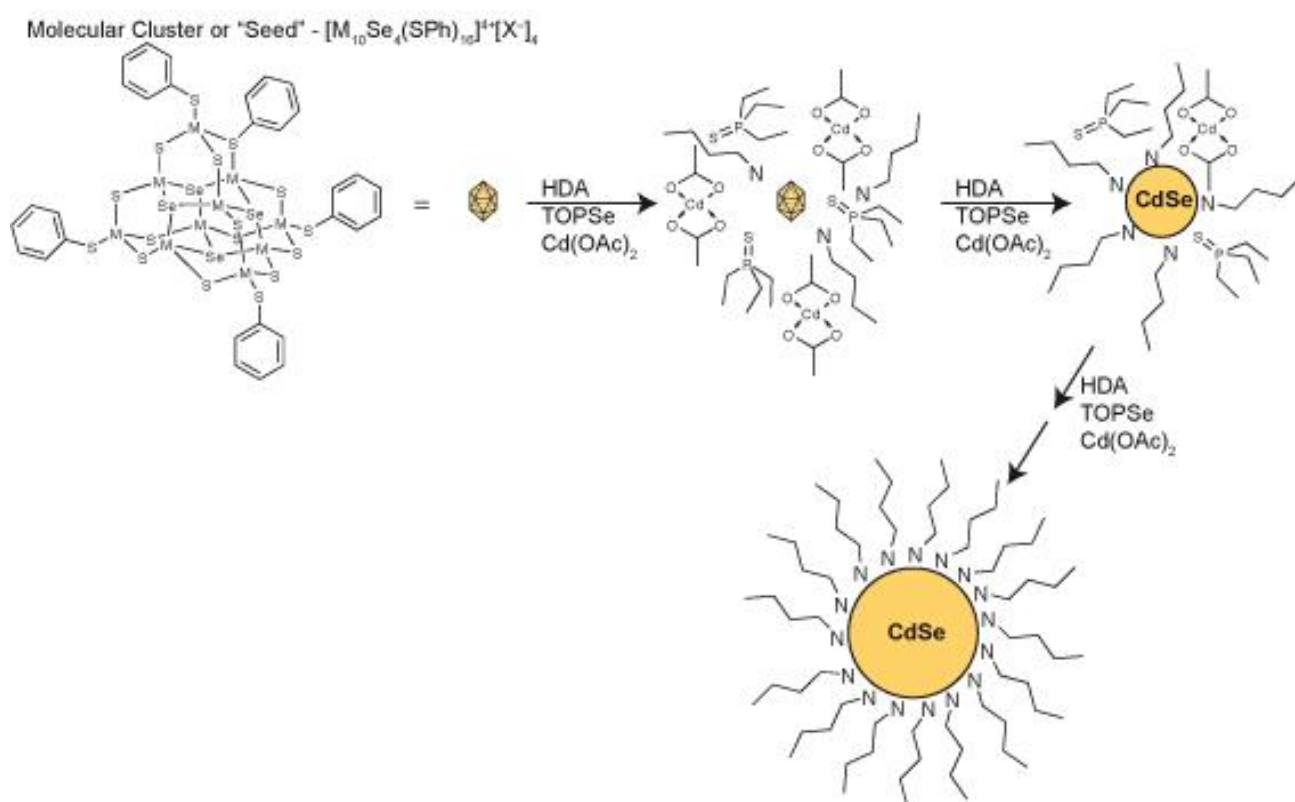


Figure 1.9 Molecular seeding synthesis of a cadmium selenide quantum dot using  $[M_{10}Se_4(SPh)_{16}][X]_4$  ( $X = Li^+$  or  $(CH_3)_3NH^+$ ) as the molecular seed and dropwise addition of cadmium acetate ( $Cd(OAc)_2$ ) and tri-*n*-octylphosphine selenide (TOP-Se) as the cadmium and selenium element-source precursors, with hexadecylamine (HDA) used as the capping agent. Reproduced from O'Brien *et al.* Preparation of Nanoparticle Materials, 2011.<sup>116</sup>

## 1.1.5. Optical and Electronic Applications of Quantum Dots

### 1.1.5.1. Displays

On account of their ability to achieve high photoluminescence QY, the tunability of the maximum emission wavelength, narrow emission linewidth and simple device configuration, QDs are becoming an increasingly important component in the display industry, especially in liquid crystal displays (LCDs) with light-emitting diode (LED) backlights. This is particularly apparent in large size, high-end televisions, where wide colour gamut (the entire range of colours available on a particular device) and features such as high dynamic range (HDR, the contrast between the brightest whites and the darkest blacks) are of great importance. In practice, QDs are deployed in a component in the display system such as LCDs, using a backlighting unit (BLU) consisting of blue LEDs which excite green and red colloidal QD nanoparticles, generating a white light with three well separated Red, Green and Blue (RGB) peaks. Therefore, three highly saturated primary colours can be obtained, leading to superior image quality<sup>117, 118</sup>

There are 3 device configurations commonly used in QD display applications: “on-chip”, “on-edge” and “on-surface”. (Figure 1.10)

*On-Chip Geometry:* The on-chip component is composed of a standard blue LED with the rare-earth-doped down conversion phosphor replaced by QDs (Figure 1.10a). This configuration can be adopted in current backlighting units without modification and is advantageous due to its design simplicity and low cost (least QD material used here). However, due to close proximity to blue LED, QDs experience high flux and temperature, adversely impacting the stability and lifetime of QDs. Also issue relating moisture in this configuration poses problems. As a result, this configuration has not been adopted in commercial products.<sup>119</sup>

*On-Edge Geometry:* In an on-edge configuration, the QDs are dispersed in an encapsulating resin and then loaded into a glass or transparent plastic tube and cured. The tube component is then inserted in front of the edge-lighting LED BLU (Figure 1.10b). The rest of device remains mostly the same but in improve the colour gamut, the colour filters and the wavelength of the blue LED are adjusted. Lifetime and stability are much improved because the QDs are located further away from the blue LED. However, to protect against effects from the blue flux,

quite stable materials and packaging are required. Also, the distance of the QDs from the blue LED impacts efficiency and colour uniformity, while the position of the edge optic on the sides of the display limit its applicability across the display market. This design provides a suitable alternative for on-chip geometry and a lower cost than on-surface, especially for large-screen TVs and has been commercially produced by Hisense and Philips as a result.<sup>117, 120, 121</sup>

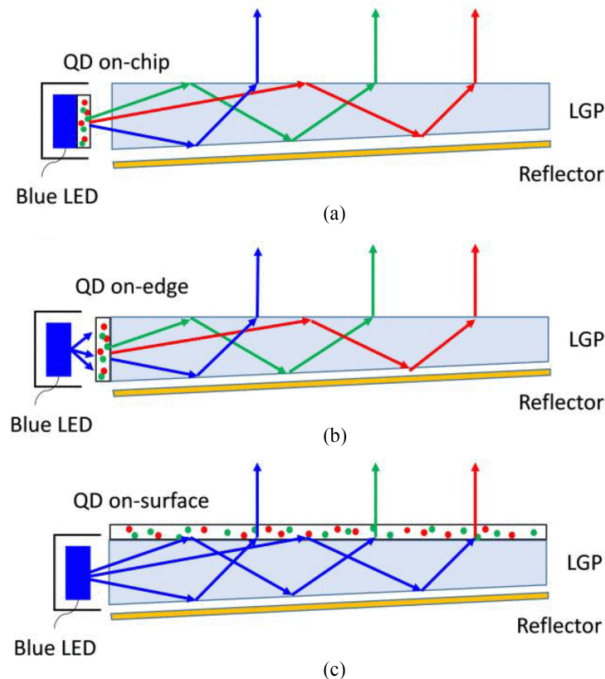


Figure 1.10 Schematic illustration of three different device geometries in QD-based displays. (a) on-chip: QDs are placed within an LED package. (b) on-edge: QDs are placed between LED and light guide plate. (c) on-surface: QDs are embedded in a film and placed on the top surface of light guide plate. (LGP: light guide plate, red dots: red-emitting QDs; green dots: green-emitting QDs). Reproduced with permission from Haiwei *et al.*, IEEE Journal of Selected Topics in Quantum Electronics, 2017.<sup>119</sup> Copyright © 2017, IEEE.

*On-Surface Geometry*: This is the most commonly used geometry. Here, QDs are dispersed in a curable resin and sandwiched between two barrier films that add extra protection against water and oxygen (Figure 1.10c). As a result, the resultant operating temperature should be close to the room temperature. Both reliability and long-term stability are enhanced significantly. The QD film replaces the diffuser sheet in traditional LCD modules. One drawback of QDs on surface geometry is the massive material consumption, especially for

large screen TVs. A QD surface may contain trillions of red and green-emitting QDs, increasing costs.<sup>119, 122</sup>

Several display manufacturers (e.g. Samsung, LG, Sony, Philips, etc.) have been adopted this promising technology with Cd-based QDs such as CdSe/CdS, CdSe/ZnCdSe/ZnS, or CdSe/ZnCdS being the preferred materials for their narrow emission spectra and high QY. 90% of the colour gamut recommended by the International Telecommunications Union (ITU), known as Rec. 2020, has been realised by Cd-based QDs with commercially available colour filters.<sup>117, 123, 124</sup> However, there are regulatory issues that complicate using Cd in QDs for display applications. For example, the Restriction of Hazardous Substances (RoHS) directive, issued by the European Union, limits the cadmium content is limited to 100 ppm in any consumer electronic product.<sup>125</sup> This has led to increasing demand to eliminate cadmium and other restricted toxic heavy metals from consumer products. Some companies are moving toward including InP-based QDs such as InP/ZnSe or InP/ZnSeS/ZnS as a replacement for CdSe-based QDs in their products. Compared to CdSe, InP QDs has a smaller bandgap thus experience stronger quantum confinement effects and emission is more susceptible to particle size variation, resulting in broader FWHMs (> 40 nm), corresponding to 70 – 80% Rec. 2020 colour gamut, depending on the colour filters employed (Figure 1.11).<sup>67</sup>

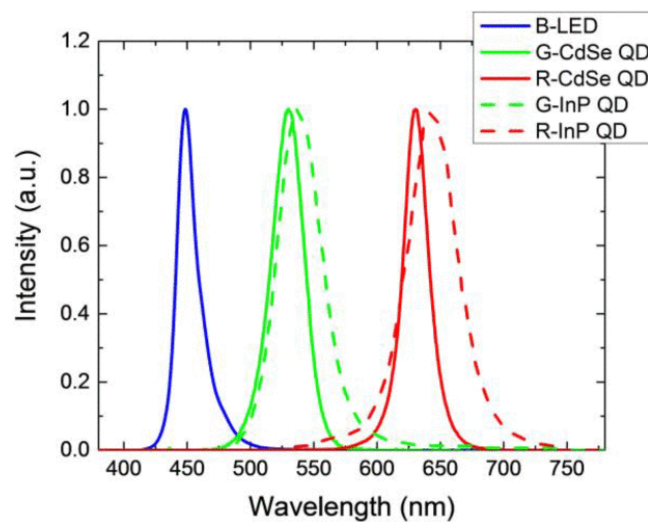


Figure 1.11 Typical emission spectra for green and red quantum dots using CdSe (solid line) and InP (dashed line). Blue LED with emission peak  $\lambda = 450$  nm is also displayed. Reproduced with permission from Haiwei *et al.*, IEEE Journal of Selected Topics in Quantum Electronics, 2017. <sup>119</sup> Copyright © 2017, IEEE.

### 1.1.5.2. Solid State Lighting

OLED technology, the current-state of the art, suffers from lacking cheap patterning methods for various colour pixels. OLEDs are made from small organic molecules and deteriorate in the solvent required for classic patterning techniques, making them expensive. In addition, typically OLEDs are characterised by a doublet with a broad long wavelength tail extending more than 100 nm, limiting the available colour gamut. This means vivid colours from OLED displays generally come at a cost – either power loss or manufacturing and performance.<sup>122,</sup>

<sup>126</sup> Quantum dot-based light emitting diodes (QLEDs) show potential to overcome these drawbacks.

The first QLEDs were developed by Alivisatos and his colleagues in 1994 and consisted of a common bilayer structure including an indium tin oxide (ITO) anode, plain CdSe QDs, a p-paraphenylene vinylene (PPV) layer, and Mg cathode. These devices emitted up to 100 cd/m<sup>2</sup> and operated up to 50 mA/cm<sup>2</sup> however showed an external quantum efficiency (EQE) of only 0.001 – 0.01%.<sup>127</sup> In 1995, Dabbousi *et al.* similarly reported a QLED where a single layer of CdSe QDs were incorporated into polyvinylcarbazole (PVK), a photostable hole conducting polymer and an oxadiazole derivative, an electron transport species, sandwiched between ITO and Al electrodes. This device exhibited a very small EQE value of ~0.0005%.<sup>128</sup> The performance achieved by these QLEDs despite the device simplicity and suboptimal QLED synthesis procedures encouraged research and since the first reports, QLEDs have increased in efficiency to levels comparable with commercial organic light emitting diodes (OLEDs). This is because of improvement in both the synthesis, understanding of photophysics, and device structures used for these devices. For instance, Yang and coworkers demonstrated a full range of blue, green, and red QLEDs exhibiting EQEs above 10% with low turn-on voltages, saturated pure colours and the reported lifetimes greater than 90,000 and 300,000 h, for the green and red devices respectively.<sup>129</sup> Also, using core/shell QDs and multilayer QLED structures, Manders *et al.* were first to achieve > 20% EQE for green QLEDs (21%) and 11.2% EQE for blue QLEDs, with impressive lifetimes of greater than 280,000h at luminance of 100 cd/m<sup>2</sup>. For green QLEDs, the EQE was equal to that of vacuum-deposited red and green OLEDs operated in AMOLED display technology which is commercially available.<sup>130</sup> Again, using tandem QLED structures where two or more electroluminescent units are serially connected via a transparent interconnecting layer (ICL), even higher EQEs were achieved in 2018. Zhang and colleagues reported full colour (red/green/blue) tandem QLEDs with

extremely high EQEs: 21.4% for blue QLEDs, 27.6% for green QLEDs and 23.1% for red QLEDs, the highest values ever reported.<sup>131</sup>

These QLED devices have application mainly in displays (particularly flexible and wearable displays) as well as areas such as phototherapy to treat various medical conditions including psoriasis, acne vulgaris, eczema, skin cancer, wound healing, neonatal jaundice, circadian rhythm disorders, and tumours.<sup>132, 133</sup> QLED low cost, high efficiency, flexibility and capacity to be a light source spread over a large area, they find application in agriculture and horticulture where QDs can be tailored to fabricate QLEDs that do not emit green light where chlorophyll does not absorb light. For instance, in 2013, Pickett *et al.* reported the use of LEDs as a primary light source with secondary source consisting of one or more QD component. This QLED system was used to optimise plant growth and it was reported that the value of the energy efficiency of QLEDs used in this case ranged from 30–70 lm/W, in contrast to 10–18 lm/W for incandescent bulbs and 35–60 lm/W for fluorescent lamps.<sup>134</sup>

#### 1.1.5.3. Energy Storage

The idea of a wide band gap semiconductor being sensitised with a narrow band gap semiconductor to harvest sunlight and to generate charge carriers, can be dated back to the 1960s.<sup>135</sup> Attractive properties of QDs such as excellent photo, thermal and moisture stability, high absorption coefficient and possibility of multiple exciton generation has motivated the investigation of quantum dot-sensitised solar cells (QDSCs), replacing organic dyes.<sup>136</sup> Usually, a QDSC consists of a QD-sensitised photoanode, an electrolyte, and a counter electrode and upon light irradiation: (i) the QDs absorb solar energy, exciting electrons in the valence band (VB) to the conduction band (CB) to generate electron–hole pairs at the interface of the metal oxide and the QDs. (ii) Electrons in the CB of the QDs are quickly injected into the CB of the metal oxide (generally TiO<sub>2</sub>) electron acceptor under the driving force of the energetic difference in the CB between the QDs and metal oxide, and at the same time, the holes oxidise the electrolyte. (iii) The electrons transfer through the TiO<sub>2</sub> mesoporous film to the fluoride-doped tin oxide (FTO) and then to the counter electrode (CE) through an external circuit. (iv) Meanwhile, the oxidized QDs are regenerated by reduced species of the redox couple in the electrolyte, while the oxidized species of the redox couple are reduced by the electrons from the external circuit under the catalysis of CE (Figure 1.12).<sup>137</sup>

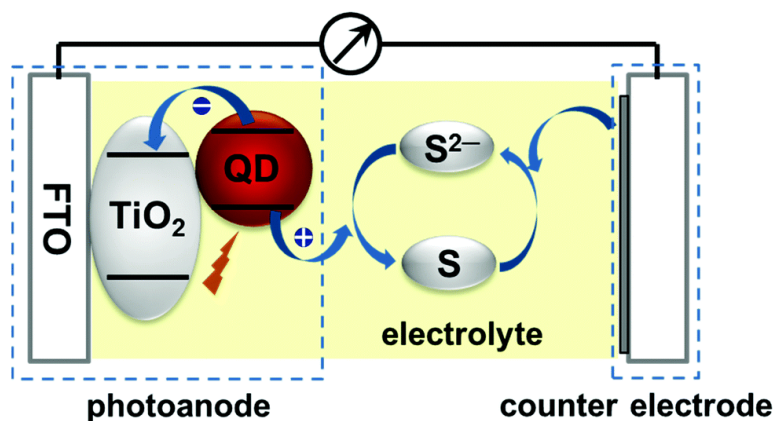


Figure 1.12 Schematic representation and QDSSCs, comprising a photoanode, QD (sensitizer), electrolyte containing a redox couple, and a counter electrode. Reproduced with permission from Pan *et al.*, Chem. Soc. Rev. 2018. <sup>137</sup>

Over the decade, the power conversion efficiency (PCE) of QDSSCs has shown a significant improvement from less than 1% to ~13%. Notably, Zhong and coworkers investigated an alloyed Zn–Cu–In–Se (ZCISe) QD sensitizer characterised by a narrow band gap and high conduction band edge simultaneously, achieving an impressive PCE of 11.61% when combined with a Ti-mesh-supported mesoporous-carbon counter electrode.<sup>138</sup> The same group improved on the efficiency of ZCISe QD-based solar cells by using Cu-deficient ZCISe QDs (Cu/In molar ratio = 0.7) to achieve a PCE of 12.57%.<sup>139</sup>

## 1.1.6. Biomedical Applications

### 1.1.6.1. Imaging

The photoluminescence of QDs is very bright and stable, making them potential candidates for biomedical imaging and therapeutic interventions. QDs conjugated with cancer specific ligands/antibodies/peptides were found to be effective for detecting and imaging human cancer cells. Gao and coworkers conjugated PEG-encapsulated CdSe/ZnS QDs to a prostate-specific membrane antigen (PSMA) antibody for in vivo targeting and imaging cancer cells. It was found that the QDs-antibody conjugates were efficiently and uniformly distributed in prostate tumours due to the specific binding between PSMA antigen in prostate cancer cells and PSMA antibody on QDs. Intense signals for QD-PSMA antibody conjugate probe were observed, with little or no interference from the mouse autofluorescence (Figure 1.13).<sup>140</sup> Cadmium-free biocompatible QDs with good PL QY were recently evaluated for their capability for lymph node mapping with the aid of an ex vivo imaging model. Subcutaneous injection of PEG-encapsulated, ZnS-shelled indium-based QDs into the paw of rats showed a strong retention confined to the regional lymph, fast localisation within minutes and stable photoluminescence. Moreover, the lack of any Class A elements (Cd, Hg and Pb) in their structure makes suitable candidates for future biomedical applications. The biocompatibility of cadmium-free QDs was evaluated and after 24 h incubation of both human breast cancer cells and human ovarian cancer cells with the NPs, negligible changes were recorded in QD-treated cells compared to untreated control cells.<sup>141</sup>

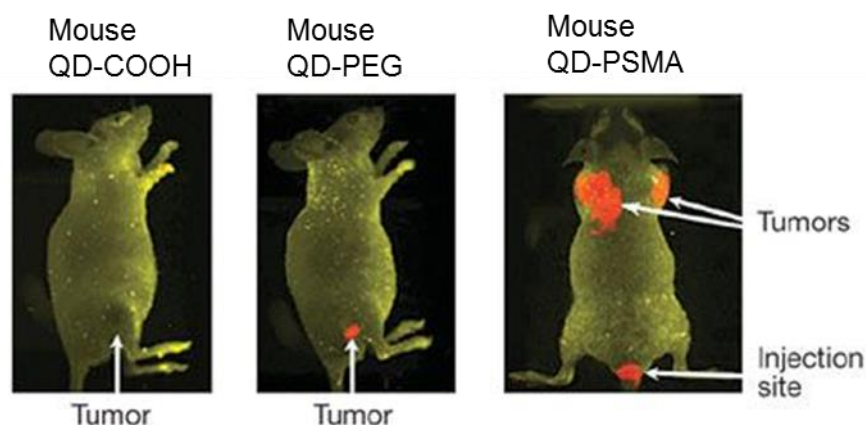


Figure 1.13 Spectrally resolved in vivo fluorescence images of live mouse models bearing human prostate tumours of similar sizes (0.5 – 1.0 cm in diameter) using QD probes with three different surface modifications: carboxylic acid groups (left), PEG groups (middle) and PEG-PSMA antibody conjugates (right). The site of QD injection was observed as a red spot on the mouse tail. Reproduced with permission from Xiaohu *et al.*, Nat Biotechnol 2004.<sup>140</sup>

QDs that emit in the near infrared region (NIR, 650–2000 nm), thus allowing for deeper penetration of photons from the excitation source and greater escape depths for the QD emission signal, have been successfully used in imaging. For example, Ag<sub>2</sub>Se QDs emitting at a peak wavelength of 1300 nm were functionalised with amphiphilic C18-PMH-PEG to obtain a stable aqueous dispersion with high photoluminescence, good photostability and a hydrodynamic diameter of ~43 nm. The imaging performance of Ag<sub>2</sub>Se QDs was compared to indocyanine green (ICG), an NIR fluorescent dye. A dose of 37 mg/kg ICG provided a weak signal and fuzzy images of the vasculature due to scattering and absorbance by tissues. On the other hand, in vivo administration of C18-PMH-PEG-Ag<sub>2</sub>Se QDs at a dose of 6 mg/kg produced clear, high spatial resolution imaging of the liver, spleen, and vasculature, under 808 nm laser excitation, within a few minutes following injection.<sup>142</sup>

#### 1.1.6.2. Drug Delivery

QDs are good candidates as theranostic platforms, as they can act as the main nanocarrier or be part of a more complex architecture as the fluorescent labels. Nanocrystals loaded with drug formulations can provide advantages such as targeted delivery, improved uptake by cells, and long circulation lifetime enhancing the therapeutic potential of the loaded drugs and contribute to specific targeted therapy. Cai *et al.* synthesised ultrasmall QDs (~3 nm) functionalized with poly(ethylene glycol) (PEG) and hyaluronic acid to target glycoprotein CD44 (transmembrane glycoprotein and a common marker overexpressed in many tumours including lung cancer and cervical cancer) in cancer cells and Doxorubicin (DOX, a chemotherapy drug) was loaded on to the pH-responsive ZnO QDs (Figure 1.14) . This drug delivery platform for intracellular controlled release of drugs could release its DOX payload under the acidic intracellular conditions and upon payload release, ZnO QDs alone showed anti-tumour activity, significantly enhancing apoptosis of cancer cells.<sup>143</sup> Yang and company loaded quercetin (QE) onto CdSe/ZnS QDs as anticancer and antibacterial nano drug delivery systems and showed that QE-loaded CdSe/ZnS QDs were more effective against drug-resistant *Escherichia coli* and *Bacillus subtilis* and then QE or CdSe QDs alone. The anticancer activity assay was focused on the proliferation and migration of gastric carcinoma (BGC-823) cells, which showed an increase in cytotoxicity of two- to sixfold compared to QE and CdSe QDs alone.<sup>144</sup>

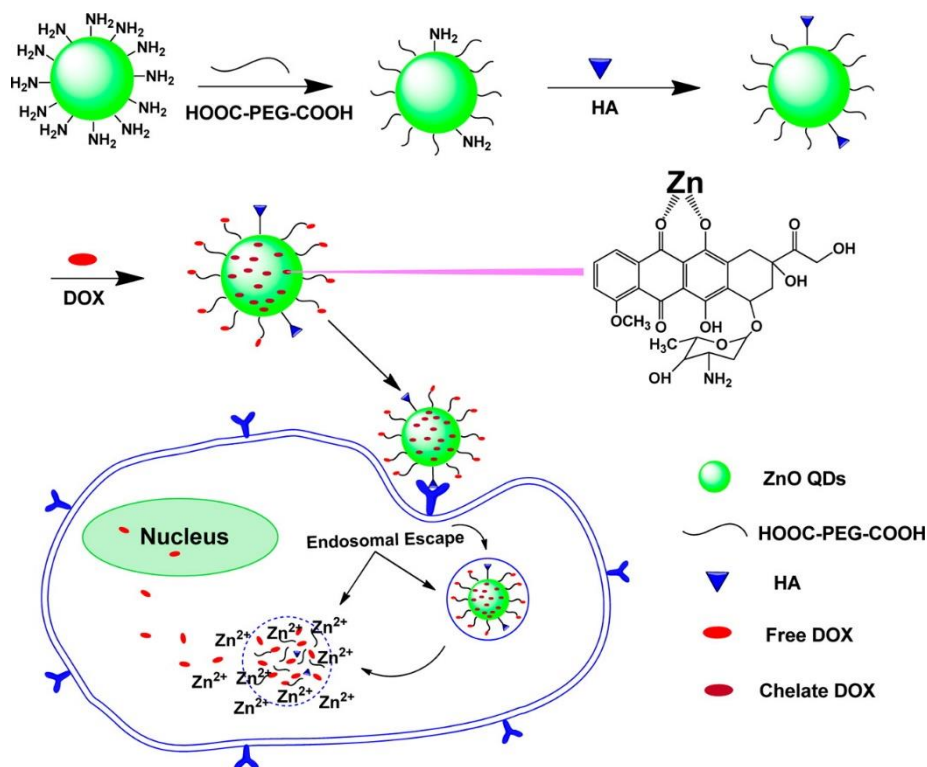


Figure 1.14 Schematic of doxorubicin-loaded hyaluronic acid PEG-encapsulated ZnO quantum dots (HA-ZnO-PEG) drug delivery system and mechanism of action. Reproduced with permission from Cai, *et al.*, ACS Appl Mater Inter 2016. <sup>143</sup> Copyright © 2016, American Chemical Society

### 1.1.6.3. Sensors

High surface to volume ratio of QDs make the surfaces of QDs highly sensitive. This combined with their photostability make QDs attractive in sensing applications. QDs can also effectively detect metal ions (such as Hg, Pb, Cu ions), drugs, organic pollutants and small biological molecules. Microwave-synthesised water-soluble AgInS<sub>2</sub>/ZnS QDs were used to determine intracellular copper(II) levels. Briefly, HeLa cells were incubated with AgInS<sub>2</sub>/ZnS QDs, and then Cu(NO<sub>3</sub>)<sub>2</sub> was used to manipulate the intracellular copper(II) level. Compared to 17 other cations, AgInS<sub>2</sub>/ZnS QDs showed a high selectivity for Cu<sup>2+</sup> ions due to strong binding of Cu<sup>2+</sup> onto the QD surface, displacing Zn<sup>2+</sup> and subsequently forming a CuS shell which quenched the QD fluorescence.<sup>145</sup> CuInS<sub>2</sub> QDs functionalised with 3-aminophenylboronic acid was used as PL probes for the detection of benzene-based organic compounds by Liu *et al.* The bioconjugated CuInS<sub>2</sub> QDs emitted in the NIR (736 nm) and the functionalised CuInS<sub>2</sub> QDs containing boronic acid functional groups were reactive toward vicinal diols, forming five- or six-member cyclic esters in an alkaline buffer which lead to photoluminescence quenching.

The authors suggested the use of the QD probes as detectors of compounds such as dopamine, catechol and gallate and were able to detect dopamine in human serum sample to levels lower than the detection limit needed in physiological conditions.<sup>146</sup>

### 1.1.7. Toxicity of Quantum Dots

QD toxicity depends on multiple factors such as chemical composition, size, concentration, charge, redox activity, surface coatings, as illustrated in Figure 1.15. These parameters and others must all be considered for toxicological assessment. The desired application of synthesized QDs will determine toxicity levels, for instance, limits of toxicity will vary greatly for QDs for antimicrobial surfaces compared to QDs intravenously injected for drug delivery applications. In addition, due to the diversity of QDs being synthesised, comparison and discussion of QD toxicity is difficult. The following is a discussion of a few of the factors affecting QD toxicity.

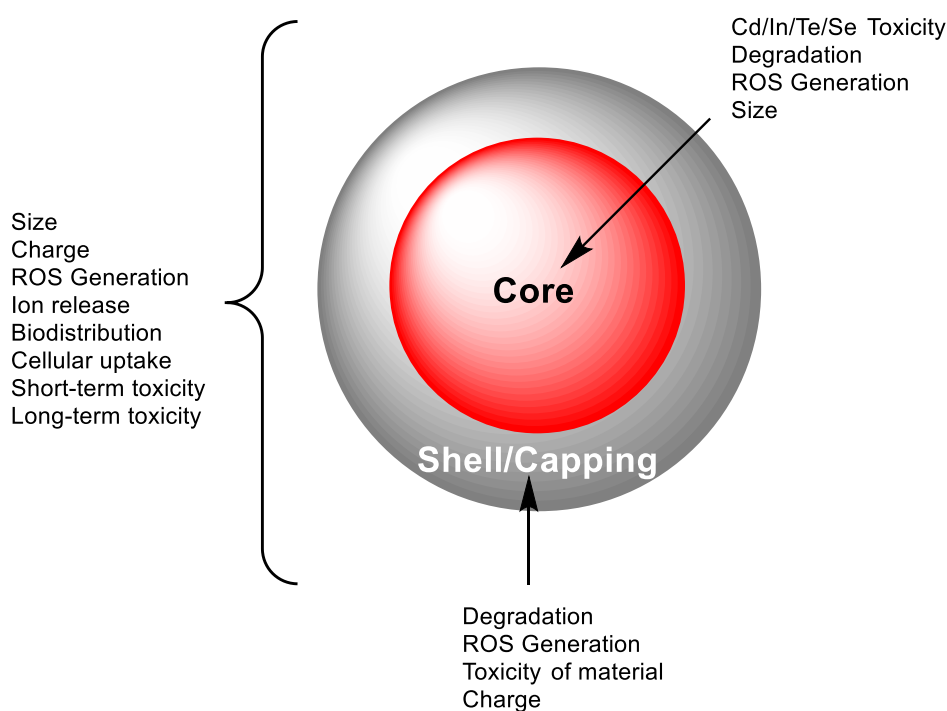


Figure 1.15 Factors affecting QD toxicity with respect to the QD core, QD shell/capping agents and the QD nanoparticle as a whole.

### 1.1.7.1. Type and Composition

In the literature, discussions relating to potential toxic effects of nanomaterials often point to the fact that in their bulk forms, many of these nanomaterials are non-toxic and have been extensively used for many years e.g. gold NPs, silver NPs and carbon nanotubes. However, in the case of QDs, the situation is compounded by the knowledge that the bulk forms of some of the constituent molecules of QDs – such as cadmium, selenium, and tellurium – are highly toxic themselves. Whether these substances are toxic on the nanoscale, in the form of quantum dots, has been discussed in several reports.<sup>147</sup> Primarily, toxicity of uncoated QDs such as CdTe and CdSe has been related to the presence of free cadmium ions in the particle suspension or the potential to degrade *in vivo*, thus releasing cadmium, selenide or other toxic metals. For instance, using primary hepatocytes as a liver model, Derfus *et al.* found that CdSe core QDs were acutely toxic due to the liberation of Cd<sup>2+</sup> ions from the CdSe lattice upon surface oxidation. Free Cd<sup>2+</sup> concentration was reported to range from 6 ppm for non-toxic CdSe (non-oxidised) to as much as 126 ppm for toxic CdSe (air-oxidised) QDs, the latter within the range of Cd<sup>2+</sup> levels known to lead to significant cell death.<sup>36</sup> Studies by Lovric *et al.* found that unmodified CdTe QDs caused apoptotic-like cell death in rat pheochromocytoma cells and induced damage to the plasma membrane, mitochondrion, and nucleus of human breast cancer (MCF-7) cells and at a concentration of 10 µg/ml. The cytotoxicity observed in these studies was consistent with cadmium toxicity from the QD core.<sup>148, 149</sup> Chen *et al.* demonstrated that Cd<sup>2+</sup> release was a major contributor to the cytotoxicity of CdTe QDs incubated in human embryonic kidney cells at 75 nM and above.<sup>150</sup> Therefore, aqueous uncoated QDs cannot be used directly for biological applications, as long term contact with biological fluids appears to result in partial desorption of the capping layer, exposure of the bare NP surface. The exposed surface can then leach toxic cadmium ions into the surrounding fluid.

In addition, many studies of NP toxicity have focused on the ability of QDs to induce oxidative stress and/or free radical-based cellular damage. Using electron paramagnetic resonance (EPR) spectroscopy and radical-specific fluorimetric assays, Ipe *et al.* measured and identified radical species generated by CdS and CdSe core QDs upon UV irradiation in aqueous solution. CdS were found to generate both hydroxyl and superoxide radicals whereas CdSe QDs exclusively generated hydroxyl radicals.<sup>151</sup> Cho *et. al.* used confocal laser scanning microscopy to image CdTe-treated cells dyed with organelle-specific dyes and determined that the significant lysosomal damage observed with CdTe-treated human breast cancer cells

was attributable not only to the presence of Cd<sup>2+</sup> but also of reactive oxygen species (ROS), which can be formed via Cd<sup>2+</sup> specific cellular pathways and/or via CdTe-triggered photo-activated energy transfer or electron transfer from excited QDs to oxygen.<sup>38</sup> While the free-radical generation is advantageous in photodynamic cancer and antimicrobial applications of QDs, the risk they may pose to healthy tissue must be considered when assessing QD toxicity.

The high toxicity of cadmium as well as selenium and telluride has led to the generation of cadmium-free QDs. The least toxic cadmium-free semiconductors include GaAs, InP, InAs and InSb. Indium phosphide is similar in physicochemical properties to cadmium selenide, thus being the best candidate for replacing CdSe but without intrinsic toxicity since InP has neither Class A elements (Cd and Hg), nor Class B elements (As and Se).<sup>70</sup> Beside being free of such elements, InP QDs have a rather low toxicity, even without an additional ZnS shell, due to the greater degree of covalent bonding. Compared to CdSe, stronger covalent bonding increases the photo-stability of InP QDs and decreases their toxicity by reducing degradation when they are used in active biological media. Brunettei *et al.* compared water soluble core/shell CdSe/ZnS and InP/ZnS QDs with similar physical and chemical properties, except the nature of the core and found InP/ZnS QDs were significantly safer alternatives to CdSe/ZnS QDs. CdSe/ZnS QDs were observed to induce cell membrane damage, oxidative stress in the cells, genetic material damage and interference with Ca<sup>2+</sup> homeostasis. All these effects were mainly ascribed to the presence of Cd<sup>2+</sup> which leached from the core despite a two-layer ZnS shell. On the other hand, though an almost identical amount of In<sup>3+</sup> ions is observed to leach from the core of InP/ZnS QDs, very low toxicity was observed, confirmed by the data on five different cell lines. In the neuronal cell line, a 46% decrease in cell viability was observed after 48h from CdSe/ZnS QDs. At the same concentration, InP/ZnS QDs showed a statistically insignificant drop in viability of <5%.<sup>152</sup> In spite of the low toxicity of the components composing InP QDs for cell cultures, they exhibit significant phototoxic action, by generating ROS via the interaction of excited electrons and holes with water and molecular oxygen.<sup>153</sup>

#### 1.1.7.2. Surface Modifications

To overcome the challenges of cadmium/selenium/telluride toxicity, QDs may be encapsulated in various coatings. Chen *et al.* compared core CdTe QDs with core-shell-shell CdTe/CdS/ZnS QDs. Intracellular Cd<sup>2+</sup> concentrations of CdTe QDs were 10-fold higher than that of CdTe/CdS/ZnS QDs at equal NP concentrations because the growth of the CdS layer

together with the ZnS shell reduced the release of Cd<sup>2+</sup> ions. This was evidenced by the near non-toxicity of the CdTe/CdS/ZnS core-shell-shell structured QDs to human embryonic kidney cells (HEK293T) and human erythroleukemia cells (K562) even at high concentrations and long exposure times whereas CdTe QDs were highly toxic.<sup>154</sup> Peng *et al.* saw that for four CdSe/ZnS QDs encapsulated within the same amphipathic polymer of poly(acrylic acid) and polyethylene glycol (PEG) coating, no obvious toxicity was observed within the tested concentration range (10-100 nM), due to the protection of the ZnS shell and the PEG coating, reducing the release of Cd and Se ions as well as preventing oxidative stress to HepG2 cells.<sup>155</sup> Chang *et al.* observed that bare CdSe/CdS QDs were more toxic to MCF-7 cells than PEG-coated CdSe/CdS QDs, due to the greater intracellular uptake of QDs via endocytosis.<sup>156</sup> The type of ligands employed in capping QDs also plays an important role in cytotoxicity. For example, a study of CdSe/ZnS QDs with different coatings in human neonatal epidermal keratinocytes (HEK) cells revealed that 20 nM QDs coated with carboxylic acid resulted in a significant loss of cell viability by 24 h, however QDs coated with PEG in the same concentration had no effect on the cell viability.<sup>157</sup> Another study revealed that the cytotoxicity of silk fibroin coated CdSe QDs was lower than the thioglycolic acid coated ones in human pancreatic carcinoma (PANC-1) cells.<sup>158</sup> Again in PANC-1 cells, cysteamine-capped CdTe (Cys-CdTe) QDs had better cellular metabolizability and lower cytotoxicity than mercaptopropionic acid capped CdTe (MPA-CdTe) QDs.<sup>159</sup>

Furthermore, in some cases, the material used to cap or modify QDs may have adverse effects, causing undesirable effects such as thrombosis and off target accumulation by reticuloendothelial cells (primarily macrophages and dendritic cells) in the liver, spleen, and lymph nodes.<sup>160-163</sup>

Surface coatings on InP QDs may reduce the cytotoxicity arising from ROS generation. Chibli *et al.* found that the generation rate of ROS depended on the thickness of a ZnS shell. Using EPR and reporter assays, InP QDs with a single layer of ZnS shell were found to produce superoxide and a small amount of hydroxyl radical under visible illumination. However, by doubling the ZnS shell, the concentration of ROS formed reduced almost 2-fold. This fact was additionally confirmed by the data on the survival of cultures in five cell lines.<sup>153</sup> Lin *et al.* systematically studied the in vivo biodistribution and long term toxicity of InP/ZnS QDs in BALB/c mice. Results indicated that though accumulation of indium element from injected

PEGylated phospholipid encapsulated InP/ZnS QDs still remained at major organs even after 84 days of injection, hematology, blood biochemistry, and histological analysis indicated that there are no acute toxic effects of the QDs-treated mice compared to the ones treated with phosphate buffer saline (PBS) solution.<sup>164</sup> Chen *et al.* compared the cytotoxicity of InP/ZnS QDs with three different surface groups (NH<sub>2</sub>, COOH, OH) in lung cell lines and showed that InP/ZnS-COOH and InP/ZnS-NH<sub>2</sub> QDs were more cytotoxic than InP/ZnS-OH QDs as they were able to enter the cells more easily, likely due to their smaller hydrodynamic size and the functional groups on the surface.<sup>165</sup>

#### 1.1.7.3. Size and Charge

The size of QD nanomaterials is an important factor affecting its toxic. Most studies have shown that the smaller QDs have the greater toxicity. Lovric saw that CdTe QD-induced death in rat cells (PC12), characterised by chromatin condensation and membrane blebbing, was more pronounced with small (2.2 nm) green emitting positively charged QDs than large (5.2 nm) positively charged red emitting QDs.<sup>148</sup> This acute size effect was confirmed in normal human lung cells. Zheng and company studied the effect of CdTe QDs of three different sizes and observed that in normal human bronchial epithelial cells (BEAS-2B), exposure to CdTe QDs < 5 nm in diameter elicited dose-dependent cytotoxicity whereas QDs > 5 nm showed negligible cytotoxicity in BEAS-2B cells.<sup>166</sup> Tang *et al.* studied the toxic effects of CdSe/ZnS QDs on zebrafish liver cells after 24 hours exposure, and the results of the study showed that 3.4 nm CdSe/ZnS QDs (IC<sub>50</sub> = 1327 nM) were more cytotoxic than 4.4 nm CdSe/ZnS QDs (IC<sub>50</sub> = 3164 nM) to zebrafish liver cells. The increase of CdSe/ZnS QDs size by 1 nm resulted in about 2.4-fold reduction in toxicity, suggesting that the smaller QDs resulted in greater toxicity.<sup>167</sup> Peng *et al.* also showed that the smaller QDs were more likely to be ingested by human liver cancer (HepG2) cells, which may be an important reason for the greater toxicity of smaller sized QDs.<sup>168</sup>

QDs that are taken up into cells enter via endocytosis and are removed via exocytosis. The charge of the QDs will affect the number of NPs taken up into cells which in turn, affects cell toxicity. Tan *et al.* found positively charged QDs were more toxic than negatively charged QDs because of increased cellular uptake. The cytotoxicity of PEG-coated cationic QDs was very low because PEG coating reduced the internalization of QDs. This is in agreement with research by Li and company who observed mice intravenously injected with CdSe/ZnS QDs

with three different surface coatings: polydiallyldimethylammonium chloride (PDDA, positive charge), carboxylic acid (CA, negative charge), and PEG (neutral), at a dose of 10 nmol/kg (equivalent to 12.5 mg/kg). In mice treated with CA-CdSe/ZnS QDs or PEG- CdSe/ZnS QDs, no animal death occurred. However, for PDDA- CdSe/ZnS QDs-treated mice, all the mice died within 24 hours post-injection, suggesting that the surface charge of QDs had a profound influence on in vivo toxicity.<sup>169</sup>

## 1.2. PHOTODYNAMIC THERAPY

### 1.2.1. Introduction & History

Photodynamic therapy (PDT), is a clinically approved, minimally invasive, light-activated therapeutic procedure that was accidentally discovered over 100 years ago by medical student Oscar Raab while studying the interaction of fluorescent dyes with infusoria (aquatic microorganisms). Raab found that intense light applied to the dye acridine hydrochloride resulted in rapid destruction of *Paramecia caudatum* algae.<sup>170</sup> Further investigation into this phenomenon by his supervisors, Hermann von Tappeiner and Albert Jesionek, confirmed that the deactivation of bacteria was not a consequence of heat, but rather a light-activated effect, a “photodynamic reaction”.<sup>171, 172</sup> By the early 1900’s, patients were being successfully treated by this process for a wide variety of cancers, particularly of the skin. Despite this early success, PDT did not achieve enough momentum and was neglected for nearly 50 years until studies by Lipson and Schwartz revealed that photosensitizing agents had not only tumour ablation capabilities but also could be used to fluoresce and demarcate tumours.<sup>173, 174</sup> Then in the 1970s, Thomas Dougherty helped to bring PDT to a worldwide audience when he revived interest in PDT while studying porphyrin compounds by creating a commercially available photosensitising drug, known as ‘haematoporphyrin derivative’ (HpD).<sup>175, 176</sup> Subsequent refinement of this compound led to the development of Photofrin, a partially purified form of HpD, with many of the less active components removed.<sup>177</sup> HpD and Photofrin are referred to as first generation photosensitisers (PS) of PDT. Although Photofrin is still the most widely employed PS and still viewed as the “gold standard” for this form of cancer therapy, it suffers from severe deficiencies: chemical impurity, poor tumour selectivity, long lasting skin photosensitivity and relatively low absorbance in the red region.<sup>178</sup>

No single product has yet been found which can be regarded as an ideal PS for PDT, however, several hundred compounds have been developed to surmount the inadequacies of first generation PS, known as second generation PS. The most promising candidates that have been used experimentally and clinically include: 5-aminolevulanic acid (ALA), protoporphyrin IX, chlorin e6, silicon phthalocyanine (Pc4) and the benzoporphyrin derivative (BPD).<sup>178-180</sup>

Since the revival of PDT, much research effort has been gone into the utilisation of PDT in applications related to tumour detection and tumour photodestruction.<sup>175, 181-189</sup> The procedure involves administration of a photosensitising agent followed by irradiation with light at a

wavelength that is effectively absorbed by the PS. In the presence of oxygen, a series of events lead to direct tumour cell death, damage to the microvasculature and induction of immune response and inflammatory reaction.<sup>179</sup> Most of the PS used in the treatment of cancerous and non-cancerous diseases are based on a tetrapyrrole structure, for example, Photofrin, chlorophyll-based chlorins and bacteriochlorins (Figure 1.16). Examples of non-tetrapyrrole based PS include Rose Bengal, methylene blue (MB), toluidine blue O (TBO) and crystal violet (CV) (Figure 1.17).

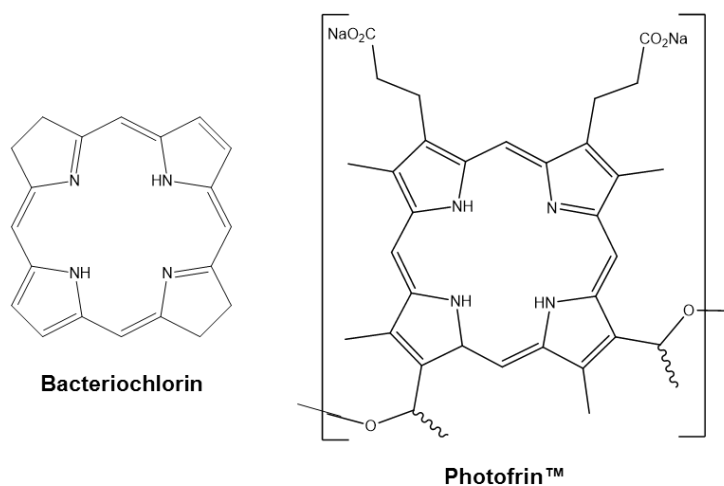


Figure 1.16 Examples of tetrapyrrole photosensitisers used in PDT.

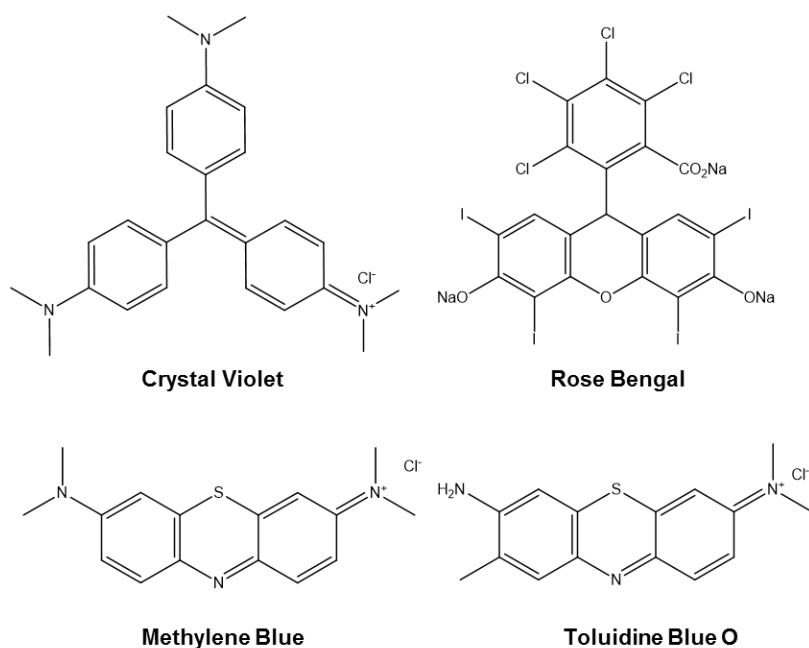


Figure 1.17 Examples of non-tetrapyrrole photosensitisers used in PDT.

In addition to cancer therapy, PDT is also powerful for use in antimicrobial applications, often referred to as antimicrobial photodynamic therapy (aPDT). In the 1960's, the lethal effects of photosensitising dyes were demonstrated in a wide variety of microorganisms. For example, Macmillan *et al.* showed rapid killing of several species of bacteria, algae, and yeast in aerobically irradiated TBO aqueous solutions. It was observed that 99% of bacteria were killed within 30 min of irradiation with 21–30 mW of light at 632 nm from a continuous-wave gas laser.<sup>190</sup> Other dyes such as neutral red, CV, MB, rose Bengal, eosine Y, acridine orange, and rhodamine 6G were also shown to be effective against bacteria.<sup>191, 192</sup> For several years, progress in aPDT was impeded by the discovery of antibiotics but with the emergence of antibiotic resistance, there has been a recent resurgence of research into new antimicrobial strategies based on aPDT.<sup>193</sup>

Key benefits of research and applications mediated by aPDT include:

- A)** Low toxicity of PS in the absence of light activation
- B)** Variety of administration routes (directly through topical application, intravenous application, etc. or indirectly through incorporation of PS into devices and surface coatings)
- C)** The mechanistic pathways of aPDT are independent of antibiotic resistance patterns

- D) More limited adverse effect profile and damage to the host tissue
- E) No resistance following multiple sessions of aPDT
- F) Broad spectrum of action compared to antibiotics since PS can act on diverse microorganisms such as bacteria, protozoa, fungi.<sup>192</sup>

In order to optimise the photodynamic properties of PS, fresh investigations into aPDT have yielded several chemically modified PS as well as new classes of PS.<sup>194</sup> Gollmer *et al.* developed a chemical modified MB derivative with the ability of additional hydrogen bonding that had a strong antibacterial effect against Gram-positive *S. aureus* and Gram-negative *E. coli* in 10 mins of irradiation (660 nm, 50 mW cm<sup>-2</sup>).<sup>195</sup> Dovigo *et al.* reported that Photodithazine<sup>®</sup> (PDZ), a commercially available water-soluble chlorin e6 derivative was able to reduce biofouling caused by clinical isolates of *Candida* biofilms by irradiating with an LED device emitting at 660 nm and delivering 25 mW cm<sup>-2</sup> light.<sup>196</sup> Three synthetic mono-substituted cationic bacteriochlorin structures, tested as PS for anti-cancer applications, were also reported to show antimicrobial activity by Huang *et al.* Irradiating with a NIR light source (700–850 nm band pass filter) at an irradiance of 100 mW cm<sup>-2</sup>, all the synthetic dyes were highly effective against both Gram-positive *S. aureus* and *Enterococcus faecalis*, one against Gram-negative *E. coli* and *Acinetobacter baumannii* and another against fungal yeasts *C. albicans* and *Cryptococcus neoformans*.<sup>197</sup> Thus, by functionalisation, the photoinactivation effect of PS on both Gram-positive and Gram-negative bacteria and other microorganisms was potentiated.<sup>192, 194, 198</sup>

### 1.2.2. PDT Mechanisms

The basic photo-physical pathways by which the combination of a PS, light and O<sub>2</sub> results in photosensitised cell death are shown in Figure 1.18. Illumination with light at the appropriate wavelength activates the photosensitising agents which then interact with molecular oxygen to produce reactive oxygen species (ROS) via electron transfer (Type I) or energy transfer (Type II) reactions.

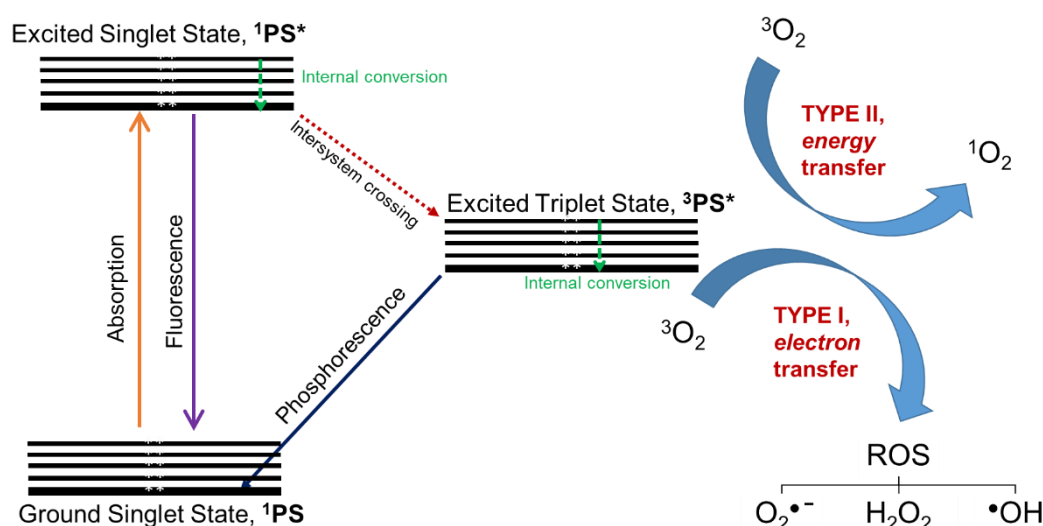


Figure 1.18 Simplified Jablonski diagram showing the processes involved in PDT when a photosensitiser undergoes energetic transitions upon light absorption. The photosensitiser in its excited singlet state can undergo radiative decay (fluorescence) or non-radiative decay via internal conversion. It may also convert to the excited triplet state via intersystem crossing. The triplet state molecule may decay radiatively by phosphorescence, non-radiatively via internal conversion, or interact with molecular oxygen via resonant energy transfer (Type II reaction). The triplet state molecule may also interact with molecular oxygen and/or other substrate molecules via electron transfer (Type I reactions).

The initial absorption of light transforms the PS from its ground singlet state (<sup>1</sup>PS) to the short-lived excited singlet state (<sup>1</sup>PS\*). Excess vibrational energy is dissipated by internal conversion and the PS may relax back to ground state by emitting a photon (fluorescence). Alternatively, via intersystem crossing (ISC), the short-lived excited singlet state (<sup>1</sup>PS\*) is transformed to the relatively long-lived electronically excited triplet state (<sup>3</sup>PS\*). The triplet state can undergo two different photochemical reactions. A direct reaction of <sup>1</sup>PS\* or <sup>3</sup>PS\* with oxygen or another substrate, resulting in electron transfer to form ROS such as superoxide

( $O_2^{\bullet-}$ ), hydroxyl radicals ( $\bullet OH$ ) and hydrogen peroxide ( $H_2O_2$ ) is known as the Type I mechanism or photo-induced electron transfer (PET). The Type II mechanism involves direct transfer of energy from  $^3PS^*$  to  $O_2$  to form excited state singlet oxygen ( $^1O_2$ ).<sup>199</sup> ROS such as  $O_2^{\bullet-}$ ,  $\bullet OH$  and  $^1O_2$  react with a large number of biological substrates and induce irreversible cellular membrane damage and enzyme deactivation ultimately leading to cell death.<sup>200</sup>

Both Type I and Type II reactions occur in parallel, and the ratio between these processes depends on the type of PS used, the concentrations of substrate and oxygen, as well as the binding affinity of the PS for the substrate. The PS requires a good triplet state QY and a long triplet state lifetime in order to promote Type I/II processes. For most PS employed in PDT, Type II photochemical reactions represent the dominant process.<sup>201, 202</sup>

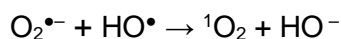
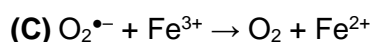
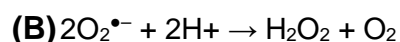
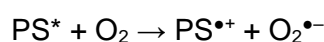
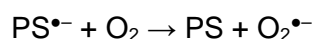
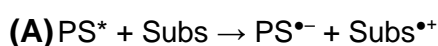


Figure 1.19 Common Type I photochemical reactions during photodynamic therapy. **(A)** Reactions of the photosensitiser upon activation to form superoxide **(B)** Dismutation of superoxide. **(C)** Fenton reaction.  $PS^*$ : excited state photosensitiser,  $PS^{\bullet-}$ : photosensitiser radical anion, Subs: substrate,  $Subs^{\bullet+}$ : substrate radical cation,  $O_2^{\bullet-}$ : superoxide radical anion,  $^1O_2$ : singlet oxygen,  $H_2O_2$ : hydrogen peroxide,  $HO^{\bullet}$ : hydroxyl radical,  $HO^-$ : hydroxide,  $Fe^{3+}$ : oxidised iron cation,  $Fe^{2+}$ : reduced iron cation.

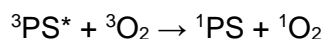


Figure 1.20 Type II photochemical reactions during photodynamic therapy.  $^3PS^*$ : excited triplet state photosensitiser,  $^1PS$ : ground state photosensitiser,  $^3O_2$ : ground state molecular oxygen,  $^1O_2$ : excited state singlet oxygen, Subs: substrate

In Type I photochemical reactions, electrons (or protons) are transferred to oxygen or other adjacent molecules to generate a mixture of radical anion or cation intermediates respectively. For example, the PS radical anion can transfer an electron to molecular oxygen to form  $O_2^{\bullet-}$  (Figure 1.19A).  $O_2^{\bullet-}$  is only moderately effective at causing oxidative damage on its own compared to  $^1O_2$ , but it can undergo dismutation, catalysed by superoxide dismutase (SOD) to produce oxygen and  $H_2O_2$ , which can pass through bacterial cell membranes to cause oxidative damage (Figure 1.19B).<sup>203</sup> In cells, where small amounts of metal such as copper and iron are present,  $O_2^{\bullet-}$  ions can act as reducing agents to produce ROS. The donation of an electron from  $O_2^{\bullet-}$  reduces the metal ions which in turn catalyse the conversion of  $H_2O_2$  into highly reactive  $\bullet OH$  in a process known as the Fenton reaction (Figure 1.19C).<sup>204</sup> Moreover,  $O_2^{\bullet-}$  can react with  $HO\bullet$  to produce  $^1O_2$  in a secondary process.<sup>205</sup>

On the other hand, Type II photochemical reactions involve the transfer of energy (not electrons) to molecular oxygen. Here, the  $^3PS^*$  can transfer its energy directly to ground state molecular oxygen to mediate the formation of  $^1O_2$ , described as one of the most potent ROS (Type II reaction, Figure 1.20).  $^1O_2$ , as an uncharged molecule, can easily diffuse through the cytoplasm and biological membranes, enabling its interaction with many important biomolecules resulting in photo-oxidative damage to vital cellular functions.<sup>201</sup>

ROS such as  $HO\bullet$  (formed via Type I electron transfer reactions) and  $^1O_2$  (formed via Type II energy transfer reactions) are extremely reactive. Because of the high reactivity and short half-life of these ROS, only cells that are proximal to the area of ROS production, i.e. the area of PS localisation and subsequent illumination, are directly affected by PDT. For example, the half-life of  $^1O_2$  in biological systems is less than  $0.04 \mu s$  and, therefore, the radius of the action of singlet oxygen is  $<0.02 \mu m$ .<sup>206</sup> The extent of damage induced by PDT is dependent on several factors including the PS type, dose administered, light exposure, amount of oxygen available, the extracellular and intracellular localisation of the PS and the time between the PS administration and light exposure. All of these factors are interdependent.<sup>207</sup>

### 1.2.3. Photodynamic Therapy by Quantum Dots

The basic principle underlying PDT is photoactivation of a PS, resulting in the generation of ROS such as  $\text{H}_2\text{O}_2$ ,  $\text{O}_2^{\bullet-}$ ,  $\bullet\text{OH}$  and  $^1\text{O}_2$ , through a series of electron and energy transfer reactions between the PS and molecular oxygen, (as illustrated in Figure 1.18) In anticancer PDT, targeted tumours are treated by applying a PS and irradiating with light to form ROS that immediately react with cell organelles, resulting in cancer cell death. Similarly, in aPDT, bacterial killing is a result of ROS attacking multiple sites in the bacterial cell, making the development of resistance unlikely. An ideal PS should be:

1. a compound with a consistent composition
2. synthesised simply with easily available precursors
3. nontoxic in the absence of light
4. possess target specificity and localise in target tissues with high selectivity and specificity
5. strongly absorbing with a high extinction coefficient at wavelengths with optimal tissue penetration
6. high quantum yield of ROS formation
7. highly resistance to photobleaching
8. minimally self-aggregating in biological media
9. quickly eliminated from the body.

Most conventional PS used both clinically and experimentally have some major drawbacks, for instance, instability in aqueous solutions, prolonged cutaneous sensitivity, chemical impurity, poor selectivity in terms of targeting diseased tissue, low extinction coefficients and weak absorption at the therapeutic wavelength.<sup>208</sup> Due to their unparalleled photo-stability, broad-band absorption (particularly in the NIR for cancer applications) and large two-photon absorption cross section, QDs have attracted much attention as potential PS for PDT.<sup>32, 209, 210</sup>

In relation to PDT, QD NPs possess several characteristics which make them attractive as a new therapeutic agents for PDT/aPDT:

1. they are compounds with a consistent composition
2. fairly simple and standardised synthesis (particularly  $\text{CdX/ZnY}$  QDs;  $\text{X} = \text{S, Se, Te}$ ,  $\text{Y} = \text{S, Se}$ )

3. relatively non-toxic in the absence of light but potentially ROS-producing under light exposure
4. surface can be coated to be water-soluble and biocompatible
5. large surface area can be functionalised for specific targeting of diseased tissues
6. the large extinction coefficient and large two-photon cross section could be exploited for inducing photosensitisation at deeper depths
7. exceptionally high threshold for photobleaching.

When QDs are photoactivated, an electron is promoted from the ground state (QD) to the excited state (QD\*), yielding an electron-hole pair. The excited electron can return to the ground state via two different pathways: radiative relaxation or non-radiative relaxation. Radiative recombination results in the emission of light in the form of fluorescence. Alternatively, excited state electrons may localise in surface traps with the bandgap, either repopulating the excited state (non-exciton emission) or thermalising into deeper trap states (non-radiative relaxation). Surface-trapped electrons are long-lived and can interact with surrounding molecules, leading to the formation of ROS via electron or energy transfer. Because of the large surface area of QDs, non-radiative relaxation at surface sites and surface traps competes with radiative recombination however, ultrafast radiative carrier relaxation processes in the band edge dominate relatively slow energy transfer to molecular oxygen resulting in poor ROS (particularly  $^1\text{O}_2$ ) production efficiency.<sup>211</sup> For example, a study by Yaghini *et al.* found that illuminated PEG-encapsulated CdSe/ZnS QDs alone did not generate any detectable  $^1\text{O}_2$  in aerated aqueous solution with an upper limit to the QY estimated as <0.003. The  $\text{O}_2^{\bullet-}$  yields were found to be low as well (0.35%).<sup>212</sup> Similarly, Tsay *et al.* found no evidence of the generation of  $^1\text{O}_2$  by peptide-coated CdSe/CdS/ZnS QDs in the absence of a PS.<sup>213</sup> In contrast, porphyrin- and phthalocyanine-based conventional PS produce ROS at much higher efficiencies (>75%).<sup>211</sup>

Therefore, both conventional PS and QDs have a number of advantages and limitations when individually applied for PDT. However, the advantages and limitations of QDs and PS drugs complement each other. Thus, several hybrids and conjugates of QD and PS have been investigated in an effort to exploit the photostability of QDs and the ROS efficiency of PS. In such a configuration, the excited singlet and triplet states of the PS may be indirectly generated by non-radiative energy transfer, also called Förster resonance energy transfer

(FRET) from photoactivated QDs. The indirect photoactivation preserves the PS by minimising photobleaching. Due to the broad absorption spectra of QDs, there are also more options for excitation sources with the QD-PS hybrids. Moreover, the large surface area and biocompatibility of QDs allow them to be conjugated with multiple PS molecules.

#### 1.2.4. Förster resonance energy transfer (FRET)

FRET involves the non-radiative transfer of excitation energy from an excited donor fluorophore (D), after absorption of a higher energy photon, to a ground-state acceptor fluorophore, (A) which can radiatively emit a lower energy photon.<sup>214</sup> Efficient FRET interactions require two key criteria be satisfied:

- Finite spectral overlap between donor photoluminescence and acceptor absorption,
- Close proximity of the donor to the acceptor, typically within 10 nm, is required as energy transfer efficiency inversely varies with the sixth power of the separation distance between the donor and acceptor pair,  $r$ .

As the process is driven by dipole–dipole interactions, it is also strongly dependent on the relative orientations of the donor and acceptor dipoles.<sup>215, 216</sup> The rate of non-radiative energy transfer from a donor to an acceptor  $k_T(r)$  is given by:

$$k_T(r) = \frac{1}{\tau_D} \left( \frac{R_0}{r} \right)^6$$

Equation 1.2

where  $r$  is the distance between the donor and acceptor,  $\tau_D$  is the lifetime of the donor in the absence of energy transfer,  $R_0$  is the Förster distance. The Förster distance is the separation at which the probability of energy transfer is 50%, i.e. half of the donor molecules decay by energy transfer and the other half decay by the usual radiative and non-radiative processes. A simplified expression for the Förster distance in Å is given by:

$$R_0 = 0.0211(\kappa^2 \phi n^{-4} J(\lambda))^{1/6}$$

Equation 1.3

where  $\kappa$  is the orientation factor ( $\kappa^2 = 2/3$ ),  $\phi$  is the quantum dot fluorescence quantum yield,  $n$  the refractive index and  $J(\lambda)$  the overlap integral. The overlap integral  $J(\lambda)$ , a quantitative measure of the degree of resonance between the donor emission and the acceptor absorption is calculated using the equation:

$$J(\lambda) = \int_0^{\infty} f_D(\lambda) \varepsilon_A(\lambda) \lambda^4 d\lambda$$

Equation 1.4

where  $f_D(\lambda)$  is the dimensionless fluorescence intensity of the donor in the absence of the acceptor,  $\varepsilon_A(\lambda)$  the molar absorption extinction coefficient of the acceptor, in units of  $M^{-1}cm^{-1}$  and  $\lambda$  is the wavelength in nanometres.<sup>215</sup> Experimentally, the FRET efficiency (E) is determined from changes in the steady-state or time-resolved fluorescence measurements, using the following equations:

$$E = 1 - \frac{f_D}{f_{DA}}$$

Equation 1.5

Or

$$E = 1 - \frac{\tau_D}{\tau_{DA}}$$

Equation 1.6

where  $f_D$  and  $f_{DA}$  are the donor fluorescence intensity in the absence and presence of the acceptor respectively; similarly,  $\tau_D$  and  $\tau_{DA}$  denote the amplitude-weighted fluorescence lifetime of the donor excited state in the absence and presence of the acceptor. FRET manifests in a loss of the donor fluorescence coupled with simultaneous enhancement of the acceptor fluorescence signal if the acceptor is an emitter. Similarly energy transfer results in a shortening of the excited state lifetime of the donor coupled with a lengthening of the acceptor exciton lifetime.<sup>216</sup>

FRET occurs when there is appreciable overlap between the emission spectrum of the donor and the absorption spectrum of the acceptor therefore careful selection of an appropriate donor/acceptor pair ensures high transfer efficiency. FRET is a powerful photophysical technique that has been extensively used in a variety of in vivo and in vitro biological investigations, including the monitoring of DNA hybridization and sequencing, protein conformation studies, diffusion dynamics, and the monitoring of intracellular receptor–ligand binding and cellular membrane dynamics.<sup>215, 217-220</sup> Fluorescent organic molecules have been widely used as energy donors and acceptors in a variety of FRET-based biological studies due to their small size, compatibility, and relatively large detection optical signals. However, they suffer from some drawbacks including pH sensitivity, susceptibility to photo/chemical degradation, relatively narrow absorption spectra, broad emission spectra, low photobleaching

threshold and small Stokes shifts.<sup>214, 215, 221</sup> Therefore the use of these fluorophores in a FRET configuration can result in significant direct acceptor excitation and substantial overlap between donor and acceptor emission.

Several reports have shown that QDs can substitute the organic dyes due to unique optical and spectroscopic properties.<sup>32, 210, 222</sup> They offer several advantages over organic dyes and can overcome a number of problems encountered by organic dyes in the FRET process as well as improve the performance of organic dyes when coupled together. Because of the broad absorption spectra of the semiconductor QDs, great flexibility in the selection of the donor excitation wavelength is afforded. Thus efficient excitation of the donor can occur at a wavelength where direct excitation of the acceptor is minimal. In addition, QDs have narrow and symmetric emission spectra reducing spectral cross-talk between the donor and the acceptor emission.

The first demonstration of efficient non-radiative energy transfer in QDs was reported by the Bawendi group.<sup>223</sup> In a thin film made of two close packed CdSe QDs with different diameters, energy transfer was observed with the smaller CdSe QDs (38.5 Å, PL maximum at 555 nm) acting as energy donors and the bigger CdSe QDs (62 Å, PL maximum at 620 nm) acting as energy acceptors. Steady-state fluorescence data showed a clear decrease in the PL from the smaller QDs along with an increase in acceptor (bigger QDs), which was corroborated by time-resolved fluorescence experiments. The first biologically relevant FRET investigation using QDs as energy donors was reported by Willard *et al.* which investigated the replication and telomerisation of surface bound DNA. Since then several groups have investigated the FRET efficiency using QDs and its application in biological systems.<sup>224</sup>

#### 1.2.4.1. QDs as Donors

Samia *et al.* first demonstrated the concept of FRET-based production of  $^1\text{O}_2$  by QD–PS pairs in a preliminary study investigating the application of QDs in cancer PDT. A complex was prepared by linking CdSe QDs to a silicon phthalocyanine (Pc4) PS through alkyl amine groups. Pc4 was selected for its high  $^1\text{O}_2$  efficiency (43%) under direct photo-activation. In the QD–Pc4 pair, QD acted as the energy donor to Pc4, and Pc4 as both an energy acceptor from QD and an energy donor to  $^3\text{O}_2$ , resulting in the generation of  $^1\text{O}_2$  and a FRET efficiency of 77%.<sup>225</sup> Following the first investigation of QD–PS pair, many researchers were attracted to

the energy transfer properties of covalent and noncovalent QD–PS pairs composed of QDs as energy donors and various chromophores such as porphyrins, phthalocyanines, inorganic complexes, and other organic dyes as energy acceptors. Below are a few examples of FRET-based applications employing QDs as donors.

#### 1.2.4.1.1. Biosensing

Systematic studies by Mattoussi and his group have probed FRET interactions between CdSe/ZnS QDs and proximal dyes. In their work QD NPs (capped with dihydrolipoic acid (DHLA)) were conjugated to engineered proteins containing site specifically labelled dye acceptors.<sup>226-232</sup> In this configuration, each QD was surrounded by a fixed number of proteins (MBP (maltose binding protein)) which attached to the QD either by electrostatic attraction or metal-affinity coordination. Therefore, QD-MBP acted as energy donors and dye-labelled proteins as energy acceptors. Steady-state fluorescence measurements showed that as the fraction of dye-labelled proteins per QD increased the QD PL systematically decreased. In the case where the acceptor was an emitter (cyanine dye), a concomitant enhancement of cyanine PL was measured. In much of their work, QD-MBP functioned as a probe for maltose, thus acting as a sugar sensor.<sup>227, 231</sup> MBP was also able to bind to cyclodextrin (a dark quencher), but with less affinity than maltose. Attachment of the cyclodextrin to the MBP led to the fluorescence quenching of the QD-MBP through FRET; however in the presence of maltose, the quencher-labelled cyclodextrin was displaced from the MBP binding site and maltose concentration dependent recovery of QD fluorescence was observed i.e., quantitative maltose sensing (Figure 1.21).



Figure 1.21 Schematic representation of a QD-protein-dye donor/acceptor pair for biosensing. Reproduced with permission from Medintz *et al.*, *Nat. Mater.*, 2003.<sup>227</sup>

#### 1.2.4.1.2. pH and ion Sensing

Several intracellular processes are controlled by changes in the concentration of local protons, therefore probes that are capable of accurately monitoring pH changes are highly desired. By coupling QDs to pH sensitive fluorescent molecules, researchers have developed highly sensitive pH sensors.<sup>233-235</sup> For example, Nocera and coworkers conjugated a pH-sensitive squaraine dye to CdSe/ZnS QDs (rendered hydrophilic via encapsulation in a poly(acrylic acid) capping layer), promoting proximal FRET interactions between QD and dye (Figure 1.22A). Because the dye's absorption profile is a function of pH, the efficiency of the FRET interactions also became a function of the environmental pH. In particular, it was shown that modulation of the FRET efficiency by varying the solution pH values below and above the  $pK_a$  of the dye ( $\sim 8.5$ ) produced net ratiometric dependence between the QD and dye emissions (Figure 1.22B), providing a unique tool to measure the solution pH, by simply analysing the ratio of the QD and dye peak intensities or comparing them to the value at the isosbestic point.<sup>233</sup> QD-based FRET systems have also been developed to detect metal ions.<sup>236, 237</sup>

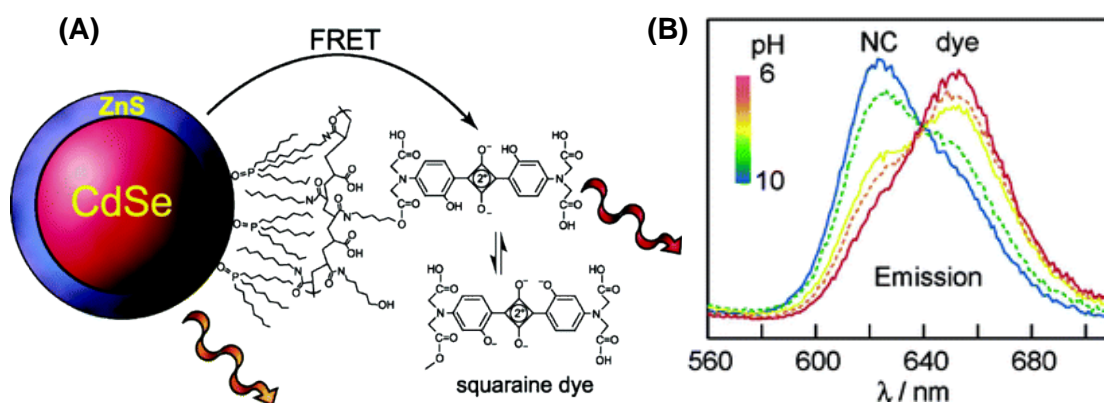


Figure 1.22 (A) Schematic of a pH sensor constructed from CdSe/ZnS QDs coupled to a pH-sensitive squaraine dye. (B) The emission profile of the QD-squaraine dye conjugate changes as a function of pH (red solid, 6.0; orange dotted, 7.0; yellow dotted, 8.0; green dotted, 9.0; and blue solid, 10) with  $\lambda_{ex} = 380$  nm. Adapted from Snee *et al.*, J. Am. Chem. Soc., 2006.<sup>233</sup> Copyright © 2006, American Chemical Society

#### 1.2.4.1.3. Probes for Enzymatic Activity

Using FRET for signal transduction is a common approach reported for detecting protease activity.<sup>238-241</sup> For example, Rao and company reported the assembly and testing of QD-substrates for sensing the activity of  $\beta$ -lactamase (Bla), a bacterial enzyme that hydrolyses

drugs such as penicillin and cephalosporins and which is responsible for bacterial antibiotic resistance. CdSe/ZnS QDs (peak emission at 605 nm) were the FRET donor, and a carbocyanine dye (Cy5) the FRET acceptor. The QD surface was coated with streptavidin, and a biotinylated lactam was labelled with Cy5. Binding of biotin to streptavidin immobilised the lactam-tethered Cy5 at the surface of the QD, thus quenching the QD fluorescence emission. When  $\beta$ -lactamase was present, the lactam ring was cleaved by the enzyme, releasing Cy5 from the QD surface and restoring the QD fluorescence emission (Figure 1.23). Addition of the lactamase enzyme to a solution of the QD-substrates resulted in time dependent changes in FRET efficiency and allowed monitoring of enzyme activity over time.<sup>238</sup>

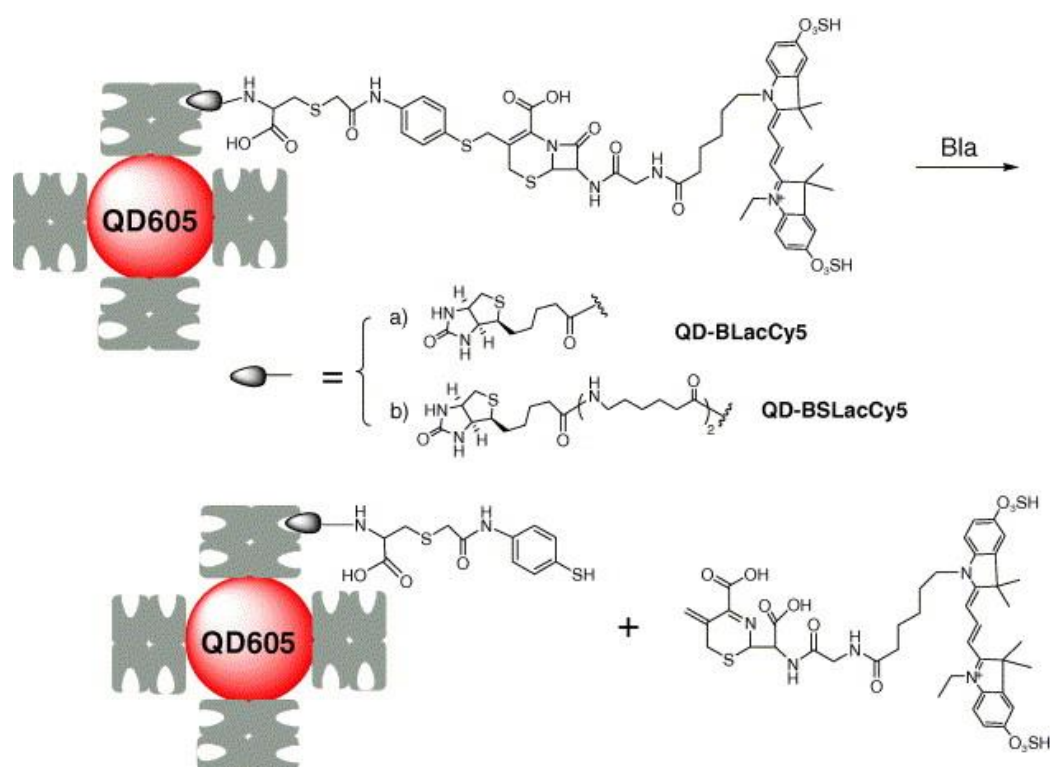


Figure 1.23 Schematic presentation of the design of the QD-based nanosensors for detecting Bla ( $\beta$ -lactamases). The Bla substrate is labelled with the FRET acceptor carbocyanine dye; (Cy5), and immobilized to QDs via the biotin and streptavidin binding. Bla activity cleaves the lactam ring and releases Cy5 to restore the QD fluorescence emission. Reproced with permission from Xu *et al.*, *Biochem. Biophys. Res. Commun.*, 2006.<sup>238</sup>

#### 1.2.4.1.4. Photodynamic Therapy

Reactive oxygen species (ROS) are known to initiate cytotoxic reactions in cells and tissues, making PDT a useful therapeutic tool to treat several types of cancer with high selectivity as

only tissues that are exposed to both the photosensitiser and photoexcitation in the presence of oxygen are affected. Rose bengal and chlorin e6, two photosensitisers (PSs) that generate singlet oxygen with relatively high yield, were covalently conjugated to CdSe/ZnS QDs and tested. By measuring the  $^1\text{O}_2$  phosphorescence signal at 1270 nm (excitation at 532 or 355 nm) and showed that indirect excitation of the photosensitiser within the QD-PS conjugate via FRET resulted in a higher yield of singlet oxygen compared to direct excitation of the PS at the same wavelength. Singlet oxygen QY as high as 0.31 for the QD-PS complex was measured using 532-nm excitation.<sup>242</sup>

#### 1.2.4.1.5. DNA Replication

Replication of DNA is an important natural process that occurs in live cells before they divide. The conjugates of QD–DNA have been widely used for detection of nucleic acids including DNA, RNA, mRNA and miRNA, and other molecular ligands. QDs conjugated to oligonucleotides have been used as FRET donors to monitor DNA replication processes in solution.<sup>230, 243, 244</sup> Hybridisation of oligonucleotides brings the acceptor in close proximity to QDs resulting in energy transfer from the QDs to the acceptors. A QD-based DNA nanosensor that used QDs as energy donors was developed by Zhang and his group to detect single point mutation in clinical samples. The nanosensor showed more than 100 times superior performance compared to popular molecular beacons.<sup>245</sup> Several other FRET-based bioanalysis of nucleic acids have also been demonstrated by other groups.<sup>246-250</sup>

#### 1.2.4.2. QDs as Acceptors

Further, QDs have been employed as energy acceptors in a number of studies as in principle, they are excellent candidates due to their large absorption cross-section, which can be an order of magnitude larger than organic dyes. The ideal FRET acceptor has (i) a large molar absorption coefficient across the entire range of donor PL for a sizeable spectral overlap integral, (ii) a large Stokes shift so that FRET acceptor PL is well resolved from the donor PL, and (iii) negligible absorption at the excitation wavelength of the donor.<sup>5</sup> QDs satisfy the first and second criteria well, but critically fail to satisfy the third, having strong absorption at all UV-visible wavelengths shorter than their PL emission. If fluorescent dyes serve as FRET donors, excitation of the dye will unavoidably excite the QD as well and an excited QD cannot serve as a FRET acceptor. Also due to the large size of the QDs, matching the dipole-dipole orientation is less likely when the QDs are acceptors. Therefore QDs are poor acceptors for

molecular dye donors. However, by selecting chemiluminescent donors (donors originate from chemical reactions rather than optical excitation therefore QDs remain in the ground state, making them excellent acceptors),<sup>251-254</sup> bioluminescent donors (biological analogue of chemiluminescence; chemical energy is converted into light energy within a biological system, typified by the action of luciferase enzymes on luciferin substrates),<sup>255-258</sup> lanthanide donors (luminescent lanthanide ions have excited-state lifetimes ~1000-fold longer than QDs, and are effective FRET donors for QD acceptors when the experimental system is properly configured and optimized)<sup>259-262</sup> or other QDs as donors<sup>223, 263-267</sup>, direct excitation of QD acceptors can be overcome.<sup>268</sup>

### 1.2.5. Charge Transfer

As discussed, electron-hole pairs generated by QD photoexcitation can recombine radiatively, emitting photoluminescence. However, a number of non-radiative relaxation pathways compete with radiative recombination of the exciton. Photoinduced charge transfer can occur from an excited state QD to a proximal redox active species, resulting in separation of carriers and QD ionisation. The transfer of an electron to molecular oxygen (or another acceptor) resulting in ROS is referred to as the reductive process, and the transfer of a hole to an electron donor such as hydrogen peroxide is called the oxidative process. The QD PL remains quenched until the charge on the QD is neutralised.<sup>153, 269</sup> Moreover, since charge transfer can occur to both the core states and the surface states of QDs, surface states are an important feature of the electronic structure of QDs. Charge can potentially transfer to the surface states of ground state QDs to yield an ionised QD where the PL is not completely quenched. Thus surface traps act as charge acceptors and yield further non-radiative pathways that compete with radiative recombination of the exciton: Auger recombination and defect-mediated recombination (see section 1.1.3.1).<sup>270, 271</sup> Efficient yields of charge transfer processes with external moieties requires efficient charge transport to the QD surface and adsorbate site if binding takes place. Efficient PET was demonstrated in InP/ZnS QDs by Chibli *et al.* who showed, with spin-trap EPR spectroscopy and reporter assays, that InP/ZnS QDs produced considerable amounts of  $O_2^{\bullet-}$  and a small amount of  $\bullet OH$  upon visible illumination.<sup>153</sup> Although charge transfer reactions involving QDs are complicated and not fully understood, applications of QDs based on PET have been widely reported in the literature. For example, Jeong *et al.* synthesised a NIR-emitting PbS/CdS/ZnS QDs conjugated to a methylene blue (MB)-containing activatable fluorescent modulator (PA-NIRQD). In the absence of

metalloproteinase (MMP), a hallmark of the cancer microenvironment, PET occurred from the PbS/CdS/ZnS to MB, quenching QD PL but in the presence of MMP, the part of PA-NIRQD containing MB was cleaved, preventing PET and restoring QD PL, enabling visualisation of colorectal tumour sites. High-resolution, real-time, non-invasive fluorescence imaging was demonstrated on ex vivo mouse colon cancer where within 10 min, increases in fluorescence of up to 300% was observed with the PA-NIRQD.<sup>272</sup> Also, Courtney *et al.* synthesised green-emitting CdTe QDs that induced light-activated growth inhibition of a number of MDR bacterial strains via PET with molecular oxygen. Using 2',7'-dichlorofluorescein diacetate (DCFH-DA) assays, flow cytometry and reduction potentials, the authors deduced that the green-emitting CdTe QDs generated  $O_2^{\bullet-}$  via electron transfer from photoexcited QDs and subsequent reactions led to the generation of more ROS, such as  $H_2O_2$ .<sup>153</sup>

## 1.3. HOSPITAL ACQUIRED INFECTIONS

### 1.3.1. Introduction

A hospital-acquired infection (HAI), also known as a nosocomial infection, is an infection acquired by patients while receiving treatment for any medical or surgical conditions and can occur in acute care settings within hospitals or in other outpatient healthcare settings such as same-day surgical centres and dialysis centres.<sup>273</sup> Nosocomial infections are a serious risk to patients, staff and visitors, causing significant complications with existing medical conditions, disability, anxiety and discomfort, even mortality to those infected. On average, infected patients require 2.5 times longer stays in hospital than uninfected patients resulting in increased costs for patients and healthcare facilities worldwide.<sup>274</sup> A study by Plowman *et al.* estimated that patients that acquire a HAI incurred hospital costs 2.9 times higher than uninfected patients.<sup>275</sup> Each year it is estimated that 2 million patients develop a HAI in the United States, representing nearly 5% of all hospitalised patients. These infections directly contribute to approximately 88,000 deaths and add an additional \$4.5 billion to healthcare costs.<sup>276</sup> In Europe, over 80,000 patients on any given day have at least one healthcare-acquired infection, about 6% of hospitalised patients, amounting to 3.2 million infected patients every year.<sup>277</sup> On a national level, 300,000 patients a year in England acquire a healthcare-associated infection as a result of care within the NHS. In 2007, methicillin-resistant *Staphylococcus aureus* (MRSA) bloodstream infections and *Clostridium difficile* infections were recorded as the underlying cause of, or a contributory factor in ~9000 deaths in hospital and primary care in England; and healthcare-associated infections were estimated to cost the NHS approximately £1 billion a year.<sup>278</sup> Action to address these problems – including new legislation, focused investment, regulation and performance monitoring – have had mixed results. The number of *C. difficile* cases reached a low of 13,362 cases in 2013/14 and since then the number of *C. difficile* infections has fluctuated. Similarly, from 2007/08 to 2013/14, total cases of MRSA infections in the UK decreased by 81%. Despite this reduction, the number of MRSA cases increased slightly in 2015/16 and has fluctuated since then. On the other hand, the total number of *Escherichia coli* infections increased by 34% between 2012/13 and 2018/19, and *E.coli* represents 55% of all Gram-negative bloodstream infections.<sup>279</sup>

### 1.3.2. Transmission of Hospital-Acquired Infections

Pathogens that cause HAIs may derive from the patient's own microbiological flora such as from the gastrointestinal tract, the respiratory tract or the skin. These types of infections are

known as endogenous infections. On the other hand, exogenous nosocomial infections are infections caused by pathogens that were not primarily part of the patient's microbiological flora but were transmitted to the patient during their hospital stay. It is impossible to completely eradicate a patient's physiological flora so endogenous HAIs are always a risk though precautions (such as skin disinfection before surgical procedures) may be taken to prevent some. However, all exogenous HAIs, in principle, are preventable through infection control measures.<sup>276</sup>

In a health-care facility, the sources of microbial contamination and subsequent transmission may be medical personnel, patients, or the inanimate environment.<sup>280</sup> Contact is by far the most common way of acquiring HAIs, either directly or indirectly. Direct contact transmission requires a direct person-to-person contact, which results in the physical transfer of a pathogen between an infected or colonised person and a susceptible host. Patient-to-patient transmission does not usually occur in health-care facilities however the drawing of blood, patient care activities, physical examinations and other kinds of medical care provide ample opportunities for symptomless medical workers to infect immunosuppressed patients or vice versa, for infected patients to directly transfer a large number of microorganisms to medical personnel. Indirect contact transmission involves contact of a susceptible host with contaminated objects as medical devices and nursing equipment. Indirect transmission may also occur when colonised or infected hosts touch and contaminate an object, an instrument, or a surface. Subsequent contact between that item and another patient is likely to contaminate the second individual who may then develop an infection. Indirect contact is the most frequent route of transmission of HAIs and as medical personnel regularly come in close contact with patients, the hands of clinical personnel serve as important drivers of HAIs, particularly taking into account the low compliance rates of healthcare workers in hand hygiene.<sup>281</sup> For example, after a *Acinetobacter baumannii* nosocomial outbreak in a neurosurgical intensive care unit, a direct correlation was found between the number of environmental isolates obtained during screening and the number of patients who were colonised or infected with the same strain during the same calendar month.<sup>282</sup> Furthermore, in a study by Boyce *et al.*, 42% of 12 nurses who had no direct contact with patients contaminated their gloves by touching objects in the rooms of patients with MRSA in a wound or urine.<sup>283</sup>

Disinfection of surfaces, particularly surfaces in the immediate environment of patients, has been described to reduce acquisition of nosocomial pathogens such as vancomycin-resistant *enterococcus* and *A. baumannii*.<sup>284, 285</sup> It is therefore advisable to control the spread of nosocomial pathogens at least in the direct inanimate environment of the patient by routine surface disinfection.<sup>286</sup> Inanimate objects can act as a reservoir for bacteria and several studies have found that the most relevant nosocomial pathogens such as *Acinetobacter* spp., *E. coli*, *Klebsiella* spp., *Pseudomonas aeruginosa*, *S. aureus*, norovirus, *C. difficile* and *Enterococcus* spp. can persist on surfaces for many days and even months.<sup>285, 287-290</sup>

### 1.3.3. Antimicrobial Resistance

Over the last 60 years, antibiotic drugs have been used to inhibit or kill bacteria. However, microbial resistance to these drugs has developed on a very large scale over time, greatly reducing their effectiveness, and is an ever growing problem. Antimicrobial resistance (AMR) poses serious challenges for the remedy and management of infections around the world, resulting in higher doses of drugs, addition of treatments with higher toxicity, longer hospital stays, and increased risk of complications and fatal outcomes.<sup>291, 292</sup> The most vulnerable groups are children and the elderly with high susceptibility to infections and reduced immune response. Other risk groups are people with compromised immune systems, such as cancer patients and people who are HIV-positive, for whom adequate antibiotic therapy to prevent and treat severe infections is essential for their survival. In addition, AMR jeopardizes advanced medical procedures such as organ transplants and implants of prostheses, where antibiotics are crucial for patient safety and to avoid complications.<sup>293, 294</sup>

Mortality as a result of infectious diseases represents a fifth of global deaths.<sup>295</sup> This is likely to increase due to the global emergence of drug-resistant bacteria as well as the decelerating development of new antibiotics threatens present and future medical advances. The burden of AMR is estimated to grow to \$100 trillion and cause 10 million deaths annually by 2050, killing more people than the number that currently die of cancer.<sup>296</sup> In the UK, official figures suggest AMR claims the lives of 5,000 people a year however experts estimate that the real figure may be at least twice as high.<sup>297</sup> Getting global figures on the problem is difficult but reliable estimates suggest 700,000 are already dying each year – one person a minute.<sup>298</sup>

The development of AMR is a natural process that occurred long before the introduction of antibiotics to healthcare, however overreliance on and misuse of antibiotics has accelerated the development and spread of drug resistance.<sup>299</sup> Resistance can be acquired as a result of genetic events causing changes in the pre-existing bacterial genome, such as point mutations and gene amplifications. The other main mechanism is horizontal gene transfer between bacteria both within and between species, introducing transposons, integrons or plasmids into a microorganism.<sup>300-302</sup> The genetic alterations in bacteria cause resistance to antibiotics in one or more of four principal ways,<sup>291, 299</sup> as shown in Figure 1.24:

1. Reduction of drug accumulation, through decreasing drug permeability, or increasing active efflux (pumping out) of the drugs across the cell surface,
2. Degradation of antibiotic by microbe,
3. Not absorbing the antibiotic, inactivation or modification of the drug,
4. Altering the usual molecular target for the antibiotics, making the drug ineffective.

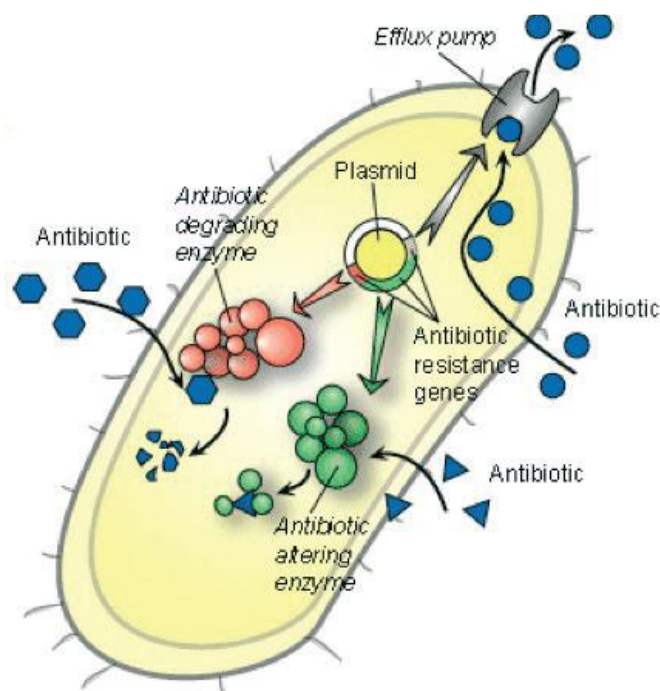


Figure 1.24 Mechanisms of resistance. Adapted from Per Nordberg *et al.*, Priority Medicines for Europe and the World. 'A Public Health Approach to Innovation – Antibacterial Drug Resistance, 2004.<sup>294</sup>

#### 1.3.4. Resistance in Common Nosocomial Pathogens

*Staphylococcus aureus* is one of the most virulent human pathogens and is the leading cause of bone, joint and soft tissue infections acquired in hospital and in the community. It also causes blood stream infections and endocarditis, and it is a frequent cause of food poisoning. Some strains of the *S. aureus* bacterium are resistant to the action of methicillin antibiotic, and other related  $\beta$ -lactam antibiotics (e.g., penicillin and cephalosporin). Since the 1980s the frequency of isolates of MRSA among *S. aureus* has increased from close to zero to nearly 70% in Japan and the Republic of Korea and around 40% in the USA.<sup>303</sup> MRSA has evolved a resistance not only to  $\beta$ -lactam antibiotics, but to several other classes of antibiotics, with an increasing number of MRSA strains susceptible only to vancomycin and other glycopeptides, and now, decreased vancomycin susceptibility has now emerged within all pandemic MRSA lineages.<sup>304</sup>

*Escherichia coli* is the most common Gram-negative bacterium isolated from blood cultures in clinical settings.<sup>277</sup> It is the most frequent cause of community and hospital-acquired urinary tract infections, is associated with peritonitis, causes synergistic wound infections and is one of the most important food-borne pathogens. Broad-spectrum penicillins such as amoxicillin were the treatments of choice before resistance started to emerge and to a large extent made them ineffective. In 2002, the proportion of *E. coli* isolates resistant to aminopenicillins was more than 30% for almost all countries in Europe.<sup>294</sup> In 2012, more than 50% of *E. coli* isolates were resistant to at least one of the antibiotics usually administered for treatment.<sup>305</sup> Extended-spectrum  $\beta$ -lactamase (ESBL) is a plasmid-associated  $\beta$ -lactamase that has been found to be produced by the members of *Enterobacteriaceae* family, predominantly *Klebsiella pneumoniae*, and *E. coli*. ESBL can hydrolyse penicillins, many narrow spectrum cephalosporins, many extended-spectrum cephalosporins, oxyimino-cephalosporins (cefotaxime, ceftazidime), and monobactams (aztreonam). In the 2017 EARS-Net study, 87.4% of the third-generation cephalosporin-resistant *E. coli* isolates were ESBL-positive as was the case with *K. pneumoniae* (76%).<sup>305</sup> Carbapenem resistance is a recently emerging threat mediated by a range of carbapenamases, which confer resistance to virtually all available  $\beta$ -lactam antibacterial drugs.

Following *E. coli*, *Pseudomonas aeruginosa* is the second most commonly isolated microorganism in hospital-acquired infections. *P. aeruginosa* is an opportunistic pathogen that

rarely affects healthy individuals, but causes high morbidity and mortality in cystic fibrosis (CF) patients and immunocompromised individuals.<sup>306</sup> It causes hospital-acquired pneumonia, bloodstream and urinary tract infections and is the leading cause of ventilator-associated pneumonia.<sup>307</sup> Management of *P. aeruginosa* in hospitals and institutional environments is problematic due to the intrinsic tolerance of the bacterium to many detergents, disinfectants and antimicrobial compounds. Furthermore, treatment is being rendered increasingly challenging due to the emergence and spread of resistance to the few therapeutic options that remain, particularly the acquisition of carbapenemases by some strains of *P. aeruginosa*; over 30% of *P. aeruginosa* isolates from HAIs were resistant to carbapenems in Europe.<sup>305, 308</sup>

### **1.3.5. Prevention Strategies**

#### **1.3.5.1. Hand Hygiene**

As the hands of health-care workers are the most frequent vehicle of HAIs, hand hygiene (hand washing and hand disinfection) is the primary preventive measure. Cross-infection *via* the hands of healthcare personnel is estimated to be responsible for 20 – 40% of HAIs.<sup>309</sup> Therefore, the decontamination of hands, both prior and following to patient contact, is vital in minimising the spread of bacteria.<sup>310</sup> Thorough hand washing with adequate quantities of water and soap removes more than 90% of superficial, flora including all or most contaminants. Killing all transient flora with all contaminants within a short time (a few seconds) requires hygienic hand disinfection using alcohol or alcoholic preparations. However hand disinfection with alcohol does not replace the need for regular and thorough hand cleansing with soap and water.<sup>311</sup>

#### **1.3.5.2. Cleaning**

One of the most basic measures for the maintenance of hygiene, and one that is particularly important in the hospital environment, is cleaning. Cleaning is the removal of foreign material (such as organic matter and soil) from objects using soap, detergents or enzymatic products. Hospital surfaces are cleaned hourly, daily or weekly depending on if the surfaces appear dirty, there are spillages, or after patient discharge. In the UK, routine cleaning is performed manually by using equipment such as mops, wipes, cloths, buckets and brushes and vacuum cleaners. Critical surfaces such as frequently touches surfaces must be cleaned thoroughly and regularly. Soaps and detergents act as solubilising agents and possess no antimicrobial activity, therefore the efficacy of the cleaning process is completely dependent on the

mechanical process. Thorough cleaning will remove more than 90% of microorganisms. However, careless and superficial cleaning is much less effective and could even have a negative effect, by dispersing the microorganisms over a greater surface and increasing the chance that they may contaminate other objects.<sup>280</sup> For example, a *P. aeruginosa* outbreak was reported in a haematology-oncology unit as a result of contamination of the surface cleaning equipment when non-germicidal cleaning solutions were used to decontaminate the patients' environment instead of disinfectants.<sup>312</sup> Therefore, the CDC recommends the use of bleach and other chemical disinfectants such as aldehydes, alcohols and quaternary ammonium compounds to eliminate microorganisms.<sup>313</sup>

#### 1.3.5.3. Disinfection

Disinfection refers to the use of chemical agents on inanimate surfaces to destroy or inhibit microorganisms, with the exception of high numbers of bacterial spores. There is no ideal disinfectant and the best compromise will depend on a number of factors including:

- 1) The number and location of microorganisms
- 2) The innate resistance of the microorganisms
- 3) The concentration and potency of the disinfectants
- 4) Duration of exposure to germicide
- 5) Nature of contaminant (organic or inorganic matter)
- 6) Presence of biofilms (these can be resistant to disinfectants and harder to remove)
- 7) Chemical and physical factors (e.g. temperature, pH, humidity and water hardness)

A range of biocides (chemical agents that inactivate microorganisms) are available for use as antiseptics including alcohols (mainly ethanol and isopropanol), chlorine and chlorine compounds, quaternary ammonium compounds and phenolics, formaldehyde, iodophors, peracetic acid, hydrogen peroxide, glutaraldehyde and ortho-phthalaldehyde.<sup>314-318</sup> Many disinfectants can be used alone or in combinations in the health-care setting. Depending on the level of activity, disinfectant may be classified as:

- (i) *High-level*: can be expected to destroy all microorganisms, with the exception of large numbers of bacterial spores. Examples: glutaraldehyde, peracetic acid.
- (ii) *Intermediate*: inactivates *Mycobacterium tuberculosis*, vegetative bacteria, most viruses, and most fungi; does not necessarily kill bacterial spores. Example: chlorine compounds, alcohols, iodophors.

- (iii) *Low-level*: can kill most bacteria, some viruses, and some fungi; cannot be relied on to kill resistant microorganisms such as tubercle bacilli or bacterial spores. Examples: phenolics, quaternary ammonium compounds.<sup>280</sup>

#### 1.3.5.4. Sterilization

Sterilization refers to a physical or chemical process that completely destroys or removes all microbial life, including spores.<sup>317</sup> By definition, it effects a reduction in the number of microorganisms by a factor of more than  $10^6$  (i.e. >99.9999%). Sterilization can be achieved by both physical and chemical means. Physical methods are based on the action of heat (autoclaving, dry thermal or wet thermal sterilization), on irradiation ( $\gamma$ -irradiation), or on mechanical separation by filtration. Chemical means include gas sterilization with ethylene oxide, hydrogen peroxide, peracetic acid or other gases; and immersion in a disinfectant solution with sterilizing properties (e.g. glutaraldehyde).<sup>313, 317</sup>

#### 1.3.5.5. Behaviours and Practices Affecting Cleaning and HAIs

Efficacy of cleaning and adherence to infection control protocols is not dependent only on the strength of the cleaning solutions alone but also the prevailing safety culture in healthcare facilities. Despite the risk of exposure to infectious agents, compliance to infection control, hygiene and personal protective equipment (PPE) protocols is often quite low, and is attributed to a number of factors.

First, there is a general lack of quality training for hospital cleaning staff and other healthcare personnel regarding modes of HAI transmission, proper hand hygiene and PPE usage.<sup>319</sup> In one study at an intensive care unit, over a 9-month period, the acquisition of Vancomycin-Resistant Enterococcus (VRE) dropped 3-fold after a period of educational intervention to improve environmental cleaning and a period of multimodal hand hygiene intervention.<sup>320</sup>

Secondly, for hospital cleaning staff, barriers encountered while performing their work has an impact on cleaning practices. One report listed not having sufficient time to perform daily cleaning and discharge cleaning properly as well as interruptions to assist with other tasks as challenges to achieving optimal cleaning and disinfection in hospitals.<sup>321</sup>

Third, institutional attitudes and policies toward safety, hygiene and infection control are important in cultivating a strong safety culture. Organisational commitment to infection control is reflected in the availability of and participation in training and refresher courses, supervisor and peer adherence to hygiene and infection control policies, organisational support for staff and patient safety and health— promoting hygiene even at the expense of efficiency, positive reinforcement of individual compliance behaviour, and negative reinforcement of noncompliance. Gershon *et. al.* found that employees who perceive a strong organisation-wide commitment to safety have been found to be more than 2.5 times more likely to adhere to safety protocols than those who lack such perceptions.<sup>319, 322</sup>

Thus, identifying root causes of noncompliance and designing interventions to address these issues ensures effective and consistent practices that reduce HAI transmission and keep acquisition of HAIs low.

## 1.4. ANTIMICROBIAL MATERIALS & SURFACES

### 1.4.1. Antimicrobial Action of Metal Nanoparticles

Metals such as silver (Ag), copper (Cu), gold (Au), titanium (Ti), and zinc (Zn) have been known to have antimicrobial activity for centuries. For instance, vessels made of Cu and Ag have been used for water disinfection and food preservation since the time of the Persian kings.<sup>323</sup> The properties of metal nanoparticles have been widely studied for their antimicrobial activity. Metal and metal oxide NPs such as gold (Au), calcium oxide (CaO), silver oxide (Ag<sub>2</sub>O), titanium dioxide (TiO<sub>2</sub>), silicon (Si), copper oxide (CuO), zinc oxide (ZnO), and magnesium oxide (MgO) have demonstrated antimicrobial activity against a spectrum of microorganisms.<sup>324-326</sup>

#### 1.4.1.1. Silver Nanoparticles

Among the best-known metal used as an antimicrobial agent, Ag NPs have received considerable attention due to their broad inhibitory behaviour towards nearly 650 species of microbes, and more importantly against antibiotic resistant bacterial strains. In general, the potency of Ag NPs to induce cell damage is shape- and size-dependent. Pal *et al.* reported that truncated triangular Ag NPs showed stronger antimicrobial activity against *E. coli* than spherical and rod-shaped Ag NPs.<sup>327</sup> Size-wise, investigations by Bera and co-workers found that smaller Ag NPs showed enhanced antimicrobial activity against Gram-positive (*S. epidermidis* and *Bacillus megaterium*) and Gram-negative bacteria (*P. aeruginosa*) as the smaller particles easily penetrated the cell wall.<sup>328, 329</sup> A number of mechanisms have been proposed for antibacterial activity of Ag NPs. These NPs have the ability to anchor to the bacterial cell wall and subsequently penetrate it, causing structural changes in the cell membrane such as in permeability, and afterward cell death.<sup>330</sup> The formation of “pits” on the cell surface increasing the accumulation of Ag NPs on the cell surface has also been proposed.<sup>331</sup> Electron paramagnetic resonance (EPR) spectroscopy suggests that when in contact with bacteria, Ag NPs form free radicals that can damage the cell membrane and make it porous leading to cell death<sup>330, 332, 333</sup> However, the release of Ag ions by Ag NPs is proposed as the main toxic mechanism. Ag ions interact with disulfide or sulfhydryl groups of enzymes that lead to disruption of metabolic processes which in turn cause the cell death.<sup>334</sup>

#### 1.4.1.2. Zinc Oxide Nanoparticles

ZnO NPs are “generally recognized as safe” by the U.S. Food and Drugs Administration and exhibit minimal toxicity to humans, high photo catalytic activity and are more biocompatible than TiO<sub>2</sub> nanoparticles.<sup>326, 335</sup> ZnO NPs have pronounced antimicrobial activity compared to their microparticles due to increased surface to volume ratio and surface abrasiveness of the nanostructures, and the bactericidal efficacy of the ZnO NPs increase with decreasing size.<sup>336, 337</sup> ZnO NPs can inhibit the growth of both Gram positive and Gram negative bacteria as well as spores resistant to high temperature and high pressure.<sup>338</sup> The growth of pathogens such as *S. aureus*, *E. coli*, *Pseudomonas fluorescens*, *Streptococcus pyogenes*, *Bacillus subtilis* and *Enterococcus faecalis* has been effectively inhibited in the presence of ZnO NPs.<sup>336, 339, 340</sup> ZnO NPs also have potent antimicrobial activity against common food-bourne pathogens such as *Campylobacter jejuni*, *Shigella dysenteriae*, *Salmonella enteritidis* and *Listeria monocytogenes*.<sup>341-343</sup> Distinctive mechanisms put forward in the literature include: direct contact of ZnO NPs with cell walls, destructing bacterial cell integrity,<sup>344-346</sup> release of antimicrobial ions mainly Zn<sup>2+</sup> ions,<sup>347, 348</sup> and ROS formation.<sup>349-351</sup> However, the toxicity mechanism varies in various media as the species of dissolved Zn may change according to the medium components besides the physicochemical properties of ZnO NPs.<sup>335</sup>

#### 1.4.1.3. Titanium Dioxide Nanoparticles

TiO<sub>2</sub> NPs have a wide spectrum of antimicrobial activity against a range of pathogenic microorganisms including bacteria, fungi, parasites and viruses and similar to ZnO NPs, they already see application in food, drugs and cosmetics.<sup>352-356</sup> TiO<sub>2</sub> NPs produce ROS under UV light and this photocatalytic ability helps to effectively eradicate microbes by damaging lipids and proteins, compromising cellular integrity.<sup>354</sup> However, the use of TiO<sub>2</sub> NPs under UV light is restricted because of genetic damage in human cells and tissues.<sup>357</sup> Doping TiO<sub>2</sub> NPs with metal ions has been shown to overcome this problem and also significantly enhance antibacterial properties by shifting the absorption range from UV to visible light.<sup>357, 358</sup>

#### 1.4.1.4. Copper Nanoparticles

In the bulk form, copper, like conventional silver, exhibits antibacterial properties. On the nanoscale, antimicrobial activity of Cu NPs has also been demonstrated against diverse species of bacteria, such as MRSA, *B. subtilis*, *Salmonella cholerasuis* and *P. aeruginosa*, and yeast species such as *Candida albicans*.<sup>359-361</sup> Cu NPs have been applied as coatings on

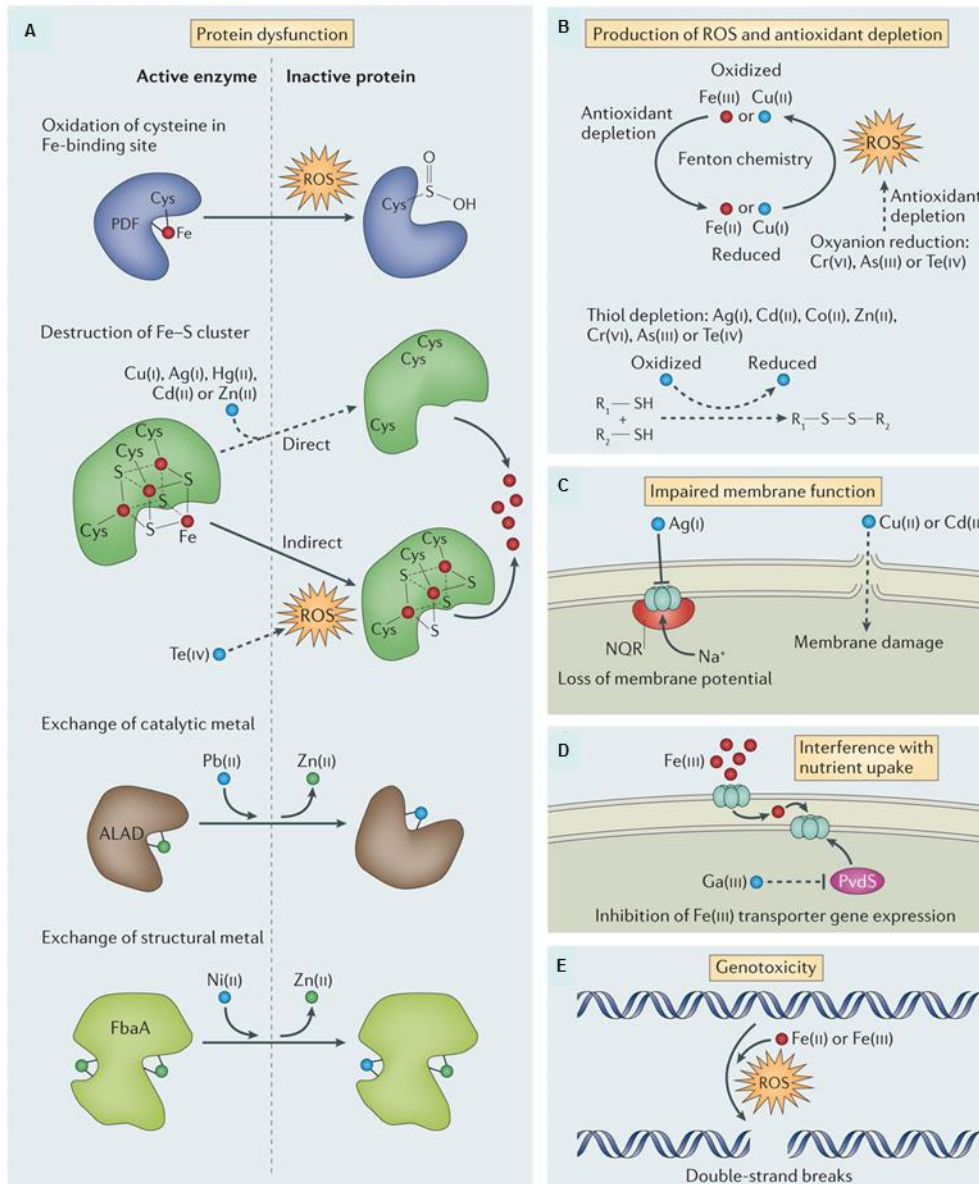
medical devices due to their antimicrobial properties however rapid oxidation of the Cu NPs on exposure to air limits their application.<sup>359, 362</sup> The bactericidal activity of Cu depends on the level of aggregation which is a common issue with Cu NPs. Minimizing aggregation results in smaller sized NPs providing more available surface area for solubilisation of copper ions and for interaction with bacterial membranes which leads to more toxicity. Metallic and ionic forms of copper produce  $\bullet\text{OH}$  radicals that damage essential proteins and DNA.<sup>363</sup> Cu NPs may also restrict bacteria growth by entering the cell via nanometric pores on the cell membrane.<sup>364</sup>

#### 1.4.1.5. Other Metal Nanoparticles

Compared to metal NPs mentioned above, gold (Au) NPs are reported to have weaker antibacterial activity of varying degrees. Au NPs are considered valuable in the development of antibacterial agents due to their nontoxicity, high capacity for functionalisation, ease of detection among other factors. Good bactericidal activity against Gram positive and Gram negative bacteria has been reported for Au NPs synthesized by reduction of the  $\text{Au}^+$  and  $\text{Au}^{3+}$  metal ions.<sup>365-367</sup> Gold NPs less than 2 nm have shown strong antibacterial activity.<sup>368</sup> Bactericidal activity of Au NPs is not due to ROS formation but has been attributed to attachment of the Au NPs to the bacterial membrane followed by membrane potential modification and adenosine triphosphate (ATP) level decrease as well as inhibition of transfer ribonucleic acid (tRNA) binding to the ribosome.<sup>369</sup>

Si NPs are considered as nontoxic with good biocompatibility and have been shown to inhibit the adhesion of bacteria to oral biofilms.<sup>370</sup> Silica nanowires can be biocidal by interrupting cell functions such as cell differentiation, adhesion and spreading of bacteria. Moreover, combination of Si NPs with other antimicrobial metals has indicated improved antimicrobial activities against *E. coli*, *S. aureus* and *C. albicans*.<sup>334, 371</sup>

CaO and MgO NPs also display strong antibacterial activity against both Gram positive and Gram negative bacteria. Antibacterial action is ascribed to the generation of  $\text{O}_2^{\bullet-}$  on the surface of these particles, and also by increased pH due to the hydration of CaO NPs and MgO NPs with water. It has also been proposed that MgO NPs damage the cell membrane and subsequently causing the leakage of intracellular contents which in turn leads to death of bacterial cells.<sup>372-376</sup> Figure 1.25 summarises the various proposed mechanism of antimicrobial action of metal and metal oxide NPs.



Nature Reviews | Microbiology

Figure 1.25 Mechanisms of metal toxicity to microbial cells. **A)** Metals can lead to protein dysfunction. **B)** They can also catalyse the generation of reactive oxygen species (ROS) and depletion of antioxidants. **C)** Certain metals have been shown to impair membrane function. **D)** Some can interfere with nutrient assimilation. **E)** Metals can also be genotoxic. Solid arrows represent pathways in which the underlying biochemistry has been elucidated, whereas dashed arrows represent a route of toxicity for which the underlying biochemical mechanism is unclear. [ALAD:  $\delta$ -aminolevulinic acid dehydratase, FbaA: fructose-1,6-bisphosphate aldolase, NQR: NADH:quinone oxidoreductase, PDF: peptide deformylase, PvdS: a  $\sigma$ -factor ( $\sigma^{24}$ ) from *P. aeruginosa*.] Reproduced with permission from Lemire *et al.*, *Nat Rev Microbiol*, 2013.<sup>323</sup>

### 1.4.2. Antimicrobial Action of Semiconductor Nanoparticles

QDs have been shown to have excellent antimicrobial activity against a range of Gram-positive and Gram-negative bacteria upon activation with light.<sup>377-381</sup> For instance, Ristic and co-workers reported the treatment of a clinical isolate of MRSA and reference strain *E. coli* ATCC 25922 with electrochemically produced graphene QDs in phosphate buffered saline (PBS). Following exposure of bacteria to 200 mg/mL of graphene QDs and irradiation with blue light (465 – 475 nm) for 15 min, *E. coli* numbers were reduced by 80% and *S. aureus* numbers by about 95%.<sup>378</sup> Similarly, Courtney *et al.* prepared green-emitting cadmium telluride (CdTe) QDs in aqueous media to which populations of MDR bacteria were exposed with and without visible light. In the presence of 100 nM CdTe and light for 8 h, the growth of patient isolates of MRSA and *Klebsiella pneumoniae* were reduced by 29% and 59% respectively. Under the same conditions, a clinical isolate of MDR *Salmonella typhimurium* showed 56% growth inhibition and two MDR *E. coli* isolates had 83% and 64% growth inhibition, respectively.<sup>377</sup> They demonstrated that superoxide was generated by photoexcitation of the QDs, and attributed the bactericidal activity to oxidative damage by this species and other ROS generated *via* the Fenton process.

#### 1.4.2.1. Combinatorial Antimicrobial Treatments with Quantum Dots

The conjugation of QDs with various materials to enhance antimicrobial performance and the target specificity has also been reported. Luo *et al.* used CdTe QDs to synergistically enhance the efficacy of rocephin, one of the most widely used antibiotic drugs. The minimum inhibitory concentrations (MIC, the lowest concentration of a drug which prevents visible growth of a bacterium) of rocephin and CdTe QDs for *E. coli* were 20  $\mu\text{gml}^{-1}$  and 1200  $\mu\text{gml}^{-1}$ , respectively. However the combination of the antibiotic with the QDs dramatically dropped the MICs to 0.5  $\mu\text{gml}^{-1}$  and 120  $\mu\text{gml}^{-1}$  for rocephin and CdTe QDs respectively.<sup>382</sup> In a similar vein, Courtney *et al.* combined superoxide-producing CdTe QDs with the set of bactericidal (ceftriaxone, ciprofloxacin, and streptomycin) and bacteriostatic (clindamycin and chloramphenicol) antibiotics of varied mechanisms of action. The QD-antibiotic combinations inhibited MDR Gram-negative clinical isolates to levels where the antibiotic GIC<sub>50</sub> (50% growth inhibition concentration) was below the clinical sensitive/resistant breakpoint and, in some cases, 1000-fold lower.<sup>383</sup>

On the other hand, Galdiero *et al.* conjugated amine-functionalised QDs to indolicidin, an antimicrobial peptide (QDs-Ind).<sup>384</sup> Though the QDs-Ind achieved a lower antibacterial activity against Gram-positive *S. aureus* ATCC 6538 than Gram-negative *P. aeruginosa* ATCC 1025, *E. coli* ATCC 11229, and *K. pneumoniae* ATCC 10031, the level of activity was still always more significant than that of indolicidin alone or the QDs alone.

In another example, Ananth and company prepared thioglycolic acid capped CdTe QDs complexed with phenolics rutin and caffeine (which have been shown to have antioxidant and antimicrobial properties) and studied the antimicrobial effect against *E. coli*. Morphological characterisation by atomic force microscopy indicated *E. coli* treated with QD-rutin conjugates showed more damage to cell wall when compared to QDs alone treated.<sup>385</sup>

### **1.4.3. Antibacterial Surfaces**

There has been a growing interest in the development of self-disinfecting antibacterial surfaces as cleaning and disinfection strategies are unable to eradicate the problem of HAIs.<sup>386</sup> The transmission of drug-resistant bacteria such as MRSA do not only cause health complications, but in a clinical setting with immunocompromised patients, transfer of bacteria can result in mortality. Effective antibacterial surfaces have the potential of preventing the spread of infections in a hospital environment by disrupting the cycle of transmission of bacteria from surfaces to patients and surfaces to healthcare workers. In addition, they can reduce microbial colonisation on frequently touched surfaces – such as door handles, telephones, computers, keyboards, bed rails and bedside tables – without staff having to spend hours manually cleaning surfaces.<sup>387-389</sup> A number of different surfaces such as glass, stainless steel and titania films have been investigated for the application of functional antimicrobial surfaces, but polymers are the most popular due to their extensive use in clinical applications, flexibility, ease of modification, low cost and durability.<sup>386, 390-392</sup>

#### **1.4.3.1. Photosensitiser-Based Light-Activated Antibacterial Surfaces**

The immobilisation of photosensitisers (PS) into polymers to develop antimicrobial polymers is a common approach for a number of reasons. The antibacterial action of certain types of PS have known for decades and have been suggested for local disinfection of wounds and ulcers, for example.<sup>193</sup> In addition, PS effect a non-site-specific, multi-site attack against microorganisms in the vicinity, making the development of bacterial resistance unlikely.<sup>393, 394</sup> Further, various types of PS have been shown to be powerfully bactericidal via the generation

of  $^1\text{O}_2$ .<sup>193</sup> Thus, materials with the capability to produce singlet oxygen offer the potential for infection control in the clinical setting.  $^1\text{O}_2$  is an extremely reactive species that is very effective in killing bacteria. However, the species is very short-lived, with a short diffusion pathway, decaying to molecular oxygen within microseconds; thus the generation of  $^1\text{O}_2$  at polymer surfaces does not increase mammalian toxicity of the material.<sup>395</sup>

Wilson prepared cellulose acetate polymers containing toluidine blue O (TBO) by co-dissolving with the PS. The author found that TBO incorporated cellulose acetate demonstrated promising light-activated antimicrobial activity against MRSA and *P. aeruginosa* (94% and 99.9% respectively) over a 24 hour period of white light illumination (60-W domestic lamp bulb); suitable to reduce microbial loads on surfaces in occupied hospital rooms.<sup>396</sup> In subsequent studies by Wilson *et al.*, it was found that the combination of PS dyes to maximise light absorption enhanced the efficiency of the photo-bactericidal process. Cellulose acetate coated with a 50:50 mixture of TBO and rose Bengal induced a 99.6% reduction in *S. aureus* bacteria after 2h illumination with 25W fluorescent lamp; after 6h, *S. aureus* was completely eliminated. Complete elimination of *C. difficile* and *E. coli* was also achieved within 4h and 16 h illumination respectively.<sup>397</sup> Interestingly, a reverse effect is observed when a combination of PS dyes was employed. Here, a greater effect is observed against Gram-positive bacteria (*S. aureus* and *C. difficile*) than against Gram-negative (*E. coli*).

Wainwright *et al.* reported the immobilisation of the methylene blue analogue, new methylene blue, in polymer resins by co-solution followed by drying and curing overnight. Both Gram-type organisms (*S. epidermis* and *E. coli*) were susceptible to the photodynamic action of the films but Gram-positive bacteria being more susceptible. Bactericidal action was observed to be positively correlated to the concentration of the PS and light dose. The type of polymer film was also important, with styrene films showing higher antimicrobial activity than acrylate films; it was postulated that this was due to different surface hydrophobicities of the polymer types.<sup>395</sup>

#### **1.4.3.2. Light-Activated Antibacterial Surfaces – Photosensitisers Combined with Other Materials**

Hend and Nabeel pioneered a rapid method of impregnating polymers with PS.<sup>398</sup> A simple instant dipping method was used to coat endotracheal tubes and urinary catheters with gendine (chlorhexidine combined with gentian violet)<sup>399</sup> and gardine (chlorhexidine combined

with brilliant green)<sup>400</sup> to produce antimicrobial devices that displayed broad-spectrum antimicrobial activity and protected against multi-drug resistant MRSA, *P. aeruginosa*, *E. coli*, and *Candida parapsilosis* biofilm colonisation.

The “swell-encapsulation-shrink”, a technique pioneered by the UCL Materials Chemistry Centre, is a simple non-covalent dipping method of impregnating polymers with NPs and has been successfully used to incorporate PS dyes and other materials into a number of polymers such as polyurethane, silicone, polyvinyl chloride and polydimethylsiloxane, endowing these with antimicrobial activity.<sup>401-410</sup> In swell-encapsulation, materials are dissolved into an appropriate solvent or solvent mixture that is capable of swelling the chosen polymer. The polymer is then submerged in the solution, expanding the polymer and enabling the diffusion of the material through the polymer matrix. Subsequent evaporation of the solvent from the polymer embeds the material into the polymer.<sup>411</sup>

Photosensitising dye-encapsulated polymers have displayed strong bactericidal activity and Gram-positive and Gram-negative pathogens when illuminated with white light<sup>407, 409, 410, 412</sup> or light of specific wavelengths.<sup>402-405</sup> Generally, polymers incorporated with PS showed no activity until photo-irradiated, likely due to the far lower PS concentrations being used in the polymers. A number of these studies also showed that the addition of NPs enhanced the photo-bactericidal activity of the PS. Swell-encapsulation-shrink can and has been used to successfully incorporate both NPs and PS dyes into polymer to enhance the photosensitising effect of dyes. For example, Perni *et al.* showed that methylene blue (MB), in addition to 2 nm gold nanoparticles, incorporated demonstrated an enhanced light-activated antimicrobial activity against Gram-positive and Gram-negative bacteria, compared to those encapsulated with MB only.<sup>402</sup> Similarly, Naik *et al.* found that the activity of MB-incorporated polyurethane (2.8 log<sub>10</sub> kill) and TBO-incorporated polyurethane (4.3 log<sub>10</sub> kill) was increased when 2 nm gold NPs were added: 3.8 log<sub>10</sub> kill for MB and 4.8 log<sub>10</sub> kill for TBO.<sup>412</sup> Sehmi *et al.* studied the effect of the addition of ZnO and MgO to the photo-antibacterial activity of crystal violet (CV)-incorporated polyurethane. Both nanoparticles when combined with CV enhanced antibacterial activity against both Gram-positive and Gram-negative bacteria, with polymers embedded with a combination of ZnO and CV showing the strongest photo-bactericidal activity against *S. aureus* and *E.coli*.<sup>407</sup>

It was noteworthy that NPs embedded in to polymers on their own often did not exhibit any antibacterial activity, with or without light exposure. However in the presence of PS, a synergistic increase in the photosensitisation of bacteria was observed. It has been postulated that the interaction of the dye and NP may influence photochemical pathways, affecting the generation of ROS as supported by EPR studies, microbiological ROS scavenger assays and  $^1\text{O}_2$  phosphorescence studies.<sup>404, 406, 409</sup>

The efficient photo-destruction of bacteria mediated by ROS generation is the objective of antimicrobial PDT.  $^1\text{O}_2$  is often described as the most potent ROS particularly as bacteria have no natural endogenous scavengers against this ROS. While the generation of  $^1\text{O}_2$  may be taken as a predictor of toxicity in other applications such as fluorescence imaging, in aPDT, the photogeneration of this species is exploited. Though  $^1\text{O}_2$  is cytotoxic in a physiological environment, the half-life of the ROS is shorter than  $1\mu\text{s}$ , with a diffusion pathway of 10 – 100 nm so when generated from surfaces,  $^1\text{O}_2$  may diffuse into bacterial cells present on the surfaces but not far enough to reach host tissue cells.<sup>402</sup> Therefore the toxicity of  $^1\text{O}_2$  and other ROS towards host cells is not an issue in the potential use of PS or NP-PS encapsulated devices in clinical applications. Compared to  $^1\text{O}_2$ ,  $\text{O}_2^{\bullet-}$  has a longer lifetime and diffusion distance and  $\text{H}_2\text{O}_2$  even longer. Though  $\text{H}_2\text{O}_2$  is not strictly a ROS, it is a powerful oxidant due to its long lifespan and neutral charge which allows easy diffusion within and between cells.  $\bullet\text{OH}$ , a subsequent product of  $\text{H}_2\text{O}_2$  is another highly reactive ROS.<sup>413, 414</sup> The combination of these different ROS overwhelm bacterial cell defences and inflict indiscriminate oxidative damage to a range of molecular substrates. Since the ROS attack different sites, the development of resistance to this oxidative attack is unlikely.

Thus, antibacterial surfaces from polymers consisting of photosensitisers in combination with nanoparticles have the potential to drastically reduce the transmission and incidence of nosocomial pathogens by destroying bacteria and preventing their growth thereby protecting against biofilm formation. This thesis explores the development of novel antimicrobial surfaces containing PS and cadmium-free quantum dots.

# CHAPTER 2. SOLUTION PHASE STUDIES OF MECHANISMS OF REACTIVE OXYGEN SPECIES (ROS) GENERATION OF QUANTUM DOTS-PHOTOSENSITISER COMPLEXES

## 2.1. Introduction

The unique photo-physical properties of QDs make them attractive in a wide range of applications. Especially in the biomedical field, QDs have been extensively studied for application in the imaging of tumours, drug delivery, fluorescent labelling, tumour ablation, and more recently, antimicrobial PDT. PDT mediated by conventional photosensitisers (PS) suffers from inherent limitations that reduce the effectiveness of this technique such as narrow absorption and broad emission ranges. To resolve this issue, nanoparticles are currently being explored as potential PDT photosensitisers. Special focus has been given to QD nanoparticles in combination with PS in PDT because in this format, critical limitations of conventional PS can be overcome.<sup>5, 32, 210, 225</sup>

When QDs and PS are in close proximity, Förster resonance energy transfer (FRET) – non-radiative energy transfer from QD donors to PS acceptors – can occur, enhancing photosensitisation. QDs make excellent FRET donors because of their high quantum yields and brightness; their capacity to bind multiple acceptor due to their large surface area; the broad absorption range of the QDs allows them to be excited far from the excitation range of the acceptor molecule, minimising direct excitation of the acceptor; and; the narrow and tunable QD emission peak can be optimally matched with the absorption spectrum of the desired acceptor.<sup>415-419</sup>

Experimentally, FRET manifests in a loss of the donor fluorescence coupled with simultaneous enhancement of the acceptor fluorescence signal if the latter is an emitter. Alternatively, a shortening of the excited state lifetime of the donor coupled with a lengthening of the acceptor exciton lifetime also indicates FRET.<sup>215, 420</sup>

Both QD donor and PS acceptor are also capable of undergoing photo-induced electron transfer reactions (PET), resulting in ionization of the QDs and PS and subsequently, partial or full photoluminescence quenching, depending on how the electrons and holes interact with QD surface states.<sup>153, 421</sup> In fact, these interactions are more likely since PET is short-range and requires close binding whereas FRET is longer range and able to occur even with donors and acceptors spatially separated within a few nm

Although much research has been undertaken into the utilisation of QDs in light-activated applications, their full potential is yet to be realised. The aim of this study is to prepare novel QD-PS complexes embedded into polymer, with superior light activated antimicrobial properties based on FRET and/or PET. Towards this goal, an in-depth analysis of the spectroscopic properties of QD-PS complexes in solution was carried out as a first step. The QDs employed were Nanoco cadmium-free, indium-based QDs, capped with electronegative ligands (CFQD<sup>®</sup>), thus making the nanoparticles negatively charged. These NPs were electrostatically attracted to the PS, crystal violet (CV), which is cationic dye in an aprotic solvent system. CV is a triphenylmethane dye with antibacterial and antifungal properties. Before the advent of antibiotics, CV was extensively used either on its own or as an adjunct in the successful treatment of a variety of diseases.<sup>422</sup> In areas with limited resources, CV is still used to prevent bacterial colonisation of the umbilical stump following childbirth; oral thrush in infants and more recently, in HIV-infected adults and children; and burn wound management.<sup>423-426</sup>

The photophysical properties of CV are unusual because its structure allows internal rotations. As a molecular rotor (molecule that undergoes internal rotation), the emissive properties of CV are strongly solvent viscosity-dependent.<sup>427</sup> CV is weakly fluorescent in fluid solvents and does not behave as a PS as its phenyl groups can rotate freely, resulting on the formation of twisted intramolecular charge transfer (TICT) states with negligible fluorescence quantum yields. However, CV is fluorescent in viscous or rigid media or when bound to proteins as internal rotations are restricted.<sup>428-430</sup> The motivations behind our choice of CV as the photosensitiser in our studies include:<sup>422, 431</sup>

- i. Strong absorption in donor emission range
- ii. Weak absorption in donor absorption range, enabling excitation of QD with little or no direct excitation of the PS

- iii. Solubility in a range of solvents
- iv. Non-toxic
- v. Inexpensive and readily available
- vi. Clinically relevant (extensively used in the clinical setting before the advent of antibiotics)
- vii. Well-characterised PS

In this chapter, systematic evaluations and investigations were carried out to determine the Type I PET and Type II FRET interactions that QD-CV complexes may engage in in solution phase. Electron paramagnetic resonance (EPR) spectroscopy was employed in an attempt to identify ROS generated as a result of PET in the QD and/or CV. Steady-state and time-resolved fluorescence studies were carried out to determine donor/acceptor spectral overlaps, donor/acceptor distances and FRET efficiencies. Finally, the potential of the QD-PS donor/acceptor pairs to generate singlet oxygen via the FRET process was also examined directly by near-infrared detection of singlet oxygen's phosphorescence.

## 2.2. Methods & Materials

### 2.2.1. Synthesis of CFQD<sup>®</sup> nanoparticles

CFQD<sup>®</sup> nanoparticles based on indium/zinc/sulphur/phosphorus alloy cores surrounded by ZnS shells were manufactured in the laboratories of Nanoco Technologies Ltd., Manchester, UK by means of proprietary synthetic procedures based on the patented molecular seeding process.<sup>115</sup> Briefly, the preparation of crude indium-based quantum dots with emission in the range of 500 - 700 nm was carried out as follows: Dibutyl ester (approximately 100 mL) and myristic acid (MA) (10.06 g) were added to a three-neck flask and degassed at ~70 °C under vacuum for 1 h, after which, nitrogen was introduced and the temperature increased to ~90 °C. Approximately 4.7 g of the ZnS molecular cluster [Et<sub>3</sub>NH<sub>4</sub>] [Zn<sub>10</sub>S<sub>4</sub>(SPh)<sub>16</sub>] was added, and the mixture was stirred for approximately 45 min. The temperature was then increased to ~100 °C, followed by the drop-wise additions of indium myristate (In(MA)<sub>3</sub>) (1 M, 15 mL) and tris(trimethylsilyl)phosphine ((TMS)<sub>3</sub>P) (1 M, 15 mL). The reaction mixture was stirred while the temperature was increased to ~140 °C, at which point, further drop-wise additions of In(MA)<sub>3</sub> dissolved in di-n-butyl sebacate ester (1 M, 35 mL) (left to stir for 5 min) and (TMS)<sub>3</sub>P dissolved in di-n-butyl sebacate ester (1 M, 35 mL) were made. The temperature was then slowly increased to 180 °C, and another round of dropwise additions of In(MA)<sub>3</sub> (1 M, 55 mL)

followed by  $(\text{TMS})_3\text{P}$  (1 M, 40 mL) was made. By addition of the precursor in this manner, indium-based particles with an emission maximum gradually increasing from 500 nm to 720 nm were formed. The reaction was stopped when the desired emission maximum was obtained (~520 nm and 615 nm for green and red QDs respectively) and left to stir at the reaction temperature for half an hour. After this period, the mixture was left to anneal for up to approximately 4 days (at a temperature ~20 – 40 °C below that of the reaction). A UV lamp was also used at this stage to aid in annealing. The particles were isolated by the addition of dried degassed methanol (~200 mL) via cannula techniques. The precipitate was allowed to settle and then methanol was removed via cannula with the aid of a filter stick. Dried degassed chloroform (~10 mL) was added to wash the solid then the solid was left to dry under vacuum for 1 day. This procedure resulted in the formation of indium-based nanoparticles on ZnS molecular clusters. Washing in dilute hydrofluoric acid (HF) increased the quantum efficiency of the resultant indium-based nanoparticles.

Growth of a ZnS shell: HF-etched indium-based core particles (20 mL portion) was dried in a three-neck flask. 1.3 g of myristic acid and 20 mL di-n-butyl sebacate ester were added and degassed for 30 min. The solution was heated to 200 °C, and 2 mL of 1 M bis(trimethylsilylmethyl) sulfide  $((\text{TMS})_2\text{S})$  was added drop-wise (at a rate of 7.93 mL/h). After this addition was complete, the solution was left to stand for 2 min, and then 1.2 g of anhydrous zinc acetate was added. The solution was kept at 200 °C for 1 h and then cooled to room temperature. The particles were isolated by adding 40 mL of anhydrous degassed methanol and centrifuging. The supernatant was discarded, and 30 mL of anhydrous degassed hexane added to the remaining solid. The solution was allowed to settle for 5 h and then centrifuged again. The supernatant liquid was collected and the remaining solid was discarded. The quantum efficiencies of the final un-functionalised indium-based nanoparticle material range from 73% to 79% for red QDs and approximately 85% for green QDs.

## **2.2.2. Material Characterisation**

### **2.2.2.1. Transmission electron microscopy (TEM) of quantum dots**

Prior to imaging, CFQDs<sup>®</sup> suspended in cyclohexane was drop cast onto 300 mesh carbon coated copper grid (Agar Scientific) and air-dried. High resolution (HR)-TEM images were acquired using a JEOL 2100 transmission electron microscope (TEM) with a LaB6 source operating at an acceleration voltage of 200 kV. Micrographs were taken on a Gatan Orius

charge-coupled device (CCD) camera with Digital Micrograph software. Particle size analysis was carried out using Gatan Suite software.

#### **2.2.2.2. Spectroscopic measurements**

UV-vis absorption spectra of suspensions were recorded using the Shimadzu UV-2600 Spectrophotometer (300 – 800 nm range). Emission spectra of suspensions was recorded with the Horiba FMax4 Fluorimeter (405 – 790 nm) at the excitation wavelength of 400 nm or 532 nm.

#### **2.2.3. Electron Paramagnetic Resonance Spectroscopy**

Aerated solutions of indium-based QDs and CV dye were prepared in cyclohexane with 250 mM 5,5-dimethyl-1-pyrroline-N-oxide (DMPO, Santa Cruz Biotechnology, USA) as the spin trapping agent. Final concentrations: red QD – 12.5 mg/mL, green QD – 40 mg/mL and CV – 0.4 mM. The solutions were loaded on to 50  $\mu$ L Blaubrand intraMARK micropipettes (VWR, UK), sealed with Cristaseal tube sealant (Hawksley, UK) and irradiated using a light-emitting diode (LED) lamp with peak emission at 455 nm (M455L2, Thorlabs, UK) before immediately placing in the EPR resonator. Continuous-wave (CW) EPR measurements were conducted either on a Bruker Elexsys E580 equipped with an EN 4118X-MD4 resonator (9.669 GHz). The experimental parameters were as follows: 6.4 mW microwave power, 0.1 mT modulation amplitude, 20.48 ms conversion time and 5.12 ms time constant. Magnetic field was calibrated with a Bruker strong-pitch standard,  $g = 2.0038$ . All measurements were recorded at room temperature. Samples were also measured in the dark to provide a baseline signal. The individual radical components of the spectra were identified by determination of the hyperfine coupling constants arising from the interaction of the unpaired electron with the nuclei of  $^1\text{H}$  and  $^{14}\text{N}$  from DMPO based on simulations using the Easyspin toolbox in MATLAB.<sup>432</sup>

#### **2.2.4. Time-Resolved Fluorescence Lifetime Measurements**

Photoluminescence lifetime of QDs was measured using time-correlated single photon counting (TCSPC). Solutions of QDs and QD-CV complexes at various CV concentrations (fixed QD concentration) were prepared and placed in a 1 cm optical path quartz cuvette. A pulsed laser diode module Edinburgh instrument Ltd., UK model EPL-405 was used to excite the samples at 405 nm at a 1 MHz repetition rate (EPL- 405, Edinburgh Instruments Ltd., UK). The emission was detected using a fast multi-alkali photomultiplier module (model H5773-04,

Hamamatusu Photonics K.K., Japan) via a long-pass filter (OG510, Schott, UK) and a monochromator (model M300, Bentham Instrument Ltd, UK). A Lyot depolarizer (Thorlabs Ltd, Ely, UK) was incorporated to minimise any polarisation anisotropy artefacts. TCSPC was carried out using a PC-mounted TCSPC board (TimeHarp 260, PicoQuant GmbH, Germany) and lifetimes were derived using Fluofit software (PicoQuant GmbH, Germany). The Instrument Response Function (IRF) was obtained from a non-fluorescent scattering Ludox solution (Sigma-Aldrich, Gillingham, UK). Optimum fitting with minimisation of the residuals was confirmed using a Chi-squared value  $\chi^2 < 1.4$ .

#### 2.2.4.1. Derivation of Fluorescence Lifetimes

The time-resolved fluorescence intensity decays were fitted to a sum of exponentials, as described below:

$$I_t = \sum_{i=1}^n A_i e^{-t/\tau_i}$$

Equation 2.1

where  $I_t$  is the intensity at time  $t$ ,  $A_i$  is the pre-exponential factor, in counts (therefore for a 50:50 mixture of two species, the values of  $A$  for each component would be 0.50),  $\tau_i$  is the lifetime of the  $i^{\text{th}}$  component. Therefore, a bi-exponential fit of the time-resolved photoluminescence decay of the donor exciton lifetime would take the form,

$$I_t = A_1 e^{(-t/\tau_1)} + A_2 e^{(-t/\tau_2)}$$

Equation 2.2

where  $A$  and  $\tau$  are the fractional amplitude and emission lifetime respectively.<sup>433</sup> Subsequently, the time-integrated signal,  $I_{int}$ , over the whole decay is expressed as:

$$I_{int} = A_1 \tau_1 + A_2 \tau_2$$

Equation 2.3

The integrated fluorescence is proportional to the weighted average of the lifetimes, mathematically equivalent to the “mean” lifetime. This same method was used to analyse singlet oxygen phosphorescence decays.

### **2.2.5. Singlet Oxygen Phosphorescence**

The singlet oxygen phosphorescence at 1270 nm of QDs and/or CV suspended in 1:1 cyclohexane/dichloromethane was detected using time-resolved photon counting. For detection in the near-IR, a thermoelectrically cooled photomultiplier (model H10330-45, Hamamatsu Photonics Ltd, Hertfordshire, UK) was used, and the emission was collected via a series of lenses from the cuvette in combination with a long-pass (950 nm cut-on, Andover Corp., US) and a band-pass filter centred at 1270 nm (Interferenzoptik Elektronik GmbH, Germany). Solutions were irradiated using a 532 nm Nd:YAG laser (Lumanova GmbH, Germany). The laser was pulsed at a repetition rate of 3 kHz and a pulse length of 3 ns and a fast photo diode (1 ns rise time, Becker-Hickl, Berlin, Germany) was used to synchronise the laser pulse with the photon counting detection system. A series of neutral density filters was used to attenuate the laser power to 2 mW. The photon counting equipment consisted of a PC-mounted multiscaler board (model MSA-300, Becker-Hickl, Berlin, Germany) and a pre-amplifier (Becker-Hickl, Berlin, Germany) which gave a resolution of 5 ns per channel. Time-resolved phosphorescence measurements were accumulated by the multiscaler board and the signals were analysed using FluoFit software (PicoQuant GmbH, Berlin, Germany) to extract the lifetime parameters. The experimental set-up is illustrated in Figure 2.1.

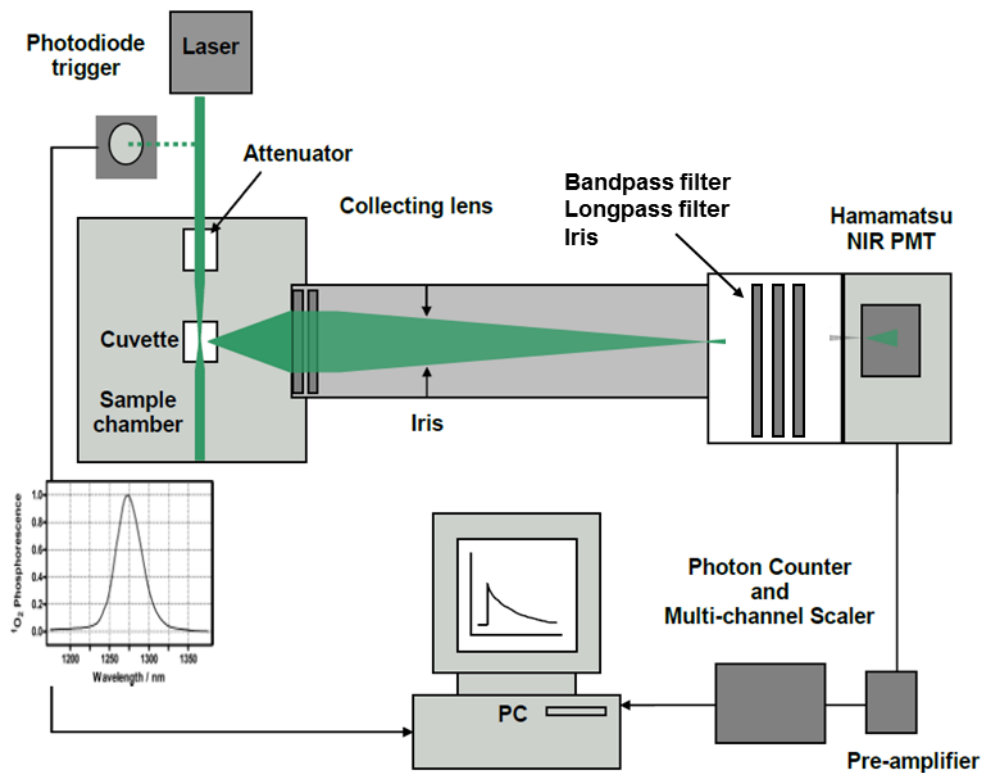


Figure 2.1 Set up for the experimental detection of singlet oxygen phosphorescence. Phosphorescence was detected at right angles to the laser excitation and collected via a series of lenses. A variable attenuator was placed in front of the laser beam to vary the incident power on the quartz cuvette. NIR: near-infrared, PMT: photomultiplier tube

## 2.3. Results & Discussion

### 2.3.1. QD Nanoparticle Synthesis and Characterisation

A scalable, and reproducible synthetic method known as molecular seeding was used to synthesise the indium-based nanoparticles. Molecular seeding uses molecules of a cluster compound that act as nucleation points where nanoparticle growth can be initiated. The method affords kilogram-scale quantities of high-quality monodisperse red and green-emitting QDs with high control over emission wavelengths, without the need for high temperatures compared to other methods (as discussed in Chapter 1.1.4.7) because a nucleation points are already available in the system provided.<sup>114-116</sup>

High-resolution TEM images showed both red- and green-emitting QDs to be small, highly crystalline, monodisperse and mainly spherical. (Figure 2.2 and Figure 2.3). Size analysis of over 150 particles of each QD gave average sizes of  $3.6 \pm 0.6$  nm for red QDs and  $2.88 \pm 0.49$  nm for green QDs. Some aggregation was observed for green-emitting QDs however generally the QDs showed good shape uniformity and narrow size distributions.

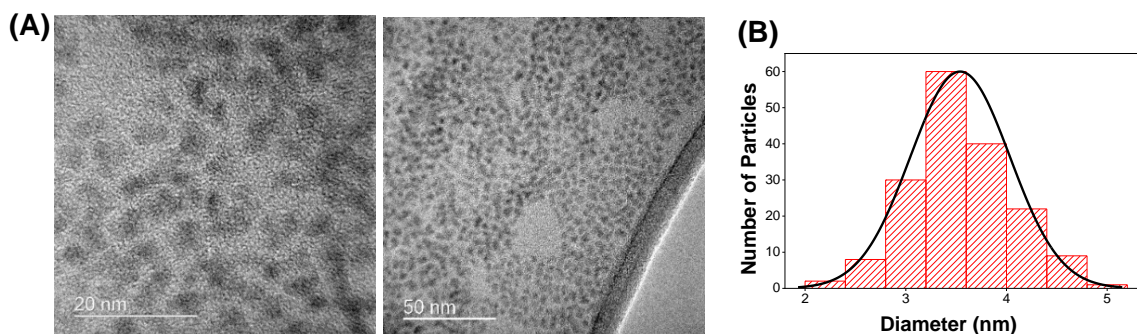


Figure 2.2 (A) High resolution TEM images of red-emitting QDs (B) red QD size distribution determined by HR-TEM.

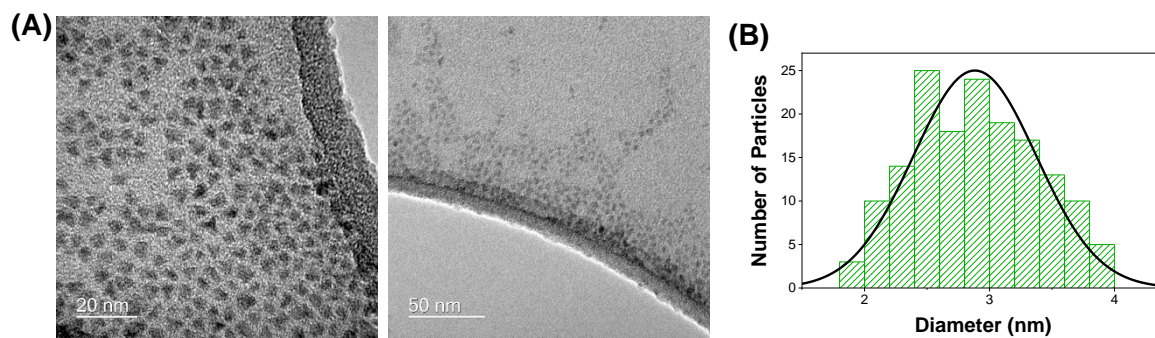


Figure 2.3 **(A)** High resolution TEM images of green-emitting QDs **(B)** green QD size distribution determined by HR-TEM

### 2.3.2. Complex formation between QD and PS

The binding of the PS crystal violet to red and green QDs to form a complex in organic solvent solution was investigated spectroscopically. Absorption spectra of all samples were recorded between 400 – 750 nm on a UV/Vis spectrometer.

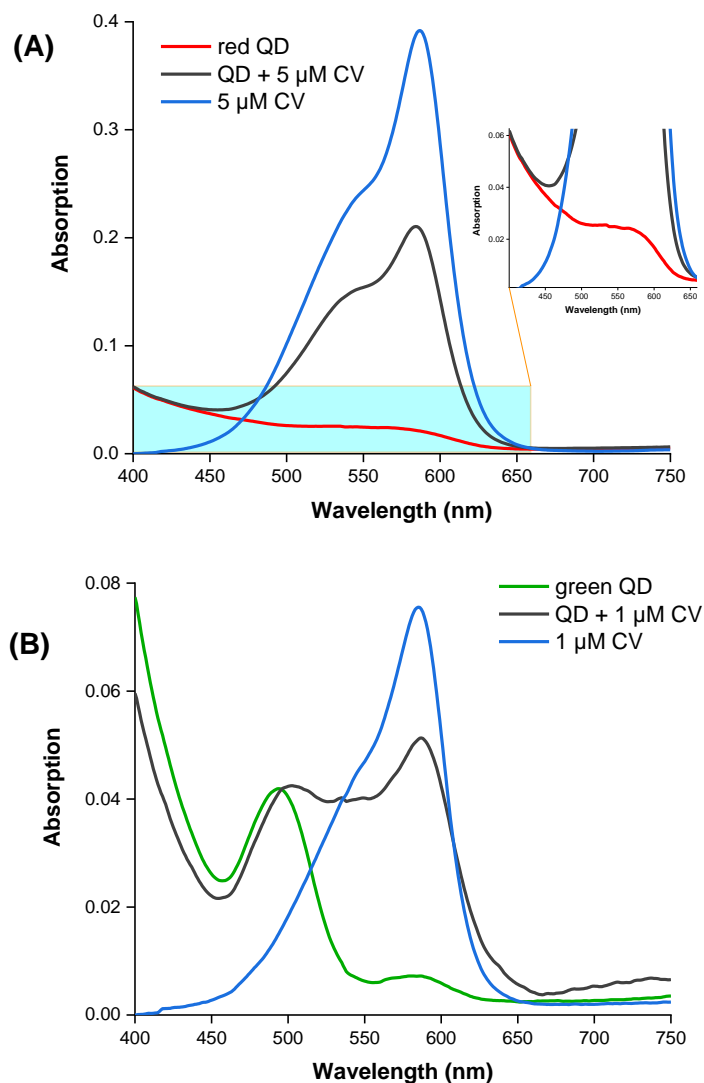


Figure 2.4 Absorption spectra for the formation of QD-PS complexes in 1:1 cyclohexane/dichloromethane solutions. **(A)** Absorption of 0.02mg/mL red QDs (red line), 5  $\mu\text{M}$  CV (blue line) and 0.02mg/mL red QDs combined with 5  $\mu\text{M}$  CV (black line). Inset: zoomed section of absorption profile to clearly show red QD absorption features. **(B)** Absorption of 0.02mg/mL green QDs (red line), 1  $\mu\text{M}$  CV (blue line) and 0.02mg/mL red QDs combined with 1  $\mu\text{M}$  CV (black line).

The peak absorption wavelength of CV alone was at 587 nm. When CV was mixed with the QD solutions, the CV absorption spectra peak were slightly modified to 584 nm and 589 nm for red and green QDs respectively. The small shift in CV absorption peak, of 3 nm to the blue region in the case of red QDs and 2 nm to the red region in the case of red QDs, upon mixture of the PS with QDs indicated a change in the microenvironment of the photosensitiser which may be ascribed to the binding of the molecule with the core/shell QD. The red-emitting QDs absorbance, which was broad and extended from the blue region up to about 600 nm peaking at ~550 nm (Figure 2.4A and inset), showed no obvious change in the absorption spectrum after combination with PS however it is impossible to tell due to the strong absorbance of the PS in the same region. On the other hand, a clear red shift in the green QD absorption spectrum is observed when mixed with CV. The green-emitting QDs absorption spectrum has excitonic peak at 494 nm which shifts to 502 nm when are mixed with CV (Figure 2.4B).

Successful complexation of QDs to CV is crucial for photo-induced electron transfer as PET requires much closer proximities of the donor and acceptor than is required with FRET. As found for a CdSe/ZnS QD/fluorescein electrostatically bound complex in heptane,<sup>434</sup> PET between QDs and CV may take place, resulting in generation of the semi-reduced CV radical with different spectral properties. In aqueous solution, the  $O_2/O_2^{\bullet-}$  redox couple is  $-0.18$  V vs. NHE (normal hydrogen electrode) (Equation 2.4) close to the  $CV^+/CV^{\bullet}$  reduction potential at  $-0.36$  V (Equation 2.5).<sup>435, 436</sup> The valence band reduction potential for InP QDs was estimated as  $0.95$  V.<sup>437</sup> Assuming binding and solvent effects to be minimal, extrapolation of the excited state redox potential implies that the photo-reduction of CV by indium-based QDs would be energetically feasible. This is especially so given the similar reduction potentials  $O_2/O_2^{\bullet-}$  and  $CV^+/CV^{\bullet}$ , and the good electron accepting properties of CV. PET from QDs to CV generates the semi-reduced CV radical QD which can then interact with molecular oxygen to generate superoxide by a secondary electron transfer reaction (Equation 2.6).<sup>153, 437</sup>



### 2.3.3. Spectral Overlap

As a cationic dye in an aprotic solvent system, CV will be electrostatically attracted to the polar surface of both QDs, which are capped with electronegative ligands, to form electrostatically bound complexes. QD-CV complexes favour PET interactions which occur over a shorter range over FRET.<sup>434, 438</sup> For QD-CV complexes to function as donor-acceptor hybrids for FRET, the spectral overlap must exist between CV absorption and QD PL. Figure 2.5 shows the absorption spectrum of CV (blue line) with a maximum absorption peak at ~590 nm and a shoulder around 550 nm. The fluorescence emission spectrum of red QDs was characterised by a symmetric profile with a full-width at half maximum (FWHM) of about 60 nm and a sharply defined maximum emission of 615 nm (Figure 1.5A). The green QDs had a narrower emission spectrum with an emission peak at 520 nm and a FWHM of 46 nm (Figure 1.5 B). There was considerable spectral overlap between the emission spectra of the QDs and absorption spectrum of CV which, in principle, should enable the occurrence of FRET between donor QDs and the acceptor dye when blue light excitation employed. To quantify spectral overlap, the overlap integral  $J(\lambda)$  was calculated using the equation:

$$J(\lambda) = \int_0^{\infty} f_D(\lambda) \varepsilon_A(\lambda) \lambda^4 d\lambda$$

Equation 2.7

where  $f_D(\lambda)$  is the dimensionless fluorescence intensity of the donor in the absence of the acceptor,  $\varepsilon_A(\lambda)$  the extinction coefficient of the acceptor, in units of  $M^{-1}cm^{-1}$  and  $\lambda$  is the wavelength in nanometres.<sup>215</sup>  $J(\lambda)$  of the QD-CV complex was calculated to be  $1.35 \times 10^{14} nm^4 M^{-1} cm^{-1}$ , for the red QD-PS complex and  $0.8 \times 10^{14} nm^4 M^{-1} cm^{-1}$  for the green QDs, both high overlap integral values, indicating strong spectral overlap of the QD-CV pairs, which would favour non-radiative energy transfer from photoexcited QD donors to ground state photosensitiser acceptor.<sup>420</sup> The corresponding Förster distance ( $R_0$ ), the distance at which the FRET efficiency is 50%, was then derived as 3.4 nm and 3.05 nm for the red and green QD-CV pairs respectively, using the equation:

$$R_0 = 0.0211(\kappa^2 \phi n^{-4} J(\lambda))^{1/6}$$

Equation 2.8

where  $\kappa$  is the orientation factor ( $\kappa^2 = 2/3$ ),  $\phi$  is the quantum dot fluorescence quantum yield,  $n$  the refractive index and  $J(\lambda)$  the spectral overlap.<sup>215</sup>

Table 2.1 displays the calculated values of  $J(\lambda)$  and  $R_0$  for both QDs.

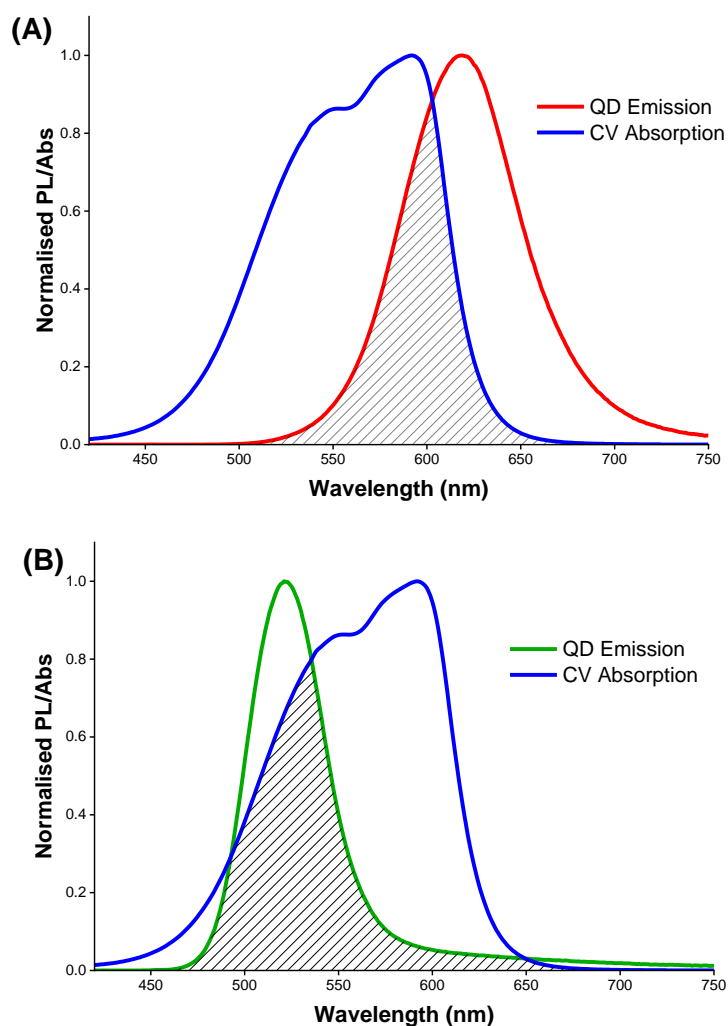


Figure 2.5 **(A)** Spectral overlap between the emission spectrum of the FRET donor (red QDs) and the absorption spectrum of the FRET acceptor (CV). Emission spectrum of red-emitting QDs (red line) and absorption spectrum of CV (blue line) and overlap region (shaded area). **(B)** Spectral overlap between the emission spectrum of the FRET donor (green QDs) and the absorption spectrum of the FRET acceptor (CV). Emission spectrum of green-emitting QDs (green line) and absorption spectrum of CV (blue line) and overlap region (shaded area)

Table 2.1 Overlap integral ( $J(\lambda)$ ) and Förster distances ( $R_0$ ) for the QD-PS donor-acceptor pairs

<b>Donor-Acceptor Complex</b>	$J(\lambda)$ <b>(<math>10^{13} \text{ nm}^4 \text{ M}^{-1} \text{ cm}^{-1}</math>)</b>	$R_0$ <b>(nm)</b>
Red QD – CV	13.5	3.4
Green QD – CV	8.04	3.05

#### 2.3.4. Steady-state Fluorescence Measurements

Steady-state fluorescence measurements were used to examine the efficiency of QD-PS complexes to perform as donor/acceptor pairs in the FRET process. Fixed concentrations of QDs and various excess concentrations of PS were prepared, and the emission measured. All samples were excited at 400 nm, which was near the minimum of the CV absorption spectrum in order to minimise interference from direct excitation of the PS acceptor. The emission spectra of the QD donor and the PS acceptor at different concentrations is illustrated for red and green QDs in Figure 2.6. In all cases, the emission of the QDs was quenched however there was no apparent CV fluorescence at longer wavelengths which was expected with the occurrence of the FRET within the QD donor and the PS acceptor. We do observe a slight distortion of the red QD spectrum at high concentrations, due to QD absorption interference. CV absorption of the QD emission at 520 nm, 615 nm and longer wavelengths could not account for the large decrease in intensity over the ranges of increasing CV concentrations.<sup>439</sup>

It has been previously reported that the FRET efficiency increases when the number of acceptors per QD increases. It was also observed that the decrease in QDs emission intensity was dependent on the CV/QD ratio and with increasing CV/QDs ratio, the QDs emission decreased progressively. If FRET occurred, then an increase in the acceptor emission should be observed. The absence of the CV emission appeared to be due to the low fluorescence efficiency of the CV even when bound to the QD which has a very high quantum yield in comparison.<sup>430 439</sup> The emission spectrum of CV could not be recorded in solution since most arylmethane dyes have typically low emission due to the strong dependence of fluorescence quantum yields on solvent viscosity. In low viscosity fluid solvents, the arylmethane groups can rotate freely resulting in the formation of twisted intramolecular charge transfer (TICT) states with negligible fluorescence quantum yields. However, this

molecular rotor effect is diminished when CV is dissolved in high viscosity solvents or bound to proteins and CV fluorescence from the first excited singlet state can then be measured<sup>428-430</sup> Likewise, when CV was encapsulated in polymer where the spatial constraint imposed by the matrix will restrict the rotor effect, the CV fluorescence was evident.<sup>405, 430</sup> Alternatively, PET between QDs and CV may account for the lack of a corresponding increase in CV emission as QD PL decreases. The semi-reduced CV radical emits in the red however its emission is weaker compared to CV itself.<sup>440</sup>

It is also possible that a recently identified mechanism, Dexter energy transfer (DET), may be occurring. DET involves direct energy transfer from the triplet state of the QDs to the sensitiser triplet state, which only emits weak phosphorescence.<sup>441, 442</sup> If this process occurs then it would also be consistent with the data. However, we do not know if this is possible for the present QD-CV complex.

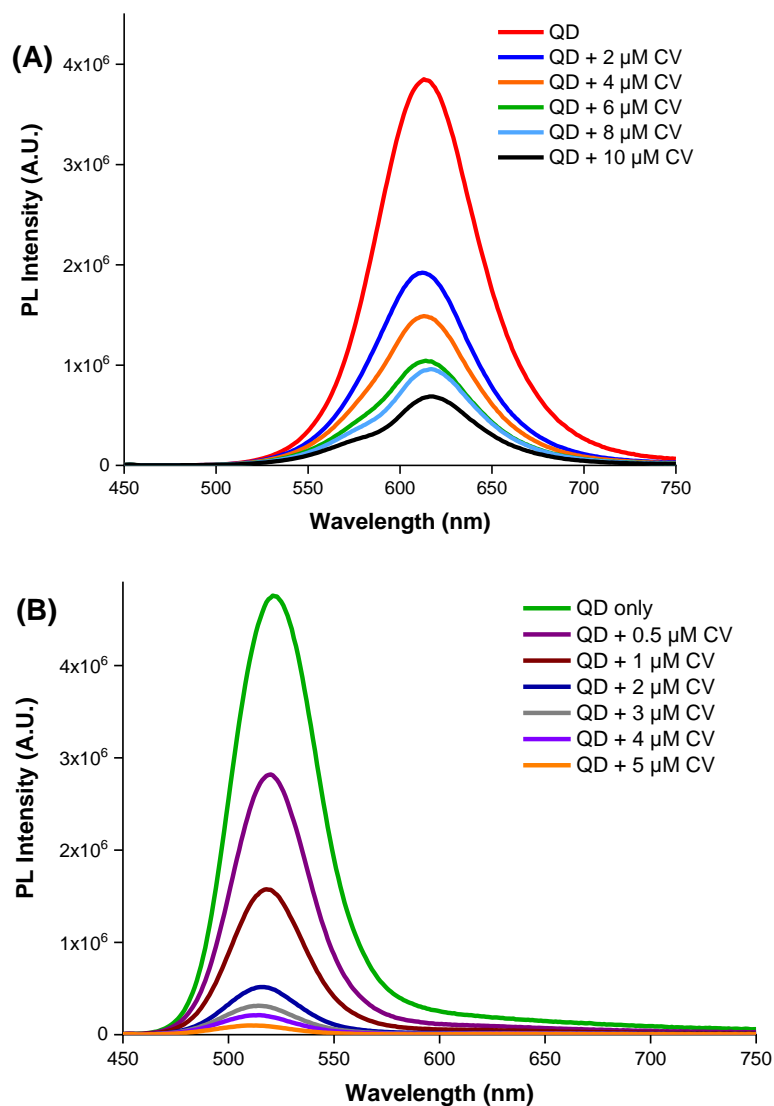


Figure 2.6 Fluorescence spectral changes in solution with fixed QDs concentration and increasing CV concentration. **(A)** Steady-state fluorescence emission spectra (400 nm excitation) of pure red QDs (red line) and QD-PS complexes with increasing CV concentration (2  $\mu\text{M}$  – 10  $\mu\text{M}$ ). **(B)** Steady-state fluorescence emission spectra (400 nm excitation) of pure green QDs (green line) and QD-PS complexes with increasing CV concentration (0.5  $\mu\text{M}$  – 5  $\mu\text{M}$ ).

### 2.3.5. Time-Resolved Fluorescence Lifetime Measurements

A comparison between the fluorescence lifetime of the donor and the fluorescence lifetime of the donor interacting with the acceptor molecule in close proximity should provide additional information on non-radiative energy transfer.<sup>215</sup> Measurements of the photoluminescence decay – of the two QDs alone as well as when the QDs are mixed with increasing CV concentrations – were carried out, using time-correlated single photon counting method (TCSPC). The donor exciton lifetime was extracted by fitting the time-resolved photoluminescence intensity ( $I_t$ ) of the QD to a bi-exponential decay (Equation 2.2). Figure 2.7 illustrates the QD fluorescence signal as a function of decay time for various QD and QD-PS mixtures. The decays are shown as logarithmic plots where the gradient scales with the lifetime, that is, the steeper the gradient, the shorter the fluorescence lifetime. Upon the addition of PS, it was observed that the overall fluorescence lifetime of the QD was significantly reduced. The exciton photoluminescence lifetime progressively shortened with the introduction of increasingly higher concentrations of the dye, suggesting that both QD-PS complexes investigated underwent the FRET process (Table 2.2 and Table 2.3). It is important to note that PET may also contribute to this QD lifetime shortening effect.

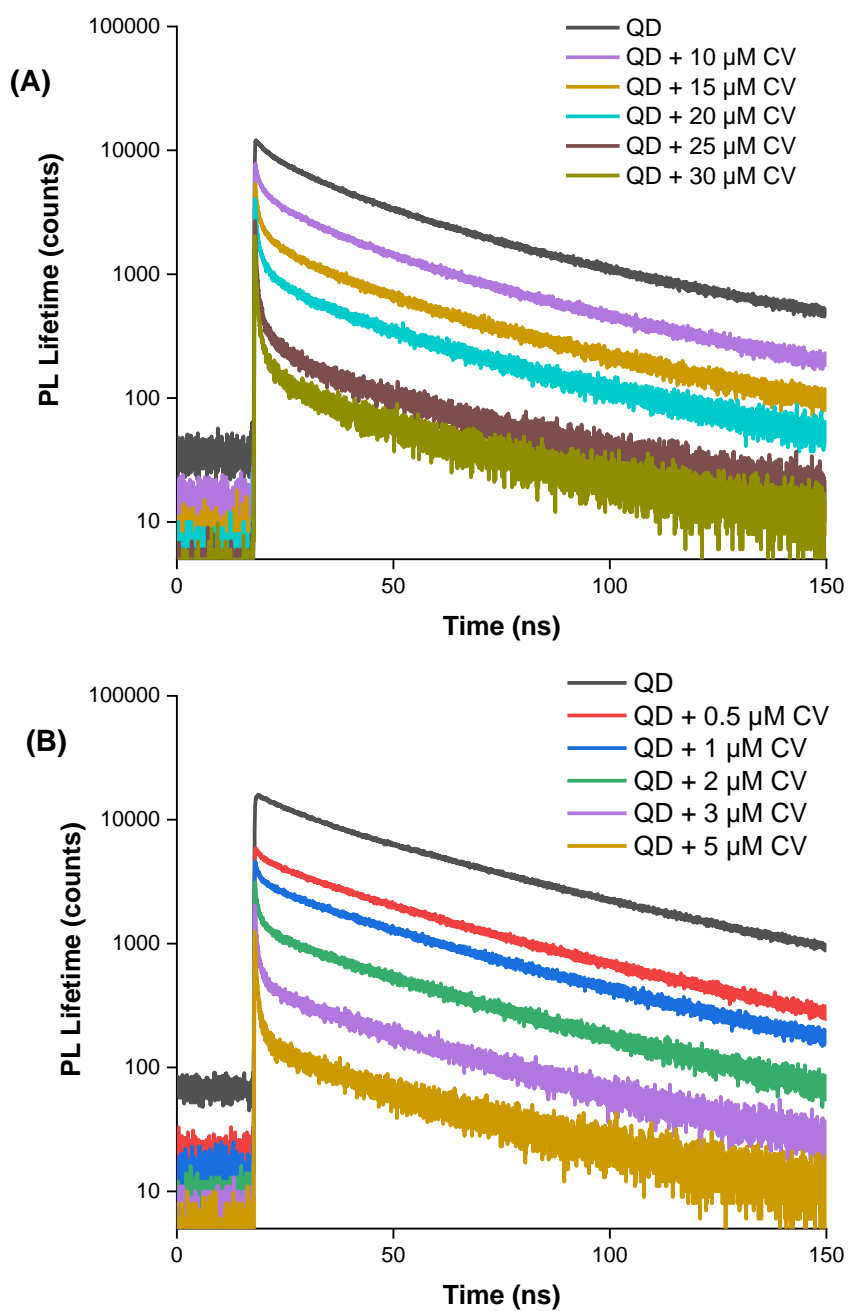


Figure 2.7 Logarithmic plots of time-resolved fluorescence intensities using the time correlated single photon counting method, recorded after pulsed excitation at 400 nm. **(A)** Red-emitting QDs and QD-CV mixtures with increasing CV concentrations (10  $\mu\text{M}$  – 30  $\mu\text{M}$ ). **(B)** Green-emitting QDs and QD-CV mixtures with increasing CV concentrations (0.5  $\mu\text{M}$  – 5  $\mu\text{M}$ ).

Table 2.2 Donor/acceptor lifetime analysis data for red QD and red QD-CV complexes. Pre-exponential components ( $A_1$  and  $A_2$ ), emission lifetimes ( $\tau_1$  and  $\tau_2$ ) and amplitude weighted lifetime ( $\tau_0$ ) of the QDs with increasing CV concentration are shown.

	$A_1$ (counts)	$\tau_1$ (ns)	$A_2$ (counts)	$\tau_2$ (ns)	$\tau_0$ (ns)
Red QD	1722	73	2152	25	46
Red QD + 10 $\mu$ M CV	756	22	865	64	44
Red QD + 15 $\mu$ M CV	446	58	248	20	44
Red QD + 20 $\mu$ M CV	351	53	215	18	40
Red QD + 25 $\mu$ M CV	181	41	103	6	28
Red QD + 30 $\mu$ M CV	92	31	50	0	20

Table 2.3 Donor/acceptor lifetime analysis data for green QD and green QD-CV complexes showing pre-exponential components ( $A_1$  and  $A_2$ ), emission lifetimes ( $\tau_1$  and  $\tau_2$ ) and amplitude weighted lifetime ( $\tau_0$ ) of the QDs with increasing CV concentration.

	$A_1$ (counts)	$\tau_1$ (ns)	$A_2$ (counts)	$\tau_2$ (ns)	$\tau_0$ (ns)
Green QD	2009	94	7089	36	49
Green QD + 0.5 $\mu$ M CV	622	90	2280	35	47
Green QD + 1 $\mu$ M CV	945	65	1523	29	42
Green QD + 2 $\mu$ M CV	644	51	367	21	40
Green QD + 3 $\mu$ M CV	276	44	65	13	38
Green QD + 5 $\mu$ M CV	203	40	43	6	34

Assuming the QD lifetime shortening was due to FRET only, the FRET efficiency (E) of donor/acceptor complexes in polymer was derived from the time-resolved fluorescence measurements, using the equation:

$$E = 1 - \frac{\tau_{DA}}{\tau_D}$$

where  $\tau_{DA}$  and  $\tau_D$  are the average fluorescence lifetime (amplitude weighted) of the donor in the presence and absence of the acceptor, respectively in 1:1 Cy/DCM solution.<sup>433, 443</sup> The FRET efficiencies of the QD-CV complexes are tabulated in Table 2.4 and Table 2.5.

Table 2.4 Amplitude weighted lifetimes ( $\tau_0$ ) and corresponding FRET efficiencies (E) for red QD-CV complexes

CV Concentration ( $\mu\text{M}$ )	$\tau_0$ (ns)	FRET Efficiency (%)
0	46.3	0
10	44.2	4.3
15	44.3	4.4
20	39.6	14
25	28.1	39
30	20.0	57

Table 2.5 Amplitude weighted lifetimes ( $\tau_0$ ) and corresponding FRET efficiencies (E) for green QD-CV complexes.

CV Concentration ( $\mu\text{M}$ )	$\tau_0$ (ns)	FRET Efficiency (%)
0	49.1	0
0.5	46.8	5
1	42.3	14
2	40.1	18
3	38.3	22
5	33.8	31
8	22.0	55

### 2.3.6. Stern-Volmer Relationship

The static or dynamic nature of the quenching processes was measured using Stern-Volmer plots. The decrease in emission intensity is described by the Stern–Volmer (SV) relationship in Equations 2.10 and 2.11:

$$F_0/F = 1 + K_{SV}[Q] \quad \text{Equation 2.10}$$

$$K_{SV}[Q] = k_q \times \tau_0 \quad \text{Equation 2.11}$$

where  $F_0$  and  $F$  are the emission intensities in the absence and presence of acceptor respectively,  $[Q]$  the quencher (crystal violet) concentration and  $K_{SV}$  the Stern–Volmer quenching constant.<sup>215</sup>

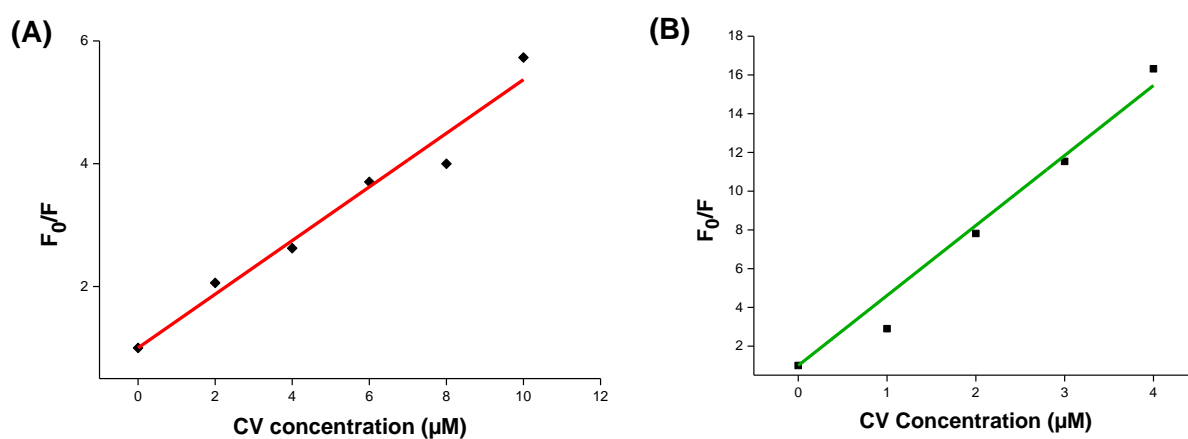


Figure 2.8 Stern-Volmer (S-V) relationships. **(A)** S-V relationship of QD quenching vs. CV concentration in solution at 620 nm. ( $\lambda_{ex}$  at 400 nm). **(B)** S-V relationship of QD quenching vs. CV concentration in solution at 500 nm ( $\lambda_{ex}$  at 400 nm).

Table 2.6 Stern-Volmer quenching constants ( $K_{SV}$ ), amplitude weighted lifetimes of QDs in the absence of quencher ( $\tau_0$ ) and bimolecular quenching constants ( $k_q$ ) of QDs upon addition of quencher in solution phase.

Quantum Dot	$K_{SV}$ ( $\text{M}^{-1}$ )	PL Lifetime, $\tau_0$ (ns)	$k_q$ ( $\text{M}^{-1}\text{s}^{-1}$ )
Red	$4.4 \times 10^5$	46	$8.9 \times 10^{12}$
Green	$3.6 \times 10^6$	49.1	$7.4 \times 10^{14}$

Dynamic quenching involves deactivation of the QD exciton upon contact with the quencher, in this case the CV molecules present in solution. Conversely, in static quenching, a complex is formed between the QD and the quencher, which in this case would arise from adsorption of the CV onto the QD surface, and the photoluminescence quenching can arise from either energy or electron transfer processes.<sup>215, 444</sup> The SV relationship ( $F_0/F$  against  $[Q]$ ) was plotted at 620 nm ( $\lambda_{ex} = 400$  nm) for red QDs and at 500 nm ( $\lambda_{ex} = 400$  nm) for green QDs with CV as the acceptor in a solvent system of 1:1 cyclohexane/dichloromethane. The results are shown in Figure 2.8. In both cases, the SV relationships are linear with slopes,  $K_{SV}$ , of  $4.4 \times 10^5 \text{ M}^{-1}$  and  $3.6 \times 10^6 \text{ M}^{-1}$  for red and green QDs respectively. This is indicative of a single class of fluorophores, all equally accessible to the quencher.<sup>215</sup> To confirm this, the bimolecular quenching constants ( $k_q$ ) was estimated from Equation 1.12 using the slopes obtained from the Stern–Volmer analyses ( $K_{SV}[Q]$ ) and the derived amplitude weighted lifetimes of the QD donors ( $\tau_0$ ) in solution. The bimolecular quenching constants ( $k_q$ ) for red and green QDs on addition of CV are summarised in Table 2.6. The  $k_q$  values are large for both QDs, more than two orders of magnitude higher than the diffusion-controlled limit for bimolecular reactions ( $\sim 10^{10} \text{ M}^{-1}\text{s}^{-1}$ ), signifying binding interactions between the QDs and CV; and that the interactions were predominantly static in nature with CV bound to the QD surface.<sup>445</sup> Therefore, in the solution-phase, adsorption of CV onto the QD surface is the key way that the donor and acceptor entities interact – thus PET reactions would be favoured as these depend on much closer-range distances than FRET. In the polymer, however, PET contributions to QD quenching (and therefore ROS production) may differ due to the different microenvironment. This is discussed further in CHAPTER 4 and CHAPTER 6.

Under the same experimental conditions, the  $K_{SV}$  value for green QDs was a whole order of magnitude higher than the  $K_{SV}$  value derived for the red QDs (Table 2.6), showing that the photophysical interaction between green QDs and CV was stronger than the red QDs.<sup>409</sup> The effect may be due to the smaller diameter of the green QDs compared to red QDs (2.9 nm versus 3.6 nm for the red QDs), in accord with the quantum confinement effect on the band gap. The larger surface to volume ratio of the green QDs will confer a higher ratio of the electronegative capping ligands per unit inorganic mass, thereby enhancing the propensity for electrostatic surface binding of the cationic CV molecule. Not only are electrostatic bindings between green QDs and CV enhanced but the stronger electronegative charge on the green

QDs may enable the array of more CV molecules per single green QD nanoparticle, producing a proportional increase in the FRET efficiency compared to a one-to-one donor-acceptor pairing. Since the solution employed for incorporation of the QDs and CV into the polymer contained a mixture of the two moieties, strong binding should promote direct uptake of QD + CV complexes into the polymer. Under this scenario, quenching of the QD PL should therefore occur in the polymer when co-administered with CV.

### 2.3.7. Singlet Oxygen Phosphorescence Measurements

Thus far, with the exception of overlap integral analyses, data from steady-state and time-resolved fluorescence studies have shown that QD-CV have been consistent with *both* FRET and PET occurring. It is not possible to conclude that FRET occurs based on these studies alone. However, since only FRET interactions produce singlet oxygen, any  $^1\text{O}_2$  generated by the QD-CV complexes would give definitive proof of FRET. With this in mind, direct measurement of  $^1\text{O}_2$  phosphorescence was carried out in solution. Using a Nd:YAG laser at 532 nm as the excitation source,  $^1\text{O}_2$  phosphorescence was monitored at 1270 nm. QD emission extends to the near-infrared though the photoluminescence around 1270 nm is very weak; however  $^1\text{O}_2$  phosphorescence has a low quantum yield and weak phosphorescence therefore at 1270 nm, QD PL was still detectable. A short-lived spike, lasting  $\sim 10 \mu\text{s}$  for green QDs and  $\sim 15\text{-}18 \mu\text{s}$  for red QDs (signal for red QD stronger at 1270 nm as its emission was nearer to IR wavelengths than green QDs which emitted at far shorter wavelengths) after the laser pulse at  $t = 0$  was ascribed to the residual QD PL. Due to the long-lived QD PL spike lasting up to about  $10\text{-}20 \mu\text{s}$ , the integrated phosphorescence signal was calculated from  $\sim 30 \mu\text{s}$  onwards up to  $50 \mu\text{s}$ , to ensure that only the phosphorescence signal was measured, an analysis method that has been used previously in other studies on  $^1\text{O}_2$ .<sup>446</sup>

In control experiments of Cy/DCM solutions containing QDs, no  $^1\text{O}_2$  phosphorescence was detected, showing that they were not able to produce any detectable amounts of  $^1\text{O}_2$ . Similarly, excitation of a CV only solution resulted in no detectable singlet oxygen despite the fact that CV absorbs strongly at the excitation wavelength of 532 nm (not shown). The absence of  $^1\text{O}_2$  was due to the molecular rotor effect that destabilises the excited singlet state and thus drastically reduces intersystem crossing to the triplet state that interacts with oxygen to generate  $^1\text{O}_2$ . In the polymer, the rotor effect is much weaker so in this environment,  $^1\text{O}_2$  can be detected from CV only polymer samples (see CHAPTER 6). In contrast,  $^1\text{O}_2$  was detected

with QD + CV solution, consistent with inhibition of the molecular rotor effect when the CV is complexed with the QD surface, providing indirect evidence for QD/CV binding. At 532 nm, both the QD and CV can be excited (unlike 405 nm – the excitation wavelength used in steady-state emission studies – which excites only the QDs) so the signal observed may be a mixture of direct excitation of CV that is bound to the QDs and energy transfer.

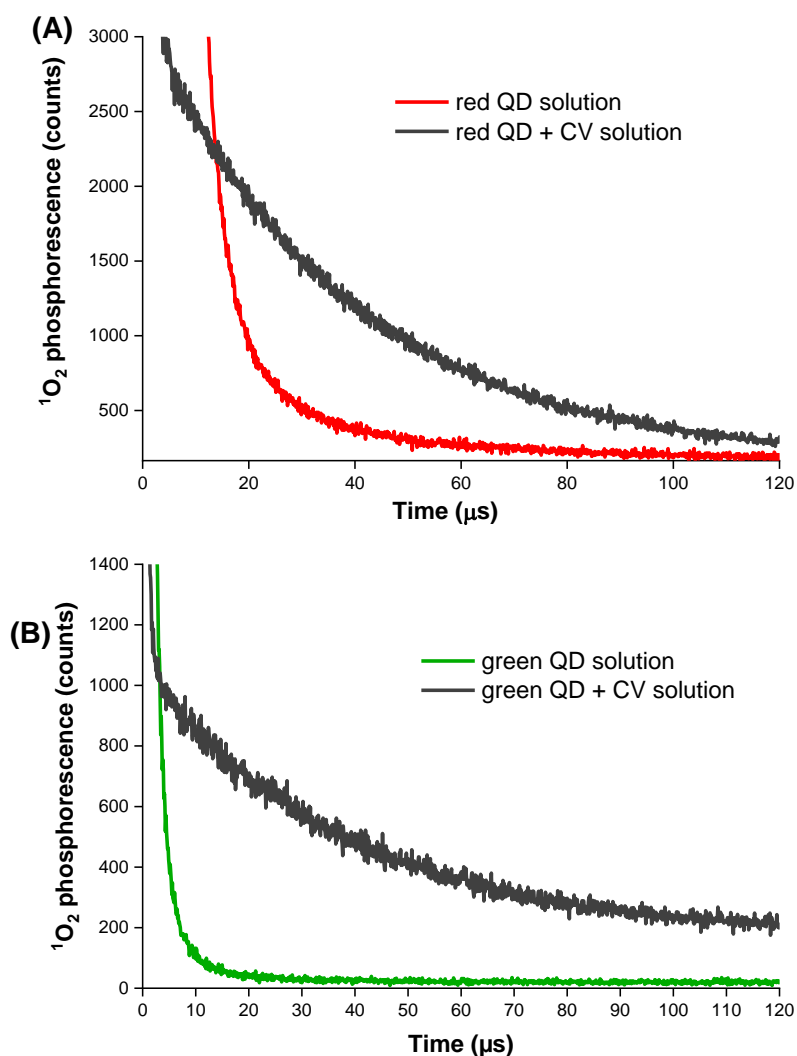


Figure 2.9 Time-resolved  $^1\text{O}_2$  phosphorescence at 1270 nm after pulsed laser irradiation of 1:1 cyclohexane/DCM solutions containing QDs only and QDs combined with CV. (A) Red QDs and red QD combined with CV. (B) Green QDs and green QDs combined with CV.

Analysis of  $^1\text{O}_2$  production by the QD-CV complexes in solution phase was carried out. The decay curves of the QD-CV complexes in a solvent system of 1:1 cyclohexane/DCM (Cy/DCM)

were fitted to a single exponential (equation 2) where  $I_t$  is the phosphorescence intensity, and  $A$  and  $\tau$  are the fractional amplitude and emission lifetime respectively (Figure 2.9). Using green QDs as an example, an average amplitude weighted  $^1\text{O}_2$  lifetime of  $3.79 \times 10^{-5}$  s was determined and subsequently, the rate constant of decay of  $^1\text{O}_2$  in 1:1 Cy/DCM was determined to be  $2.64 \times 10^4 \text{ s}^{-1}$  from the reciprocal of this value.  $^1\text{O}_2$  photo-generated via FRET can be quenched by both Cy and DCM and in a mixed system of these 2 solvents, the decay rate constant of  $^1\text{O}_2$  ( $k_d$ ) may be expressed as follows:

$$k_d = x_1 k_1 + x_2 k_2 \quad \text{Equation 2.12}$$

where  $x_1$  and  $x_2$  are the mole fractions of Cy and DCM in the systems respectively and  $k_1$  and  $k_2$  are the  $^1\text{O}_2$  decay rate constants from the reported  $^1\text{O}_2$  lifetimes in each solvent.<sup>447</sup> In 1:1 Cy/DCM,  $x_1 = x_2 = 0.5$ . The literature reports  $^1\text{O}_2$  lifetimes as  $2.3 \times 10^{-5}$  s in Cy and  $9.9 \times 10^{-5}$  s in DCM, yielding values of  $4.3 \times 10^4 \text{ s}^{-1}$  and  $1.0 \times 10^4 \text{ s}^{-1}$  for the  $^1\text{O}_2$  decay constant in Cy and DCM respectively.<sup>448, 449</sup> Applying Equation 2.12, this corresponded to a literature  $^1\text{O}_2$  decay rate constant of  $2.68 \times 10^4 \text{ s}^{-1}$  of in 1: 1 Cy/DCM. This value was in excellent agreement (within 2%) with the experimental  $^1\text{O}_2$  decay rate constant of  $2.63 \times 10^4 \text{ s}^{-1}$ , indicating that in solution,  $^1\text{O}_2$  quenching occurred only through interaction with solvent vibrational modes and not the CV or QD solute. The detection of  $^1\text{O}_2$  in QD + CV solutions is consistent with the hypothesis that in addition to PET, green QD-CV and red QD-CV complexes undergo FRET interactions in solution-phase.

### 2.3.8. Electron Transfer Interactions

Photoexcitation of either the QDs or CV may result in electron donation to CV, which is a good electron acceptor, and the reduced CV radical can then interact with oxygen to form  $\text{O}_2^{\bullet-}$ , as has been previously demonstrated by various groups.<sup>421, 430, 450</sup> To investigate the occurrence of PET mechanisms in the QD-CV complex, electron paramagnetic resonance (EPR) studies were performed. EPR spectroscopy is a technique used to detect species with unpaired electrons (a species with unpaired electrons is paramagnetic). EPR is based on the detection of the transitions of unpaired electrons in an applied magnetic field. An electron has a spin which gives it a magnetic property known as a magnetic moment. When an external magnetic field is applied, the unpaired electrons can either orient in a direction parallel or antiparallel to the direction of the magnetic field. This creates two distinct energy levels for the unpaired electrons and allows measurement as they are driven between the two levels. The separation

between the two spin states ( $m_s = \pm 1/2$ ) is called the Zeeman effect and is proportional to the magnetic field. Microwave frequencies are applied and absorbed when the energy of the microwaves exactly match the energy level separation of the spin states (known as the resonance condition). Only species with unpaired electrons are detectable by EPR making EPR spectroscopy useful across several disciplines including chemistry, medical sciences and biology. This method is the technique of choice for the study of free radicals as it is highly sensitive and specific for measuring low concentrations and while other techniques provide information, only EPR spectroscopy yields direct evidence of the presence of free radicals.<sup>451, 452</sup> Free electrons, particularly in liquid systems, are very short-lived therefore ROS such as  $\bullet\text{OH}$ ,  $\text{O}_2^{\bullet-}$  and alkyl radicals ( $\bullet\text{R}$ ) cannot be detected conventionally. To overcome this, a spin trapping can be added to the system under consideration. A spin trapping agent is a diamagnetic molecule that readily reacts with the primary unstable radical of interest to form stable, paramagnetic spin adducts that are more persistent and whose concentration can reach detectable levels. DMPO (5,5-dimethyl-1-pyrrolyne N-oxide) is a chemical commonly used as a spin trap, particularly for the detection of  $\bullet\text{OH}$  or  $\text{O}_2^{\bullet-}$ .<sup>451, 453</sup> It has been reported that irradiated InP QDs can generate  $\text{O}_2^{\bullet-}$  and earlier in this chapter, we showed that it is energetically feasible for CV with InP QDs to generate  $\text{O}_2^{\bullet-}$  so DMPO was an appropriate choice.<sup>153</sup> The generation of free radicals with indium-based QDs in cyclohexane was measured using the spin trapping technique in combination with EPR spectroscopy. DMPO dissolved in cyclohexane served as the spin trapping agent. We did not try TEMPO (2,2,6,6-Tetramethylpiperidine 1-oxyl) for  $^1\text{O}_2$  detection as it can be misleading.<sup>454, 455</sup>

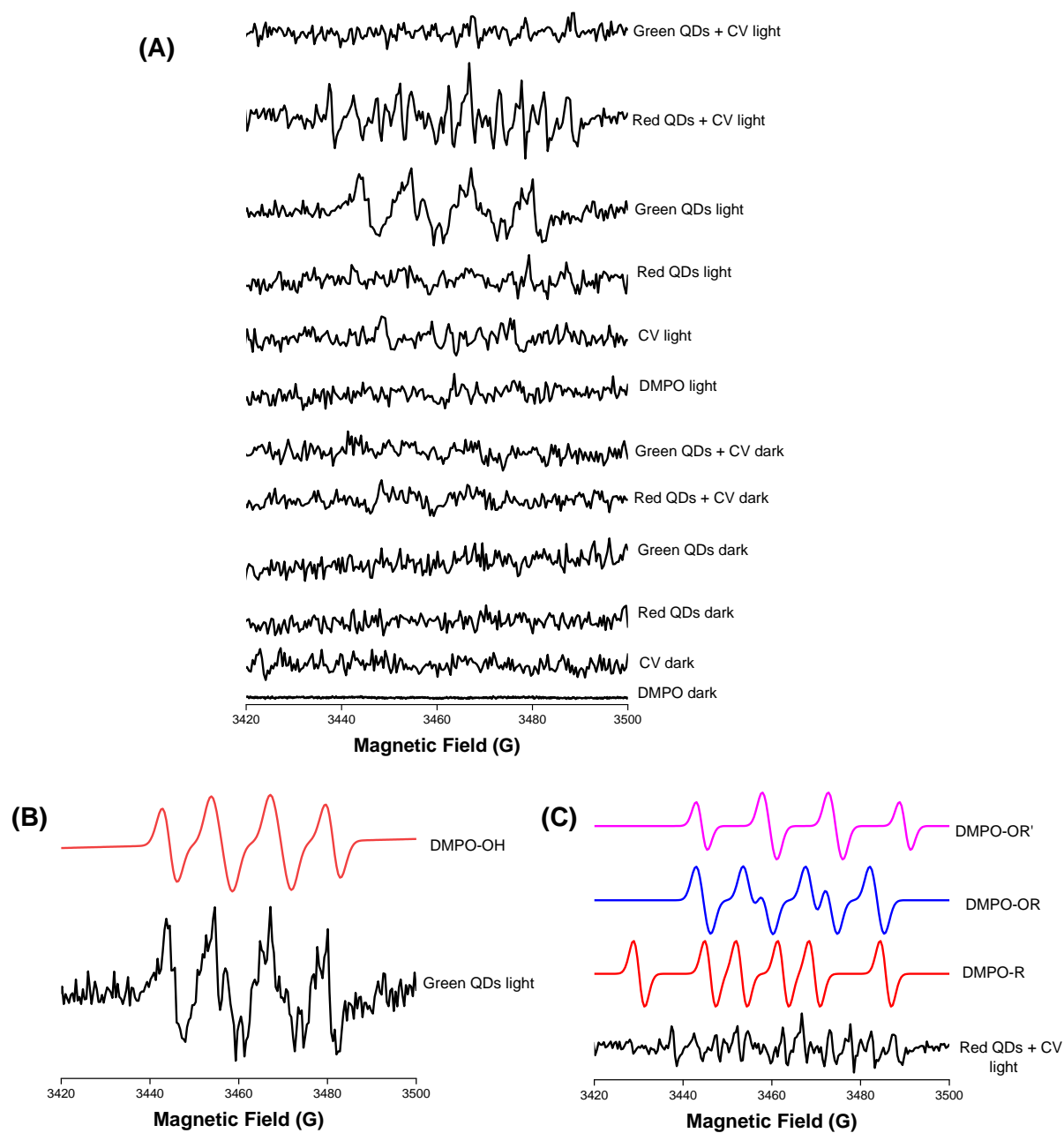


Figure 2.10 **(A)** EPR spectra for QDs with/without CV with controls. **(B)** EPR spectrum of irradiated green QDs and computer simulation for DMPO/hydroxyl adduct (red trace). **(C)** EPR spectrum of irradiated red QDs mixed with CV and computer simulations of oxygen-centred DMPO adducts (purple and blue traces) and a carbon-centred DMPO adduct (red trace). Final concentrations – DMPO: 250 mM; red QD – 12.5 mg/mL; green QD – 40 mg/mL; CV – 0.4 mM

Freshly prepared solutions of QDs and QDs + CV in cyclohexane (final concentrations of red QD – 12.5 mg/mL, green QD – 40 mg/mL and CV – 0.4 mM) and DMPO was added to the solutions with a final concentration of 250 mM. Samples were illuminated with 455 nm light for 10 minutes and the EPR measurements were performed immediately afterwards. Control studies on the solutions without light illumination were also performed. Figure 2.10 displays the signals that were obtained. Signals were obtained only for green QDs on their own (illuminated) and red QDs combined with CV (illuminated) (Figure 2.10A and B). Illuminated CV in solution did not produce an EPR signal as triarylmethane dyes are naturally EPR silent. Due to the molecular rotor effect, free photoexcited CV will not generate ROS unless bound. For example, using EPR, Brezova and colleagues were able to demonstrate that the photo-generation of  $O_2^{\bullet-}$  from CV only after binding CV to paper to minimise rotor effects.<sup>456</sup> Furthermore, as illustrated by a lack of signal, no  $O_2^{\bullet-}$  or  $\bullet OH$  were generated by the red-emitting QDs within the signal resolution of the spectrometer (Figure 2.10A). This was the case even after extending the irradiation times to 12 min and 15 min. This was in contrast to the green QDs which produced EPR signals corresponding to spin adducts formed by the reaction of DMPO with hydroxyl radicals (Figure 2.10B). This was very likely to be simply due to the higher exciton energy of the green QDs – they emit at a shorter wavelength so the energy level is higher which will make the direct electron transfer more favourable energetically. We also observed that red QDs mixed with CV produced EPR signals corresponding to the production of carbon-centred radicals (Figure 2.10C).<sup>457, 458</sup> The EPR spectrum observed when red QDs and CV are mixed together in solution implied that PET processes took place between the red QD and CV when in close proximity.

Additionally, no ROS were detected by EPR when green QDs were combined with CV dye. This result, along with the observation that CV was bleached following irradiation of green QDs + CV in solution, indicated the green QDs appeared to oxidise the molecular dye. It may be that the ROS produced by the green QDs are what caused the CV dye to photo-bleach. The larger bandgap for green QDs enables production of more  $O_2^{\bullet-}$  and  $\bullet OH$  however it does not appear to produce enough to cause a loss in bacterial cell when embedded in polymer (see CHAPTER 3).<sup>153</sup> Another plausible reason for the negative EPR results in solution when using the green QD/CV mixtures may have to do with the strength of the electrostatic binding between the green QDs and CV. If we assume that PET plays an important role for the green QD/CV mixtures then it is possible that the ion pairs may undergo charge recombination resulting in quenched QD and CV being unchanged.<sup>459</sup> This process can be very fast so there

may not be enough time for the CV radical anion to interact with oxygen to form superoxide. Since the binding of CV to the green QDs appears to be stronger from the Stern-Volmer data, then this mechanism may well be important and explain the absence of EPR signals. Conversely, with the red QDs perhaps charge separation is longer-lived and may explain why evidence of ROS was observed with the red QD/CV combination. In line with the rationale, it is worth noting that the PL lifetime profile of the green QDs in solution does not change much at higher CV which would be consistent with very fast charge recombination quenching. Even at low CV concentrations, the amplitude (A) component of the green QD lifetime declined substantially which may be a result of rapid charge recombination (Table 2.3).

## 2.4. Conclusion

This study presented a novel QD-PS nanocomposite composed of indium-based cadmium-free QDs and CV. Steady-state and time-resolved photoluminescence measurements indicated that the complex engaged in both PET and FRET. PET interactions between the acceptor and donor was supported by redox potential evaluations, showing that electron transfer reactions from excited QDs to CV were energetically feasible followed by subsequent electron transfer reactions with molecular oxygen to form  $O_2^{\bullet-}$ . PET interactions were supported in part by EPR spectroscopy. Further, FRET interactions were confirmed between the QDs and CV using singlet oxygen phosphorescence. Since  $^1O_2$  was a product of energy transfer, the generation of  $^1O_2$  when QDs were combined with CV in solution provided conclusive evidence of the occurrence of FRET.

# CHAPTER 3. QUANTUM DOTS IN POLYMER AS LIGHT-ACTIVATED ANTIMICROBIAL AGENTS

## 3.1. Introduction

Self-disinfecting light-activated surfaces are increasingly being widely studied as a means to reduce the bacterial contamination on surfaces and the transmission of bacteria from inanimate surfaces to humans. In the clinical setting, this is particularly important as indirect contact, the transmission of infections via contact with inanimate surfaces after contamination by colonised or infected hosts, is the biggest driver of hospital acquired infections.

A particular advantage of light-activated surfaces is the low likelihood of microbes developing resistance, as singlet oxygen utilises a non-specific, multi-site mechanistic mode of destroying microorganisms. Substrates such as titania, glass and stainless steel have been investigated for this application<sup>390-392, 460-463</sup>, however generally, impregnation of polymers with light-activated agents offers a more versatile and simple solution to the problem due to the flexibility, relative cheapness and durability of polymers. Silicone, cellulose acetate, polyurethane as well as polymer resins are examples of polymers that have been combined with many different dyes and nanoparticles and utilised for this purpose.<sup>395, 397, 402, 405, 408</sup>

Attachment of nanoparticles and dyes to the surface of polymers can be achieved via such methods such as physical deposition, chemical deposition and co-solution.<sup>464</sup> Swell-encapsulation-shrink is another technique that has been successfully employed to integrate active antimicrobial agents into polymers such as polyurethane, silicone, polyvinyl chloride and polydimethylsiloxane, endowing these with antimicrobial activity.<sup>401-405</sup> In swell-encapsulation, the polymer substrate is immersed in a swelling solution made up of the active material dissolved in an appropriate solvent. The solution expands the polymer, creating space for the antimicrobial agents to impregnate the polymer matrix. Evaporation of the solvent simultaneously shrinks the polymer back to its original size and locks in the active material.<sup>411</sup>

QDs are attractive as PS due to their broad absorption, allowing activation by conventional lamps; their large surface area that can be functionalised; their high thermal and photo

stability; and their ability to generate reactive oxygen species (ROS) upon light exposure. This makes them ideal as light-activated antimicrobial agents.

In this section, fluorescent indium-based QD nanoparticles were incorporated into polyurethane using swell-encapsulation-shrink and subsequently characterised via a range of spectroscopic measurements. The bactericidal activity of QD-incorporated polymer substrates was then evaluated, in the dark and upon exposure to white light, against clinically important Gram-negative and Gram-positive bacteria.

## **3.2. Materials & Methods**

### **3.2.1. Synthesis of Indium-based Nanoparticles**

Please see the previous chapter for nanoparticle synthesis methods

### **3.2.2. Polymer Samples Preparation**

All work used flat medical grade polyurethane sheets (American Polyfilm Inc, USA) of 0.8 mm thickness, cut to 1 cm<sup>2</sup> squares, unless otherwise stated.

### **3.2.3. Optimisation of QD Uptake into Polymer from Solvent**

1 cm<sup>2</sup> polyurethane squares were immersed in the following cyclohexane:dichloromethane (Cy:DCM) ratios – 1:0, 2:1, 1:1, 1:2 and 0:1. They were allowed to swell for 24 h in the dark, removed, air-dried overnight, and subsequently washed with dH<sub>2</sub>O and towel-dried.

### **3.2.4. Polymer Samples for Antibacterial Testing**

Polymer samples were prepared using the 'swell-encapsulation-shrink' method adapted from Perni *et al.*<sup>403</sup> The following modified polyurethane samples (1 cm<sup>2</sup>) were prepared for antimicrobial testing:

1. Control samples: Polyurethane was treated in neat 1: 1 Cy/DCM solvent mixture for 24 h removed, air-dried overnight, and subsequently washed with deionised water and air-dried.
2. Red/green QD-encapsulated polyurethane: Stock concentrations of QDs (red or green) were made in Cy at 2 mg/mL concentration. From the stock, dipping solutions at 1mg/mL QD concentration were prepared in 1: 1 Cy/DCM solvent. 10 mL of the QD

dipping solution was added to a sample vial and then 4 polyurethane squares were immersed in the vials for 24 h in the dark. Subsequently, the squares were removed, air-dried overnight, and washed with deionised water and air-dried. (Figure 3.1)

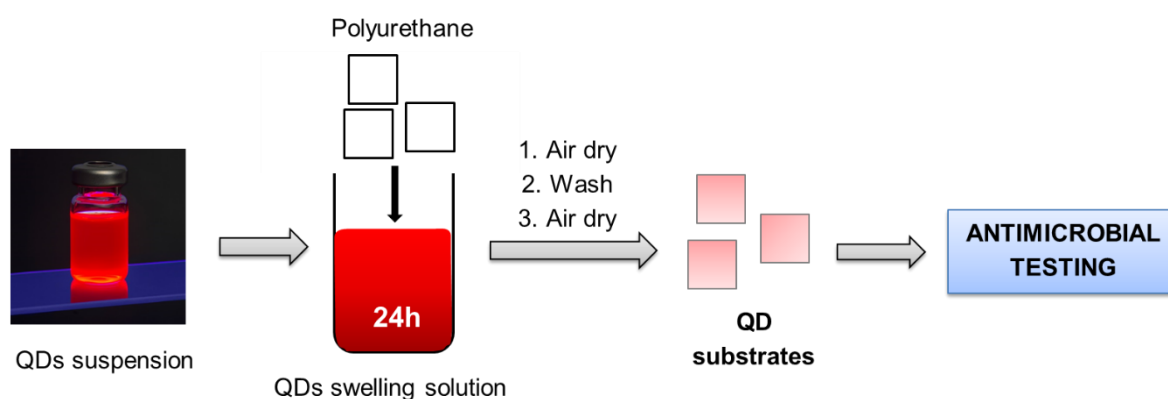


Figure 3.1 Schematic diagram illustrating the preparation of QD-encapsulated polyurethane from QD solution via swell-encapsulation-shrink for antimicrobial testing

### 3.2.5. Characterisation of Modified Polymer Samples

A Shimadzu UV-Vis spectrometer (400 – 750 nm range) was used to measure the absorption spectra of all modified polymer samples. Absorption of the dipping solutions before and after swell-encapsulation-shrink was also measured to estimate QD uptake by the polymer. Emission spectra of suspensions was recorded with the Horiba FMax4 Fluorimeter (405 – 790 nm) at the excitation wavelength of 400 nm. X-ray photoelectron spectroscopy (XPS) analysis was performed using a Thermo Scientific *K-Alpha* spectrometer to detect indium and zinc as a function of polymer depth, and all binding energies were calibrated to the carbon 1s peak at 284.4 eV

### 3.2.6. Antibacterial Activity

#### 3.2.6.1. Bacterial Strains

Laboratory strain *Staphylococcus aureus* (*S. aureus* NCTC 8325-4), methicillin-resistant *Staphylococcus aureus* (MRSA NCTC 13143) were obtained from the National Collection of Type Cultures (PHE, Colindale). EMRSA 4742, a clinical strain of epidemic MRSA was obtained from P. Wilson, University College London Hospital. *Escherichia coli* (*E. coli* ATCC 25922) was obtained from the American Type Culture Collection (USA). *E. coli* 1030, a

multidrug resistant clinical strain of *E. coli* which produces both NDM-1 and OXA-48 carbapenemases, was obtained from J. Wade, King's College Hospital, London.

### 3.2.6.2. Microbiology Assay

The following 1 cm<sup>2</sup> polyurethane samples were prepared:

- i. solvent treated polyurethane (control PU)
- ii. red quantum dot-encapsulated polyurethane (rQD PU) and green quantum dot-encapsulated polyurethane (gQD PU)

The antibacterial activity of these samples was tested against laboratory strain *E. coli* ATCC 25922, *E. coli* 1030, *S. aureus* 8325-4, and EMRSA 4724. These organisms were stored at -70°C in Brain-Heart Infusion broth (BHI, Oxoid) containing 20% (v/v) glycerol and propagated onto either MacConkey agar (MAC, Oxoid) in the case of *E. coli* or Mannitol Salt agar (MSA, Oxoid) in the case of *S. aureus* for a maximum of 2 subcultures at intervals of 2 weeks. BHI broth was inoculated with 1 bacterial colony and cultured in air at 37°C for 18 h with shaking, at 200 rpm. The bacterial pellet was recovered by centrifugation, (20 °C, 2867.2 g, 5 min), washed in PBS (10 mL), centrifuged again to recover the pellet (20 °C, 2867.2 g, 5 min), after which the bacteria were finally re-suspended in PBS (10 mL). The washed suspension was diluted 1,000-fold to obtain an inoculum of ~10<sup>6</sup> cfu/mL. In each experiment, the inoculum was confirmed by plating 10-fold serial dilutions on agar for viable counts. Triplicates of each polymer sample type were inoculated with 25 µL of the inoculum and covered with a sterile cover slip (2.2 cm<sup>2</sup>). The samples were then incubated in the dark and in the light (General Electric 28 W Watt Miser™ T5 2D compact fluorescent lamp) emitting an average light of 6600 ± 990 lux at a distance of 25 cm) for up to 4 h for the modified polyurethane samples, for Gram-negative and Gram-positive microorganisms respectively. After incubation, the inoculated samples and coverslips were added to PBS (450 µL) and mixed using a vortex mixer. The neat suspension and 10-fold serial dilutions were plated on agar for viable counts and incubated aerobically at 37 °C for 24 h (*E. coli*) or 48 h (*S. aureus*).

### 3.2.6.3. Log and Percentage Reductions in Antimicrobial Studies

The antimicrobial effectiveness of the test materials was determined by counting the number of colony forming units (CFUs) of a given bacteria present after treatment on the test material and comparing this to the number of CFUs on the control material. The difference between

the control and the test materials was expressed as either a log reduction or a percentage reduction.

$$\text{Log Reduction} = \log_{10}(A/B)$$

$$\text{Percentage Reduction} = (A - B) \times 100 / A$$

Where A = the number of bacterial CFUs present before treatment (control material)

B = the number of CFUs present after treatment (test material)

#### 3.2.6.4. Statistical Analysis

The experiment was repeated three times and the statistical significance was analysed using the student's T-test to compare QD-incorporated polymer vs. control polymer. Error bars show the standard deviation from the mean. Statistically significant results have  $p < 0.05$ . \* denotes  $p < 0.05$ , \*\* denotes  $p < 0.01$  and \*\*\* denotes  $p < 0.001$ .

### 3.3. Results & Discussion

#### 3.3.1. Optimisation of Polymer Swelling

The nanoparticles were incorporated into polyurethane using a simple and efficient 'swell-encapsulation-shrink' method (Figure 3.1). This method has proven highly successful at introducing antibacterial functionality to polymers by impregnating a wide range of small nanoparticles into their matrices.<sup>403, 404, 406, 408</sup> Swell-encapsulation depends on factors such as the polarity and volatility of the solvent, the thickness of the polymer and the length of swelling time all affect the rate of NP uptake.<sup>405, 411</sup> The extent of polymer swelling is proportional to the rate of QD uptake and polymer swelling is greatly affected by the solvent system employed. An important consideration when impregnating polymers via swell-encapsulation-shrink is that although a higher rate of swelling positively correlates to higher nanoparticle uptake, over-expansion of the polymer by the solvent may cause misshapeness of the substrate, changing the polymer physical properties and making antimicrobial testing difficult. To avoid this issue, a series of cy/DCM solvent ratios were tested to determine the best solvent for QD encapsulation. To determine the best solvent system for QD-encapsulated polymers, 1cm<sup>2</sup> polyurethane (PU) squares were submerged in a number of solvents and solvent mixtures. The increase in size of 1cm<sup>2</sup> PU squares in different solvent systems, after immersion for 24 h to maximise PU expansion, is displayed in Table 3.1.

Only appropriate organic solvents were considered as the indium-based QDs were suspended in organic solvent and attempts to make them water-soluble would have required additional manipulation that would increase their overall size and thus change their fundamental properties, as discussed in CHAPTER 1 (Section 1.1.4). The indium-based core/shell QDs were suspended primarily in cyclohexane (Cy) however, PU does not expand in Cy alone therefore dichloromethane (DCM) was explored as a miscible solvent. DCM is a very polar solvent and on its own, caused the polymer to swell to double its size in 24 h. However, after evaporation of DCM, the resulting PU was deformed. Bending was also observed for the 1:2 Cy/DCM solvent-swelled PU after swelling to 70% its size. The best condition that caused PU expansion without bending or deformity was 1:1 Cy/DCM, which expanded the PU to 50%. Therefore, a 1:1 Cy/DCM solvent mixture was used to swell-encapsulate QDs into PU.

Table 3.1 Percentage polymer swelling of 1 cm<sup>2</sup> polyurethane samples after submersion in in different ratios of cyclohexane and dichloromethane for 24 h

<b>Cy:DCM Ratio</b>	<b>Extent of Polymer Swelling after 24 h (%)</b>	<b>State of Polymer after Swelling</b>
1:0	0	No deformity
2:1	40	No deformity
1:1	50	No deformity
1:2	70	Bent
0:1	100	Highly deformed

A range of methods may be used to incorporate antimicrobial agents into polymers including physical deposition and chemical deposition, co-solution and swell-encapsulation. Physical deposition techniques use Van der Waals forces, dipolar interactions or weak easily broken hydrogen bonds to form surface coatings whereas chemical deposition techniques change the surface by forming covalent bonds at the interface of NP and surface.<sup>465</sup> Both techniques build thin layers of active material at the surface which is particularly advantageous with expensive nanoparticles, however these techniques are often complicated and laborious. The primary means of NP incorporation into polymers is co-solution, the direct addition of NPs into the fabrication process, achieving an even distribution of NPs into the polymer matrix. For antimicrobial applications, this distribution may prove disadvantageous as the active material is often not required in the polymer bulk, only at the surface or just beneath the surface. In comparison, swell-encapsulation-shrink offers a facile means of incorporating antimicrobial agents into polymer. By controlling the solvent used, the length of immersion in the swelling solvent and the type of polymer, active material can be impregnated on the surface or further into the bulk.

### 3.3.2. Characterisation of QD-Incorporated Polyurethane

After swell-encapsulation, QD-incorporated PU looked very mildly discoloured compared to the control PU, a visual indication of QD uptake, confirmed by emission spectroscopy (Figure 3.2).

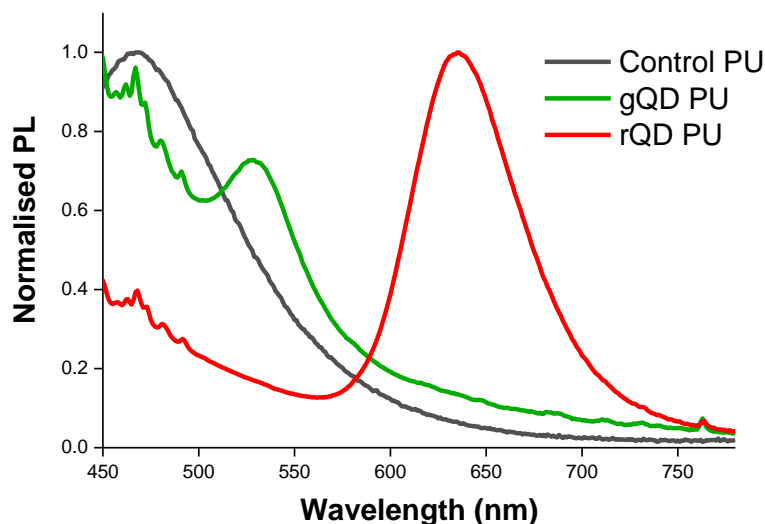


Figure 3.2 Plot showing normalised emission spectra of polyurethane solvent-treated (black line), encapsulated with green QDs (green line) and polyurethane encapsulated with red QDs (red line)

XPS was used to determine the efficacy of the 'swell-encapsulation-shrink' method for incorporating quantum dots into the polymer (Figure 3.3 and Figure 3.4). The control polymer and red/green QD-incorporated polymers displayed peaks attributed to the presence of carbon 1s (284.4 eV), nitrogen 1s (399.3 eV) and oxygen 1s (531.9 eV) on the surface, with no significant difference in percentage element composition between the samples (data not shown). XPS depth profile analysis for all samples demonstrated little change in carbon and nitrogen composition, but a decrease in oxygen content with polymer depth.

The presence of indium, which is present in the core of the QD nanoparticles, was detected on the polyurethane surface and within the substrate as peaks correlating to 444.3 eV and 451.9 eV (Figure 3.3A). Zn (2p) was also detected on the surface and in the bulk of QD-incorporated polyurethane substrates, at peaks of 1021.9 eV and 1044.7 eV. (Figure 3.3B)

For both In and Zn elements, the content was higher within the bulk of the red QD-embedded polymer in comparison to the surface. This trend was reversed in green QD-incorporated polyurethane substrates. Higher In (444.5 and 451.6 eV peaks) and Zn (1021.4 and 1044.6

eV peaks) contents were observed on the surface of the gQD PU substrates and less in the bulk (Figure 3.4).

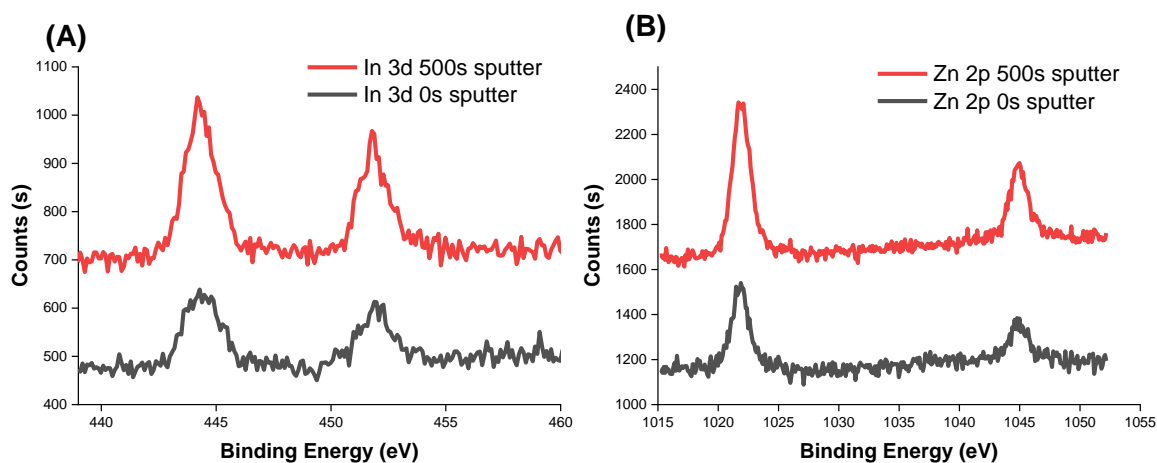


Figure 3.3 **(A)** In (3d) region XPS spectra for red QD-incorporated polyurethane at the surface, sputtered 0 s (black line) and red QD-incorporated polyurethane in the bulk, sputtered 500 s (red line). **(B)** Zn (2p) region XPS spectra for red QD-incorporated polyurethane at the surface, sputtered 0 s (black line) and red QD-incorporated polyurethane in the bulk, sputtered 500 s (red line).

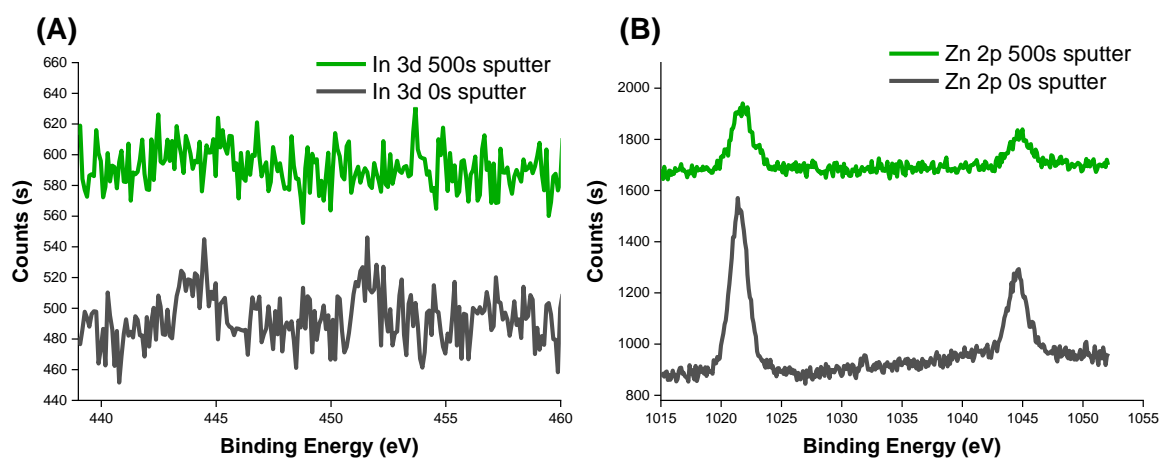


Figure 3.4 XPS analysis. **(A)** In (3d) region XPS spectra for green QD-incorporated polyurethane at the surface, sputtered 0 s (black line) and green QD-incorporated polyurethane in the bulk, sputtered 500 s (green line). **(B)** Zn (2p) region XPS spectra for green QD- incorporated polyurethane at the surface, sputtered 0 s (black line) and green QD-incorporated polyurethane in the bulk, sputtered 500 s (green line).

### 3.3.3. Antibacterial Activity

The antibacterial activity of the polymer samples modified via swell-encapsulation in 1mg/mL QDs suspensions was tested against two nosocomial pathogens: Gram-positive *S. aureus* (laboratory strain *S. aureus* NCTC 13143 and epidemic strain EMRSA 4742) and *E. coli* (laboratory strain *E. coli* ATCC 25922). Figure 3.5 illustrates the results for red QD-encapsulated polyurethane (rQD PU) against *S. aureus* after 1 h of white light illumination at  $6600 \pm 900$  lux (Figure 3.5A) and against *E. coli* after 2 h white light illumination at  $6600 \pm 900$  lux (Figure 3.5B). In all cases, the control PU did not display any significant kill of *S. aureus* or *E. coli*. For MRSA, neither rQD PU substrates incubated in the dark nor illuminated rQD PU substrates caused any significant kill of MRSA bacteria but rather, it appeared that the bacterial levels were slightly higher than the control PU however, they were still with the starting inoculum numbers. This indicated that there was no significant bactericidal effect against *S. aureus* associated with the presence of red QDs in the polymer. For *E. coli*, rQD PU caused a  $\sim 0.2 \log_{10}$  reduction and a  $0.5 \log_{10}$  reduction in the dark and after illumination respectively. However, the reductions were statistically insignificant ( $p > 0.05$ ) so rQD PU was ineffective against this Gram-negative bacterium as well.

Figure 3.6 shows the antibacterial performance of green QD-encapsulated polyurethane (rQD PU) against *S. aureus* after 1 h of white light illumination at  $6600 \pm 900$  lux (Figure 3.6A) and against *E. coli* after 2 h white light illumination at  $6600 \pm 900$  lux (Figure 3.6B). gQD PU caused a  $0.2 \log_{10}$  reductions of EMRSA in the dark and light respectively. There were also  $\sim 0.2 \log_{10}$  and  $0.4 \log_{10}$  reductions for *E. coli* in the dark and light respectively. Again, statistically, the observed activities were insignificant ( $p > 0.05$ ).

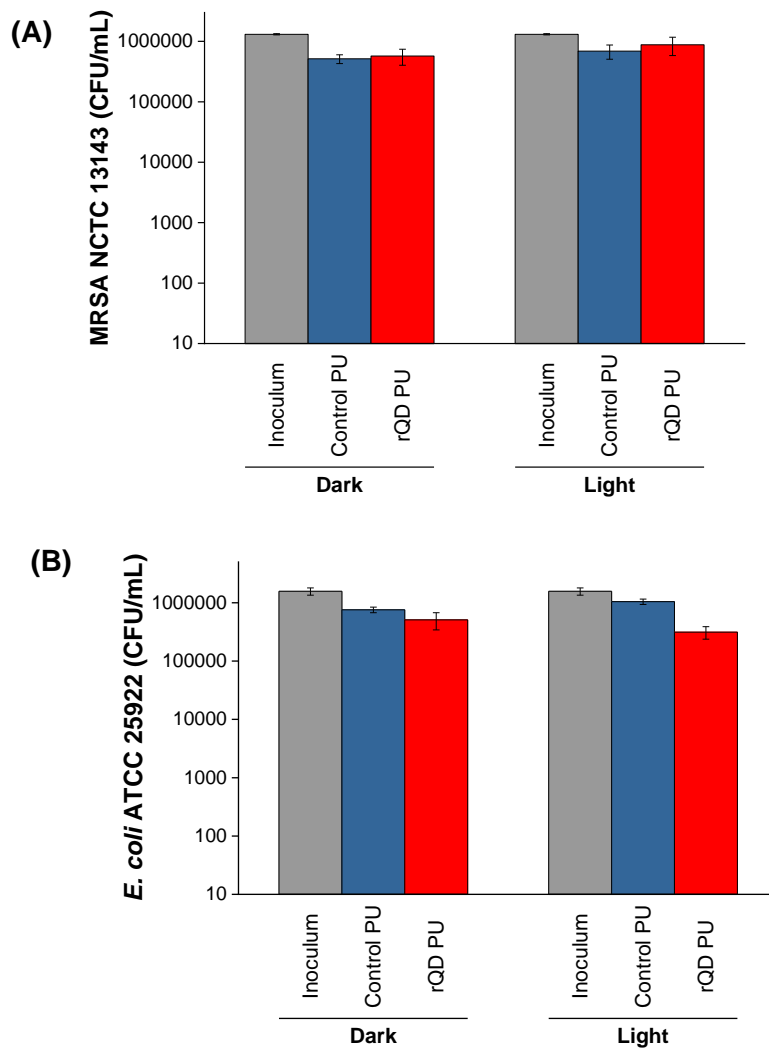


Figure 3.5 Testing of red QD-encapsulated polyurethane against Gram-positive and Gram-negative bacteria. **(A)** Counts of MRSA after incubation on solvent-treated polyurethane (blue bar) and incubation on polyurethane incorporated with red QDs (red bar) after 1 h white light illumination ( $6600 \pm 900$  lux). **(B)** Counts of *E. coli* after incubation on solvent-treated polyurethane (blue bar) and incubation on polyurethane incorporated with red QDs (red bar) after 2 h white light illumination ( $6600 \pm 900$  lux). The grey bar indicates the starting inoculum. (QD concentration used in swelling solution: 1 mg/mL)

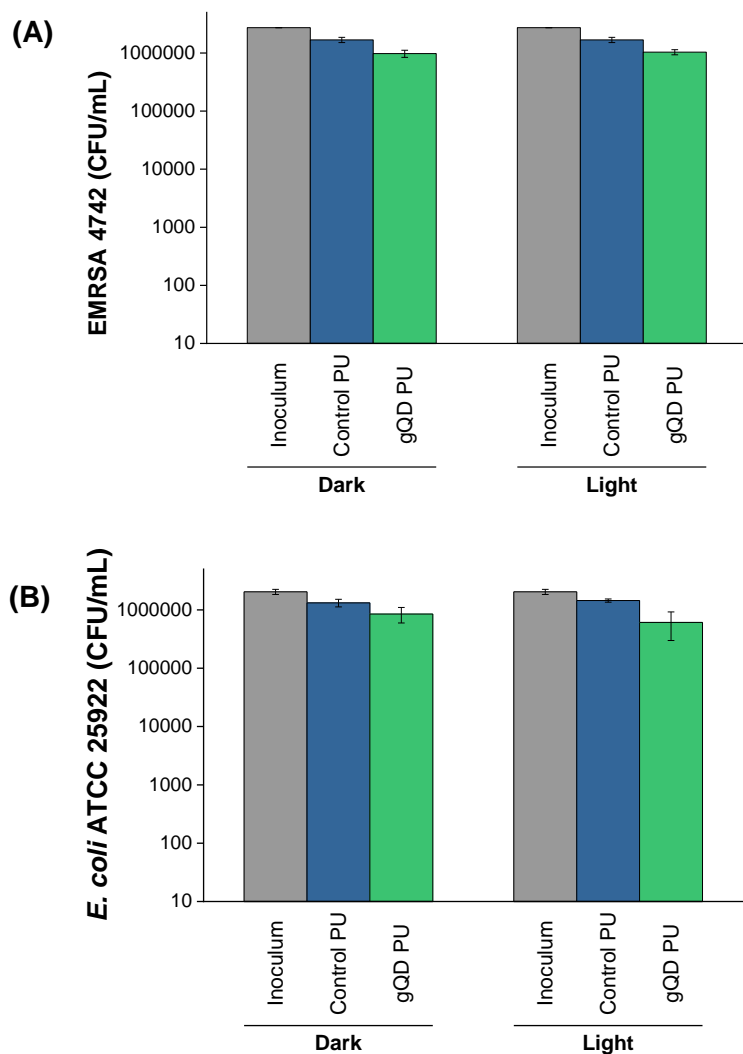


Figure 3.6 Testing of green QD-encapsulated polyurethane against Gram-positive and Gram-negative bacteria. **(A)** Counts of EMRSA after incubation on solvent-treated polyurethane (blue bar) and incubation on polyurethane incorporated with green QDs (green bar) after 1 h white light illumination ( $6600 \pm 900$  lux). **(B)** Counts of *E. coli* after incubation on solvent-treated polyurethane (blue bar) and incubation on polyurethane incorporated with green QDs (green bar) after 2 h white light illumination ( $6600 \pm 900$  lux). The grey bar - starting inoculum. (QD concentration used in swelling solution: 1mg/mL)

### 3.3.4. Effect of Increasing QD Concentration

By increasing the incubation time from 2 h to 6 h and the QD concentration (of the dipping suspension) from 1 mg/mL to 3 mg/mL, we observe a statistically significant increase in antibacterial activity of rQD PU – from 0.2 log<sub>10</sub> (with 1 mg/mL rQD) to ~1.3 log<sub>10</sub> reduction (with 3 mg/mL rQD) in *E. coli* numbers in the light (Figure 3.7A). In the dark, there is an increase from 0.2 log<sub>10</sub> kill to 1.4 log<sub>10</sub> kill of *E. coli*. The similar levels of kill in the light and dark of rQD PU substrates indicated that at high QD concentration, the mechanism of bacterial destruction was unlikely to be photochemical that is, bacterial killing did not involve ROS generation.

It is plausible that the rQD PU substrates intended for dark incubation may have been exposed to light during experiment set-up and that these residual levels of light may have activated the substrates resulting in antibacterial activity. While this may explain why ‘dark’ samples would exhibit bactericidal activity, it follows that much greater activity would be expected for ‘light’ samples which experience far greater exposure to visible light as they are irradiated with white light of high intensity at close distance for an extended period of time (6 h). On this basis, we can reject this line of reasoning.

QD dipping suspensions of even higher concentration (7 mg/mL) were prepared and used to make modified PU substrates with higher QD content. After 6 h incubation in the dark, *E. coli* numbers were reduced by 1.7 log<sub>10</sub> and in the light, *E. coli* numbers were reduced by ~2 log<sub>10</sub> (Figure 3.7B). Therefore, a stronger ‘dark’ toxicity of rQD PU was evident with an increase in QD content in the substrates. This observation, and the fact that activity levels in the dark and after illumination were comparable, supported the conclusion that the antibacterial activity was not photo-activated.

Likely, antibacterial activity resulted from a release of NPs from the substrate via leaching. If NPs escaped from the polymer, bacterial cell death may occur via a number of mechanisms. Released QDs may bind to the cell membranes of Gram-positive bacteria and direct electron transfer from the QDs results significant loss of cell membrane potential (depolarisation).<sup>466</sup> It has also been shown that interaction of QDs with the phospholipid layer of outer membrane of Gram-negative bacteria leads to cell membrane shrinkage and the cell may rupture.<sup>467, 468</sup> Due to their nanoscale sizes, QDs can diffuse across membranes, accumulating inside the

cell and inhibiting various cellular processes such as adenosine triphosphate (ATP) production, cellular respiration and division.<sup>469, 470</sup> Inside the cell, QDs could engage in electron transfer, resulting in oxidative damage caused by the excessive production of ROS. Finally, QD cores could release heavy metal ions into the cytoplasm of the bacterial cell. These ions can accumulate in vesicle bodies, causing cytotoxicity.<sup>471, 472</sup>

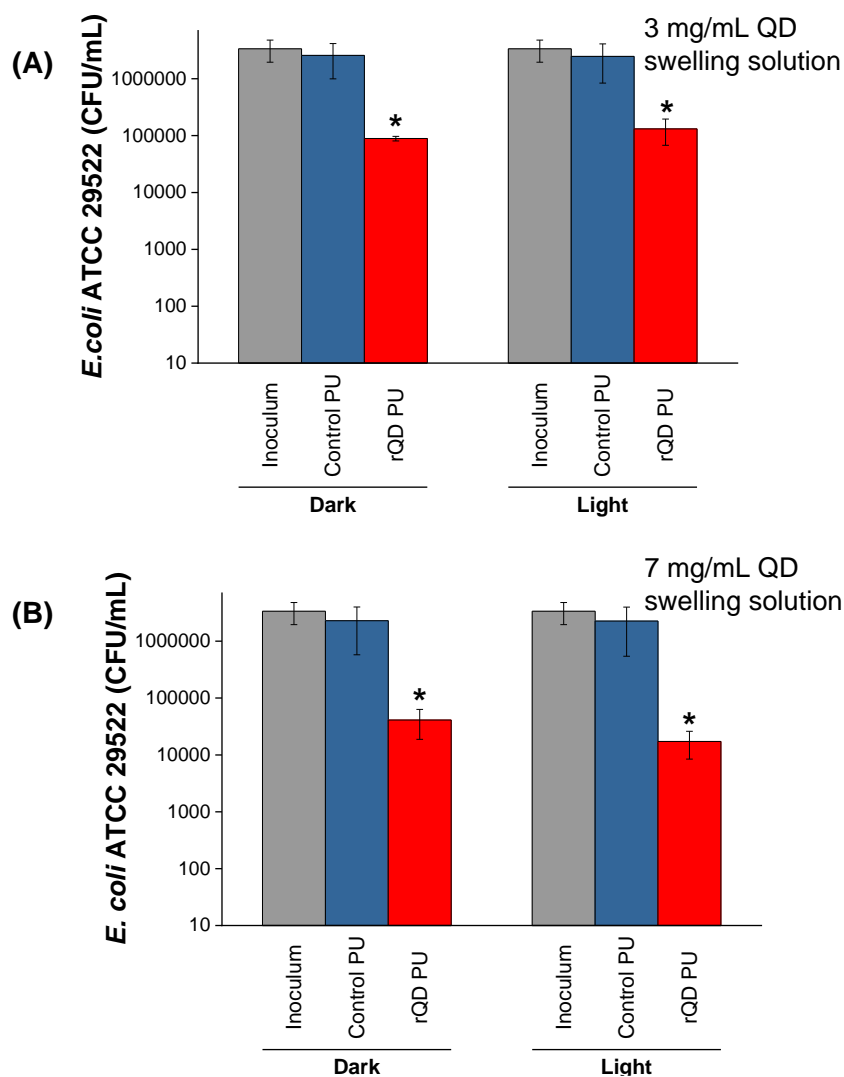


Figure 3.7 Effect of QD concentration and illumination time on antibacterial activity of QD-encapsulated polyurethane. **(A)** Counts of *E. coli* after incubation on solvent-treated polyurethane (blue bar) and on polyurethane swell-encapsulated in 3 mg/mL red QDs suspension (red bar) after 6 h white light illumination ( $6600 \pm 900$  lux). **(B)** Counts of *E. coli* after incubation on solvent-treated polyurethane (blue bar) and incubation on polyurethane swell-encapsulated in 7 mg/mL red QDs suspension (red bar) after 6 h white light illumination ( $6600 \pm 900$  lux). \* indicates  $p < 0.05$ .

Therefore, interpretation of the data suggested that when only QD nanoparticles were present in the polymer, the antibacterial activity depended, not on photo-irradiation of the surfaces, but rather, direct contact of the QDs with bacteria on the surface. QDs may have direct contact with bacteria if there is residual nanomaterial on the surface from the swell-encapsulation-shrink procedure used to functionalise the polymers. Alternatively, the QDs may have leached out of the polymer – although this seems unlikely since they are hydrophobic – and at higher concentrations of QD, the likelihood of leaching was even greater hence, greater antibacterial activity was observed.

Overall, it appeared that regardless of the QD concentration on the swelling solutions, the final QD concentration with the polymer itself was not sufficient to induce cytotoxic effects via *photochemical means* i.e. to produce ROS, or to produce sufficient ROS to overwhelm cellular defences and induce bacterial death.

### 3.3.5. Estimation of Quantum Dot Uptake by Polymer

In order to estimate the QD content in the QD-encapsulated polymers and thus understand the lack of photo-activity observed in QD PU substrates, spectroscopic measurements were conducted. However, it was impossible to confirm uptake using UV-Vis absorbance spectroscopies of the red QD PU and green QD PU substrates. The absorption of the polymer in itself was very strong and effectively blocked the QD spectroscopic features, making these impossible to resolve, as illustrated by the typical absorption plot display in Figure 3.8 below.

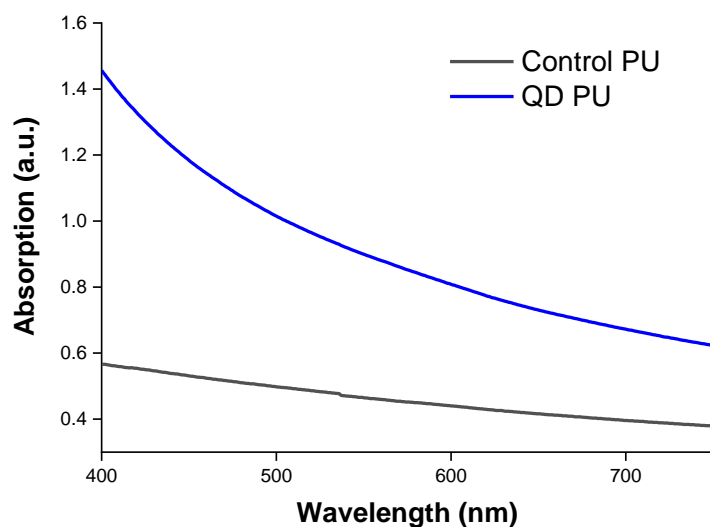


Figure 3.8 Typical plot of near detector absorbance of solvent-treated polyurethane absorbance (black line) alongside QD-encapsulated polyurethane (blue line).

Since QD uptake could not be confirmed and subsequently analysed directly, an analysis of the dipping suspensions used to make the QD-embedded substrates was carried out. By evaluating the absorption spectra of the dipping solvents before and after polyurethane immersion and; assuming no loss of solvent via evaporation, and that material no longer present in the solution had been taken up by the polymer, an approximation of QD uptake could be made. The change in absorption and other data used to estimate QD uptake is summarised in Table 3.2. The amount of NPs encapsulated into the polymer was calculated as follows:

$$10 \text{ mg} \times 1 - \left( \frac{QD_{before} - QD_{after}}{QD_{after}} \right)$$

where  $QD_{before}$  indicates the absorption of the QD suspension before the encapsulation and  $QD_{after}$  represents the absorption of the QD suspension after the treatment. 10 mg is the weight of QDs in a 10 mL solution of  $1\text{ mgmL}^{-1}$  concentration.

Table 3.2 QD Uptake by Polymer. Data utilised in the analysis of QD material uptake by polymer.

<b>QD Concentration</b>	1 $\text{mgmL}^{-1}$
<b>Volume of QD suspension used to swell-encapsulate polymer</b>	10 mL
<b>Average loss of absorbance after swell-encapsulation</b>	15%
<b>Polymer squares per QD suspension</b>	4
<b>Polymer Area</b>	1 $\text{cm}^2$

The overall uptake of QDs after each swell-encapsulation treatment was about 15%, based on UV-vis absorption measurements, equating to 1.5 mg QD material. Four  $1\text{ cm}^2$  polymer squares were treated in each procedure, therefore QD uptake per polymer square was estimated to be ~4% per polymer square, i.e.  $0.4\text{ mg QDs/cm}^2\text{ PU}$ . This analysis confirmed that QD uptake by polyurethane via swell-encapsulation-shrink was very modest and explained why little to no antibacterial activity was observed when the QDs were embedded in polyurethane. This also explained why an increase in QD concentration of the swelling solutions led to increased antibacterial activity as the amount of QD uptake per PU square increased. Each  $1\text{ cm}^2$  polyurethane substrates treated with  $3\text{ mgmL}^{-1}$  and  $7\text{ mgmL}^{-1}$  QD swelling suspensions took up 1.15 mg and 2.7 of QD material respectively. However, the activity observed with these QD PU substrates (ranging from 1.3 – 2  $\log_{10}$  kill) did not justify the use of such high QD concentrations in the swelling protocols, as a large proportion of the NPs was lost when they were not assimilated by the polymer. This is an important point as a balance between good antibacterial activity and cost is essential to the translation of these materials to clinical use and other applications.

Previous studies have shown that QDs optimised for superoxide generation can display excellent bactericidal light-activated properties. For instance, green-emitting cadmium telluride (CdTe) QDs were directly prepared in aqueous media to which populations of multi-drug resistant (MDR) bacteria were exposed, with and without visible light, by Courtney *et al.* In the presence of 100 nM CdTe and light for 8 h, the growth of patient isolates of MRSA and *Klebsiella pneumoniae* were reduced by 29% and 59% respectively. Under the same conditions, a clinical isolate of MDR *Salmonella typhimurium* showed 56% growth inhibition and two MDR *E. coli* isolates had 83% and 64% growth inhibition, respectively.<sup>377</sup> They demonstrated that  $O_2^{\bullet-}$  was generated by photoexcitation of the QDs and attributed the bactericidal activity to oxidative damage by this species and other ROS generated via the Fenton process. This study screened a number of  $O_2^{\bullet-}$  producing QDs however since they all contained toxic cadmium, clinical application is restricted. Similarly, Ristic *et al.* treated of a clinical isolate of MRSA and laboratory strain *E. coli* with electrochemically produced graphene QDs in phosphate buffered saline (PBS). Following exposure of bacteria to 200 mgmL<sup>-1</sup> of graphene QDs and irradiation with blue light (465 – 475 nm) for 15 min, *E. coli* numbers were reduced by 80% and *S. aureus* numbers by about 95%.<sup>378</sup>

However, the above studies were carried in aqueous media where QD nanoparticles were in direct contact with microorganisms. In this work, the objective was to keep QDs always physically separated from the microbes and for killing to occur via photochemical means. This meant bactericidal activity was to be solely reliant on the production of ROS which diffused out of the polymer. However, due to the low QD uptake by polyurethane, it appeared that the ROS production of the QD PU substrates may have been insufficient to induce a cytotoxic effect on bacteria.

### 3.4. Conclusion

In this chapter, the effect of solvent and solvent mixtures on polymer swelling and therefore nanoparticle uptake was examined to decide the best solvent systems for QD encapsulation in polyurethane. QD-encapsulated polyurethane was tested against Gram-positive and Gram-negative bacteria. No significant activity was observed with polyurethane modified by swell-encapsulation in 1 mgmL<sup>-1</sup> QD suspensions however, with increasing QD concentration, significant antibacterial effect is observed in the light and dark, indicating that bacterial kill was not due to photo-illumination but mostly nanoparticle leaching or by direct contact of bacteria

with NPs left on the surface after substrate fabrication. Investigation in the amount of QD uptake by polyurethane was carried by analysing the absorption spectra of the dipping solvents by which QD PU substrates were produced, before and after swell-encapsulation. The analysis revealed that QD uptake by polyurethane was low, at 4%, explaining the lack of photo-activity of QD PU. In an effort to boost QD activity in the polymers and avoid waste of comparatively expensive QD material, PS with well-characterised photo-antibacterial activity was complexed with QDs as discussed in the following chapter.

# CHAPTER 4. LIGHT-ACTIVATED ANTIMICROBIAL SURFACES: QUANTUM-DOT – PHOTSENSITISER COMBINATIONS IN POLYURETHANE

## 4.1. Introduction

The immobilization of photosensitisers (PS) on surfaces is one promising application of the bactericidal properties of conventional PS molecules. As with photodynamic therapy (PDT), irradiation of the surface activates the embedded photosensitiser, leading to lethal sensitisation of bacteria colonising the surface. In the Type I mechanism, excitation of the PS generates superoxide, hydroxyl radicals, hydrogen peroxide and other reactive species through electron transfer. In the Type II mechanism, energy transfer from the excited triple state photosensitiser to the ground state molecular oxygen generates singlet oxygen. (see Figure 1.18) PS dyes such as methylene blue, crystal violet and toluidine blue O have been used to create functional light-activated antimicrobial surfaces for of medical grade polymers using a simple “swell-encapsulation-shrink” method to embed the photosensitiser.<sup>401-405</sup> Though effective as antimicrobials, PS dyes suffer from several drawbacks such as chemical instability, low photo-stability and narrow absorption spectra.

Owing to their unique size-related properties, nanoparticles have received much attention in PDT. One promising approach to enhance PDT efficacy is to conjugate photosensitisers with nanoparticles.<sup>473, 474</sup> Quantum dots have been particularly studied in this capacity as their properties can enhance energy transfer efficiencies and facilitate the design of donor–acceptor systems.<sup>268, 475</sup> Broad absorption spectra, large molar absorption coefficients, size-tunable PL, high quantum yields, large surface area and high resistance to photobleaching are among the benefits of pairing QDs as donors with conventional PS dyes as acceptors. As illustrated in Figure 4.1, QDs are able to sensitise photosensitisers through a Forster resonance energy transfer (FRET) mechanism, generating  $^1\text{O}_2$  through indirect activation of the photosensitiser.<sup>5</sup> However application of QDs have been limited due to concerns associated with the use of cadmium-containing semiconductor nanoparticles, which release  $\text{Cd}^{2+}$  ions.<sup>36, 38</sup> However, indium-based cadmium-free QDs have been reported with significantly lower toxicity at least in murine models.<sup>141, 476</sup>

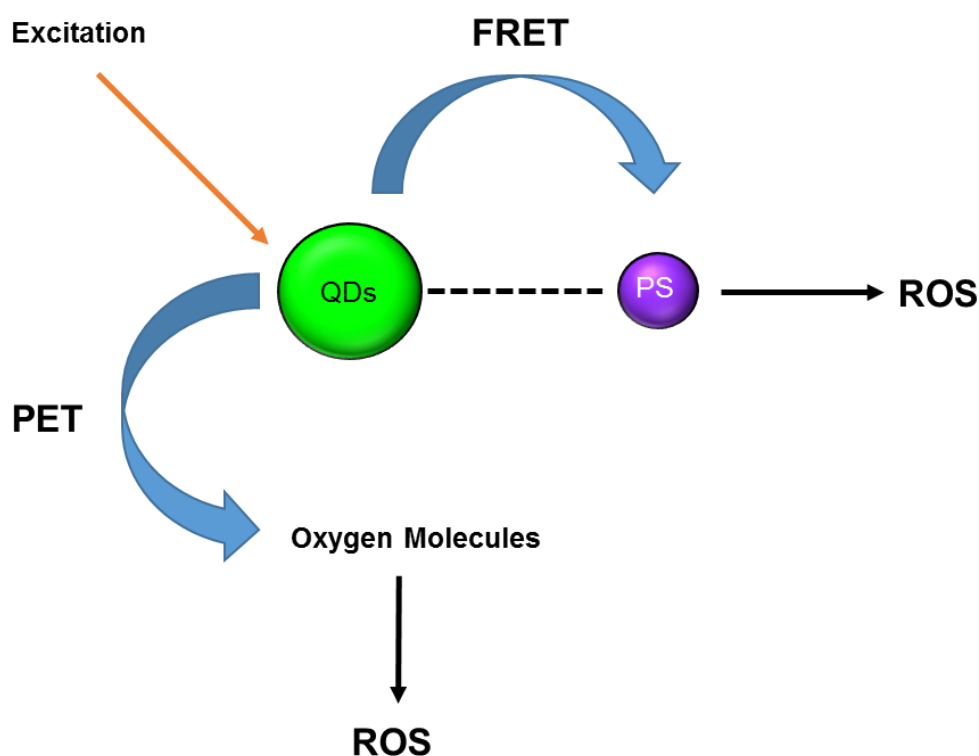


Figure 4.1 Schematic illustrating the activation of a nearby photosensitiser molecule (PS) via energy transfer (FRET) after excitation of QDs, leading to generation of reactive oxygen species (ROS). Excitation of QDs may also enable generation of ROS via electron transfer processes (PET).

In the previous chapter, the incorporation of QD nanoparticles into polyurethane substrates via swell-encapsulation-shrink failed to produce antimicrobial surfaces that were effective against Gram-negative and Gram-positive bacterial pathogens. This was attributed to a combination of factors: the low uptake of QDs into the polymer via swell-encapsulation-shrink and because QDs have a low ROS yield when employed as photosensitisers on their own.

In this chapter, the effect of the combination of crystal violet, a conventional PS molecule with known antimicrobial properties, and cadmium-free indium-based QDs was examined. Quantum dot and crystal violet-incorporated polymer substrates were tested against Gram-positive and Gram-negative bacteria and through a consideration of putative mechanisms underlying the activity of the polymer substrates, optimization of antibacterial action was achieved.

## 4.2. Materials & Methods

### 4.2.1. Quantum Dot Nanoparticles

Cadmium-free indium alloy-based QDs were synthesised via molecular seeding and supplied by Nanoco Technologies Ltd. (Manchester, UK). See CHAPTER 2 (Section 2.2.1) for synthesis details.

### 4.2.2. Nanoparticle Characterisation

A Shimadzu UV-Vis spectrometer (400 – 750 nm range) was used to measure the absorption spectra of all modified polymer samples. Absorption of the dipping solutions before and after swell-encapsulation-shrink was also measured to estimate QD uptake by the polymer. Emission spectra of suspensions was recorded with the Horiba FMax4 Fluorimeter (405 – 790 nm) at the excitation wavelength of 400 nm.

### 4.2.3. Polymer Samples

#### 4.2.3.1. Chemicals and Reagents

Medical grade flat polyurethane sheets (thickness 0.8 mm) were purchased from American Polyfilm Inc. (Branford, CT, USA). To prepare the polymer surfaces, the following reagents were used: CV (Sigma, UK); and CFQDs NPs (Nanoco Technologies Ltd, UK) suspended in cyclohexane (Cy) (Sigma, UK) and dichloromethane (DCM) (VWR, UK). Deionised water was used (resistivity 15 M $\Omega$  cm) to wash polymer squares during sample preparation.

#### 4.2.3.2. Polymer Samples for Antibacterial Testing

Polyurethane samples (1 cm<sup>2</sup>) were modified via the swell-encapsulation-shrink technique adapted from Perni *et al.*, in either a *two-step procedure* or a *modified one-step method*.<sup>402</sup>

The two-step encapsulation method was employed to prepare the following samples for antibacterial testing:

- a) Control samples (control PU): Polyurethane immersed in neat Cy swelling solution for 24 h in the dark, removed, air dried, washed then air dried again.
- b) Crystal violet-coated samples (CV PU): Polyurethane squares were dipped into an aqueous CV solution (concentration: 1 mM) for 72 h, removed, washed and air dried.

- c) Quantum dot-encapsulated samples (QD PU): Polyurethane immersed in a Cy swelling solution containing red-emitting QDs (rQD PU) or green-emitting QDs nanoparticles (gQD PU) for 24 h. (QD concentration: 0.1 – 7 mgmL<sup>-1</sup>)
- d) Quantum-dot encapsulated, CV-coated samples (rQD/CV PU and gQD/CV): Polyurethane squares were prepared by: (i) immersion in a Cy swelling solution containing red or green QD NPs (24 h), followed by (ii) immersion in crystal violet aqueous solution for 72 h in the dark. (QD concentration: 0.1 – 1 mgmL<sup>-1</sup>; CV concentration: 1 mM)

On the other hand, the modified one-step encapsulation method produced the following samples for antibacterial testing:

- e) Control samples (control PU): Polyurethane immersed in neat 1:1 Cy/DCM solvent for 24 h in the dark.
- f) Crystal violet-encapsulated samples (CV PU): Polyurethane squares were (i) immersed in a 1:1 Cy/DCM swelling solution containing CV (concentration: 0.5 mM) for 24 h in the dark, removed, washed and air dried.
- g) Quantum dot-encapsulated samples (QD PU): Polyurethane immersed in a 1:1 Cy/DCM swelling solution containing 1 mgmL<sup>-1</sup> red-emitting QDs (rQD PU) or green-emitting QDs nanoparticles (gQD PU) for 24 h in the dark.
- h) Quantum-dot and CV-encapsulated samples (rQD + CV PU and gQD + CV PU): Polyurethane squares were prepared by a 24 h immersion in a 1:1 Cy/DCM swelling solution containing a combination of red QDs and CV or green QDs and CV.

#### **4.2.4. Material Characterisation**

##### **4.2.4.1. Spectroscopic measurements**

UV-vis absorption spectra of polymer substrates were recorded using dual beam spectrophotometers (PerkinElmer Lambda 950 or Shimadzu UV-2600). Emission spectra of suspensions were recorded with a spectrofluorimeter (Horiba FMax4 Fluorimeter); from 405 – 790nm (400 nm excitation) and from 550 – 790 nm (532 nm excitation). Quartz cuvettes were employed of 1 cm path length. For the emission spectroscopy measurements of the polyurethane substrates, which are strongly light-scattering, samples were mounted diagonally at 45° incidence to the excitation beam, and a long-pass Schott filter (RG435 for

400 nm excitation wavelengths; OG550 for 532nm excitation wavelengths) was installed in the emission port to filter out the blue/green excitation scattered light.

#### 4.2.4.2. Water Contact Angle

Equilibrium water contact angle measurements (~10.0  $\mu\text{L}$ ) were taken using an FTA 1000 Drop Shape Instrument to determine the differences in surface hydrophobicity of treated polymer samples. Contact angle measurements were averaged from 10 measurements using a droplet of deionised water dispensed by gravity from a gauge 30 needle. A camera, fitted side on, photographed the samples and the data were analysed using FTA32 software.

#### 4.2.5. Antibacterial Activity

##### 4.2.5.1. Bacterial Strains

*Escherichia coli* (*E. coli* ATCC 25922) was obtained from the American Type Culture Collection (USA). Methicillin-resistant *Staphylococcus aureus* (MRSA NCTC 13143), *Salmonella typhimurium* (*S. typhimurium* ATCC 14028) and *Listeria monocytogenes* (*L. monocytogenes* NCTC 7973) were obtained from the National Collection of Type Cultures (PHE, Colindale). EMRSA 4742, a clinical strain of epidemic methicillin-resistant *Staphylococcus aureus* (*S. aureus*) was obtained from P. Wilson, University College London Hospital. *E. coli* 1030, a multidrug resistant clinical strain of *E. coli* which produces both NDM-1 and OXA-48 carbapenemases, was obtained from J. Wade, King's College Hospital, London.

##### 4.2.5.2. Microbiology Assay – Nosocomial Bacteria

The following 1  $\text{cm}^2$  polyurethane samples were prepared:

- a) solvent treated polyurethane (control PU)
- b) crystal violet-encapsulated polyurethane (CV PU)
- c) quantum dot-encapsulated polyurethane (rQD PU and gQD PU)
- d) quantum dot and CV- encapsulated polyurethane (rQD/CV PU and gQD/CV PU **or** rQD + CV PU and gQD + CV PU)

The antibacterial activity of these samples was tested against laboratory and clinical strains of representative nosocomial Gram-negative and Gram-positive pathogens. These organisms were stored at  $-70^\circ\text{C}$  in Brain-Heart Infusion broth (BHI, Oxoid, UK) containing 20% (v/v) glycerol and propagated onto either MacConkey agar (Oxoid, UK) in the case of *E. coli* or

Mannitol Salt agar (Oxoid, UK) in the case of *S. aureus* for a maximum of two subcultures at intervals of two weeks. BHI broth was inoculated with one bacterial colony and cultured in air at 37°C for 18 h with shaking, at 200 rpm. The bacterial pellet was recovered by centrifugation, (20 °C, 2867.2 g, 5 min), washed in PBS (10 mL), centrifuged again to recover the pellet (20 °C, 2867.2 g, 5 min), after which the bacteria were finally re-suspended in PBS (10 mL). The washed suspension was diluted 1,000-fold to obtain an inoculum of  $\sim 10^6$  cfu/mL (colony forming units/mL). In each experiment, the inoculum was confirmed by plating 10-fold serial dilutions on agar for viable counts. Triplicates of each polymer sample type were inoculated with 25  $\mu$ L of the inoculum. The samples were then incubated in the dark and in the light (General Electric 28 W Watt Miser™ T5 2D compact fluorescent lamp) emitting an average light of  $6600 \pm 900$  lux at a distance of 25 cm) for up to 4 h for the modified polyurethane samples, for Gram-negative and Gram-positive microorganisms respectively. After incubation, the inoculated samples and coverslips were added to PBS (450  $\mu$ L) and mixed using a vortex mixer. The neat suspension and 10-fold serial dilutions were plated on agar for viable counts and incubated aerobically at 37 °C for 24 h (*E. coli*) or 48 h (*S. aureus*).

#### 4.2.5.3. Microbiology Assay – Food-Borne Bacteria

Testing the antibacterial activity of the polyurethane samples against the following food-borne bacteria: the Gram-negative, *S. typhimurium*, and the Gram-positive, *L. monocytogenes* was carried out in the following manner:

From frozen stocks (stored at -70°C in BHI broth containing 20% glycerol), a sterile inoculating loop was used to scrape a small quantity of frozen material. This was streaked for isolated colonies on MacConkey agar (for *S. typhimurium*) or BHI agar (for *L. monocytogenes*) and incubated overnight (18–24 h) at 37°C. Using a sterile disposable plastic inoculating loop, a single, freshly isolated colony of bacteria was picked up. The inoculum was introduced into sterile BHI broth in a culture tube by gently swirling the loop within the broth. The culture was then incubated at 37°C with orbital shaking at 200 rpm for 18 h. To obtain a starting inoculum of  $10^6$  cfu/mL, the overnight culture was diluted to an OD<sub>600</sub> of 0.6 – confirmed by plating 10-fold serial dilutions on agar for viable counts. Triplicates of each polyurethane substrate were inoculated with 25  $\mu$ L of the inoculum and left uncovered at room temperature. The samples were then incubated in the dark or irradiated with a white light source (General Electric 28 W Watt Miser™ T5 2D compact fluorescent lamp) emitting a light intensity of  $6600 \pm 900$  lux at a distance of 25 cm for 4 h (*S. typhimurium*) or 1.5 h (*L. monocytogenes*). After incubation,

the inoculated samples were added to PBS (450  $\mu$ L) and mixed using a vortex mixer to re-suspend the bacteria. The neat suspension and 10-fold serial dilutions were plated on agar for viable counts and incubated aerobically at 37 °C for 24 h (*S. typhimurium*) or 48 h (*L. monocytogenes*).<sup>477</sup>

#### 4.2.5.4. Log and Percentage Reductions in Antimicrobial Studies

The antimicrobial effectiveness of the test materials was determined by counting the number of colony forming units (CFUs) of a given bacteria present after treatment on the test material and comparing this to the number of CFUs on the control material. The difference between the control and the test materials was expressed as either a log reduction or a percentage reduction.

$$\text{Log Reduction} = \log_{10}\left(\frac{A}{B}\right)$$

$$\text{Percentage Reduction} = \frac{(A - B) \times 100}{A}$$

Where A = the number of bacterial CFUs present before treatment (control material)

B = the number of CFUs present after treatment (test material)

#### 4.2.5.5. Statistical Significance

The experiment contained two technical replicates and was repeated a minimum of two times. The statistical significance of the following comparisons was analysed using the student's T-test: (i) control polyurethane vs. inoculum; (ii) CV-incorporated polyurethane vs. control polyurethane; (iii) QD-incorporated polyurethane vs. control polyurethane; (iv) QD and CV-incorporated polyurethane vs. control polyurethane, (v) QD and CV-incorporated polyurethane vs. CV-incorporated polyurethane. Results were considered significantly different for  $p < 0.05$ . Error bars show the standard deviation from the mean. \*, \*\* and \*\*\* annotation on QD-CV surfaces denote  $p < 0.05$ ,  $p < 0.01$  or  $p < 0.001$  p-values when QD-CV PU compared to CV PU.

## 4.3. Results & Discussion

### 4.3.1. Characterisation

#### 4.3.1.1. Quantum Dots

Figure 4.2 shows the absorption and emission spectra of the two nanoparticles. The indium-based QDs both display broad absorption spectral features ranging from the blue to red regions, with the strongest absorbances observed in the blue region. The first excitonic peaks are at ~550 nm and ~490 nm for red-emitting and green-emitting QDs, respectively. The emission spectra of the QD nanoparticles are narrow and symmetrical as typical of these materials, with emission peaks at 520 and 615 nm for the red and green QDs respectively. The emission spectra of the green QDs is narrower, with a FMWH of about 45 nm, than the red QDs PL which has a FMWH of 60 nm. A more depth discussion of the QDs in suspension is presented in CHAPTER 2.

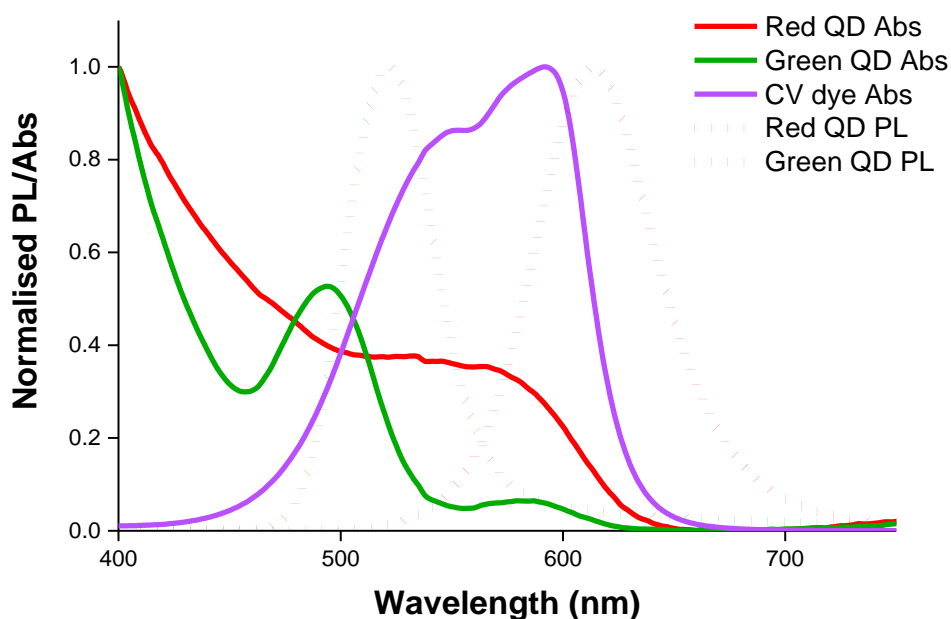


Figure 4.2 Graph showing absorption spectra of red QDs (red line), green QDs (green line), crystal violet (purple line); and emission spectra following excitation at 400 nm for red QDs (red dotted line) and green QDs (green dotted).

#### 4.3.1.2. Crystal Violet

CV is a highly coloured triphenylmethane dye with an extensive history as an anti-bacterial and anti-fungal agent (Figure 4.3). The compound was first synthesised in 1861 by Charles

Lauth, a French chemist. In 1884, Hans Gram discovered that CV was preferentially taken up and retained by Gram-positive bacterial cells even after washing with ethanol, a discovery which formed the basis of the Gram stain still used today to categorise bacteria. In the early 1900s, the bacteriostatic activity of CV against Gram-positive bacteria was reported and right through the first half of the 20<sup>th</sup> century, it was employed in the treatment of wide range of diseases including cutaneous and systemic infections oral thrush, eczema and as a blood additive to prevent transmission of Chagas' disease.<sup>401, 422, 431, 478</sup> However, in the 1940s, CV fell out of favour with clinical community following the discovery of antibiotics. With the emergence of antibiotic resistance, there has been a resurgence in interest in the use of CV and other photosensitisers for clinical use. CV is inexpensive, readily available and chemically stable.<sup>422</sup> Trials using CV have shown no or very mild adverse effects and no cases of cancer has been linked to CV despite more than a century of use.<sup>478-480</sup> FDA-approval of the clinical application of CV in wound dressings highlights the safety of this conventional PS.<sup>481</sup>

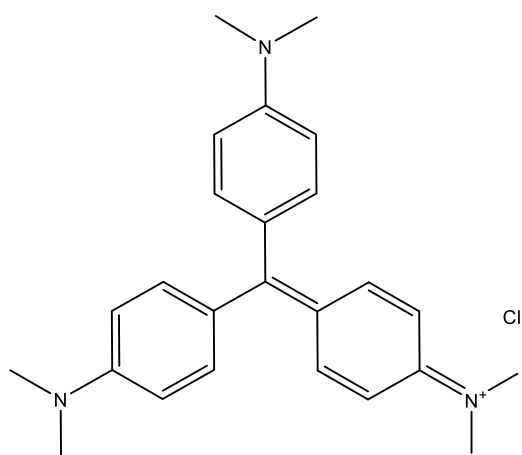


Figure 4.3 Molecular structure of crystal violet, a photosensitiser with extensive history of use as an antiseptic.

In addition to its reputation as a safe and effective antimicrobial, CV was selected as the photosensitiser in these studies because the absorption spectra of the dye matched the emission spectra of the indium-based QD nanoparticles, which were mainly fabricated with emission peaks within the green and red regions of the visible light spectrum. QDs can absorb light of wavelengths lower than their emission, therefore pairing the QDs with CV meant that there was potential for better light harvesting. The dye absorbs strongly in the red region so more of the visible light spectrum range could be exploited for photoactivity. It was

hypothesised that this would enhance bactericidal activity of functional surfaces containing the QD and CV pair. Along with better light harvesting, it was also hypothesised that the weak absorption of the dye molecule in the regions of high QD absorption would allow QDs activation with little to no direct activation of the PS, which is important if QDs are to be efficient donors in an energy transfer mechanism.

Compared to the QD absorption spectra, crystal violet has a narrow absorption range from about 500 – 650 nm. The absorption spectra in 1:1 cyclohexane/DCM is characterised by an overlapped doublet spectrum with the maximum absorption peak at 590 nm and a shoulder around 550 nm (Figure 4.2).<sup>482</sup> The emission spectrum of CV could not be recorded in solution due to CV's low fluorescence quantum yield in this environment. This is a characteristic typical of most phenylmethane dyes which possess phenyl groups that are free to rotate in solvents of low viscosity, giving rise to twisted intramolecular charge transfer (TICT) states with negligible fluorescence quantum yields. However, when the dye is in a solvent of high viscosity or bound to proteins, the movement of its molecular groups is restricted and this molecular rotor effect is attenuated, enabling measurement of CV fluorescence.<sup>428-430</sup>

#### **4.3.2. Incorporation of QDs and CV into Polyurethane**

The swell-encapsulation-shrink technique<sup>403, 404</sup> is a simple means of incorporating material into polymer, particularly at the surface, without the need for complex and often expensive covalent conjugation.<sup>411</sup> The fabrication of QD/CV PU substrates required two steps, illustrated in Figure 4.4. In the first step, unmodified medical grade flat polyurethane squares were immersed in a 0.5 mgmL<sup>-1</sup> QD suspension for 24 h in the dark to make QD-encapsulated PU. Following this, a second dipping procedure is carried out by immersing the QD-encapsulated PU in an aqueous CV (1 mM) for 72 h in the dark to allow CV to coat the polymer, resulting in purple-stained samples which after drying were used for antimicrobial testing. Embedded QD nanoparticles were very unlikely to leach out of the polymer during or after this process due to their hydrophobicity and large size.

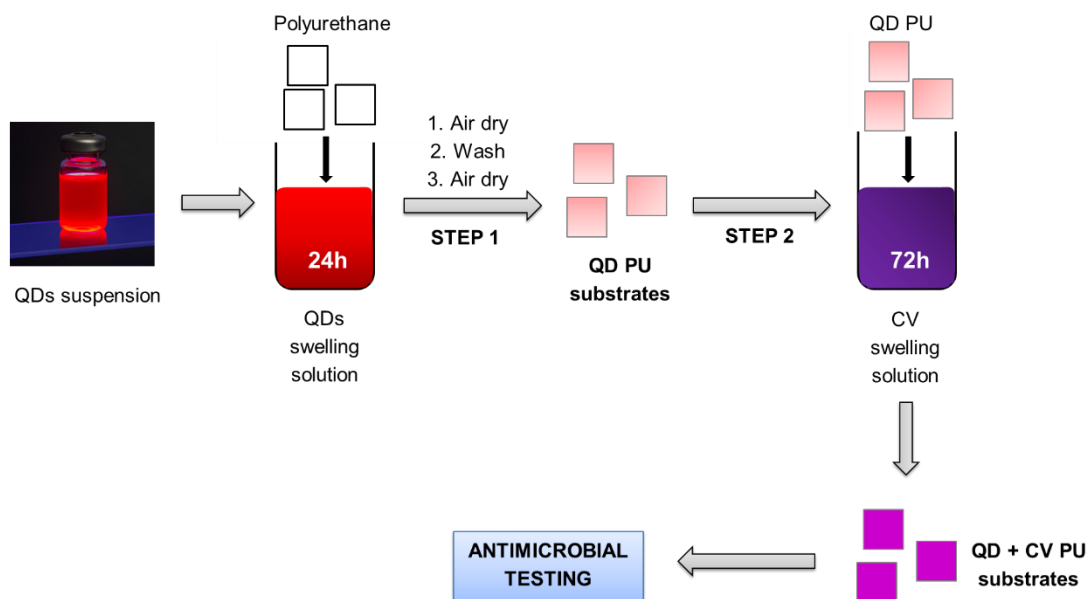


Figure 4.4 Scheme showing two-step 'swell-encapsulation-shrink' technique used to produce polyurethane substrates containing both QDs and CV.

Successful incorporation was verified by emission spectroscopy (Figure 4.5). Upon swell-encapsulation of CV into the polymer, an emission spectrum was detected for CV PU with a peak of 690 nm. Contrary to what occurred in solution where CV fluorescence could not be measured due to the free rotation of TICT states, when CV was encapsulated in polymer, the fluorescence of the PS was observable. This was likely because the microenvironment of the polymer matrix imposed a spatial constraint similar to a solvent of high viscosity, thus restricting the rotor effect and increasing the CV fluorescence quantum yield so that the emission of the dye from the first excited singlet state to the ground state was now evident and measurable.<sup>405, 430</sup>

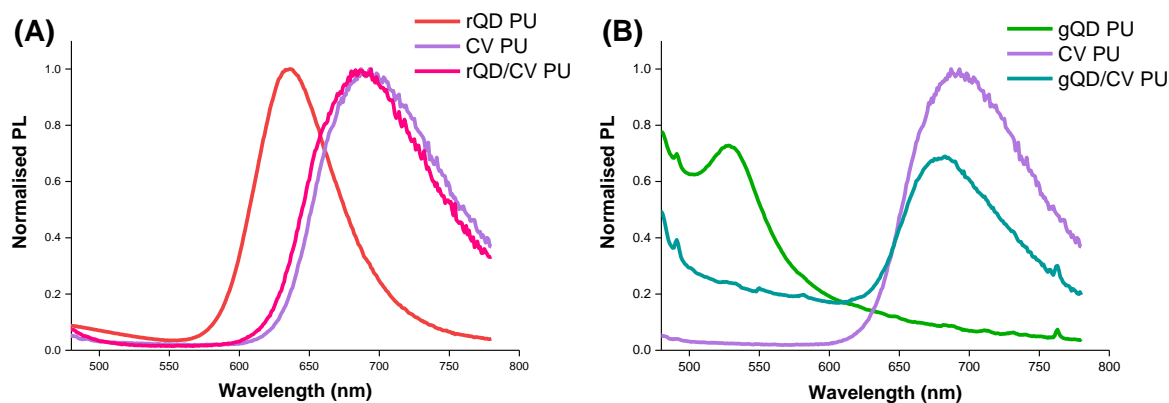


Figure 4.5 Characterisation of modified polymers. **(A)** Normalised emission spectra of red QD-encapsulated polyurethane (red line), CV-coated polyurethane (violet line), red QD-encapsulated and CV-coated polyurethane (pink line). **(B)** Normalised emission spectra of green QD-encapsulated polyurethane (green line), CV-coated polyurethane (violet line), green QD-encapsulated and CV-coated polyurethane (dark green line).

The incorporation of the QDs into polyurethane caused a slight red shift in the emission peak of the QDs compared to in solution (Figure 4.5). Red QD-incorporated polyurethane (rQD PU) emitted at a maximum of about 630 nm and green QD-incorporated polyurethane (gQD PU) at about 530 nm. Combining the PS and QDs, we noticed a significant red shift in the QDs emission. rQD PU had an emission peak of around 630 nm which shifted to ~685 nm upon the addition of CV (rQD/CV PU). An even larger red shift in emission was observed for the gQD PU which saw a change in peak emission wavelength of about 150 nm, from ~530 nm to 680 nm when CV was added to green QDs in PU (gQD/CV PU).

For the CV PU, the CV emission spectrum also appeared to be strongly red-shifted to ~700 nm. This red-shift effect described for all CV-containing polymers was CV-concentration-dependent and was ascribed to absorption of the shorter wavelength portion of the CV emission spectrum which suppressed emission nearer 600 nm and lead to the red-shift.<sup>409</sup> Theoretically the red-shift effect could also be due to the molecular rotor effect as the TICT state can emit in the red however this does not happen for the TICT state of CV unlike some other rotor molecules.<sup>483</sup>

It appeared that the emission of CV dominated the QD emission when the two are combined. This was likely to do with the amount of CV incorporated in the polymer: the degree of CV

uptake by PU was high due to the solubilizing solvent. Dichloromethane, the solvent in which CV was dissolved, was very effective at swelling PU (see Table 3.1), allowing good integration of the PS in the polymer substrate. After preparing and characterizing the new polymer surfaces, antimicrobial tests were carried out to evaluate light-activated bactericidal properties of the functional surfaces.

### 4.3.3. Antibacterial Activity

#### 4.3.3.1. Low QD Content

Antibacterial activity was initially tested with polymers dipped in a low concentration QD suspension – 0.1 mg/mL – and a CV solution of 1 mM. The samples were irradiated for three hours under a white light source emitting an average light of  $6600 \pm 990$  lux, with a further set of samples kept in the dark. Figure 4.6 demonstrates the lethal photosensitisation of *E. coli* when exposed to the solvent treated polyurethane (control PU), crystal violet-coated (CV PU), red and green quantum dot-encapsulated (rQD PU and gQD PU respectively) and red or green quantum dot-encapsulated, crystal violet-coated polyurethane samples (rQD/CV PU and gQD/CV PU respectively). Following 3 hours of incubation in the dark, none of the samples showed significant kill of *E. coli*. However, exposure to the white light source for a period of 3 hours induced a reduction in *E. coli* of about  $2.1 \log_{10}$  with CV alone ( $p = 0.013$ ). The high variability in the log reduction for CV PU treatments was due to one set of biological replicates showing higher attenuation of *E. coli*, perhaps due to the bacterial inoculum having a high susceptibility to the photodynamic treatment applied.

Interestingly, the addition of red quantum dots at a concentration of 0.1 mg/mL to CV-containing polyurethane (rQD/CV PU) did not enhance the bactericidal activity demonstrated by CV alone ( $p = 0.25$ ), that is, rQD/CV PU also induced a  $2 \log_{10}$  kill. On the other hand, a  $2.4 \log_{10}$  reduction of *E. coli* numbers was achieved for gQD/CV PU ( $p = 0.012$ ). No significant kill was achieved for control, rQD or gQD samples.

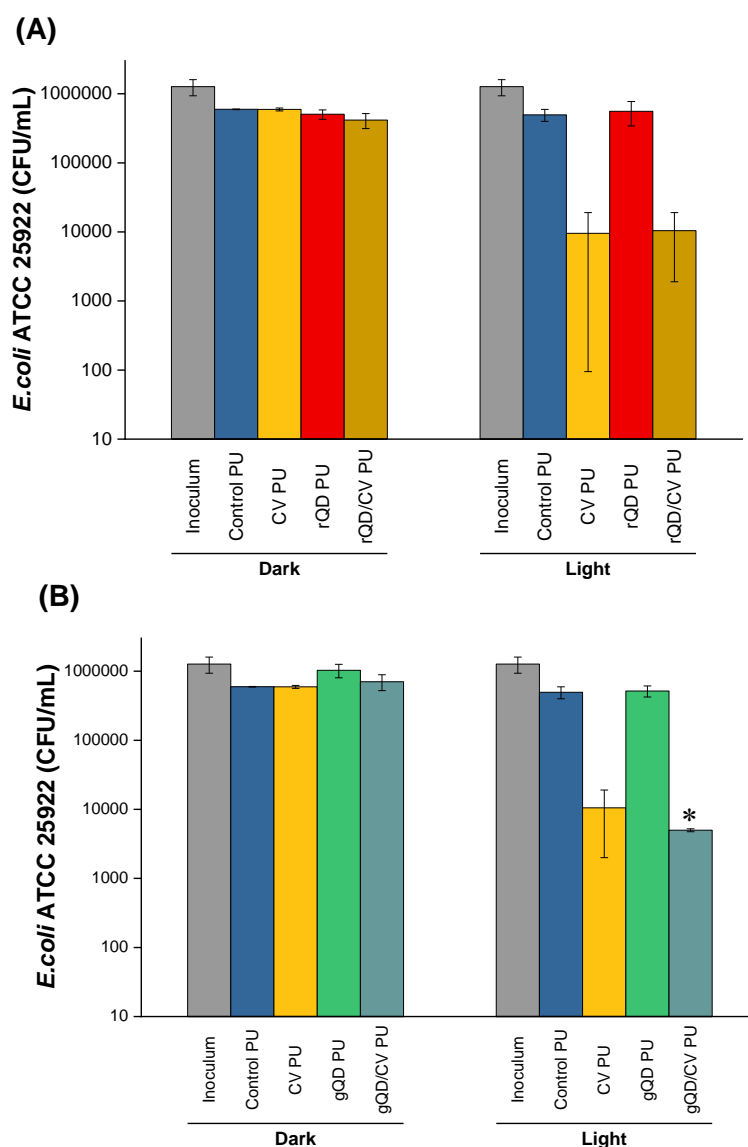


Figure 4.6 Antibacterial action of modified polyurethane substrates. Viable counts of *E. coli* ATCC 25922 bacteria after 3 h incubation at 20°C in the dark and under white light (6600 ± 990 lux) on **(A)** red QD-encapsulated and CV-coated polyurethane and **(B)** green QD-encapsulated and CV-coated polyurethane. (Concentrations of swelling solutions used to modify PU: QDs – 0.1 mgmL<sup>-1</sup>; CV – 1 mM)

These results did not show that the combination of CV and nanoparticle enhanced kill compared to either alone, however they did confirm that the presence of a PS dye was imperative for lethal photosensitisation, as QDs on their own yielded little to no antibacterial effect (discussed in the preceding chapter).

#### 4.3.3.2. Effect of Increasing QD Content in Polymer on Antimicrobial Activity

To improve the bactericidal activity of the QD/CV combinations, higher concentration QD suspensions, 0.5 mg/mL, were prepared and used in the swelling protocol, while keeping the concentration of CV the same. The antimicrobial tests were repeated, keeping the same conditions as used in Section 4.3.3.1. The results are displayed in Figure 4.7. As expected, none of the modified PU substrates demonstrated significant kill of *E. coli* following incubation in the dark.

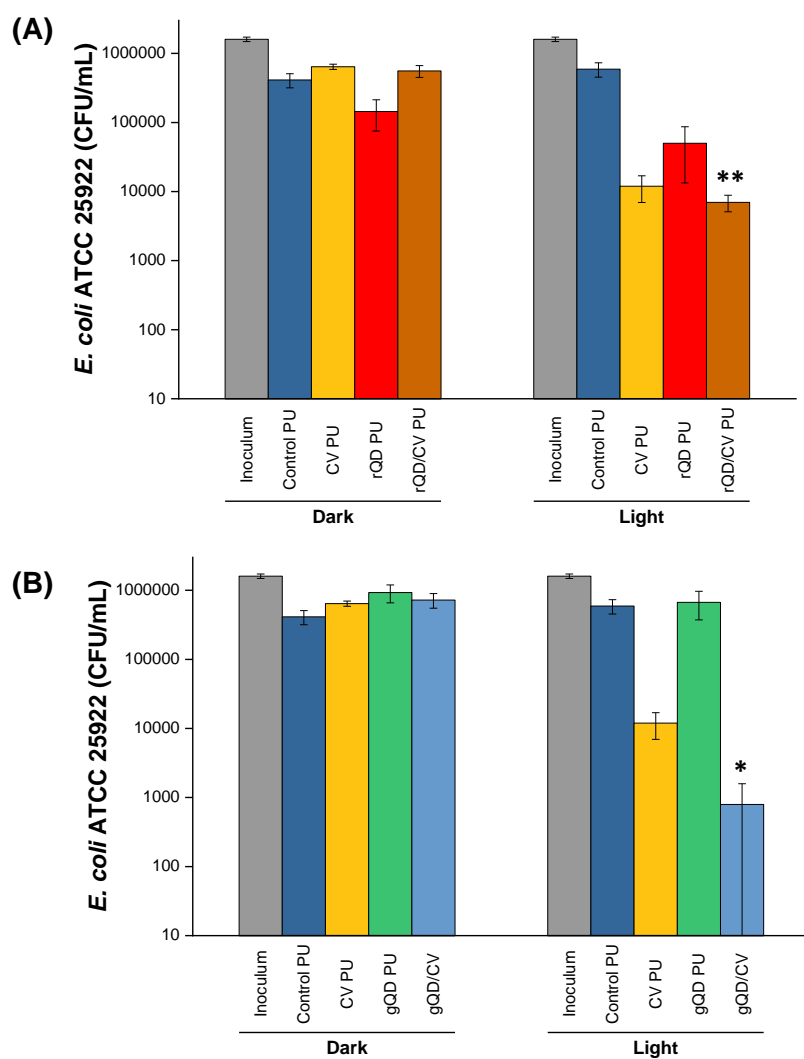


Figure 4.7 Antibacterial action of modified polyurethane substrates. Viable counts of *E. coli* ATCC 25922 bacteria after 3 h incubation at 20°C in the dark and under white light (6600 ± 990 lux) on (A) red QD-encapsulated and CV-coated polyurethane and (B) green QD-encapsulated and CV-coated polyurethane. (Concentrations of swelling solutions used to modify PU: QDs – 0.5 mgmL<sup>-1</sup>; CV – 1 mM)

Red quantum-containing polyurethane (Figure 4.7A) showed 1 log<sub>10</sub> reduction in the dark though not biologically or statistically significant. Statistically, the effect is not significant as the p-value is greater than 0.05 ( $p = 0.075$ ), meaning that it is likely that the difference may have occurred by chance alone. Biologically, this effect is not significant because it is not observed consistently in our antimicrobial experiments.<sup>484</sup> The control PU, CV PU and rQD/CV PU samples showed no antibacterial effect in the dark. The control substrate continued to show no activity upon exposure to light whereas samples containing CV alone showed a 2.1 log<sub>10</sub> reduction ( $p < 0.01$ ), rQD PU samples showed a 1.5 log<sub>10</sub> reduction ( $p = 0.041$ ) and the rQD/CV PU combination achieved 2.3 log<sub>10</sub> reduction of *E. coli* numbers ( $p < 0.01$ ).

In common with the control PU, CV PU and gQD/CV PU samples, green QD-incorporated PU showed no significant activity in the dark (Figure 4.7B). White light irradiation again induced an approximately 2 log<sub>10</sub> reduction in *E. coli* numbers with PU substrates containing only CV while the addition of green QDs to CV-containing PU resulted in a large decrease in *E. coli* numbers of 3.3 log<sub>10</sub>. ( $p = 0.025$ ). Complete kill was achieved with all the gQD/CV PU samples bar one, explaining the high variability observed in Figure 4.7B. A comparison of the results when QD concentration was increased is given in Table 4.1.

Table 4.1 Resulting antibacterial effectiveness of surfaces against laboratory strain of *E. coli* according to nanoparticle and photosensitiser concentrations used to make them

<b>Red QD/CV</b>	<b>Red QD Concentration (mgmL<sup>-1</sup>)</b>	<b>CV Concentration (mM)</b>	<b>Attenuation of <i>E. coli</i> (from 10<sup>6</sup> CFU/mL)</b>
<b>Swelling Solutions</b>	0.1	1	2.1 log <sub>10</sub>
	0.5	1	2.3 log <sub>10</sub>
<hr/>			
<b>Green QD/CV</b>	<b>Green QD Concentration (mgmL<sup>-1</sup>)</b>	<b>CV Concentration (mM)</b>	<b>Attenuation of <i>E. coli</i> (from 10<sup>6</sup> CFU/mL)</b>
<b>Swelling Solutions</b>	0.1	1	2.4 log <sub>10</sub>
	0.5	1	3.3 log <sub>10</sub>

Thus, with green QD-CV combinations, a positive correlation existed between the concentration of QDs in the polymer and the reduction of *E. coli* numbers, implying a synergistic effect between the photosensitiser and nanoparticles. However, this effect was not apparent with the rQDs, as red QD-CV combinations so far, have failed to yield bactericidal activity any higher than that obtained with samples containing CV alone. If bactericidal activity of the quantum dots is enabled, wholly or partly, by reactive oxygen species (ROS) generated through Förster resonance energy transfer (FRET), then to improve the bactericidal activity observed with rQD/CV substrates, we must take into account the criteria needed for efficient FRET interactions. Since the intent of this study was to induce bactericidal activity through ROS generation and it was thought that the combination of QD and CV would produce ROS through FRET (evidence for this interaction was observed in solution in CHAPTER 2), we next considered the criteria required for efficient FRET interactions to take place.

### 4.3.4. Improving Antibacterial Activity of QD-CV Polymer Substrates

#### 4.3.4.1. Red QD-CV Polymer Substrates

FRET involves the non-radiative transfer of excitation energy from an excited state donor molecule to a ground state acceptor molecule. The conjugation of QDs and CV dye facilitates energy transfer interactions where QDs serve as donors and CV dyes as acceptors. As discussed in CHAPTER 1 Section 1.2.4, efficient FRET interactions requires two key conditions:

1. sizeable spectral overlap between the donor QD emission and dye acceptor absorption profiles and,
2. close proximity between donor and acceptor, due to the short range nature of the interactions.<sup>215</sup>

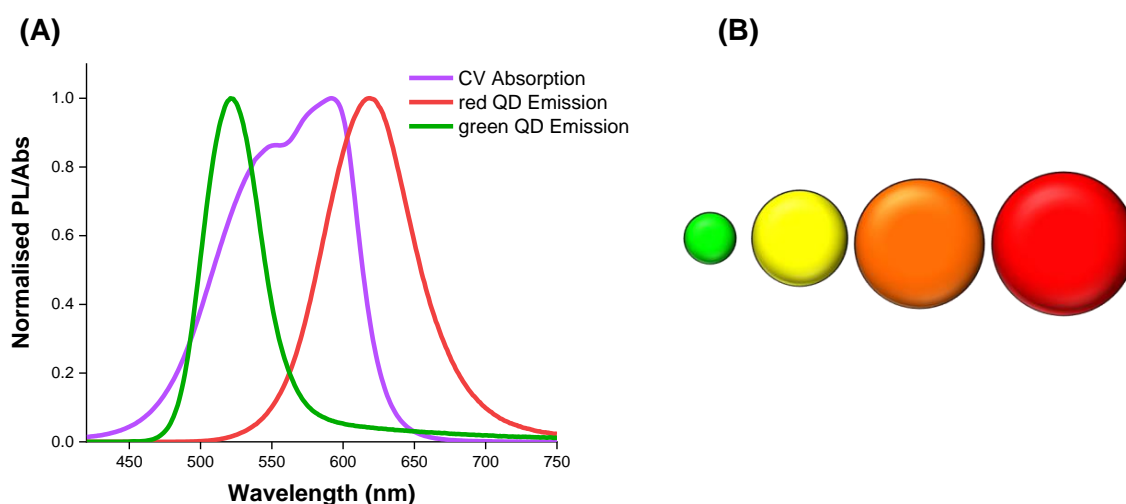


Figure 4.8 Förster resonance energy transfer (FRET) considerations. **(A)** Absorption spectrum of CV dye superimposed with emission spectra of green and red QDs in solution, normalised. **(B)** The size-dependent colour of quantum dots (not drawn to scale). Red-emitting QDs are characteristically larger than their green counterparts.

The choice of CV as the acceptor in the putative FRET-based functional surfaces was appropriate as the dye exhibits strong absorption in the emission range of both QD nanoparticles (Figure 4.8A). Thus the first requirement was fulfilled by careful selection of photosensitiser. The calculated overlap integral of QDs donor PL spectra with CV acceptor absorption spectrum indicated that red QD experienced greater spectral overlap with CV than

green QDs, therefore we expected better antibacterial action via FRET in red QD-CV conjugate surfaces compared to green QD-CV surfaces. (Table 2.1)

On the other hand, the second requirement of proximity disfavoured red emitting QDs which, by nature, were larger in radius than their green counterparts (3.6 nm versus 2.9 nm for the green QDs) (Figure 4.8B). The larger radius results in increased centre-to-centre separation distance between red QD donor and CV acceptor which, in turn, lowers FRET efficiencies. The radius of a QD nanoparticle emitting at a particular wavelength is fixed and cannot be adjusted without changing its properties. This is because the properties of semiconductor NPs are highly size-dependent hence, the QD radius may act as a limiting factor in donor-acceptor separation distances. In biomedical applications, this is particularly important as certain coatings that make QDs water soluble and more biocompatible can significantly increase the radius length, altering spectral overlap and therefore FRET efficiency. On the other hand, these coatings have advantages as they improve QD quantum yield, resulting in increased rates of FRET.<sup>83, 85, 268</sup> In our studies, core indium-based QDs were etched in dilute hydrofluoric acid and subsequently encased in a ZnS shell to improve quantum yield. However since QDs were not being directly utilized in biological studies, and were intended to be embedded in polymer, the nanoparticles were supplied un-functionalised, thus keeping the dots at the smallest radii possible.

Although the radius of the red-emitting dots could not be changed, the large spectral overlap of the red QDs with CV showed promise for efficient FRET interactions between the complex, therefore the method of red QD and CV dye incorporation into polyurethane was considered and a modification of the dipping process was developed to limit the centre-to-centre separation distance between the donor and acceptor as much as possible, and in turn, improve bactericidal activity. The swell-encapsulation-shrink technique is traditionally employed as a two-step process when impregnating polymers with both nanoparticles and dyes mainly due to the different solubilities of the nanomaterials and the dyes.<sup>403, 404</sup>

It is important to note that synergism of the QD-CV polymers may also result from PET mechanisms, with QDs and CV acting as electron donors and acceptors respectively. Both FRET and PET generate more cytotoxic ROS, amplifying antibacterial activity. Fluorescence quenching studies, through Stern-Volmer analyses, revealed that  $K_{SV}$  values (Stern-Volmer

quenching constant) were substantially higher for green QDs than red QDs in solution phase ( $3.6 \times 10^6 \text{ M}^{-1}$  for green QDs vs  $4.4 \times 10^5 \text{ M}^{-1}$  for red QDs). This meant that at a given CV concentration, green QDs were more effectively quenched than red QDs. This result was attributed to the smaller average size and thus larger surface to volume ratio of the green QDs. A larger surface to volume ratio enhances the electronegative charge on the green QDs and enables the array of a higher number of CV dye molecules per single nanoparticle, producing a proportional increase in the FRET and PET efficiency compared to a one-to-one donor-acceptor pairing.<sup>420</sup>

Furthermore, quenching constants ( $k_q$ ), orders of magnitude higher than the diffusion controlled limit for bimolecular reactions, are observed on addition of CV for both QDs. This shows that the interactions were predominantly static in nature with CV bound to the QD surface in solution phase.<sup>445</sup> Thus in solution, direct interaction between the QDs and CV takes place via adsorption of CV onto the QD surface to enable FRET/PET. However, in the polymer, in addition to intact QD-CV complexes, a proportion of the CV may reside in the matrix in close proximity to the QDs but not bound at the QD surface. Therefore here, we expect that PET may be less important as these interactions occur over a shorter range than FRET.

Taking the above considerations into account, a two-step process may reduce effectiveness of functional surfaces as the synergistic mechanisms that augment antimicrobial activity often require close proximity. Consequently, through a systematic process of trial and error, a novel one-step process was designed to improve co-localisation of the QD and CV in the polymer and complex formation. This was achieved by mixing the QDs and CV in a miscible 1:1 cyclohexane/dichloromethane solvent system (Figure 4.9). A mixed solvent system was required since the QDs were supplied suspended in cyclohexane whereas CV was not directly soluble in this solvent. For this reason, a stock solution of CV dissolved in DCM and a stock QD suspension in cyclohexane was first prepared before mixing with the QDs and CV to obtain a mixture with a final concentration of  $1 \text{ mgmL}^{-1}$  QDs and  $0.5 \text{ mM}$  CV. The polymer samples were then treated with this solution for 24 h resulting in purple-stained samples which, after drying, were used for antimicrobial testing.

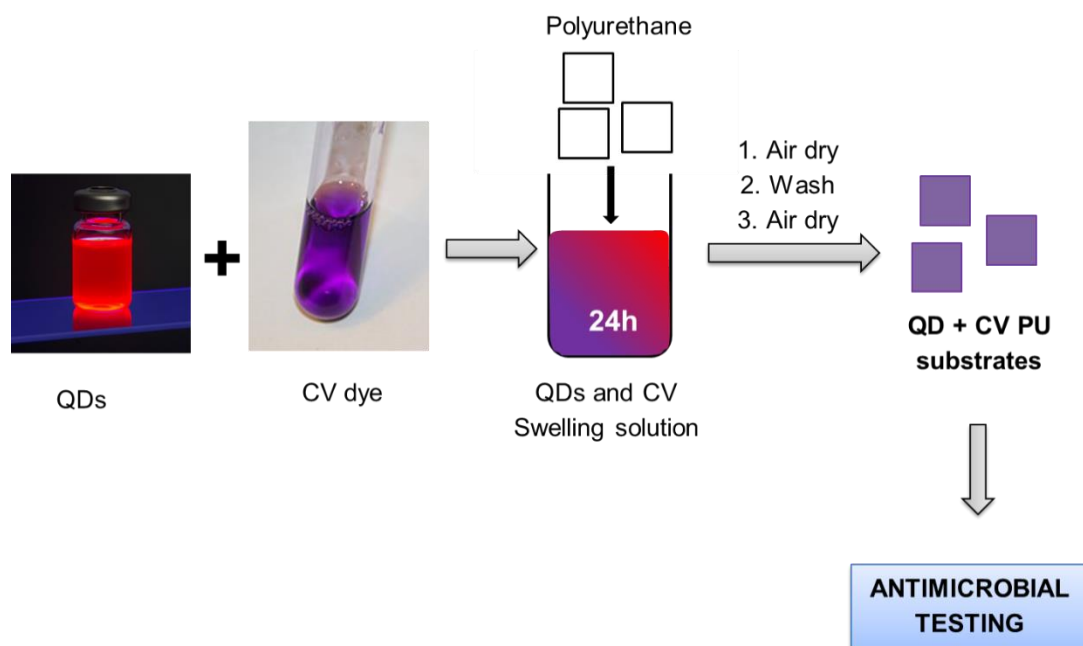


Figure 4.9 Scheme illustrating the modified swell-encapsulation-shrink technique used to prepare the new quantum dot and CV-encapsulated polyurethane substrates. Polyurethane squares were dipped in a 1:1 cyclohexane/DCM solvent mixture containing QDs ( $1 \text{ mgmL}^{-1}$ ) and CV dye ( $0.5 \text{ mM}$ ) for 24h.

Combining red QDs and CV in a miscible 1:1 cyclohexane/dichloromethane solvent system for 24 hours, this novel approach circumvented the need for the lengthy 72-hour CV-coating step. Again, visible colour changes and fluorescence measurements of the polymers after modification confirmed uptake of the QD and/or CV (Figure 4.10). The wetting properties of the untreated and treated polyurethane samples were measured to see if the new incorporation technique caused any changes in surface hydrophobicity of the samples. The water contact angles of untreated samples indicated that polyurethane had a hydrophobic surface. The addition of either the nanoparticles or the photosensitiser caused negligible changes in the hydrophobicity of the material, with contact angles varying by  $\pm 1^\circ - 2^\circ$ .

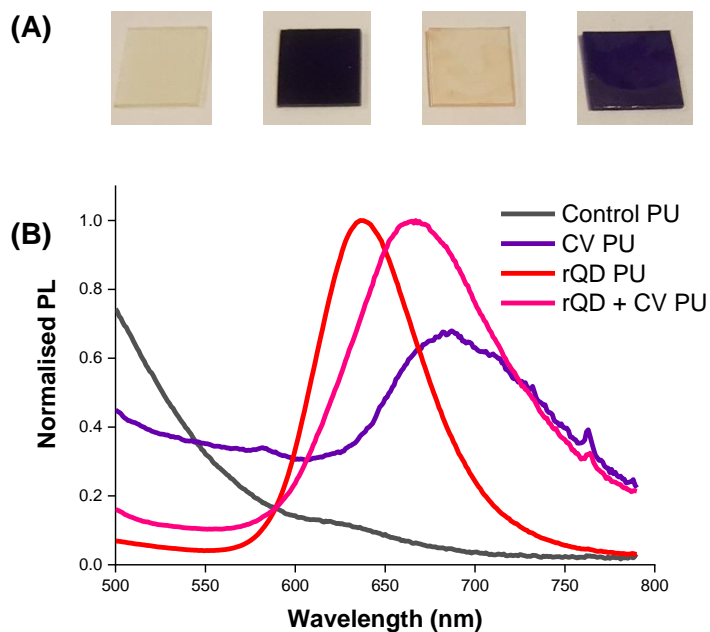


Figure 4.10 Confirmation of nanomaterial and photosensitiser uptake. **(A)** Image showing polymer substrate after modification. From left to right: Appearance of polymer after treatment with plain solvent (control PU), with CV solution only (CV PU), with red QD QD solution only (rQD PU) and red QD combined with CV solution (rQD + CV PU). **(B)** Emission of polymer after preparation using new swell-encapsulation-shrink technique.

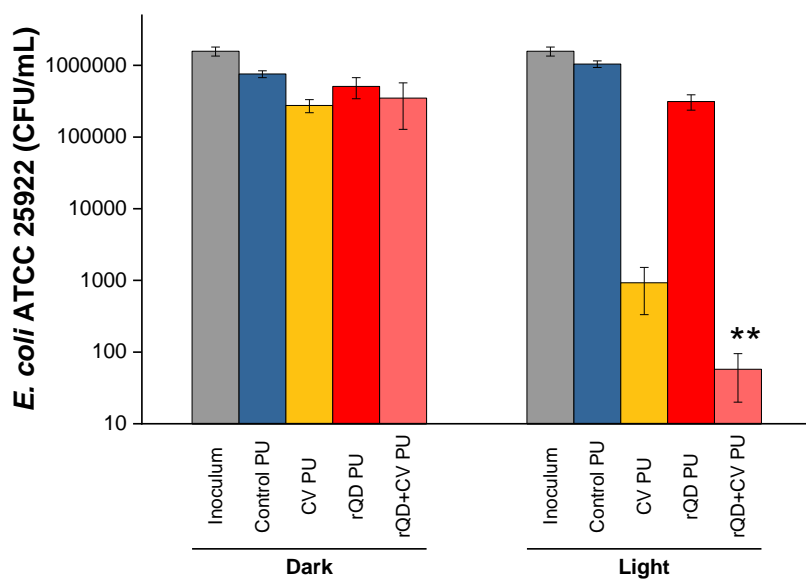


Figure 4.11 Antibacterial action of polyurethane substrates produced using the 1-step swell-encapsulation-shrink method. Viable counts of *E. coli* ATCC 25922 bacteria after 2 h incubation at 20°C in the dark and under white light (6600 ± 990 lux) on red QD and CV-encapsulated polyurethane. (Concentrations of swelling solutions used to modify PU: red QDs – 1 mgmL<sup>-1</sup>; CV – 0.5 mM)

As in the above cases, laboratory strain *E. coli* ATCC 29522 was used to test the antibacterial activity of the polymers impregnated with red QDs and CV via the modified 1-step swelling process (Figure 4.11). The swelling suspension prepared consisted of double the QD concentration and half the CV concentration used in Section 4.3.3.2. In the dark, no activity was observed from any of the polyurethane surfaces. After a 2 h incubation under a 6000 lux white light source, control PU and rQD PU samples again showed no significant activity, as before. However, polyurethane containing CV alone (CV PU) displayed a 2.6 log<sub>10</sub> reduction in bacterial numbers ( $p < 0.01$ ) and samples with the combination of red QD and CV (rQD + CV PU) induced a 4.3 log<sub>10</sub> reduction ( $p < 0.01$ ) in the numbers of *E. coli*. A comparison of antimicrobial activities of the surfaces depending on the method of the substrate preparation is presented in Table 4.2.

The potentiation of antibacterial activity upon adjustment of the QD-CV dye encapsulation technique strongly indicated synergistic interactions between QDs and CV in the polymer via FRET and possibly PET. This improvement in activity was noteworthy in light of the fact that the CV concentration was halved in the swelling solution therefore activity was more dependent on synergistic interactions than in previous experiments. Additionally, high antibacterial activity was

achieved with less irradiation time compared to the 2-step swelled polymers. Thus, the new surfaces simultaneously provided stronger and faster antibacterial action.

Table 4.2 Comparison of the antibacterial activities of rQD + CV substrates prepared by either the original 2-step dipping process or the novel single-step dipping procedure

<b>Swell-Encapsulation Method (Red QD-CV)</b>	<b>2-step</b>	<b>1-step</b>
<b>Length of Irradiation</b>	3 h	2 h
<b><i>E. coli</i> ATCC 25922 Kill</b>	2.3 log <sub>10</sub>	4.3 log <sub>10</sub>

#### 4.3.4.2. Red QD-CV Substrates by 1-Step Encapsulation against Clinical Strains of Bacteria

Laboratory bacterial strains are grown in standardised ideal conditions and having been sub-cultured for years since their first isolation, might have lost important pathophysiological characteristics typical of newly-isolated clinical strains.<sup>485</sup> Therefore, it is crucial to test QD-CV surfaces against clinical bacterial isolates recently isolated from hospitalised patients. An added benefit of testing clinical strains is that we know the full history of the pathogen. This is harder to ascertain with strains from the ATCC (American Type Culture Collection) and NCTC (National Collection of Type Cultures), which have been subcultured for decades. The ROS produced as a result of electron transfer or energy transfer by the surfaces, can engage in multiple modes of attack, reducing the likelihood of development of resistance. Thus we expect that our surfaces will be effective against both laboratory and clinical strains of bacteria that are drug-resistant. To that end, the antibacterial activity of the red QD and CV encapsulated PU samples produced by the new 1-step swell-encapsulation-shrink process were tested against a number of clinical strains of multi-drug resistant bacteria.

The bactericidal activity of the various polymer surfaces against Gram-positive methicillin-resistant isolate of *Staphylococcus aureus* (MRSA) NCTC 13143, in the dark and following 1 h of exposure to a white light source with an average light intensity of  $6600 \pm 990$  lux is presented in Figure 4.12A. Following 1 h of incubation in the dark, neither the control PU nor the rQD PU samples showed significant kill of MRSA. Similarly, exposure to white light for a period of 1 h also did not result in any bactericidal activity from the rQD PU. In fact, compared to the irradiated control PU, there was a slight increase in bacterial numbers for rQD PU of  $0.3 \log_{10}$ , though not statistically significant. In contrast, in the absence of light, CV PU and rQD + CV PU samples showed a  $1.2 \log_{10}$  ( $p < 0.001$ ) and  $0.7 \log_{10}$  ( $p < 0.001$ ) reduction in bacterial numbers, respectively. This 'dark' cytotoxicity of the CV-containing polymers against *S. aureus* is explained by the intrinsic antimicrobial properties of CV towards Gram-positive microorganisms as supported by a number of studies – in aqueous solutions<sup>422</sup> and also using polyurethane substrates, where it was observed that crystal violet-incorporated surfaces exhibited limited dark toxicity against a laboratory strain of *S. aureus*.<sup>406</sup> The observation that the presence of QD reduced the activity of CV was believed to be a concentration effect. It was noted that when a swelling protocol was carried out to simultaneously embed QD and CV into polyurethane, the resultant QD + CV PU had a weaker purple colour compared to CV PU.

It indicated that perhaps less CV was taken up by the polymer and consequently, lower 'dark' antibacterial activity.

In the presence of white light for a short period of 1 h, CV alone (CV PU) produced a 2.7 log<sub>10</sub> reduction in bacterial numbers ( $p = 0.027$ ) and the combination of red quantum dot and CV (rQD + CV PU) caused the greatest kill of MRSA with numbers reduced by 3.7 log<sub>10</sub> (99.98%;  $p = 0.027$ ).

In addition to MRSA NCTC 13143, the red QD-CV functional surfaces were also tested against a clinical isolate of epidemic MRSA (EMRSA 4742). The surfaces showed a similarly high level of activity against this strain after 1 h irradiation (Figure 4.12B). Photo-irradiated rQD + CV functional surfaces attenuated EMRSA numbers by 4.4 log<sub>10</sub> ( $p < 0.001$ ). Irradiated surfaces containing CV alone achieved a 2.9 log<sub>10</sub> kill of bacteria ( $p < 0.001$ ) while the solvent treated surface (control PU) exhibited no significant photo-bactericidal action and QD surface (rQD PU) showed a 0.1 log<sub>10</sub> reduction (not statistically significant). Without photo-irradiation, CV PU and rQD + CV PU both achieved ~0.8 log<sub>10</sub> kill of EMRSA ( $p < 0.001$ ) and again control PU and rQD PU were inactive against the bacteria. This was a reassuring result as 'dark' responses of CV-containing polymers against two different strains of MRSA was similar.

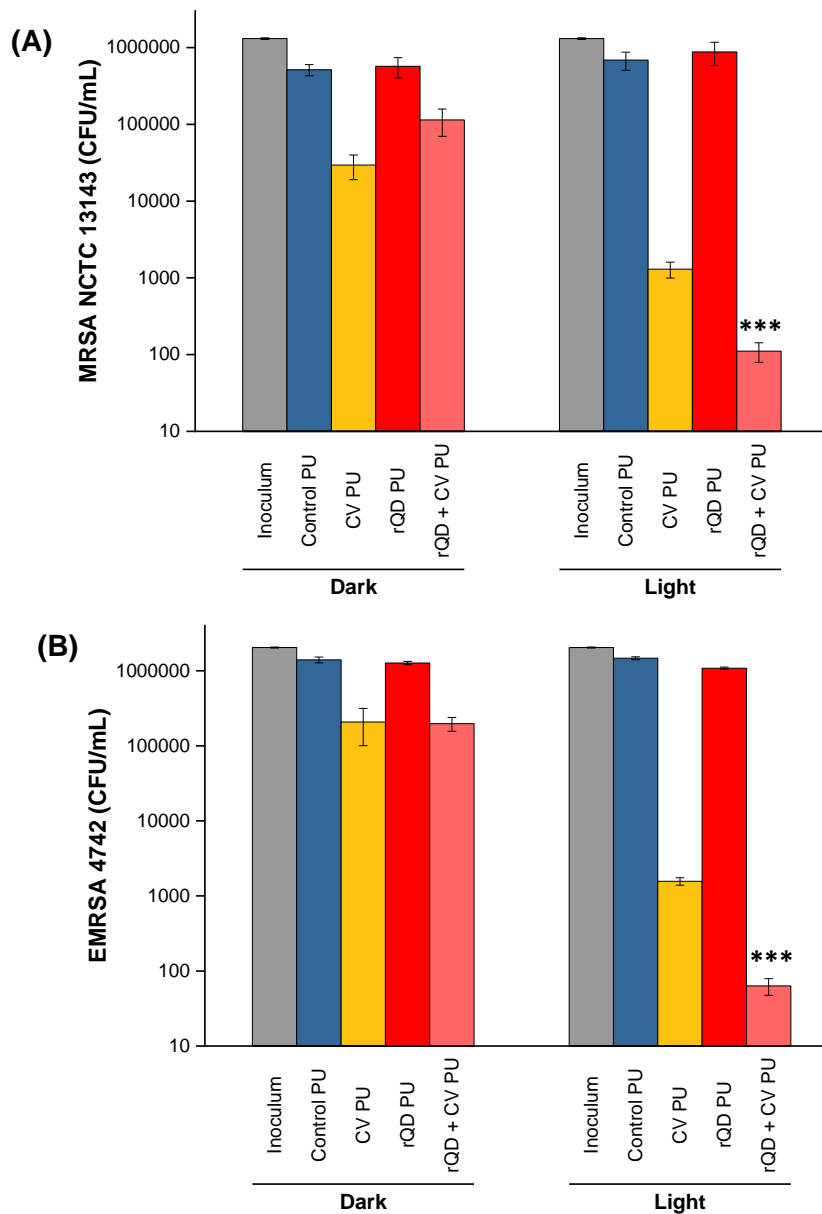


Figure 4.12 **(A)** Viable counts of MRSA NCTC 13143 on unmodified and modified polyurethane substrates incubated at 20°C under dark conditions and under white light (6000 lux  $\pm$  990 lux) for 1 h; **(B)** Viable counts of clinical strain EMRSA 4742 on unmodified and modified polyurethane substrates incubated at 20°C under dark conditions and under white light (6000 lux  $\pm$  990 lux) for 1 h. Concentrations of swelling solutions (made in 1:1 Cy/DCM solvent) used to modify PU: QDs – 1 mgmL<sup>-1</sup>; CV – 0.5 mM.

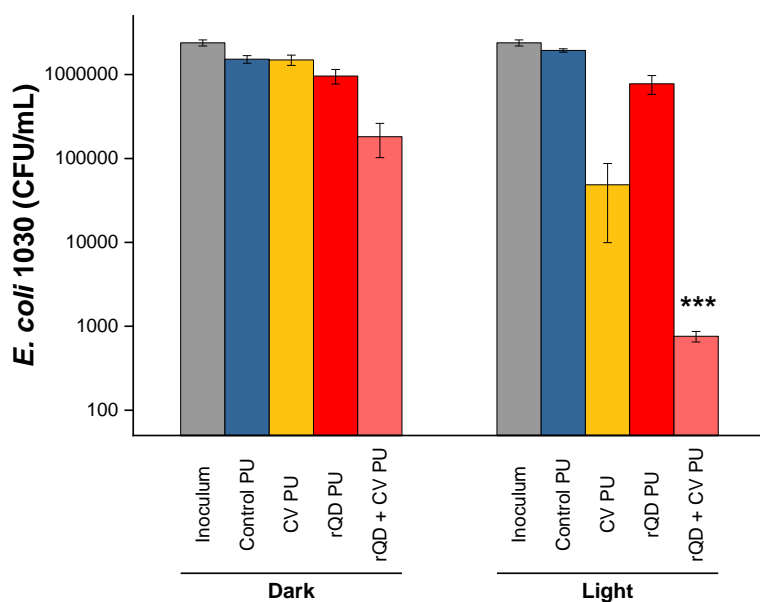


Figure 4.13 Antibacterial action of red QD + CV polymer made by the 1-step swell-encapsulation-shrink method. Viable counts of *E. coli* 1030 on unmodified and modified polyurethane substrates incubated at 20°C under dark conditions and under white light (6000 lux  $\pm$  990 lux) for 4 h. Concentrations of swelling solutions used to modify PU: red QDs – 1 mgmL<sup>-1</sup>; CV – 0.5 mM

The photo-bactericidal activity of the polyurethane surfaces was tested against Gram-negative multi-drug resistant (MDR) *E. coli* 1030, under the same conditions but for an extended period. Figure 4.13 shows the activity of the samples after 4 h of incubation in the absence and presence of ~6000 lux white light. Only the rQD + CV PU substrate showed activity in the dark, inducing a 0.9 log<sub>10</sub> reduction in *E. coli* numbers after 4 h ( $p < 0.001$ ). White light illumination for a period of 4 h resulted in no significant bactericidal activity on the control PU material as expected, a 1.6 log<sub>10</sub> reduction in bacterial numbers was observed with CV PU ( $p < 0.001$ ), and a 0.4 log<sub>10</sub> reduction with QD PU ( $p < 0.01$ ). QD + CV PU showed increased bactericidal activity compared to CV PU alone, resulting in a 3.4 log<sub>10</sub> reduction in bacterial numbers following light exposure for 4 h ( $p < 0.001$ ).

#### 4.3.4.3. Green QD-CV Substrates by 1-Step Encapsulation

Through modification of the swell-encapsulation-shrink procedure, it was found that the activity of red QD-CV substrates could be optimised. Similarly, it was hypothesised that by applying the same treatment to green QD-CV substrates that had already performed well in preliminary tests, better activity could be realised. Green QDs and crystal violet were simultaneously incorporated into

polyurethane via the 1-step swell-encapsulation technique and initially tested against *E. coli* ATCC 25922 (Figure 4.14).

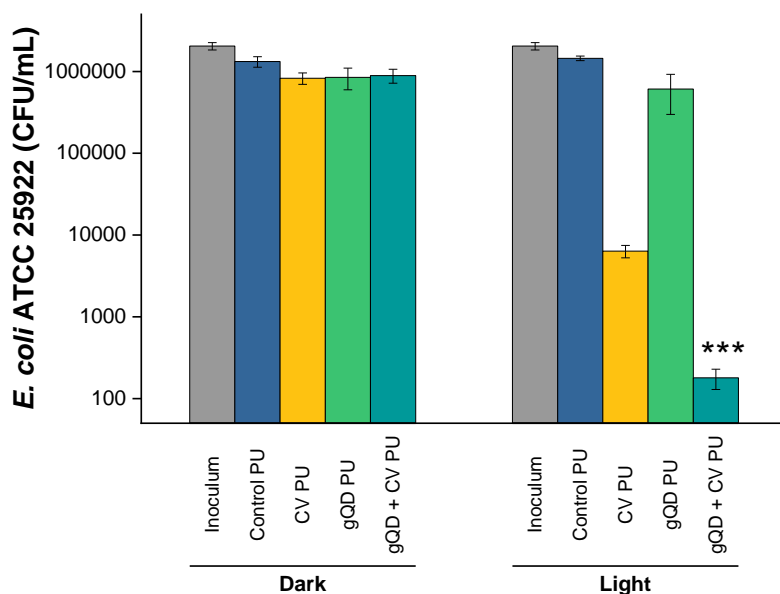


Figure 4.14 Antibacterial action of polymer embedded with green QDs and CV using the 1-step swell-encapsulation-shrink method. Viable counts of lab strain *E. coli* ATCC 25922 bacteria after 2 h incubation at 20°C in the dark and under white light (6600 ± 990 lux) on green QD and CV-encapsulated polyurethane. (Concentrations of swelling solutions used to modify PU: green QDs – 1 mgmL<sup>-1</sup>; CV – 0.5 mM)

Two-hour incubation of green QD and CV-incorporated functional surfaces (gQD + CV PU) and constituent surfaces PU in the dark yielded no significant antibacterial activity. The application of 6000 lux white light for 2 h led to no significant antibacterial activity for control PU while gQD PU surfaces displayed ~0.2 log<sub>10</sub> reduction (but  $p > 0.05$ ) however, it was observed that the *E. coli* numbers diminished by 2.4 log<sub>10</sub> ( $p < 0.001$ ) on CV PU surfaces and by 3.9 log<sub>10</sub> on gQD + CV PU surfaces ( $p < 0.001$ ). Clearly, the effect of gQD + CV on this strain of *E. coli* was even stronger when functional surfaces were produced from the 1-step swell-encapsulation-shrink technique compared to the 2-step technique, as summarised in Table 4.3. This result solidified the rationale for adopting the new 1-step dipping procedure as the standard method of functional surface manufacture, moving forward.

Table 4.3 Comparison of the antibacterial activities of gQD + CV substrates prepared by either the original 2-step dipping process or the novel single-step dipping procedure

<b>Swell-Encapsulation Method (Green QD-CV)</b>	2-step	1-step
<b>Length of Irradiation</b>	3 h	2 h
<b><i>E. coli</i> ATCC 25922 Kill</b>	3.3 log <sub>10</sub>	3.9 log <sub>10</sub>

#### 4.3.4.4. Green QD-CV Substrates by 1-Step Encapsulation against Clinical Strains

The bactericidal action of gQD + CV PU substrates against clinical isolates was analysed against both Gram-positive and Gram-negative strains (Figure 4.15). In the absence of light, incubation of the Gram-positive, EMRSA strain (4742) on CV PU and gQD + CV PU surfaces induced 0.5 log<sub>10</sub> and 0.59 log<sub>10</sub> kill of the bacterial strain, however, this was not statistically significant (no antibacterial activity observed with control PU and gQD PU in the dark). Photo-irradiation for a 1 h period attenuated EMRSA numbers by 2.7 log<sub>10</sub> on CV PU and 4.07 log<sub>10</sub> on gQD + CV PU surfaces (statistically not significant decrease of ~0.1 log<sub>10</sub> observed with gQD PU after photo-irradiation) (Figure 4.15A).

Against a clinical Gram-negative isolate, *E. coli* 1030, gQD + CV PU induced ~4 log<sub>10</sub> kill following white light irradiation for 4 h (Figure 4.15B). Photo-irradiation of CV PU also led to a 2.8 log<sub>10</sub> reduction of *E. coli* 1030 but no significant activity was observed for gQD PU and control PU. In the dark, no significant antibacterial activity was seen for any of the PU substrates.

Therefore, (red and green) QD + CV PU surfaces diminish the levels of laboratory and clinical strains of bacteria with comparable effectiveness, suggesting that the functional surfaces may operate via mechanisms independent of resistance routes. The light-activated surfaces work by generating ROS which attack bacteria at multiple intracellular sites, making the development of resistance unlikely.<sup>486</sup>

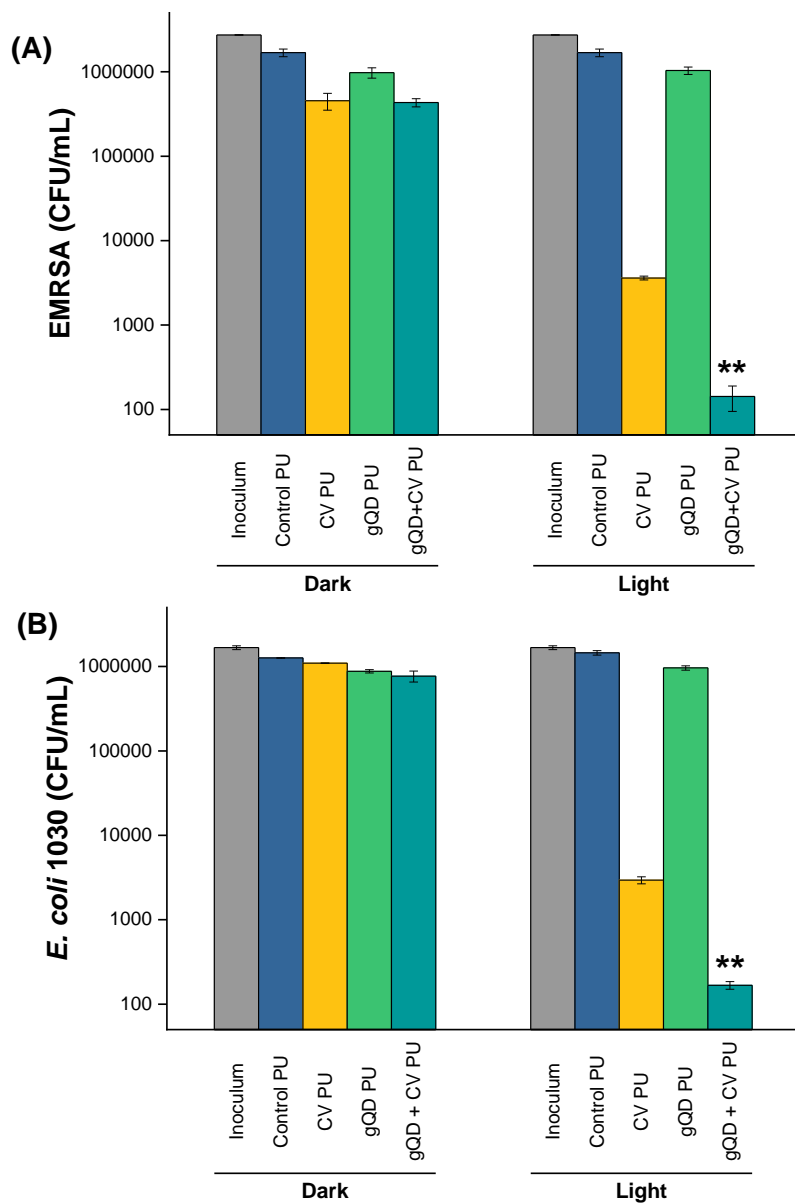


Figure 4.15 Antibacterial action of gQD + CV polymers against **(A)** clinical strain of EMRSA 4742 (1 h, 6600lux white light irradiation, 20°C incubation) and **(B)** clinical strain of *E. coli* (*E. coli* 1030, 6600lux white light irradiation for 4 h, 20°C incubation). Concentrations of swelling solutions used to modify PU: green QDs – 1 mgmL<sup>-1</sup>; CV – 0.5 mM

#### 4.3.5. Foodborne Pathogens

Food pathogens are a widespread and increasing health concern throughout the world, even in countries with enhanced food safety measures.<sup>487</sup> The full burden of foodborne disease is unknown due to underreporting and underdiagnoses but in the US, CDC estimates that annually foodborne illnesses affect nearly 48 million Americans, hospitalising 128,000 people and killing over 3000.<sup>488</sup> Major causes of food contamination include poor sanitation, poor food management, insufficient refrigeration, undercooking, inappropriate cooking temperatures, spoiled ingredients, cross contamination, and inadequate use of instruments.

Pathogens that cause foodborne illness include certain strains of *E. coli*, *Campylobacter* spp., *Salmonella* spp., *L. monocytogenes*, Norovirus and *Shigella* spp. Depending on an individual's health, nutritional status and age and the virulence of the pathogen, adverse health effects of foodborne illnesses can range from mild (e.g. nausea, vomiting and diarrhoea) to severe (e.g. kidney and liver failure, neurological disorders, septicaemia) and even death.<sup>489</sup> Milk and milk products, meat, poultry, fruits and vegetables, fisheries and marine products, grain processing and consumer products are food sectors where high levels of food-borne bacteria are present.<sup>487</sup> Food can become contaminated at many stages of the food chain, beginning in the environment and primary production, through to manufacture, distribution and retailing and ending with handling and consumption.

The following investigation was prompted by recent outbreaks in UK hospitals caused by the food contaminated with *Listeria* provided by a food supply chain.<sup>490</sup> While most microorganisms do not affect food quality or safety, some bacteria associated with raw unprocessed foods thrive and multiply in food processing environments. The accumulation of food residues on inert surfaces such as conveyors and product transport boxes can act as reservoirs for these harmful bacteria.<sup>491</sup> Domestic food surfaces can also play an important role in the transmission of foodborne disease in terms of cross-contamination during food preparation.<sup>492</sup>

Installing antimicrobial QD-CV surfaces in food processing facilities – composed of cadmium-free, QDs and an FDA-approved PS<sup>481</sup> – can aid in reducing bacterial reservoirs on food processing and preparation surfaces. To that end, the efficacy of the QD + CV PU substrates against representative Gram-negative and Gram-positive food-borne bacteria was explored.

#### 4.3.5.1. **Salmonella**

*Salmonella* infection (salmonellosis) is a common bacterial disease that affects the intestinal tract. *Salmonella* spp. are Gram-negative bacteria of the family Enterobacteriaceae, divided into two species – *Salmonella enterica* (*S. enterica*) and *Salmonella bongori* (*S. bongori*). Most cases of salmonellosis are caused by food infected with *S. enterica*, including *S. typhi*, *S. enteritidis*, *S. paratyphi* and *S. typhimurium*. Various animals (especially poultry, pigs, cattle, and reptiles) can be reservoirs for *Salmonella*, and humans generally become infected by eating poorly cooked, contaminated food. Food-borne infections caused by *Salmonella* are characterised by fever, diarrhoea, abdominal pain and vomiting. While most healthy people recover in a few days, in some cases diarrhoea associated with salmonellosis can be so dehydrating as to require hospitalisation. Life-threatening complications also may develop if the infection spreads beyond the intestines. In addition, post-infectious complications, such as reactive joint inflammation occur in about 10% of the cases. The elderly, infants and young children, transplant recipients, pregnant women, and people with weakened immune systems are more prone to developing serious complications, sometimes leading to death.<sup>493, 494</sup> CDC estimates *Salmonella* bacteria cause about 1.35 million infections, 26,500 hospitalizations, and 420 deaths in the United States every year.<sup>495</sup> In the European Union in 2018, salmonellosis was the second most common zoonosis, with 91,857 confirmed human cases, as well as the most frequent cause of food-borne outbreaks accounting for 30.7% of all cases reported. The latest data from humans, animals and food show that a large proportion of *Salmonella* bacteria are multidrug-resistant (resistant to three or more antimicrobials).<sup>496</sup>

*Salmonella typhimurium*, a leading cause of gastroenteritis, was tested against polyurethane substrates containing green QDs and CV. The bactericidal efficacy of gQD + CV PU surfaces and constituent surfaces against *S. typhimurium* ATCC 14028 – with or without a 4 h, 6000 lux white light illumination – is displayed in Figure 4.16. White light illumination of gQD + CV PU inoculated with *S. typhimurium* resulted in a 2.2 log<sub>10</sub> reduction in bacterial numbers after 4 h. Photo-irradiation of CV-treated PU and gQD-treated PU resulted in 0.5 log<sub>10</sub> and 0.7 log<sub>10</sub> reductions respectively. No statistically significant reduction of *S. typhimurium* was observed in the absence of photo-irradiation for any of the PU substrates (including gQD + CV PU).

Interestingly, after 4 h white light irradiation, CV PU had a very low antibacterial effect on *S. typhimurium* ATCC 14028, in contrast to the other Gram-negative nosocomial pathogens

considered thus far (*E. coli* ATCC 25922 and *E. coli* 1030). This data was in agreement with previous studies which show that *Salmonella* has a higher survival rate than *E. coli* in non-host environments and can better withstand a lack of nutrients and harsh ecological conditions.<sup>497, 498</sup> For example, despite containment and decontamination protocols, *Salmonella* can survive for 10-15 days in a septic system whereas *E. coli* has a negative growth rate in this environment.<sup>498</sup> In soil, *Salmonella* can survive and multiply for at least 1 year whereas *E. coli* has an average half-life of only 3 days in this ecosystem.<sup>498</sup> On inanimate surfaces, studies have revealed that *Salmonella* can persist longer than *E. coli* – *S. typhimurium* has the ability to survive for up to 4 years on dry surfaces and *E. coli* for up to 16 months.<sup>286</sup> The enhanced inherent resistance of *Salmonella* to external stresses may explain the lack of bactericidal activity of CV PU against *S. typhimurium*. Nevertheless, the gQD + CV PU surface was still effective reducing the numbers of *S. typhimurium* 100-fold.

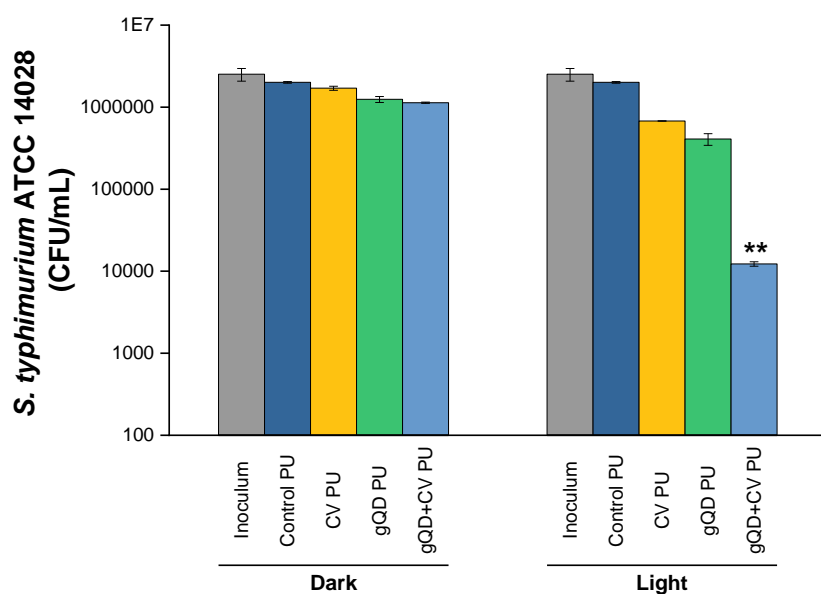


Figure 4.16 Antibacterial action of gQD + CV polymer made by the 1-step swell-encapsulation-shrink method. Viable counts of lab strain *S. typhimurium* ATCC 14028 after 4 h incubation at 20°C in the dark and under white light (6600 ± 990 lux). Concentrations of swelling solutions used to modify PU: green QDs – 1 mgmL<sup>-1</sup>; CV – 0.5 mM

#### 4.3.5.2. *Listeria*

Listeriosis is a relatively uncommon disease caused by the ubiquitous Gram-positive bacterium *Listeria monocytogenes*. Unlike most other food-borne pathogens, *L. monocytogenes* can grow in food at fairly low moisture, a high salt concentration and at refrigeration temperatures. The ability to persist and multiply in the food environment makes *L. monocytogenes* especially difficult to control.<sup>489</sup> *L. monocytogenes* has been associated with such foods as raw milk, soft cheeses, raw vegetables, fermented raw-meat sausages, raw and cooked poultry, raw meats, and raw and smoked fish. Though the incidence of listeriosis is relatively low, it is an important foodborne disease as it causes a high proportion of severe cases and deaths in risk groups such as elderly and immunocompromised persons as well as pregnant women and infants.<sup>499</sup> In 2018 in the USA, 126 *Listeria* cases caused 121 hospitalisations and 26 deaths (equivalent to a 21% mortality).<sup>500</sup> In Europe, over 2500 cases of listeriosis were reported in 2016, of which almost all required hospitalisation (97.7%) and 247 cases were fatal.<sup>501</sup> The above figures illustrate the public health impact of listeriosis and particularly in settings where risks groups are served (e.g. hospitals, nursing homes), *Listeria* infection is a major problem.

The number of listeriosis cases continues to increase, calling for more attention to the prevention and control of the disease and outbreaks. QD + CV PU surfaces are highly effective in reducing the levels of surface-contaminating *L. monocytogenes* as illustrated in Figure 4.17. After photo-irradiation with 6000 lux white light for just 1.5 h, gQD + CV PU substrates were able to reduce *L. monocytogenes* numbers to below the detection limit from a starting inoculum of  $\sim 10^6$  cfu/mL. Photo-irradiation of CV PU reduced *L. monocytogenes* numbers by 3 log<sub>10</sub> and gQD PU surfaces induced a 0.35 log<sub>10</sub> kill. In the absence of photo-irradiation, none of the polyurethane substrates showed any significant bactericidal activity against *Listeria*.

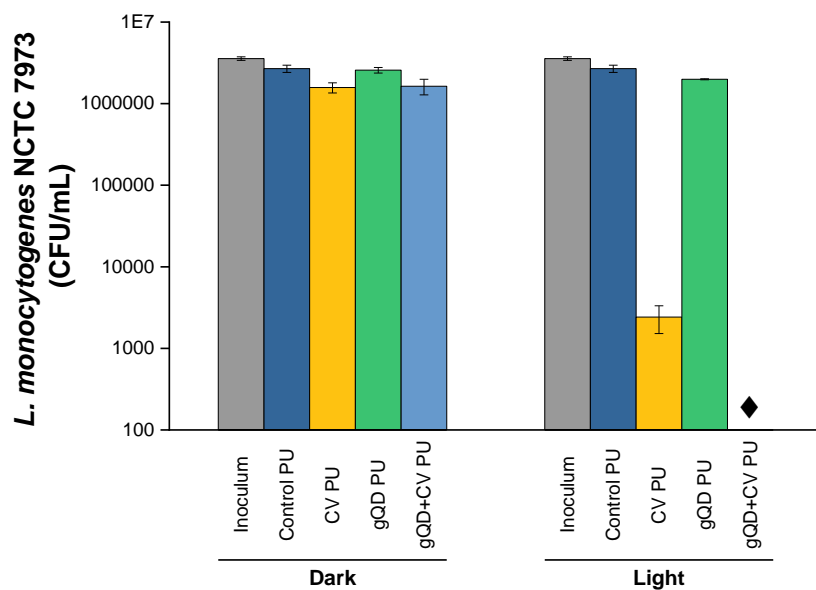


Figure 4.17 Antibacterial action of gQD + CV polymer made by the 1-step swell-encapsulation-shrink method. Viable counts of *L. monocytogenes* NCTC 7973 after 1.5 h incubation at 20°C in the dark and under white light (6600 ± 990 lux). Concentrations of swelling solutions used to modify PU: green QDs – 1 mgmL<sup>-1</sup>; CV – 0.5 mM. ♦ indicates bacteria numbers are below the detection limit of 100.

The total elimination of *Listeria* from gQD + CV surfaces appeared to be a result of the Gram-positive bacterium being more susceptible to the irradiated photosensitiser surfaces (CV PU), yielding a 3 log<sub>10</sub> reduction, compared to CV PU against *S. aureus* which typically yielded antibacterial activity < 3 log<sub>10</sub>. The synergistic effects when QDs are added to CV in the polymer generated a sufficient amount of ROS to eradicate the remnant bacteria from the surface.

#### 4.3.6. Evaluation of Synergistic Effects

Synergistic photo-bacterial destruction by rQD + CV and gQD + CV polymer surfaces was assessed using a method adapted from Drewinko *et al.*<sup>502</sup> Synergism when QDs and CV are present in polyurethane was calculated using the following equation:

$$\alpha = F_{QD} \times F_{CV} / F_{QD+CV}$$

Equation 4.1

where  $F$  is the fractional bacterial viability, relative to the control material – for a control viability (cfu/mL) of  $10^6$  and a viability after treatment of  $10^2$ , the fractional viability is  $10^{-4}$ .  $F_{QD}$  and  $F_{CV}$  in the numerator denote the fractional viability of the separate therapies, QD PU and CV PU.  $F_{QD+CV}$  in the denominator is the fractional viability observed following the combination treatment.  $\alpha$  is the ratio of the cumulative effect of the two separate therapies tested independently to the net effect of combining the two therapies together.  $\alpha$  describes whether the summative effect of the therapies was synergistic, additive or antagonistic. If  $\alpha > 1$  then the result is synergistic,  $\alpha = 1$  represents an additive effect and an antagonistic effect is denoted by  $\alpha < 1$ .<sup>503, 504</sup> Table 4.4 and Table 4.5 show the fractional viabilities and alpha values for each bacterium tested on rQD + CV PU and gQD + CV PU after 6000 lux white light irradiation.

Table 4.4 Test for synergy between red QDs and CV for each strain: tabulated fractional viabilities and derived values for  $\alpha$ . The values are greater than unity in each case which demonstrates a synergistic interaction.

Bacterial Strains		$F_{rQD}$	$F_{CV}$	$F_{rQD+CV}$	$\alpha$
Gram-negative	<i>E. coli</i> ATCC 25922	0.30	$8.9 \times 10^{-4}$	$5.5 \times 10^{-5}$	4.8
	<i>E. coli</i> 1030	0.40	$2.5 \times 10^{-2}$	$3.9 \times 10^{-4}$	25.7
Gram-positive	MRSA NCTC 13143	1.30	$1.9 \times 10^{-3}$	$1.6 \times 10^{-4}$	14.9
	EMRSA 4742	0.74	$1.1 \times 10^{-3}$	$4.3 \times 10^{-5}$	18.2

Table 4.5 Test for synergy between green QDs and CV for each strain: tabulated fractional viabilities and derived values for  $\alpha$ . The values are greater than unity in each case which demonstrates a synergistic interaction. \*  $\alpha = \infty$  at the detection limit of the test.

Bacterial Strains		$F_{gQD}$	$F_{CV}$	$F_{gQD+CV}$	$\alpha$
Gram-negative	<i>E. coli</i> ATCC 25922	0.42	$4.4 \times 10^{-3}$	$1.2 \times 10^{-4}$	15.0
	<i>E. coli</i> 1030	0.66	$2.1 \times 10^{-3}$	$1.2 \times 10^{-4}$	11.6
	<i>S. typhimurium</i> ATCC 14028	0.20	0.34	$6.1 \times 10^{-3}$	11.2
Gram-positive	EMRSA 4742	0.61	$2.0 \times 10^{-3}$	$8.5 \times 10^{-5}$	15.6
	<i>L. monocytogenes</i>	0.74	$9.0 \times 10^{-4}$	0	$\infty^*$

Comparison of the fractional viabilities for each surface type showed that for each bacterium, the functional surface containing the combination of QDs with CV ( $F_{QD+CV}$ ) had the lowest surviving fractions while surfaces containing QDs only had the highest surviving fractions. This meant that QD + CV PU provided the best antibacterial activity and QD PU the lowest in each study. Overall, the  $\alpha$  values were far greater than 1 for rQD + CV PU and gQD + CV PU surfaces, indicating that high degrees of synergism were observed for all strains tested for all surfaces produced by the novel one-step swell-encapsulation-shrink technique. Generally, longer irradiation times were required for Gram-negative bacteria (4 h vs ~1 h for Gram-positive), therefore Gram-positive bacteria were more susceptible to the lethal activity of QD + CV surfaces. This was ascribed to the greater strength and thickness of the double-membraned cell wall of Gram-negatives compared to Gram-positives which only possess a single-membraned cell wall. It was likely that initial ROS generated by the surfaces were quenched upon interaction with the cell wall.<sup>505</sup> Thus a higher concentration of exogenous ROS (generated through longer light activation of the QD + CV PU) was required to accumulate before a loss in cell viability of Gram-negative bacteria followed.

The effectiveness of CV PU and QD + CV PU substrates do not vary much between the Gram-positive species, as evidenced by the similar values of  $\alpha$  for EMRSA 4742 and MRSA NCTC 13143, indicating that the mutations that differentiate the two Gram-positive bacteria do not confer abilities that protect the bacteria from light-activated killing by CV and QDs. Between the Gram-negative species *E. coli* ATCC 25922 and *E. coli* 1030, *E. coli* 1030 showed a higher  $\alpha$  value because the effect of CV PU was more pronounced in the laboratory strain *E. coli* ATCC 25922. *E. coli* 1030 is a multidrug resistant clinical strain of *E. coli* which produces both

New Delhi-metallo-beta-lactamase 1 (NDM-1) and oxacillinase-48 (OXA-48) carbapenemases. The NDM-1 and OXA-48 genes are normally carried on a variety of plasmids along with other resistance factors. NDM-1 confers on its host bacteria almost all  $\beta$  lactam resistance and is accompanied by the expression of multiple efflux systems, porin loss and altered membrane permeability.<sup>506, 507</sup> This increased efflux activity and reduced membrane permeability of *E. coli* 1030 likely resulted in reduced interactions of the bacterium with surface CV. While the exact mechanism of action of CV is unknown, one hypothesis attributes the antimicrobial effects of CV to its ability to penetrate and form adducts with bacteria. This theory forms the basis of the Gram stain – CV is highly effective against Gram-positive bacteria because it can penetrate their cell wall and covalently bond with proteins but is less effective against Gram-negative bacteria due to the dye's inability to penetrate the lipids surrounding the cell wall. Presumably, the structural and metabolic changes induced by NDM-1 and OXA-48 production by *E. coli* 1030 further diminished the antimicrobial effect of CV. Despite the longer exposure of *S. typhimurium* to gQD + CV PU substrates, we observe a similar  $\alpha$  value of this bacterium compared to the two *E. coli* spp. This was attributed the natural features of *S. typhimurium* which allow the bacterium to survive longer and thrive better on inanimate surfaces.<sup>286</sup>

#### 4.4. Conclusion

Surfaces containing crystal violet photosensitisers and QDs were shown to be effective light-activated antibacterial surfaces against both Gram-negative and Gram-positive nosocomial and food-borne bacteria. A novel approach – a single-step swell-encapsulation-shrink method – was employed to prepare functional surfaces that aided uptake of QD nanoparticles in the polymer during the swelling process and improved co-localisation of the QD-CV complex. Better co-localisation of nanoparticles and photosensitiser enhanced the efficiency of FRET and/or PET which in turn, improved light-activated antibacterial efficiency. Other benefits of this approach were: faster and easier preparation times; less waste of QDs thus lowering costs and reducing environmental impact; and finally, the new process requires less CV which makes for substrates that are more aesthetically pleasing. The method may also be well-suited to produce other polymer substrates that combine one or more NPs (such as Au and Ag NPs) with one or more photosensitisers (such as methylene blue and toluidine blue) as it may improve surface plasmon resonance and boost ROS generation.

Crucially, in this chapter, it has been established that the presence of a photosensitiser was imperative for lethal light-activated antibacterial activity, as QDs on their own show little to no antibacterial activity. Polymers containing QDs combined with CV showed synergistic effects, enhancing the activity of the constituent polymers. The potentiation of photo-antibacterial action after modifying the fabrication process to better satisfy FRET requirements strongly suggested FRET was occurring. The ROS produced oxidise multiple intracellular sites within the bacteria thus offering a means of infection control with a low likelihood of resistance development. The non-selective action of ROS was well demonstrated by the QD + CV surfaces' ability to efficiently eliminate both laboratory bacterial strains and clinical bacterial strains which are not domesticated and thus more representative of wild strains circulating in hospitals. The powerful activity of QD + CV PU substrates against susceptible and resistant strains of bacteria highlights the motivation behind the development of these surfaces that do not rely on antibiotics thus preserving and preventing the overuse and misuse of these valuable drugs. In the next chapter, the efficacy of antibacterial action of the functional surfaces will be evaluated under low intensity lighting conditions.

# CHAPTER 5. LOW LIGHT INTENSITY ANTIBACTERIAL ACTIVITY OF QD + CV PU SURFACES

## 5.1. Introduction

Increasing antimicrobial resistance (AMR) in bacteria coupled with the unmet need for new antibiotics has aroused interest in alternative antimicrobial therapies, including antimicrobial therapies that reduce the incidence of AMR by avoiding the use of antibiotics. Antimicrobial photodynamic therapy (aPDT) involves the simultaneous application of light, oxygen and photosensitisers (PS) to generate ROS through type I and type II mechanisms – a promising strategy to eradicate bacteria without inducing antibiotic resistance.<sup>508</sup> In aPDT, a light source is required to provide the energy necessary to initiate the activation of the PS and while the energy required to activate a PS depends on its molecular structure, in all cases, it is ideal to have strong light output.<sup>200</sup> However, high intensity light sources can be disadvantageous as this can drastically reduce the stability of conventional dye-based therapies which are susceptible to photobleaching. In addition, the use of ultraviolet ionising radiation as an energy source for photoinactivation and aPDT poses major health risks.<sup>509</sup> Furthermore, acquiring, operating and maintaining special light sources (e.g. lasers and wavelength-filtered light sources) for aPDT on an institution-wide scale may be impractical due to high costs and in some regions, low accessibility and availability.<sup>510</sup> This is an important, yet often overlooked, criterion for light-activated antimicrobial therapies as it determines the feasibility and successful translation to clinical use: the need for aPDT applications to be effective under lighting conditions used in the environments for which they are designed. In the hospital setting, general lighting criteria (for example, in wards, reception areas and treatment rooms) to which hospitals must conform often require light intensities less than 1000 lux.<sup>511</sup> At these low light levels, aPDT applications are often ineffective, resulting in low antimicrobial activity.

Gram-negative bacteria account for more than 70% of urinary tract infections (UTIs); *E. coli* and *Pseudomonas aeruginosa* (*P. aeruginosa*) are among the most common uropathogen and as Gram-negative pathogens, are inherently harder to eradicate due to the protective double-membraned cell wall.<sup>512</sup> *P. aeruginosa* is an opportunistic Gram-negative bacterium

that causes infection primarily in immunosuppressed individuals. It commonly colonises moist environments within the hospital including sinks, sluices and showers and these can act as sources of infection during outbreaks.<sup>513, 514</sup> *P. aeruginosa* causes hospital-acquired pneumonia (including ventilator-associated pneumonia), bloodstream and urinary tract infections. Several factors, such as its ability to colonise multiple environmental niches, to utilise many compounds as energy sources and its inherent tolerance to many detergents, disinfectants and antimicrobial compounds, make management of *P. aeruginosa* in hospitals and other healthcare facilities difficult.<sup>515</sup> Furthermore, treatment of infections caused by the bacterium is being rendered increasingly ineffective due to the emergence and spread of resistance to the few therapeutic options that remain, particularly the acquisition of carbapenemases by some strains of *P. aeruginosa*.<sup>305, 308</sup> Cystic fibrosis (CF) patients are at increased risk from chronic *P. aeruginosa* lung infections that accounts for the majority of the morbidity and mortality in CF. Besides the lungs, *P. aeruginosa* can colonise and infect virtually all tissues and is frequently found in burn wounds and eye infections.<sup>515</sup> *P. aeruginosa* has also been found to contaminate hospital surfaces such as bed rails, floors and sinks as well as surfaces of medical devices such as joint replacements, indwelling venous and urinary catheters and ventilators and is transmitted by close contact to contaminated surfaces thus posing a high risk for CF patients. Hygienic measures to prevent colonisation of CF patients include high-level disinfection of non-disposable equipment and surfaces.<sup>516-518</sup>

*Escherichia coli* (*E. coli*) is a Gram-negative bacterium that normally lives in human and animal intestines as it is needed for bowel function and is an important part of a healthy human intestinal tract. However, it is also a common cause of hospital-acquired urinary tract infections, septicaemia and meningitis. In common with *P. aeruginosa*, *E. coli* and other members of the Enterobacteriaceae thrive in moist hospital environments which can act as sources of infection.<sup>519, 520</sup> AMR in *E. coli* develops either through mutations or by acquisition of mobile genetic elements encoding resistance mechanisms, such as the production of beta-lactamases and extended spectrum beta-lactamases (ESBLs), conferring resistance to beta-lactam antibiotics such as ampicillin, amoxicillin and third generation cephalosporins. Carbapenems usually resist the effect of ESBLs and sometimes offer one of the few treatment options for severe infections. However, the horizontal acquisition of carbapenem resistance mediated by a range of carbapenemase enzymes is a growing problem and, may confer resistance to all available beta-lactam antibiotics.<sup>305</sup>

*E. coli* and *P. aeruginosa* colonise hospital water environments and there is opportunity for genetic exchange between them (with the potential for exchange of antibiotic resistance genes and virulence factors).<sup>521</sup> In addition, biofilms formed by these bacteria are resilient, difficult to eradicate and are a common source of many persistent and chronic infections.<sup>522, 523</sup> Therefore, use of a material able to reduce colonisation by these bacteria would reduce biofouling, limit the opportunity for antibiotic resistance gene transfer and also decrease the transmission of hard-to-treat Gram-negative hospital-acquired infections.

In the previous chapter, quantum dot and crystal violet incorporated surfaces were shown to be effective light-activated agents against both laboratory and clinical strains of Gram-positive and Gram-negative bacteria. This antibacterial effect was stronger than the effect observed with constituent surfaces, containing only QDs or CV. The synergistic effect was attributed to the occurrence of FRET and PET in the hybrid system, boosting the production of ROS by the combinatorial functional surfaces. In this chapter, it was demonstrated that using light-activated green QD-CV antibacterial surfaces is an effective means to reduce levels of *P. aeruginosa* and *E. coli* bacteria despite their natural intrinsic resistances, even at light intensities deemed ineffective for efficient photodynamic therapy. Light intensities are reduced by >10-fold compared to previous experiments, to realistically mimic lighting in clinical settings. This chapter also begins to analyse some of the mechanism responsible for antibacterial activity observed.

## **5.2. Materials & Methods**

### **5.2.1. Quantum dot nanoparticles**

Only green-emitting QDs were employed for this part of the study as red QDs were in short supply from our suppliers, Nanoco Technologies. These QDs had a peak emission at ~520 nm.

### **5.2.2. Incorporation of nanoparticles and dye into polymer**

Green emitting cadmium-free indium-based QDs (CFQD<sup>®</sup> nanoparticles) and crystal violet dye (CV) were embedded into polyurethane using the 1-step 'swell-encapsulation-shrink' dipping technique.<sup>404</sup> Stock solutions of QDs in cyclohexane (2 mg/mL) and CV in dichloromethane (1 mM) were used to prepare dipping solutions of the following final concentrations: 1 mg/mL

QD + 0.5 mM CV, 1 mg/mL QD, and 0.5 mM CV in a solvent system of 1:1 cyclohexane: dichloromethane (Cy/DCM). Polymer squares (1 cm<sup>2</sup>) were dropped into each solution and left to swell in the dark for 24 h inside a closed vial containing 10 mL of dipping solution. Subsequently, samples were left to dry in the dark at room temperature for 24 h, washed with dH<sub>2</sub>O and air dried, producing polymer substrates consisting of a combination of QDs and CV (QD + CV PU); QDs only (QD PU); and CV only (CV PU) respectively. As controls, polymer samples were swollen in neat 1:1 Cy/DCM solvent.

### **5.2.3. Material Characterisation**

#### **5.2.3.1. Transmission Electron Microscopy**

Prior to transmission electron microscopy (TEM) imaging of quantum dots, CFQDs<sup>®</sup> suspended in cyclohexane was drop cast onto 300 mesh carbon coated copper grid (Agar Scientific) and air-dried. High resolution (HR)-TEM images were acquired using a JEOL 2100 transmission electron microscope (TEM) with a LaB6 source operating at an acceleration voltage of 200 kV. Micrographs were taken on a Gatan Orius charge-coupled device (CCD) camera with Digital Micrograph software. Particle size analysis was carried out using Gatan Suite software.

#### **5.2.3.2. Fluorescence Microscopy**

Modified polyurethane samples were embedded vertically in paraffin blocks. 15 µm thick cross-sections were cut using a microtome and the sections were mounted on microscope slides for fluorescence imaging. The sections were imaged using a cooled scientific-grade 16-bit digital CCD camera (Princeton Instruments Inc., Model PIXIS 512) operated by WinSpec software, coupled to an inverted fluorescence microscope (Olympus UK Ltd., Model IMT-2). The samples were imaged using a 10x objective, and the fluorescence signal from crystal violet present in the polyurethane was detected via a bandpass filter centred at 640 nm (Omega Optical Inc., 640DF35) using excitation by a 532 nm laser diode (Thorlabs Inc.). The images were subsequently analysed using ImageJ software (National Institutes of Health, U.S.A.).

#### **5.2.4. Bacterial strains**

A multi-drug resistant (MDR) clinical strain of *Escherichia coli* (*E. coli* 1030) which produces both NDM-1 and OXA-48 carbapenemases, an environmental isolate of *Pseudomonas aeruginosa* (P12) recovered from a sink within the liver intensive care unit and an isolate of *P.*

*aeruginosa* (P1068) from a cystic fibrosis (CF) patient, were obtained from J. Wade, King's College Hospital, London. For superoxide detection assays, EMRSA 4742 was obtained from P. Wilson, University College London Hospital. Bacteria were stored at  $-70\text{ }^{\circ}\text{C}$  in BHI containing 20% (v/v) glycerol and propagated onto either MAC agar in the case of *E. coli* and *P. aeruginosa* or MSA in the case of EMRSA, for a maximum of two subcultures at intervals of two weeks before reviving once more from freezer stocks.

### 5.2.5. Antibacterial Activity

QD + CV PU, QD PU, CV PU and control PU substrates were tested against bacteria using the same protocol as described in the preceding chapter (Section 4.2.5.2). However the light source used in low light studies was the Osram 58 W/865 LUMILUX T8, which gave an incident light intensity of  $499 \pm 19$  lux. Also the incubation time of inoculated samples in the absence or presence of light was 18 h for *E. coli* and 24 h for *P. aeruginosa*. After incubation, processing of inoculated samples and plating of serial dilutions on agar followed the usual protocol.

#### 5.2.5.1. Log and Percentage Reductions in Antimicrobial Studies

Log and percent reductions were used to express the magnitude of the change in bacteria colony numbers before and after treatment, and derived as follows:

$$\text{Log Reduction} = \log_{10}\left(\frac{A}{B}\right)$$

$$\text{Percentage Reduction} = \frac{(A - B) \times 100}{A}$$

Where A = the number of bacterial CFUs present before treatment (control material)

B = the number of CFUs present after treatment (test material)

### 5.2.6. Detection of Superoxide

To investigate the mechanism of bactericidal activity, superoxide dismutase (SOD) in PBS (50 U/mL) was added to the bacterial suspension and antibacterial tests were carried out on the polyurethane substrates using the protocol described in Section 4.2.5.2. The purpose of SOD was to deactivate any superoxide radicals emanating from the polymer surface. SOD from

bovine erythrocytes was purchased from Sigma-Aldrich, UK and filter sterilised using a 0.2 µm PES syringe filter (VWR, UK).

### **5.2.7. Statistical Analysis**

See Section 4.2.5.5.

## 5.3. Results & Discussion

### 5.3.1. Material Characterisation

The indium-based green-emitting QDs were small, monodispersed and mainly spherical, as evidenced by high-resolution TEM images (

Figure 5.1A). Analysis of TEM images using Gatan Suite software determined the average size of the green QDs to be  $2.9 \pm 0.5$  nm and the nanoparticles were characterised by good shape uniformity and narrow size distribution (

Figure 5.1B). Polymer substrates were subsequently imaged using fluorescence microscopy to analyse the extent of the diffusion of QD and/or dye through the polymer. Examples of images obtained using fluorescence microscopy are displayed in false colour (

Figure 5.1C,D). Each image shows roughly one half of the polymer examined on the right hand side of each image, providing an overview of the NP and CV diffusion gradient through the polymer. On the false colour scale, black/blue corresponds to low fluorescence and red/white corresponds to high fluorescence. Profile plots were also generated using ImageJ software and correlated to a graphical representation of the fluorescence distribution through the polymer. The distributions of fluorescence, for both polymer substrates embedded with QD only ( $1\text{mgmL}^{-1}$ ,

Figure 5.1E) and that embedded with a combination of QD and dye ( $1\text{mgmL}^{-1}$  QD +  $20\ \mu\text{M}$  CV,

Figure 5.1F), were quite even throughout the polymer, indicating that encapsulation was not localised to the surface but actually the QD and/or dye were encapsulated into the polymer bulk as well. This was in line with what is expected when swell-encapsulation-shrink is carried with a solvent that causes a high degree of polymer swelling (see effect of dichloromethane in Table 3.1) compared to what is observed with other solvents such as 100% water and 9:1 water/acetone where impregnation is predominately at the surface as these solvents do not have a strong swelling effect on the polymer.<sup>405, 408</sup>

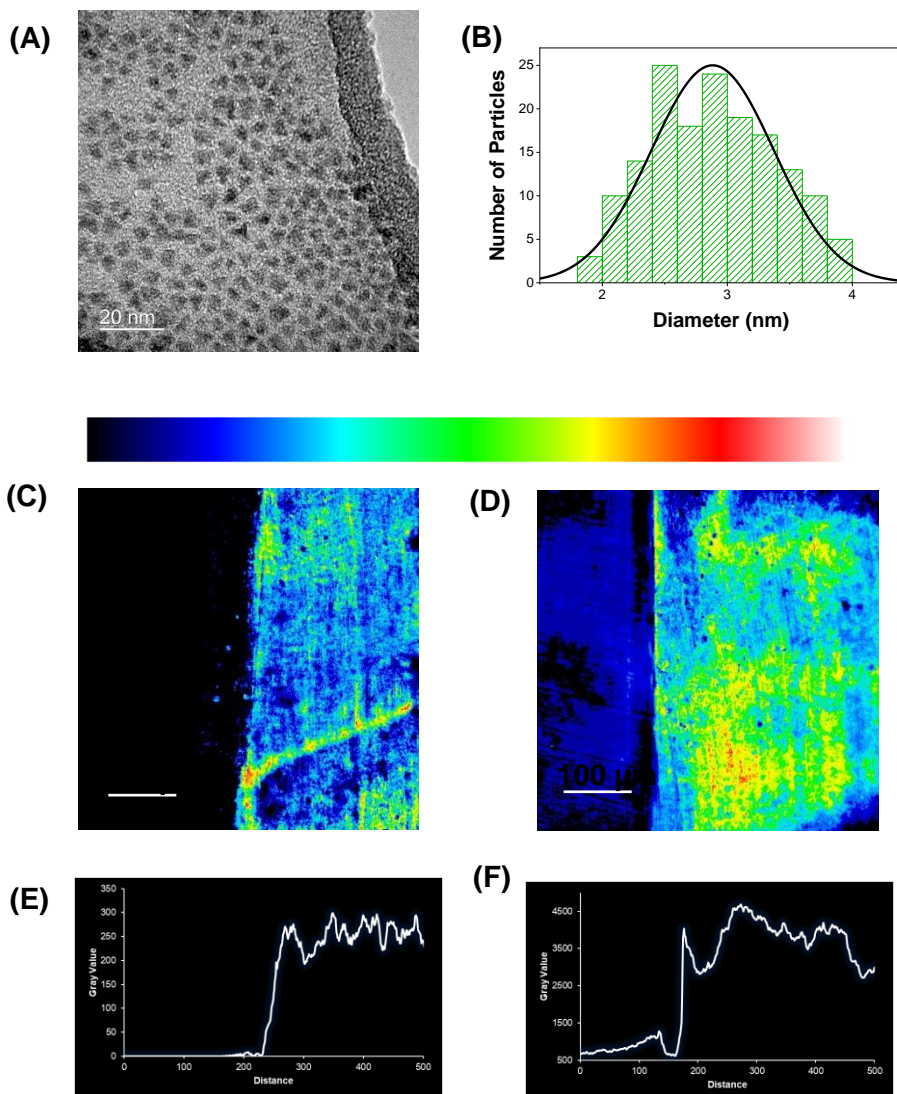


Figure 5.1 **(A)** HR-TEM image of green-emitting indium-based quantum dots. **(B)** Histogram of size distribution of green-emitting QDs. **(C)** and **(D)** CCD false coloured fluorescence microscope images of 15 micron thick sections of modified polyurethane sections (control subtracted). The polymer is shown from the right hand side of the images. Colour intensity (top) ranges from black (no fluorescence or background) to red/white (corresponding to maximum fluorescence). Image resolution: 512 x 512 pixels (557 x 557 microns). Scale: 100 microns. **(C)** Polymer prepared via swell-encapsulation-shrink in 1mg/ml-1 green QD suspension (1:1 cy/DCM); **(D)** Polymer prepared via swell-encapsulation-shrink in a suspension of 1mg/ml-1 green QD and 20  $\mu$ M crystal violet (1:1 cy/DCM). **(E)** and **(F)** The distribution of the fluorescence, for both polymer substrates in C and D respectively.

### 5.3.2. Antimicrobial Testing

The photo-active surfaces were inoculated with *P. aeruginosa* P12, *P. aeruginosa* P1062 or *E. coli* 1030 and irradiated for up to 24 h with a white light source of 500 lux intensity. As controls, solvent-treated polyurethane (control PU), QD-incorporated polyurethane (QD PU) and CV-incorporated polyurethane were also tested. To increase the relevance of the protocol, the light source intensity was carefully restricted to a maximum of 500 lux as this was close or equivalent to the recommended light levels for a number of settings and treatments in the hospital such as reception desks (500 lux), laboratories (500 lux), clinical beds (400 lux), anaesthesia rooms (500 lux), scrub-up areas (500 lux), general nursing care at bedsides (300 lux), and examination or treatment at bed positions (1000 lux).<sup>511</sup>

*P. aeruginosa* P12 is generally sensitive to many antibiotics and was recovered from a patient sink within an Intensive Care Unit at King's College Hospital, London. Environmental isolates, which are a known source of infection, are often sensitive to antibiotics compared to patient isolates, suggesting that resistance develops after infection.<sup>524</sup> The efficacy of the doped polyurethane substrates against *P. aeruginosa* P12 was investigated following 24 h in the dark and 24 h exposure to a low intensity white light source with intensity averaging  $499 \pm 19$  lux (Figure 5.2A). Following 24 h dark incubation, there was no significant change in the numbers of *P. aeruginosa* P12 on the control PU and QD PU substrates indicating no antibacterial activity, while CV PU and QD + CV PU samples showed a  $0.3 \log_{10}$  and  $1.0 \log_{10}$  reduction in bacterial numbers, respectively. Similarly, exposure to 500 lux white light for 24 h showed no antibacterial activity for the control PU or QD PU but the addition of CV (CV PU) produced a  $0.9 \log_{10}$  reduction in bacterial numbers. When quantum dot and CV were combined in polyurethane (QD + CV PU) and irradiated, the greatest bactericidal activity was observed with the numbers of *P. aeruginosa* P12 being reduced by  $3.3 \log_{10}$  (99.95%;  $p = 0.03$  compared to CV PU).

*P. aeruginosa* P1068 is a clinical isolate derived from a CF patient that was tested with the functional surfaces (Figure 5.2B). No statistically significant difference was observed for any of the substrates in the dark nor from the control or QD PU surfaces illuminated with light of 500 lux. However, following low level light illumination, CV PU elicited a  $0.9 \log_{10}$  reduction in the numbers of *P. aeruginosa* P1068 and the combination of QD + CV in the surface resulted in a  $3.4 \log_{10}$  reduction in bacterial numbers, corresponding to a 99.96% efficiency ( $p = 0.025$ ).

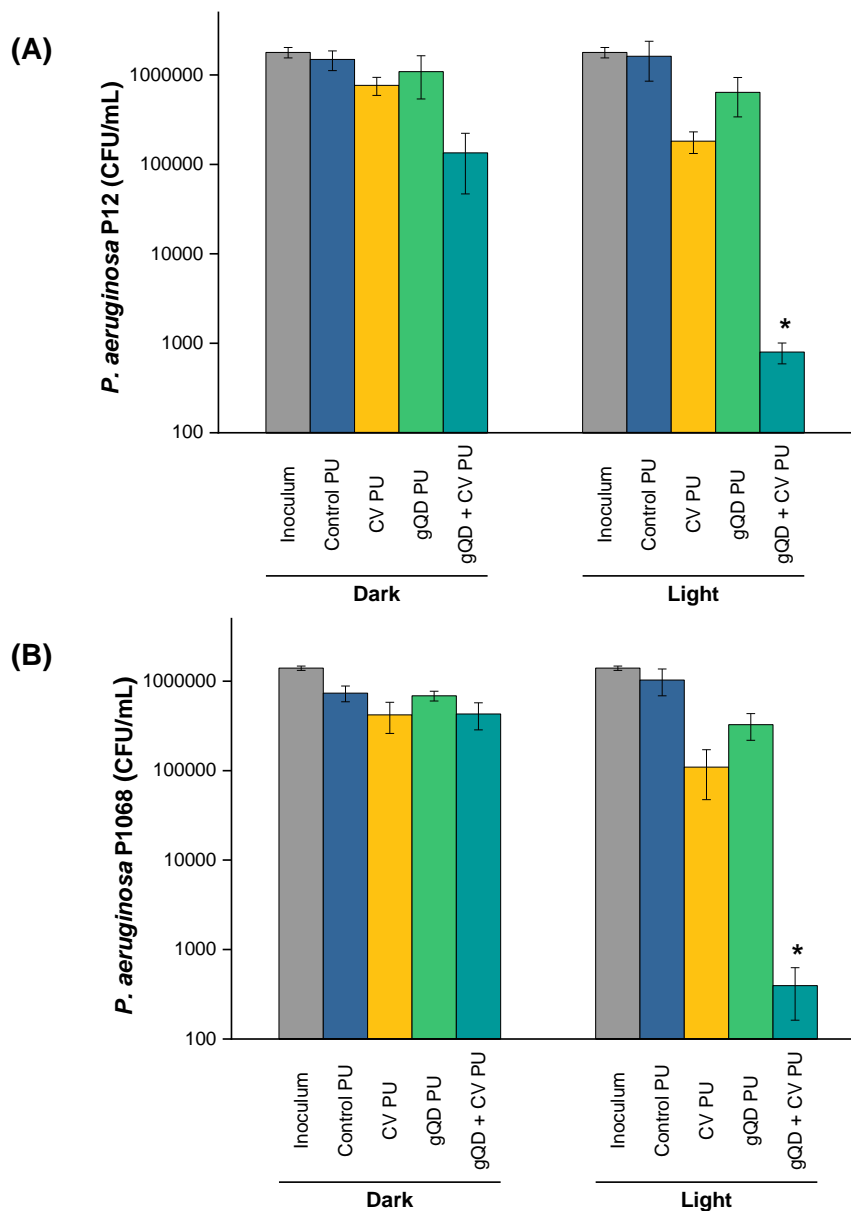


Figure 5.2 Low light intensity antibacterial activity of gQD + CV substrates. Viable counts of **(A)** environmental *P. aeruginosa* P12 on modified polyurethane surfaces after 24 h irradiation at 500 lux, **(B)** clinical *P. aeruginosa* P1068 on modified polyurethane surfaces after 24 h irradiation at 500 lux. (Concentrations of swelling solutions used to modify PU: green QDs – 1 mgmL<sup>-1</sup>; CV – 0.5 mM)

The activity of the substrates against *E. coli* 1030, a carbapenemase-producing clinical strain was also analysed (Figure 5.3). Following 18 h incubation in the dark, there was no significant antibacterial effect on any of the PU substrates. On the other hand, 18 h irradiation resulted

in a 1.8 log<sub>10</sub> reduction in the numbers of *E. coli* for the CV PU substrates and a 2.9 log<sub>10</sub> reduction in bacterial numbers for the QD + CV PU substrates (99.88%,  $p = 0.001$  compared to CV PU). Again, the control PU and QD PU substrates showed no significant bactericidal activity.

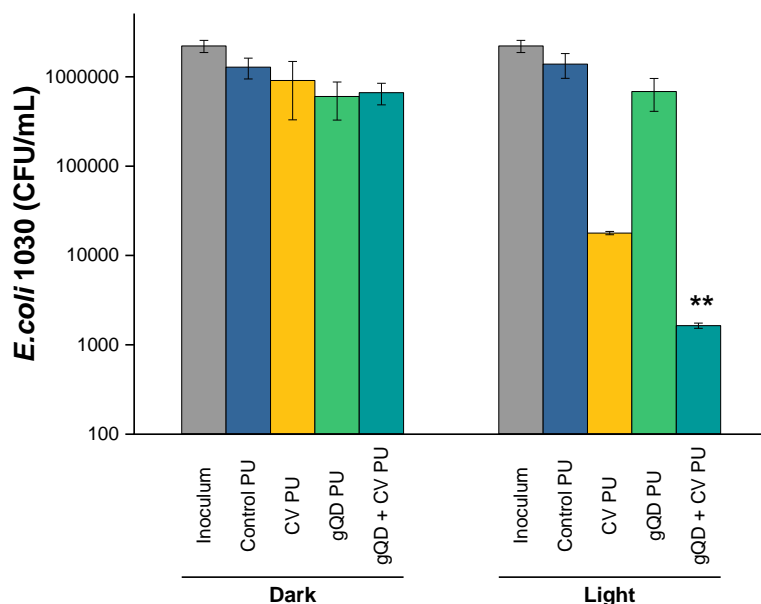


Figure 5.3 Low light intensity antibacterial activity of gQD + CV substrates. Viable counts of multi-drug resistant *E. coli* 1030 on modified polyurethane surfaces after 18 h irradiation at 500 lux. (Concentrations of swelling solutions used to modify PU: green QDs – 1 mgmL<sup>-1</sup>; CV – 0.5 mM)

The functional surfaces were expected to perform at similar efficiencies against the two Gram-negative bacteria *E. coli* and *P. aeruginosa* as they share similar structural characteristics. However, to achieve the similar level of bacterial destruction, a longer illumination time was required for *P. aeruginosa*. This may be explained by the fact that *E. coli* possesses both non-specific large general porins and substrate-specific channels on its outer membrane, whereas *P. aeruginosa* does not display such large general porins, allowing only specific diffusion of various small molecules.<sup>525</sup> The lack of general porins in *P. aeruginosa* means that penetration of ROS is reduced compared to *E. coli*, resulting in a slower disinfection rate of *P. aeruginosa* from the QD-CV surface. By the same token, if there was any leakage of CV and/or QD particles from the QD-CV surface, this would have a reduced effect on *P. aeruginosa*. However, QD nanoparticles are very unlikely to leach out of the polymer due to their hydrophobicity and large size. Furthermore, *P. aeruginosa* may be capable of withstanding a

highly oxidative environment for longer periods of time due to its lower cell permeability (~100-fold lower cell permeability than *E. coli*)<sup>526</sup> as well as adaptive mechanisms such as the ability to produce pigments such as pyomelanin, which have been shown to confer a degree of tolerance to oxidative stress generated by photo-activation of photosensitisers.<sup>527, 528</sup>

In each test, polyurethane containing only quantum dots showed no bactericidal activity. This was previously noted in our other studies and is attributed primarily to the limitations in nanoparticle uptake by the polymer via the non-covalent incorporation method employed as well as the lower QD absorption of the light source used compared to UV light sources.<sup>411</sup> Additionally, we note a low but significant reduction of *P. aeruginosa* on CV PU in the absence of illumination. This limited dark toxicity against the bacterium is likely a result of CV's intrinsic antimicrobial properties that, for decades prior to the discovery of antibiotics, made CV an effective broad-spectrum therapeutic agent.<sup>422, 529</sup> After illumination, the presence of CV in the polymer caused a significantly higher increase in bactericidal activity in combination with the QD compared to the dark. This implied that the interaction between QDs and CV presented additional sources of ROS production via Förster resonance energy transfer (FRET) and/or photoelectron transfer (PET). In order to demonstrate that the QDs and CV could physically interact in the polymer microenvironment, optical spectroscopic studies were carried out.

### 5.3.3. Photophysics

The PL of the green-emitting indium-based QDs is efficiently quenched by the addition of CV in Cy/DCM solution in a dose-dependent manner. (Figure 5.4A) However, a simultaneous increase in CV fluorescence is not observed as expected due to the formation of TICT states which rapidly relax to the ground state in solution, yielding a low fluorescence yield.<sup>483</sup> A time-resolved measurement of the QD PL when incorporated into polyurethane is displayed in Figure 5.4B. Again, the PL lifetime of the QDs decreases with increasing CV concentration, in agreement with the trend observed for steady QD emission in solution. Taken together, these data indicate that QDs must be in close proximity to CV within the polymer.

Generally, a decrease in PL lifetime in the presence may result from non-luminescent exciplex formation, energy transfer or electron transfer. However, the lack of change in the shape of the absorption spectra appeared to rule out exciplex formation (Figure 2.4). The occurrence of FRET is favoured and supported by 2 factors:

1. the large  $J(\lambda)$  integral for the gQD-CV complex ( $8.0 \times 10^{13} \text{ nm}^4 \text{ M}^{-1} \text{ cm}^{-1}$ ) (Figure 2.5) and;
2. the synergistic improvement in antimicrobial activity observed when QDs and CV are combined.

In addition to FRET (and the resulting  $^1\text{O}_2$  formation), photoelectron transfer (PET) may also occur leading to generation of ROS, principally  $\text{O}_2^{\bullet-}$ , thus contributing to antimicrobial effects in the functional surfaces. Photoexcited indium-based QDs have been shown to be capable of reducing oxygen to produce superoxide<sup>153</sup> however evidence from our studies show that, when incorporated into polymer,  $\text{O}_2^{\bullet-}$  yield is not enough to attenuate the levels of bacterial contamination, whether excited under high intensity or low intensity white light. (cf. Sections 4.3.4.3 and 4.3.4.4). PET is also possible between the QD and CV when in close proximity. For instance, photoexcitation of either the QDs or CV could result in electron donation to CV, which is a good electron acceptor, and the reduced CV radical can then interact with oxygen to form  $\text{O}_2^{\bullet-}$ , as has been previously demonstrated by various groups.<sup>421, 430, 450</sup>

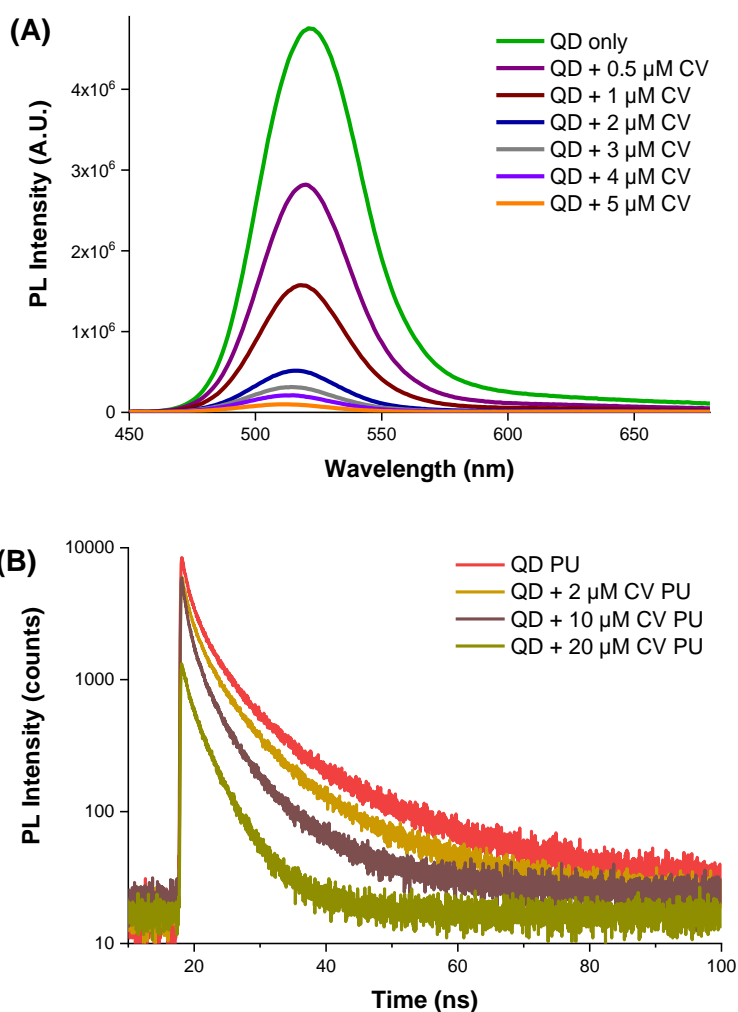


Figure 5.4 **(A)** Steady-state emission of green QD with increasing CV concentration in **solution** (1:1 cyclohexane/DCM) at 400 nm excitation. **(B)** Time-resolved emission of green QD alone or in combination with increasing concentrations of CV in **polyurethane**. The concentrations represent those used to swell the polyurethane. QD concentration in all swelling solutions:  $1\text{mgmL}^{-1}$ .

### 5.3.4. Preliminary Type I Mechanism Investigations

Superoxide dismutase (SOD) acts as a scavenger of superoxide, a radical generated by PET as discussed above. SOD works by catalysing the conversion of superoxide to water and hydrogen peroxide ( $2\text{O}_2^{\bullet-} + 2\text{H}^+ \rightarrow \text{H}_2\text{O}_2 + \text{O}_2$ ) as described in Chapter 0. To assess the possible contribution of Type I electron transfer pathways, the bactericidal activity of the control PU, CV PU and QD + CV PU substrates were tested against EMRSA 4742 after 1 h

of white light treatment, both under standard conditions as well as in the presence of SOD. After 1 h exposure to light, no significant antibacterial activity is demonstrated by the control PU or QD PU, both in the absence of SOD and in the presence of 50 U/mL SOD. Conversely, CV PU and QD + CV PU bactericidal activities were significantly diminished in the presence of SOD. The antibacterial activity of CV PU and QD + CV PU substrates decreased by  $\sim 2.5 \log_{10}$  (from 99% to 66.9%) and  $\sim 3 \log_{10}$  (from 99.996% to 96.4%) respectively when 50 U/mL SOD was added (Figure 5.5).

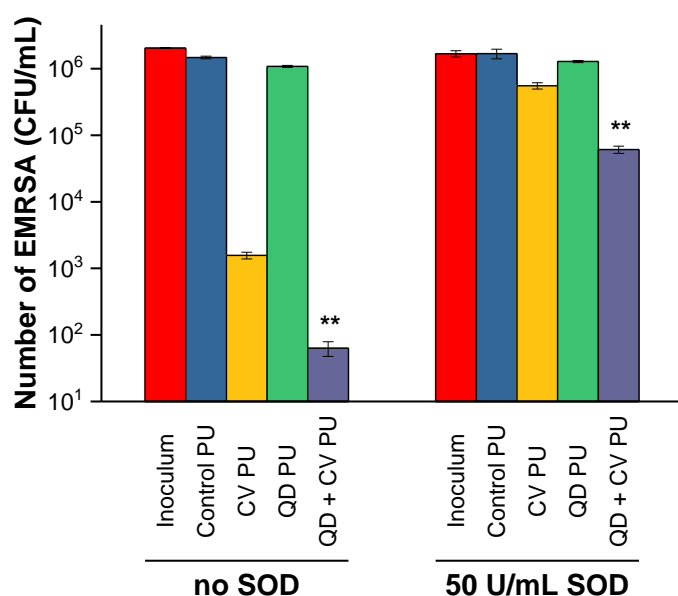


Figure 5.5 Viable counts of EMRSA 4742 on unmodified and modified polyurethane polymers tested under standard conditions (20°C, 1 h white light treatment at 6000 lux) without SOD (left) and in the presence of 50 U/mL SOD (same temperature and lighting conditions as standard test) (right). Concentrations of swelling solutions (made in 1:1 Cy/DCM solvent) used to modify PU: QDs – 1 mg/mL; CV – 500  $\mu$ M. (\*\* indicates significance of  $p < 0.01$  compared to CV PU)

The effectiveness of SOD in inhibiting the potent kill of CV PU and QD + CV PU upon irradiation indicates that  $O_2^{\bullet-}$  is formed by the materials then subsequently scavenged before oxidative damage occurs to the bacteria. Since we know that  $^1O_2$  is generated as well (from solution studies), we conclude that the synergistic enhancement in antibacterial activity of QDs combined with CV is due to the combined action of ROS generated by both Type I and Type II mechanisms. The range of mechanisms of ROS generation using QDs and CV is distinct from our lab's previous work using 2 nm diameter Au or ZnO NPs and CV in polymer

substrates. In those studies where the NPs exhibit negligible absorption in the visible range, FRET interaction would not apply and electron transfer interactions are likely to have taken place only via excitation of the CV.<sup>405, 406</sup>

## 5.4. Conclusion

In this chapter, studies have shown that prolonged low level light intensity do not elicit any antimicrobial activity from polymer surfaces that contain only QDs, as is the case under short bursts of high light intensity. Also, the efficacy of the QD + CV PU was greater than the effect elicited by the constituent surfaces (QD PU and CV PU) combined and thus demonstrated that a synergistic interaction occurs with this combination to potentiate the antimicrobial efficacy. Interestingly, the results observed under low light levels differed in an interesting way from our previous studies where much higher light intensities were employed to achieve bactericidal activity.<sup>409</sup> Under high light intensities, the CV dye also contributed much more significantly to the observed kill, whereas the contribution of CV to the overall kill was relatively low under ambient light. However, the overall antimicrobial efficacy of the QD-CV surfaces were not compromised. Another key observation was the activity of the functional surfaces may vary with different pathogens as we observed that a longer illumination time was required for *P. aeruginosa* compared to *E. coli*, due to natural features of the *P. aeruginosa* bacterium that render it highly intrinsically resistant. *P. aeruginosa*'s low permeability and lack of general porins may be responsible for the observation that exogenous ROS required longer exposure to elicit an antibacterial effect. Nevertheless, a high level of bactericidal activity was evident under ambient light after 24 h, an effect which was comparatively fast, bearing in mind that bacteria can survive for several weeks and months on inanimate surfaces.<sup>530</sup> Thus, even at ambient light levels, functional QD-CV surfaces offer a powerful means of reducing bacterial levels and potentially reducing the transmission of hospital-acquired infections through contact with surfaces. Earlier singlet oxygen data conducted in solution phase along with steady-state and time-resolved photoluminescence provided evidence of the occurrence of FRET in the QD-CV surfaces; and preliminary superoxide detection assays suggest the occurrence of PET as well in this hybrid polymer system. In the next chapter, a more in-depth analysis of the mechanisms underpinning the activity of functional surfaces will be considered.

# CHAPTER 6. EVALUATION OF MECHANISMS OF REACTIVE OXYGEN SPECIES (ROS) GENERATION OF QUANTUM DOTS-PHOTOSENSITISER COMPLEXES

## 6.1. Introduction

As mentioned earlier, when QD and CV are held in close proximity, there is a possibility for two distinct photochemical pathways: Type I electron transfer or Type II energy transfer. A Type II reaction involves direct energy transfer from the PS triplet state to molecular oxygen generating highly reactive singlet oxygen ( $^1\text{O}_2$ ). In microorganisms,  $^1\text{O}_2$  is a highly damaging ROS since microorganisms do not possess any specific scavengers to regulate this ROS.<sup>413</sup> Although it is rapidly quenched by physical interaction with water molecules in aqueous solution which limits its mean diffusion distance, it is more stable in aprotic microenvironments such as polymers.

Type I mechanisms involve electron transfer reactions from the excited QD or PS to oxygen to generate cytotoxic free radicals. Superoxide ( $\text{O}_2^{\bullet-}$ ) is the main initial free radical species, formed by a one-electron reduction of molecular oxygen.<sup>413</sup> Its biological effect stems from the fact that depending on the solution environment (i.e. pH and fluctuations), its reduction potential changes. In aqueous solution,  $\text{O}_2^{\bullet-}$  may act as a weak oxidizing agent and can oxidise ascorbic acid and thiols, or it may act as a very strong reducing agent, and reduce iron complexes of cytochrome c and ferric EDTA.<sup>414</sup> In biological systems,  $\text{O}_2^{\bullet-}$  is relatively short-lived (although longer-lived than  $^1\text{O}_2$ ) owing to its rapid reduction to hydrogen peroxide ( $\text{H}_2\text{O}_2$ ) either spontaneously or enzymatically by superoxide dismutase (SOD).<sup>531</sup> Although  $\text{H}_2\text{O}_2$  is not a ROS in the strictest sense, it is a powerful and toxic oxidising agent that plays an important role in oxygen toxicity.<sup>532</sup> As a non-radical derivative of  $\text{O}_2$ ,  $\text{H}_2\text{O}_2$  is less reactive than  $\text{O}_2^{\bullet-}$  however, it has a longer biological lifespan and; combined with its neutral charge that allows easy diffusion within and between cells,  $\text{H}_2\text{O}_2$  makes a strong cytotoxic agent.<sup>533</sup> Hydroxyl radicals ( $\bullet\text{OH}$ ) are a subsequent product of  $\text{H}_2\text{O}_2$ , formed by the reaction of  $\text{H}_2\text{O}_2$  with either  $\text{O}_2^{\bullet-}$  or perhydroxyl radicals.  $\bullet\text{OH}$  is among the strongest oxidants ever described

(standard reduction potential of 2.31 V) and can cause biological damage to a more acute degree than both  $\text{H}_2\text{O}_2$  and  $\text{O}_2^{\bullet-}$ .<sup>413, 414</sup>

The antimicrobial photodynamic effect of the functional surfaces is dependent on the efficiency of the operation of Type I and/or Type II processes. In the previous chapter, a preliminary study of ROS was set out. In this chapter, more extensive exploration of the mechanism operating in the QD-CV conjugates when embedded in polymer was carried out. Various methods – direct and indirect – were employed to distinguish between the different types of ROS produced by the functional surfaces during white light activation. On the basis of these, the contribution of Type I and Type II photochemical pathways to the QD-CV antimicrobial activity was determined.

## **6.2. Materials and Methods**

### **6.2.1. Materials**

XTT sodium salt ((2,3-bis(2-methoxy-4-nitro-5-sulfophenyl)-2H-tetrazolium-5-carboxanilide), catalase, mannitol and L-histidine were purchased from Sigma-Aldrich.

### **6.2.2. Steady-state Emission**

Samples were mounted diagonally at 45° and a longpass filter (RG435 and OG550, Schott, England) was installed into the fluorimeter (Horiba FMax4 Fluorimeter (ex. 400nm)) to reduce scattered light from the excitation wavelength before measuring emission.

### **6.2.3. Time-Resolved Lifetime Measurements**

See Section 2.2.4 for a description of how measurements of time-resolved photoluminescence lifetime were performed for solution samples. For polymer samples embedded with QDs and/or CV, the substrates were mounted on microscope glass slides first before and signals were detected in the same manner as QD and QD-CV solutions.

### **6.2.4. Singlet Oxygen Phosphorescence**

Polyurethane samples were mounted diagonally in a quartz cuvette and irradiated using a 532 nm Nd:YAG laser (Lumanova GmbH, Germany) with the beam axis aligned at 45° to the

surface plane of the sample in order to optimise detection of  $^1\text{O}_2$  within the polymer. For full details of the experimental set-up and parameters, please refer to Section 2.2.5.

#### **6.2.5. Detection of Superoxide by XTT Reduction**

QD-CV and CV-embedded polyurethane substrates ( $1\text{cm}^2$  squares) were placed in flat-bottomed wells in clear 24 well plates (TPP). 2 mL aliquots of 2 mM XTT sodium salt reagent (dissolved in distilled water) were deposited into wells to completely cover the surface of and submerge the polymer squares. Samples were exposed to a light source emitting at either 455 nm or 595 nm using an LED (Thorlabs Ltd., UK), at distance of 10 cm from the bottom of the well plate, for set intervals. Absorbance readings were taken immediately before ( $t = 0$ ) and irradiation at each time interval. Absorbance readings at 470 nm were acquired using a Pelkin-Elmer Lambda 950 or Shimadzu UV-2600 UV/Vis spectrophotometer; or an Infinite 200 Pro plate reader. Control groups included polyurethane polymer samples without CV, without QDs, without both or  $\text{dH}_2\text{O}$  alone (without XTT).

#### **6.2.6. Reactive Oxygen Species Generated by Materials**

To investigate the nature of ROS generated by the QD + CV PU materials against bacteria, a  $\text{H}_2\text{O}_2$  scavenger (catalase,  $400\text{ U mL}^{-1}$ ), a hydroxyl radical scavenger (mannitol, 33 mM) and a  $^1\text{O}_2$  scavenger (L-histidine, 4 mM) were added to the bacterial suspension (methicillin-resistant *S. aureus*, EMRSA 4742) and exposed to the polyurethane substrates to deactivate the respective ROS emanating from the polymer surface. Catalase, mannitol and L-histidine were purchased from Sigma-Aldrich, UK and filter sterilised using a  $0.2\ \mu\text{m}$  PES syringe filter (VWR, UK). The control PU, CV PU and QD + CV PU substrates were tested against EMRSA 4742 illuminated with a white light source ( $6600 \pm 900\text{ lux}$ ) intensity for a period of 30 mins, using the same antibacterial testing protocol described in previously (see CHAPTER 4). As a control, a separate experiment was conducted in the absence of any ROS quenchers. Light source: General Electric 28 W Watt Miser™ T5 2D compact fluorescent lamp.

## 6.3. Results & Discussion

### 6.3.1. Steady-State and Time-Resolved Emission Studies of QD-CV Polymer Surfaces

As discussed in CHAPTER 2, the emission of the two QDs in suspension was effectively quenched by the presence of CV dye. This effect was CV concentration-dependent. However, though steadily increasing CV concentration resulted in further weakening of QD emissions, no corresponding increase or change in CV was evident as is usual in energy transfer processes. The lack of any discernible peaks for CV emission was ascribed to the low viscosity of the solvent in which the QD-CV suspensions were prepared in. 1:1 cyclohexane/dichloromethane, the solvent in which the QD and QD-CV combinations are suspended, exhibits very low viscosity. This allows free movement and rotation of the dye's functional groups leading to the formation of twisted intramolecular charge transfer (TICT) states which rapidly relax to the ground state.<sup>483</sup> This phenomenon resulted in low CV fluorescence yield and thus peaks for the CV dye are not apparent in the emission spectra. On the other hand, by impregnating polyurethane with QD-CV mixtures, CV fluorescence was recovered to a degree because as a rigid polymer, polyurethane offered an extremely viscous microenvironment, restricting the development of TICT states. Figure 6.1A and B show the emission spectra for polyurethane incorporated with red QD and/or CV and green QD and/or CV respectively. Generally, again, a decrease in QD emission is obvious with increasing CV concentration. In addition, compared to the QD emission, the CV emission is quite low, a feature that is particularly noticeable in Figure 6.1B, as the emission of the green QDs (at ~520 nm) does not overlap with the CV emission peak (~600 nm). Furthermore, as the peak emission of the QDs decreased and CV emission increased with increasing concentration of CV, a concentration-dependent bathochromic shift (shift to the right) in the CV emission peak was detected. For instance, the addition of 5  $\mu\text{M}$  to 1  $\text{mgmL}^{-1}$  red QDs swelling solution caused a red shift from 630 nm to 647 nm. Adding 50  $\mu\text{M}$  CV caused a further bathochromic shift to 663 nm. This concentration-dependent red-shift effect was attributed to absorption of the shorter wavelengths of the CV emission causing suppression of the signal approaching to 600 nm. This phenomenon is also observed with the dye in polymer in the absence of QDs.<sup>409</sup> TICT states can also exhibit red-shifted fluorescence but not in the case of CV, therefore this mechanism can be ruled out.

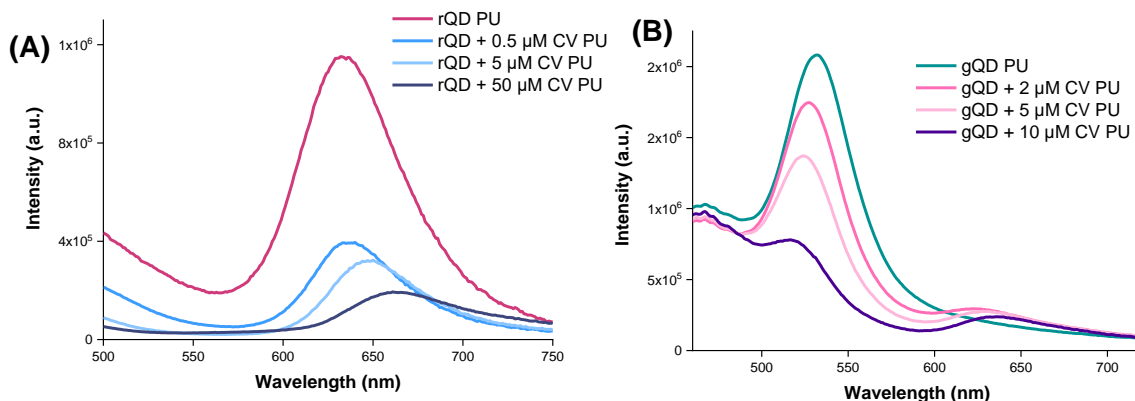


Figure 6.1 Emission spectra of polyurethane substrates when incorporated with 1mgmL<sup>-1</sup> QD only or in combination with increasing concentrations of CV (excitation at 400 nm). **(A)** shows the spectra for red-emitting QDs and **(B)** for green-emitting QDs.

Steady-state emission data demonstrate that QD emission quenching does take place in the polymer samples in the presence of CV. Time-resolved photoluminescence (PL) data was acquired to confirm occurrence of energy transfer or photo-electron transfer. By analysing time-resolved PL data, it is possible to discern decreases in donor PL intensity caused by facile reabsorption effects. For instance, in a previous study, it was observed that the mixtures of PEGylated CdSe/ZnS QDs with toluidine blue O dye could enhance bacterial kill in aqueous solutions following visible illumination. However, time-resolved emission measurements of the QD donor revealed no evidence for FRET interaction and the authors in that study concluded that the associated lifetime shortening, and the enhanced activity was attributed to reabsorption of QD emission by the dye.<sup>534</sup>

For time-resolved PL measurements, the indium-based QDs were excited at 405 nm where QD absorption was strong but CV absorption was negligible. The QD lifetime is also long compared to CV fluorescence lifetime which is < 5 ns in viscous solvents or when bound to protein.<sup>430, 535</sup> The QD PL decay when only QDs were embedded in polyurethane as well as the QD decay when QDs combined with varying concentrations of CV were incorporated into polyurethane are displayed in Figure 6.2 for red and green QD/QD-CV substrates respectively. Upon measuring the time-resolved PL, the donor exciton lifetime was derived by fitting the decay ( $I_t$ ) to a bi-exponential decay. It was observed that the QD emission lifetime in the presence of CV ( $\tau_{DA}$ ) was significantly shorter than the QD emission lifetime in the absence of CV ( $\tau_{DA}$ ). The exciton PL lifetime progressively shortened with the introduction of

increasingly higher concentrations of the dye into the polymer (Figure 6.2). In the absence of the photosensitiser, the mean fractional amplitude weighted lifetime of the red-emitting QDs was  $\tau_D = 32.0$  ns which was significantly reduced to  $\tau_{DA} = 6.8$  ns in the presence of 50  $\mu\text{M}$  CV. For green QDs,  $\tau_D = 12.1$  ns and  $\tau_{DA} = 7.4$  ns in the presence of 5  $\mu\text{M}$  CV.

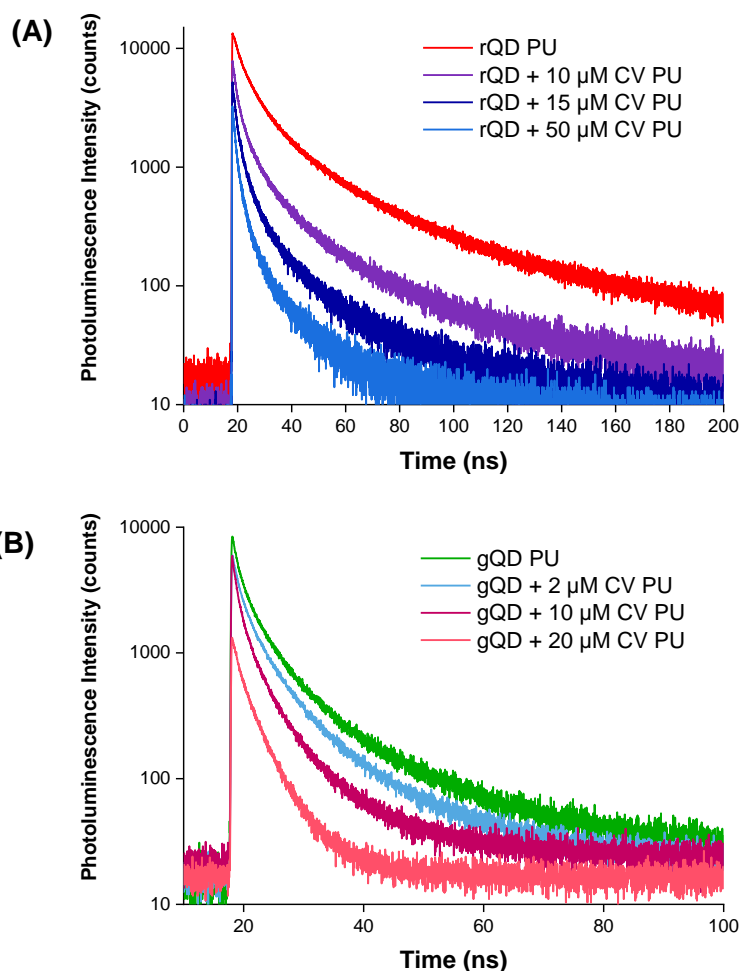


Figure 6.2 Logarithmic plots of time-resolved photoluminescence measurements of pure QDs and QD-CV combinations embedded in polyurethane via swell-encapsulation-shrink. (A) Time-resolved emission lifetimes of red QDs and red green QD-CV combinations at 620 nm. (B) Time-resolved emission lifetimes of green QDs and green QD-CV combinations at 520 nm. In all cases, final QD concentration in swelling solutions was kept constant at  $1\text{ mg mL}^{-1}$ .

Assuming that QD lifetime quenching was a result of FRET, the FRET efficiency ( $E$ ) of donor/acceptor complexes in polymer was computed from the time-resolved fluorescence measurements. Table 6.1 and Table 6.2 display the FRET efficiencies of the QD-CV with

increasing CV concentration. At the highest crystal violet concentration, the FRET efficiency was calculated as 79%. Note however that the CV concentration given is that of the dipping solution and we assume an approximately linear dependence between these values and the polymer uptake. We also assume that the use of the single-stage swell-encapsulation loading with both agents combined resulted in uptake of intact QD-CV complexes and CV residing in the matrix but in close proximity to the QDs.

It is important to note that the lifetime quenching observed is also consistent with the occurrence of PET therefore on the basis of these studies alone, we cannot be certain that FRET does take place in addition to PET.<sup>444</sup> However since the PET mechanism should not lead to singlet oxygen generation, any  $^1\text{O}_2$  produced by the QD-CV polymers would give distinct evidence of FRET. Therefore, in addition to steady-state and time-resolved PL studies, the generation of  $^1\text{O}_2$  by the polymer samples was examined.

Table 6.1 Mean fractional amplitude weighted red QD emission lifetimes and calculated FRET efficiencies of pure QD and QD-CV complexes with increasing CV concentrations (in the swell-encapsulation medium) when incorporated into polyurethane via swell-encapsulation-shrink

<b>CV Concentration (<math>\mu\text{M}</math>)</b>	<b>Mean <math>\tau</math> (ns)</b>	<b>FRET Efficiency (%)</b>
0	32.0	0
5	28.2	12
10	21.6	33
20	14.7	54
50	6.8	79

Table 6.2 Mean fractional amplitude weighted green QD emission lifetimes and calculated FRET efficiencies of pure QD and QD-CV complexes with increasing CV concentrations (in the swell-encapsulation medium) when incorporated into polyurethane via swell-encapsulation-shrink

<b>CV Concentration (<math>\mu\text{M}</math>)</b>	<b>Mean <math>\tau</math> (ns)</b>	<b>FRET Efficiency (%)</b>
0	12.1	0
0.5	10.8	10.7
1	9.1	24.7
2	8.7	28.0
5	7.4	39.0

### 6.3.2. Singlet Oxygen Phosphorescence Studies of QD-CV Polymer Surfaces

The generation of  $^1\text{O}_2$  in the polymer was investigated using time-resolved near-IR detection based on the  $^1\text{O}_2$  phosphorescence at 1270 nm. The PS crystal violet is capable of producing  $^1\text{O}_2$  via energy transfer however, in aqueous solution, the efficiency of  $^1\text{O}_2$  generation is very low because the CV excited singlet state is deactivated by the molecular rotor effect. In viscous solvents or the polymeric microenvironment, this effect is repressed which permits  $^1\text{O}_2$  generation, and it has been shown experimentally that CV dye alone impregnated in silicone polymer can generate  $^1\text{O}_2$  upon excitation at 532 nm.<sup>536</sup> Figure 6.3A shows  $^1\text{O}_2$  decay curves for polyurethane (PU) samples made from swelling solutions containing 50  $\mu\text{M}$  CV alone (black), 1mgmL<sup>-1</sup> red QDs (bright red) or a 1mgmL<sup>-1</sup> red QD + 50  $\mu\text{M}$  CV combination. Likewise, Figure 6.3B displays  $^1\text{O}_2$  decay curves for PU samples made from swelling solutions containing 20  $\mu\text{M}$  CV alone (black), 1mgmL<sup>-1</sup> green QDs (bright green) or a 1mgmL<sup>-1</sup> green QD + 20  $\mu\text{M}$  CV combination. The singlet oxygen phosphorescence plots are presented as logarithmic intensity plots so that differences in quasi-mono-exponential decay lifetimes may be more readily discerned (insets shows plots in linear scale).

For CV PU (black traces in Figure 6.3A and Figure 6.3B), a characteristic rise in signal followed by an exponential decay was observed, in agreement with other  $^1\text{O}_2$  phosphorescence studies<sup>536</sup> using CV and other dyes such as methylene blue (MB).<sup>537</sup> The initial rise in signal is governed by the rate of conversion of triplet oxygen to singlet oxygen by the quenching of excited CV to its ground state. The subsequent exponential decay is a result of the medium (i.e. polymer matrix) quenching the formed singlet oxygen to regenerate molecular oxygen.<sup>536</sup> The very short-lived sharp spike at  $t < 1 \mu\text{s}$  corresponded to CV fluorescence and was therefore disregarded in our subsequent analysis. Fitting the initial rise to a bi-exponential function (Equation 2.2) with a negative  $A_2$  component – corresponding to the rise in signal – yielded a rise-time ( $\tau_2$ ) of 3.7  $\mu\text{s}$  for 50  $\mu\text{M}$  CV PU; and 3.9  $\mu\text{s}$  for 20  $\mu\text{M}$  CV PU. The lifetime of singlet oxygen in the polyurethane substrates where only CV was present, derived by fitting the signal to a mono-exponential decay, was determined to be 36  $\mu\text{s}$  (50  $\mu\text{M}$  CV PU) and 38  $\mu\text{s}$  (20  $\mu\text{M}$  CV PU). The values were therefore in agreement with each other and indicated that decay kinetics were not largely affected by the CV concentration within the ranges measured. In addition, the experimental values derived for the lifetime of  $^1\text{O}_2$  in polyurethane were in good agreement with the reported  $^1\text{O}_2$  lifetime of CV embedded in a similar polymer (silicone, 40  $\mu\text{s}$ ).<sup>536</sup>

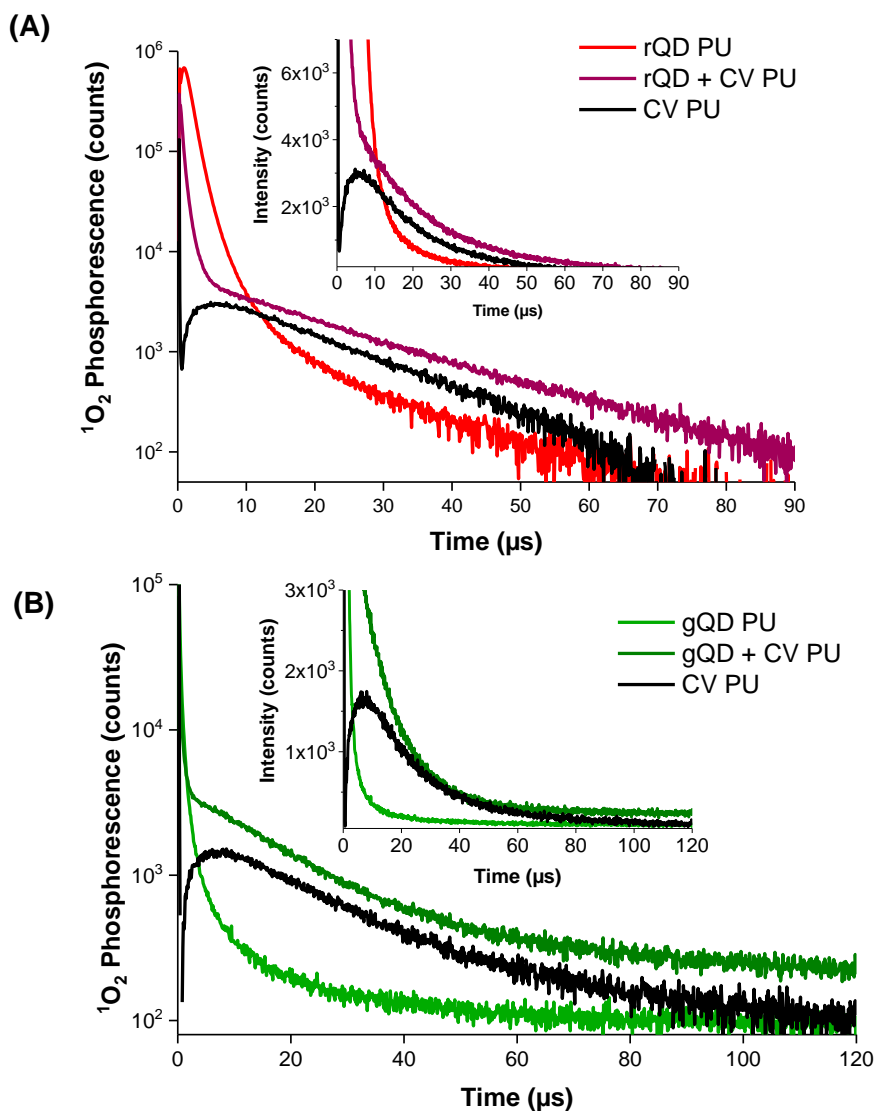


Figure 6.3 Logarithmic time-resolved singlet oxygen phosphorescence recorded at 1270 nm following pulsed laser irradiation of modified polyurethane. (A) Singlet oxygen phosphorescence signals for polymer containing red QDs (bright red), containing CV only (black), and a combination of red QD and CV (dark red). (Concentrations: QDs – 1 mg/mL; CV – 50 $\mu\text{M}$  CV). (B) Singlet oxygen phosphorescence signals for polymer containing green QDs (bright green), containing CV only (black), and a combination of green QD and CV (dark green). (Concentrations: QDs – 1 mg/mL; CV – 20 $\mu\text{M}$  CV). Insets for (A) and (B): Linear scale plot over the same time range. All signals have been subtracted from the control (untreated polyurethane).

When only QDs were present in the polymer matrix (bright red line or bright green line in Figure 6.3A and Figure 6.3B respectively), a highly intense signal was observed for a relatively short time lasting  $\sim 10 - 15 \mu\text{s}$ . This signal is ascribed to the long near-IR tail of the QDs photoluminescence.<sup>538</sup> Although photoluminescence signals for the QDs are weak at such long wavelengths, singlet oxygen has a low quantum yield and thus the phosphorescence that can be detected at 1270 nm is also very weak. Due to these factors, the QD photoluminescence presented as a strong signal for polymers containing both red-emitting and green-emitting QDs. Comparatively, rQD PU substrates displayed a longer lasting initial signal than gQD PU and this was ascribed to the fact that characteristically, red-emitting QDs have emission peaks at longer wavelengths than green-emitting QDs. Exponential decays were not observed for either rQD PU or gQD PU as the generation of  $^1\text{O}_2$  upon photo illumination is an energetically unfavourable process in indium-based QDs.<sup>153</sup> In previous studies of CdS-based QDs, no direct singlet oxygen generation could be observed with an upper limit to the quantum yield estimated as  $< 0.003$ .<sup>212</sup> Using spin-trap electron paramagnetic resonance (EPR) spectroscopy and reporter assays, Chibli et. al. found no evidence for the generation of singlet oxygen in indium phosphide based QDs.<sup>153</sup>

The combination of QD and CV in the polymer matrix (dark red line and dark green line in Figure 6.3A and Figure 6.3B respectively) gave rise to decay profiles similar to CV PU but with important differences. Firstly, a key observation from this comparative study is that the overall intensity of the singlet oxygen signal with the QD/CV PU combinations were higher than for CV PU alone. Secondly, the short but rapid decay in signal seen at early times  $< 10 \mu\text{s}$  in the presence of CV matches that observed in our previous QD FRET studies<sup>538</sup> and is consistent with the QD donor PL being quenched by the CV. Particularly for rQD + CV PU, the signal ascribed to QD PL in the decay profile is much shorter compared to rQD PU (Figure 6.3A). The quenching of QD emission by CV occurred in the polymer can be ascribed to a combination of photo-electron transfer and/or energy transfer to generate either superoxide or singlet oxygen. At 532 nm (the laser excitation wavelength), red QDs have a good absorption and there is still residual green QD absorption therefore it is possible for FRET-induced singlet oxygen generation to take place and thus contribute to the observed signal. Also, at 532nm, CV have a relatively strong absorption compared to its peak absorption near 600 nm so some

of the signal may also originate from CV bound within the matrix that is remote from the QD and possibly from direct excitation of CV bound to the QD.

Though the combination of QD and CV caused a major change in the initial features ( $t < 10 \mu\text{s}$ ) of the decay curves, namely, the rise time seen for CV PU alone was replaced by an intense short-lived spike, at later times ( $t > 10 \mu\text{s}$ ), the decay curves for rQD + CV PU and gQD + CV PU closely matched that observed for CV PU with a congruent  $^1\text{O}_2$  lifetime. This is consistent with the assumption that the same decay kinetics for singlet oxygen should apply for each type of polymer sample. The key observation from this comparative study is that the overall intensity of the singlet oxygen signal with the QD/CV combination was higher than for CV alone.

### 6.3.3. Superoxide Generation by QD-CV Substrates

When indium phosphide QDs are photo-excited, direct generation of singlet oxygen is energetically unfavourable but indium-based QDs can directly generate superoxide radical anions by reducing oxygen via a Type I mechanism.<sup>153</sup> In aqueous solution, the reduction potential of the  $\text{O}_2/\text{O}_2^{\bullet-}$  redox couple is  $-0.18 \text{ V}$  vs. NHE (normal hydrogen electrode) (Equation 2.4), a value that is near to that of  $\text{CV}^+/\text{CV}^\bullet$  reduction potential at  $-0.36 \text{ V}$  (Equation 2.5).<sup>435, 436</sup> CV is a good electron acceptor and due to the similar potentials, is readily photo-reduced by the QDs to generate the semi-reduced CV radical. By extrapolation of excited-state redox potentials estimated for other indium-based QDs emitting at comparable wavelengths to the QDs employed here, reduction of CV should be energetically feasible: the conduction and valence band reduction potentials for InP QDs are estimated as  $-1.04 \text{ V}$  and  $0.95 \text{ V}$ <sup>153, 437</sup> This assumes that effects of binding and the different solvent on redox potentials are minimal. The CV radical generated by PET from the QDs can subsequently interact with molecular oxygen to generate superoxide by electron transfer which should be energetically possible due to the positive redox potential ( $+0.18 \text{ V}$ ) of the reaction (Equation 2.6).



Various studies provide evidence indicating that these Type I processes take place. For instance, electron paramagnetic resonance (EPR) spectroscopy studies conducted in

aqueous solution have detected the formation of  $O_2^{\bullet-}$  following illumination of CV solutions with NADH (nicotinamide adenine dinucleotide), which donated an electron to the excited CV triplet state to form the CV radical.<sup>421, 539</sup>

Photoexcitation of dimers of CV may also act as a source of  $O_2^{\bullet-}$  via electron-transfer reactions as postulated previously for MB-doped polymer substrates.<sup>537</sup> Direct generation of superoxide by electron transfer to oxygen by the CV triplet state has been postulated by Reszka *et al.* and Fischer *et al.*<sup>421, 539</sup> but was confirmed by Brezova and colleagues who demonstrated irradiated polycrystalline samples of CV prepared by passing CV dissolved in aprotic solvent through paper generated  $O_2^{\bullet-}$  using EPR.<sup>456</sup> Therefore  $O_2^{\bullet-}$  should be generated in illuminated polymer samples with CV alone and CV with QDs. In solution, we expect that PET plays an important role for the QD/CV mixtures as electrostatic interactions that form geminate ion pairs are strong. However, these geminate ions pairs may recombine resulting in quenched QD and an unchanged CV.<sup>459</sup> This process can be very fast and may compete with the PET reaction of the CV radical anion with oxygen to form  $O_2^{\bullet-}$ . Uptake into the polymer may separate ion pairs and reduce charge recombination effects after PET, thus allowing more  $O_2^{\bullet-}$  generation. In addition, photoexcitation of CV dimers may also act as a source of  $O_2^{\bullet-}$  via PET reactions as previously postulated for MB-doped polymer substrates.<sup>537</sup> Furthermore, instead of the QDs unreacted monomer in the polymer matrix, may also be able to promote a Type 1 process, and contribute to the cytotoxicity observed with CV alone. Thus, it was expected that  $O_2^{\bullet-}$  should be generated in illuminated polymer samples with CV alone and CV with QDs, and then be able to diffuse into the surrounding solution containing the bacteria.

#### **6.3.4. Chemical Detection of Superoxide Release by Polymer Substrates: XTT Assay**

To determine whether the functional surfaces were capable of generating  $O_2^{\bullet-}$  radicals, XTT (2,3-bis(2-methoxy-4-nitro-5-sulfophenyl)-2H-tetrazolium-5-carboxanilide) absorption assays were carried out. The XTT assay is a colorimetric assay for probing total superoxide capacity. XTT is a sulfonated tetrazolium salt that is reduced in the presence of superoxide, forming the XTT formazan which causes a change in colour (Figure 6.4). The degree of colour change is dependent on the concentration of  $O_2^{\bullet-}$  generated and the absorbance of this coloured solution can be quantified by measuring at a certain wavelength (usually at 470 nm) by a spectrophotometer.<sup>540, 541</sup>

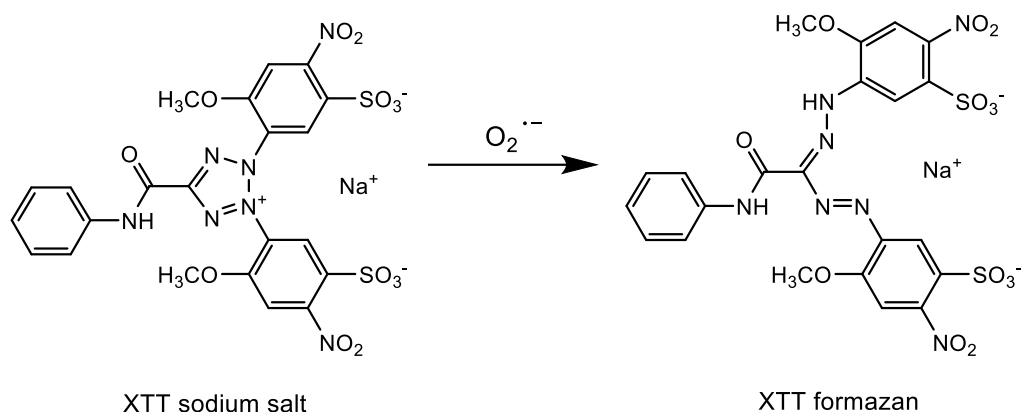


Figure 6.4 XTT reduction to formazan by superoxide

XTT is considered as more advantageous over other tetrazolium salts such as MTT (3-(4,5-dimethylthiazol-2-yl)-2,5-diphenyltetrazolium bromide), INT (3-(4-Iodophenyl)-2-(4-nitrophenyl)-5-phenyl-2H-tetrazol-3-ium chloride) and NBT (2,2'-bis(4-Nitrophenyl)-5,5'-diphenyl-3,3'-(3,3'-dimethoxy-4,4'-diphenylene)ditetrazolium chloride). In particular, unlike the above tetrazolium compounds, the formed XTT formazan is water soluble due to the presence of two sulfonic acid groups in XTT. Since the formazan product is water soluble, additional solubilisation steps are avoided, allowing convenient and accurate spectroscopic measurement and analysis in supernatants without solvent extractions.<sup>542-544</sup> Direct measurement of the release of superoxide into the surrounding medium by the functional surfaces using the spectroscopic method would be difficult to accomplish as the polymer itself absorbs strongly in the lower wavelengths where superoxide absorption peaks (245 nm in aqueous solution).<sup>545</sup> Superoxide is also highly reactive and rapidly quenched in protic solvents therefore distinguishing the contributions of superoxide to the optical signal from the contributions of the polymer and the surrounding solution would be unfeasible.<sup>546</sup> Therefore, using XTT tetrazolium salt dissolved in the surrounding medium as a superoxide probe, a spectroscopic technique was developed which was to be highly selective for superoxide anions. The XTT reagent is sensitive to  $O_2^{\bullet-}$  anions and in its presence, converts to an orange-coloured formazan product which exhibits absorption at 470 nm. The method was expected to remain sensitive only to  $O_2^{\bullet-}$  ions released by the functional surfaces into the aqueous solution as XTT is water-soluble and the polyurethane substrates are hydrophobic.

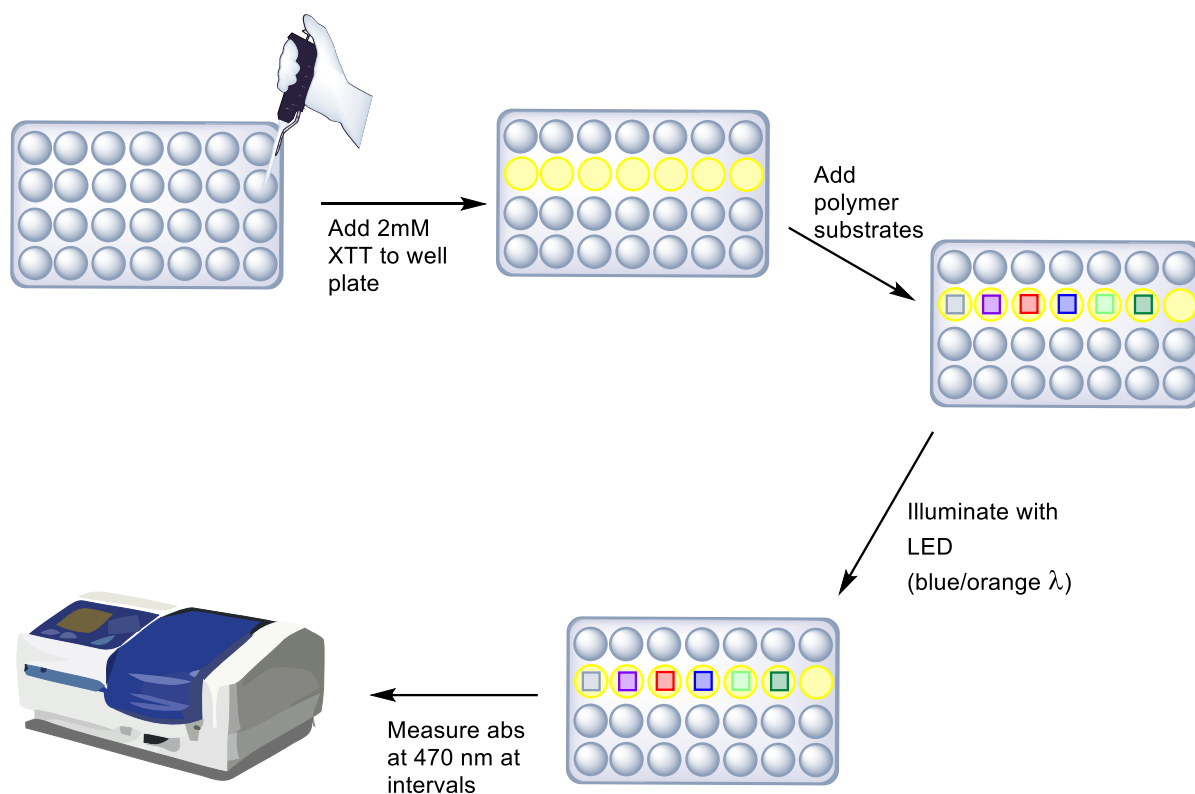


Figure 6.5 Experimental setup of polymer samples used for superoxide anion ( $O_2^{\bullet-}$ ) detection with XTT reagent. Release of  $O_2^{\bullet-}$  from QD and/or CV-incorporated polyurethane leads to reduction of XTT solution lying in direct contact with the polymer surface to form the orange formazan product which produces a detectable optical signal at 470 nm.

Polymer squares were placed in a 24 well-plate and submerged in an aqueous solution of XTT reagent. Subsequently, samples were exposed to either 455 nm or 595 nm wavelength light using an LED. Absorbance readings were taken immediately before irradiation and at various intervals post-irradiation. Control groups included unmodified polyurethane polymer samples submerged in XTT solution or unmodified polymer squares in  $dH_2O$ . The experimental set-up is illustrated in Figure 6.5 and was adapted from a protocol employed by Bovis et. al.<sup>537</sup> No signals were observed for control wells containing the unmodified polymer squares in water. Absorbance readings for the control well containing the neat polymer in XTT were subtracted for each point.

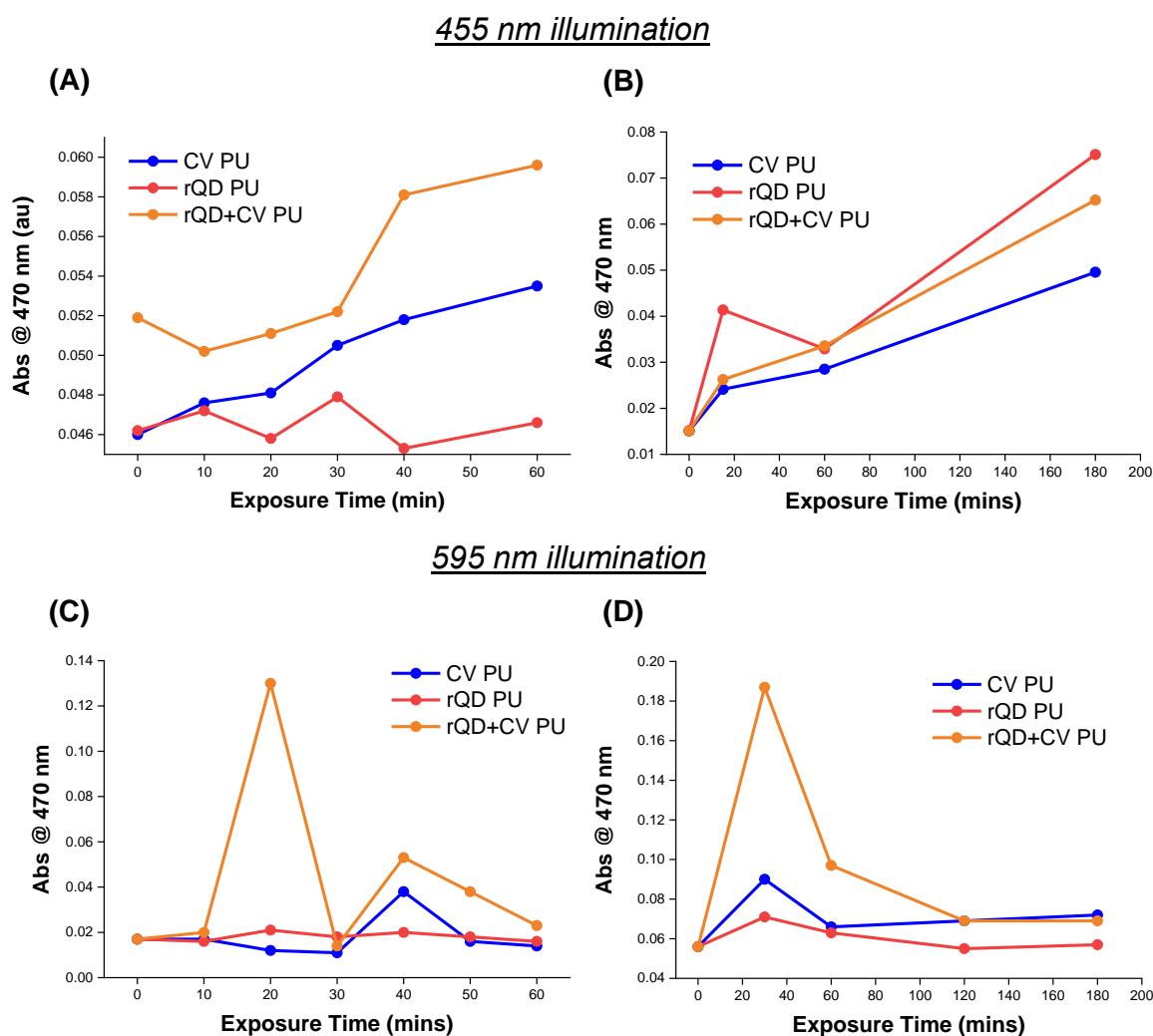


Figure 6.6 Measurement of XTT formazan formation as a result of superoxide generation. Absorbance of 470nm. Representative results when CV PU, rQD PU and rQD + CV PU are exposed to XTT and irradiated with 455 nm light at shorter time intervals **(A)** and longer time intervals **(B)**. Respectively, **(C)** and **(D)** show representative results when CV PU, rQD PU and rQD + CV PU are exposed to XTT and irradiated with 595 nm light at shorter time intervals and longer time intervals. The control (well with only XTT) has been subtracted for each point.

Figure 6.6 shows the formation of XTT formazan when rQD PU, CV PU and rQD + CV PU were irradiated with light at 455 nm where QD absorption is high and CV absorption low (A and B) or 595 nm where QD absorption is low and CV absorption is high (C and D). Figure 6.6 also shows the formation of XTT formazan when absorbance is measured at shorter time intervals (A and C) or longer time intervals (B and D). Experiments were repeated at least three times and it was not possible to reproduce any prevailing trends to a satisfactory level.

For instance, in Figure 6.6A, rQD + CV PU appeared to release the highest levels of superoxide followed by CV PU and the lowest rQD PU at 455 nm light irradiation where mainly only the red QDs were activated. However, in Figure 6.6B, under the same conditions (but over a longer time period), the trend was completely reversed, and rQD PU > rQD + CV PU > CV PU in terms of formazan production at 455 nm light irradiation.

At 595 nm light when both red QDs and CV were activated in the polymer, different patterns were observed. A common similarity that was seen under 595 nm was that the peak superoxide formation, as a function of absorbance at 470 nm, was reached quite early in all the samples. This spike profile may have been due to a photodegradation effect whereby a signal is initially observed but the oxidised photoproduct is itself degraded. The fluence rates of the LEDs are higher compared to room lighting (used in antibacterial testing). Particularly at 595 nm where CV strongly absorbs, the rate of photobleaching would be faster than at 455 nm, where CV is weakly absorbing. While rQD + CV PU and rQD PU peaked at roughly the same times in the experiments (~20 min in Figure 6.6C and D), there was a disparity in the peak absorbance for CV PU (~20 min in Figure 6.6C and ~40 min in Figure 6.6D). Overall, it appeared  $O_2^{\bullet-}$  formation was in the order: rQD + CV > CV PU > rQD PU.

While it was possible to draw some useful information from the XTT assays, the data was unreliable as results were not reproducible. Human or systematic error was ruled out as the cause of the irreproducibility of the tests by conducting several repeats as well as taking measurements using different spectrophotometers. One possibility was that the light source may have been scattered by the plastic well-plate. Light scattering would have limited the amount of light reaching the samples submerged in XTT, which in turn, limits superoxide release and XTT formazan production. Even without light scattering, the distance of the light source from the polymer square is an important factor especially since the squares were submerged in aqueous XTT solution. The barrier created by the surrounding aqueous solution may have prevented the light from reaching the samples, affecting ROS production in the surfaces. Additionally, over longer periods of time, it is also possible that evaporation of the XTT solution may have occurred which could also impact absorbance readings. Moreover, supposing any dye and or nanoparticle was leached from the samples, this may have led to artificially high absorbance readings, particularly in the case of QD + CV PU substrates. Also, it has been suggested that the presence of dye absorption peak (~600 nm for CV) can cause

an artificially enhanced absorbance measured at 470 nm, leading to an overestimate of superoxide production. Nanoparticles, depending on their size, have a potential to interact with detection probes or interfere with detection systems resulting in unreliable data.<sup>547</sup> Hence, for one or more of the above factors, the XTT assay was unsuitable as a probe to detect  $O_2^{\bullet-}$  anions in this scenario and was subsequently abandoned.

### 6.3.5. ROS Detection with ROS Scavengers

Another method of superoxide detection was then tested. Identification of reactive oxygen species via bacteriological assays have been previously employed successfully to determine the contribution of Type I and Type II processes occurring in antimicrobial polymer substrates.<sup>406</sup> Adapting the method used by Sehmi *et al.*,  $O_2^{\bullet-}$  production by the functional surfaces was detected by testing the photo-bactericidal effectiveness of polymer substrates under normal conditions and then comparing the effectiveness of the substrates in the presence of an excess amount of a  $O_2^{\bullet-}$  scavenger. The same bacteriological protocol was followed for the latter experiment with the only difference being that the  $O_2^{\bullet-}$  scavenger (superoxide dismutase (SOD)) was added to the buffer solution in which the bacteria were suspended. Superoxide dismutase is an enzyme that catalyses the dismutation of two superoxide anions to form hydrogen peroxide and molecular oxygen,<sup>548</sup> the overall reaction as follows:  $2O_2^{\bullet-} + 2H^+ \rightarrow H_2O_2 + O_2$

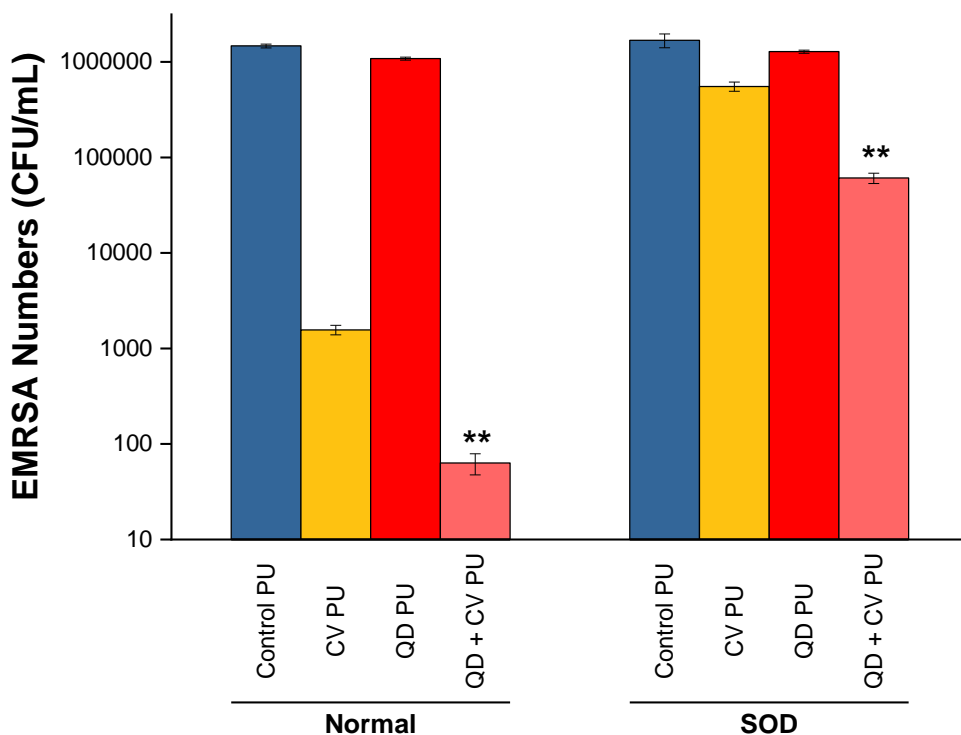


Figure 6.7 Viable counts of EMRSA 4742 on unmodified and modified polyurethane polymers tested under standard conditions (20°C, 1 h white light treatment at 6000 lux) without SOD (left) and in the presence of 50 U/mL SOD (same temperature and lighting conditions as standard test) (right). Concentrations of swelling solutions (made in 1:1 Cy/DCM solvent) used to modify PU: QDs – 1 mg/mL; CV – 500  $\mu$ M. (\*\* indicates significance of  $p < 0.01$  compared to CV PU)

The antimicrobial activity of the control PU, QD PU, CV PU and QD + CV PU substrates was tested against EMRSA 4742 after 1 h white light treatment, both under normal conditions and in the presence of 50 U/mL SOD. After illumination, control PU and QD PU demonstrated no significant antibacterial activity. This was also true in the presence of excess SOD. In contrast, antibacterial activities of CV PU and QD + CV PU substrates were significantly attenuated in the presence of SOD. The antibacterial activity of CV PU decreased by  $\sim 2.5 \log_{10}$  (from 99% to 66.9%) and the antibacterial activity of QD + CV PU decreased by  $\sim 3 \log_{10}$  (from 99.996% to 96.4%) when excess SOD was present (Figure 6.7). SOD very effectively weakened the potency of both CV PU and QD + CV PU, indicating that  $O_2^{\bullet-}$  is formed by these materials then subsequently scavenged before oxidative damage occurs to the bacteria.

Detecting  $O_2^{\bullet-}$  through the assay by which antimicrobial activity was tested proved to be a reliable and highly reproducible method of detecting ROS. This approach was favourable as

it not only detected the release of  $O_2^{\bullet-}$  by the functional surfaces but in addition, direct comparisons of antimicrobial activity could be made, showing how the release of superoxide anions affected activity directly and vice versa. Whereas, the former XTT technique would have provided information on the relative increase or decrease in  $O_2^{\bullet-}$  production, at best. Following success in determining the presence and effect of  $O_2^{\bullet-}$  on the antimicrobial action of the functional surfaces, experiments were conducted featuring scavengers to detect other ROS. In addition to the above advantages, applying this method to other quenchers circumvented the need for spectroscopic analysis, which is not a difficulty with many ROS quenchers and probes, as demonstrated by the XTT assay above.<sup>548</sup>

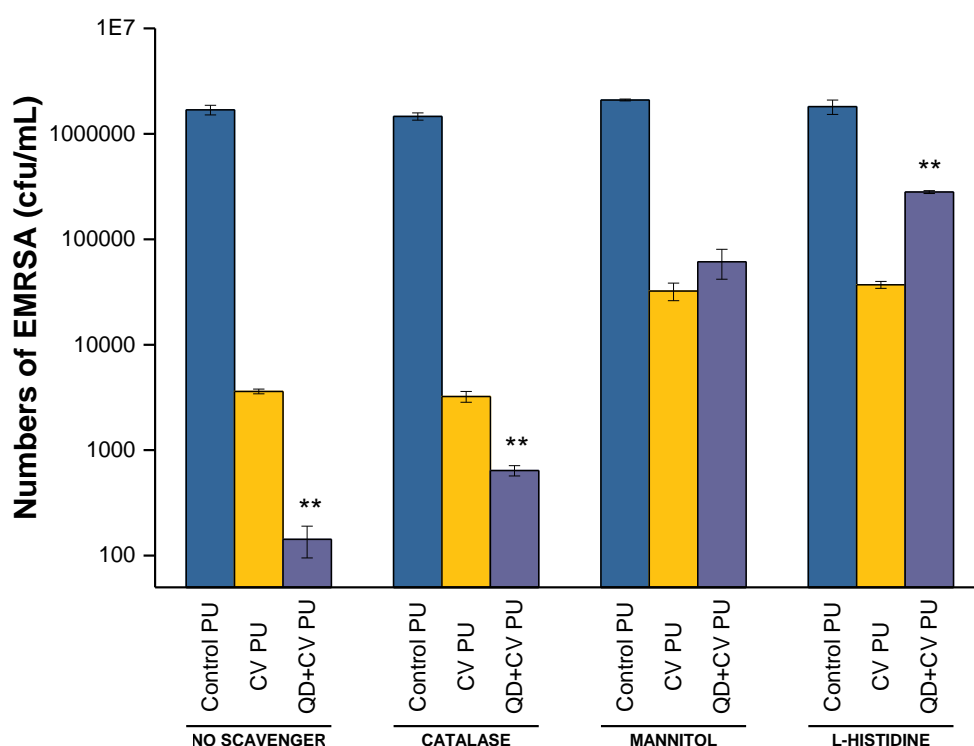


Figure 6.8 Photo-bactericidal activity of control PU, CV PU and QD + CV PU against EMRSA in the absence of ROS scavengers ('no scavenger') and in the presence of catalase ( $H_2O_2$  scavenger), mannitol (hydroxyl scavenger) and L-histidine ( $^1O_2$  scavenger). \*\* indicates that QD + CV PU has  $p \leq 0.01$  compared to CV PU. The experiment labelled "no scavenger" was the control, where no ROS quencher was added. The subsequent experiments labelled "catalase", "mannitol" and "L-histidine" are the results when that quencher was present.

Specific ROS scavengers were introduced into microbiological assays to identify the particular oxygen species produced by the surfaces and thus determine the contribution of energy transfer and electron transfer processes to the system. ROS scavengers of Type I and Type II pathway products were added to the antimicrobial testing protocol to investigate their effect on the bactericidal performance. A hydrogen peroxide scavenger (catalase), a hydroxyl radical scavenger (mannitol) and a singlet oxygen scavenger (L-histidine) were used in the microbiological investigation against EMRSA 4742. The outcome when the antibacterial efficacy of photo-irradiated control PU, CV PU, and QD + CV PU against EMRSA 4742 with and without the addition of each of the three ROS scavengers is presented in Figure 6.8. The experiment labelled “no scavenger” was the control, where no ROS quencher was added, in order to demonstrate and compare the effect of adding each scavenger separately in each set of experiments. The subsequent experiments labelled “catalase”, “mannitol” and “L-histidine” are the results in each of the quenchers were present. Only the QD PU was not included in these experiments as the addition of QD PU had no significant effect under normal conditions.

Catalase is a highly specific enzyme that is solely active against hydrogen, methyl and ethyl peroxides. It causes the conversion of hydrogen peroxide ( $\text{H}_2\text{O}_2$ ) to water namely:  $2\text{H}_2\text{O}_2 \rightarrow \text{H}_2\text{O} + \text{O}_2$ .<sup>532</sup> Following irradiation, the bacterial count on the control polymers was unaffected by the presence of catalase. On the other hand, bacterial numbers on CV PU were decreased to 2.6  $\log_{10}$  in the presence of catalase compared to 2.8  $\log_{10}$  reduction when no scavenger was present. Similarly, QD + CV PU surfaces were decreased to 3.4  $\log_{10}$  in the presence of catalase compared to the 4.2  $\log_{10}$  reduction when the experiment contained no quenchers. The presence of  $\text{H}_2\text{O}_2$  likely resulted from the production of  $\text{O}_2^{\bullet-}$  by the light-activated surfaces (Figure 6.7). Since the main source of  $\text{H}_2\text{O}_2$  is the dismutation of superoxide, it followed that the effect of catalase on the light-activated surfaces directly correlated to the contribution of  $\text{O}_2^{\bullet-}$  in the system. Overall, it appeared that QD + CV PU produced more  $\text{H}_2\text{O}_2$  than CV PU as CV PU activity is much less affected by the presence of catalase. This may be attributed to the fact that in QD + CV PU substrates, superoxide (and subsequently  $\text{H}_2\text{O}_2$ ) may be generated in four distinct ways:

- photoexcited QDs can directly produce  $\text{O}_2^{\bullet-}$ .<sup>153</sup>
- the molecular dye can produce  $\text{O}_2^{\bullet-}$  either by direct photoexcitation of CV to its triplet state.

- direct photoexcitation of CV to its singlet state in the QD + CV PU is possible. In this case, the CV is assumed to be in close proximity to or adsorbed onto the surface of the QDs and electron transfer to CV's excited singlet excited state would occur through interaction with the conduction band of the QD nanoparticle. This has been shown for a system composed of the ethyl ester of fluorescein (FLEt) and colloidal TiO<sub>2</sub> particles interacting under visible light irradiation.<sup>549</sup>
- QDs may act as electron donors to CV, resulting in the CV radical which may react with oxygen to produce O<sub>2</sub><sup>•-</sup>.

In contrast, CV PU substrates may produce O<sub>2</sub><sup>•-</sup> (and subsequently H<sub>2</sub>O<sub>2</sub>) through fewer routes:

- direct photoexcitation of the molecular dye to its triplet state
- interaction of the CV with unreacted monomer in the polymer matrix
- photoexcitation of CV dimers.<sup>537</sup>
- It is possible for the CV triplet state to interact with O<sub>2</sub> to generate O<sub>2</sub><sup>•-</sup> however the quantum yields for these reactions tend to be low.

Having fewer sources of O<sub>2</sub><sup>•-</sup> production meant that less of the species was generated by CV PU and thus subsequent dismutation generated less H<sub>2</sub>O<sub>2</sub>. In addition, these events may also simultaneously occur in QD + CV polymers, thus producing even more superoxide.

Likewise, when mannitol was present in the assays, QD + CV PU activity was more attenuated than CV PU activity. CV PU antimicrobial activity diminished to achieve only 1.68 log<sub>10</sub> kill in the presence of mannitol (2.8 log<sub>10</sub> reduction when no scavenger was present) and QD + CV PU achieved only 1.5 log<sub>10</sub> microbial kill in the presence of mannitol (4.2 log<sub>10</sub> reduction when no scavenger present). Mannitol is an effective scavenger hydroxyl radicals (<sup>•</sup>OH).<sup>550</sup> No significant change was observed with the control polymer with or without mannitol. The efficacy of CV PU and QD + CV PU surfaces were reduced to about the same level in the presence of mannitol however since the initial performance of QD + CV PU (in the absence of scavenger) was stronger, QD + CV PU surfaces were more negatively affected by the hydroxyl radical scavenger. We can infer that more <sup>•</sup>OH was being released by the QD + CV PU surfaces than the CV PU surfaces. This deduction was in agreement with the above assays that showed higher O<sub>2</sub><sup>•-</sup> and H<sub>2</sub>O<sub>2</sub> production in QD + CV PU functional surfaces.

The aromatic amino acid, L-histidine, is a well-known scavenger of singlet oxygen that chemically reacts with  $^1\text{O}_2$  at a high reaction rate to efficiently deactivate  $^1\text{O}_2$ .<sup>551-554</sup> Upon addition to the assay, the antimicrobial activity of CV PU substrates dropped from 2.8 log<sub>10</sub> kill to 1.8 log<sub>10</sub> kill. The significant attenuation of CV PU activity in the presence of L-histidine proves that the substrates produces singlet oxygen. As a molecular rotor, the photo-physical properties of CV is highly solvent-dependent. In solvents of low viscosity as cyclohexane and dichloromethane, the fluorescence quantum yield of CV is low and the molecular dye does not produce singlet oxygen.<sup>483</sup> However, in a high viscosity microenvironment, such as that afforded by polyurethane, intramolecular twisting of the dye's phenyl groups is restricted, and  $^1\text{O}_2$  can be produced via Type II energy transfer from the CV triplet state to the ground state of molecular oxygen. The results from this L-histidine microbiology assay evidenced this.

Similarly, the effectiveness of QD + CV PU substrates dropped from 4.2 log<sub>10</sub> kill to 0.8 log<sub>10</sub> kill. While  $^1\text{O}_2$  may be generated not only via direct excitation of CV embedded in polymer, but also photo-activated QDs can act as energy donors and transfer energy non-radiatively to ground-state CV acceptors which, react with nearby oxygen molecules to form cytotoxic  $^1\text{O}_2$  species (FRET).<sup>268</sup> The presence of L-histidine attenuated QD + CV PU antimicrobial activity to a much greater extent than CV PU lesser extent. Therefore the combinatorial system produced more  $^1\text{O}_2$  than the dye polymer alone. This meant that direct excitation of CV was not the only source of  $^1\text{O}_2$  generation and proved that FRET was the mechanism by which QD + CV PU activity was boosted. As previously discussed in CHAPTER 2, in the solution phase, QD and CV predominately form strong electrostatic interactions (as indicated by high  $K_{SV}$  values) which encourage PET however in the polymer, QD and CV may not form tight nanocomposites as in solution because the CV can also bind to adjacent polymer chains, altering the balance between FRET and PET. In the polymer, the QD and CV are on average localised further apart since CV can also bind to the polymer matrix. This may favour more FRET interactions and thus increase  $^1\text{O}_2$  generation in QD + CV PU as FRET occurs over longer ranges than PET.

Overall, from the ROS scavenger assays, it was clear that the superior antimicrobial action of QD + CV functional surfaces was due to the occurrence of both Type I and II photochemical mechanisms, however, there appears to be a greater contribution from Type II mechanisms as bactericidal action is most strongly attenuated in the presence of the  $^1\text{O}_2$  scavenger. This

is important to antimicrobial activity as  $^1\text{O}_2$  is deemed to be the most potent ROS.<sup>414</sup> Further, comparing CV PU and QD + CV PU with regard to the effect of the ROS scavengers, it was noted that CV PU also underwent both Type I and Type II mechanisms, producing all the ROS tested for:  $\text{O}_2^{\bullet-}$ ,  $\text{H}_2\text{O}_2$ ,  $\bullet\text{OH}$  and  $^1\text{O}_2$ . However, CV PU generated only a minimal amount of  $\text{H}_2\text{O}_2$  and generated significantly less  $\text{O}_2^{\bullet-}$ ,  $\bullet\text{OH}$  and  $^1\text{O}_2$  than QD + CV PU. As the ROS are responsible for lethal activity, this explained the lower activity of CV PU against both Gram-positive and Gram-negative bacteria. Studies have shown that photodynamic effect do not correlate with singlet oxygen yields but rather the ability of the photosensitising system to take part in the Type I mechanism.<sup>413</sup> As evidenced by the strong attenuation of the QD + CV surfaces by Type I ROS quenchers, the QD + CV functional surfaces are very efficient at Type I processes, making their photodynamic activity more effective.

These data are consistent with other studies using nanoparticle/CV combinations. For example, Sehmi *et al.* studied ROS production when ZnO nanoparticles and CV photosensitising dye were incorporated into polymer (CVZnO) and irradiated with white light intensity levels at ~6000 lux against laboratory strains of *E. coli* and *S. aureus*. In this study, specific quencher assays established the operation of both Type I and II mechanistic pathways in the lethal activity of the CVZnO system, however Type II processes provided a greater contribution.<sup>406</sup>

## 6.4. Conclusion

In this study, steady-state and time-resolved photoluminescence measurements has confirmed the ability of QD-CV complexes *embedded in polymer* to induce the formation of ROS through Type I photo-induced electron transfer or Type II energy transfer mechanisms, as has been confirmed for QD-CV complexes in organic solution. Further, analysis of time-resolved  $^1\text{O}_2$  phosphorescence data has revealed that QDs in polymer are incapable of producing singlet oxygen whereas CV in polymer (as a result of restricted intramolecular twisting) and QD + CV in polymer could efficiently release  $^1\text{O}_2$ , thus proving the occurrence of Type II energy transfer in these surfaces. To provide further evidence for the photochemical processes that CV and QD + CV PU functional surfaces take part in, inhibitors of ROS were added to bacteriological assays and the subsequent effects analysed and compared. The data has shown that while QD PU does not engage in Type I mechanisms. Along with  $^1\text{O}_2$  phosphorescence data, the present study has revealed that indium-based QD nanoparticles

on their own in polymer do not generate any ROS under light illumination, explaining the lack of photo-bactericidal activity against both Gram-positive and Gram-negative. On the other hand, both Type I and II photochemical processes are involved in photo-bacterial activity of CV-incorporated surfaces. When QD nanoparticles are added to CV, both Type I and II mechanisms are enhanced, producing more ROS. Comparatively,  $^1\text{O}_2$  played a more significant role in photo-destruction of bacteria, denoting that Type II mechanism is more dominant in the combinatorial functional surfaces.

# CHAPTER 7. CONCLUSIONS AND FUTURE WORK

## 7.1. Summary of Thesis

Hospital-acquired infections (HAIs) pose a serious risk to patients and medical personnel and result in increased morbidity and mortality to those infected. This is especially so due to the spread of AMR resulting in HAIs that are unresponsive to the antibiotics commonly used to treat them. Contaminated objects, instruments and surfaces serve as bacterial reservoirs and are the most important drivers of HAIs, underpinning the need for antibacterial surfaces that can reduce or prevent bacterial colonisation. Thus effective antibacterial surfaces have the potential to reduce the incidence of HAIs by disrupting the cycle of transmission of bacteria from surfaces to patients or medical personnel. In this thesis, polyurethane surfaces impregnated with a combination of quantum dots (QDs) and crystal violet photosensitiser (CV PS) were developed that demonstrated potent light-activated antibacterial activity based on PDT. The combination of QDs and CV dye was an advantageous strategy as it allowed exploitation of the photostability of QDs and the reactive oxygen species (ROS) efficiency of PS, while overcoming the low photobleaching threshold of the conventional PS. Additionally, the co-localisation of QDs and PS provide new interaction opportunities – electron transfer or non-radiative energy transfer (Förster resonance energy transfer, FRET) from photoactivated QDs to CV – that boost ROS generation thus enhancing bactericidal efficacy.

The QDs employed were prepared by Nanoco Technologies Ltd which has trademarked them as 'CFQDs®'. They are cadmium-free, indium-based semiconductor nanoparticles (NPs) with intrinsically lower toxicity than most commercial QDs.<sup>141, 476</sup> CV was selected owing not only to previous studies using Au and ZnO NPs but also the potential for photophysical interactions with the QDs favouring ROS generation.<sup>405, 406</sup> CV is also a well-known bactericidal agent that has been FDA approved for clinical application in wound dressings.<sup>481</sup>

In CHAPTER 2 the potential of indium-based quantum dot and CV dye as components in light-activated surfaces was initially probed by investigating the ability of QD-CV mixtures to act as FRET complexes in solution phase spectroscopically. Red-emitting and green-emitting indium-based QDs were mixed with crystal violet PS, leading to electronic interactions between the negatively charged QDs and the cationic CV. Photo-induced electron transfer

(PET) reactions that lead to the production of superoxide were shown to be feasible in the electrostatically bound complexes as evidenced by redox potentials extrapolations and Stern-Volmer analyses. Steady-state and time-resolved photoluminescence measurements revealed significant quenching of the QDs with increasing CV concentration. Together with the substantial spectral overlap between the donor emissions and acceptor absorption, this indicated the good probability of FRET interactions as well. Conclusive evidence of FRET interactions between the QDs and CV in solution was obtained using singlet oxygen phosphorescence spectroscopy. Using the TCSPC technique,  $^1\text{O}_2$  phosphorescence spectroscopy showed that illuminated red and green-emitting indium-based QDs were only able to generate  $^1\text{O}_2$  in the presence of CV, showing that in solution QDs and CV made effective FRET donor/acceptor pairs.

In the same chapter, PET between the QDs and CV was further explored using EPR spin trapping. Mixed results were observed with this method – irradiated green QDs produced signals corresponding to  $\cdot\text{OH}$  and irradiated red QDs/CV mixture resulted in the formation of carbon-centred radicals; and negligible EPR signals for all other QDs and/or CV solutions. It was believed that the higher exciton energy of the green QDs (larger band gap than red QDs) made direct electron transfer to  $\text{O}_2$  more favourable. The negative EPR results with green QD/CV mixtures observed in solution were attributed to fast charge recombination of the green QD/CV ion pair. This was supported by Stern-Volmer data which showed green QD/CV nanocomposites formed stronger electrostatic binding than red QD/CV nanocomposites. In summary, the study showed that in the presence of CV, red and green-emitting indium-based QDs could participate in FRET (Type II) processes. Moreover, additional PET (Type I) processes can occur as not only can the QDs and CV on their own engage in Type I photochemical reactions but in close proximity, excited QDs can also donate electrons to CV through energetically favourable pathways.

CHAPTER 3 describes the development of polyurethane substrates containing only QD NPs and their effectiveness as antibacterial surfaces. ‘Swell-encapsulation-shrink’, a simple, non-covalent dipping procedure, was used to impregnate medical-grade polyurethane squares as described for other nanomaterials and PS.<sup>404, 408</sup> This incorporation method expands the polymer using a solvent, making space for NPs and small molecules to be embedded. Removal of the solvent via evaporation causes the polymer to shrink, locking in the embedded

materials. Since swelling is greatly affected by the solvent system employed, optimisation studies were carried out to determine the organic solvent mixtures that encourage a high swelling rate (and thus high QD uptake) without over-expanding the polymer. It was found that no swelling occurred in neat cyclohexane, the solvent in which the QDs were supplied in. In 1:2 cyclohexane/dichloromethane (Cy/DCM) solvent mixture, polymer size increased by 70% however, after solvent evaporation, the polymer was misshapen. The best solvent ratio that encouraged swelling but caused no substrate deformity was 1:1 Cy/DCM, which swelled polyurethane up by 50% of its original size. The antibacterial tests revealed that red QD-incorporated polyurethane (rQD PU) and green QD- incorporated polyurethane (gQD PU) had no significant antibacterial effect against either *E. coli* or *S. aureus* when the substrates were made from a swelling solution containing 1 mg/mL QDs. Upon increasing the concentration of the red QDs in the swelling solution to 3 mg/mL and 7 mg/mL and extending irradiation times, the rQD PU surfaces were able to induce an antibacterial effect against *E. coli*, reducing bacterial numbers by 1.3 log<sub>10</sub> and 2 log<sub>10</sub> respectively. However, since similar levels of antibacterial activity were observed in the absence of white light irradiation for both the 3 mg/mL and 7 mg/mL rQD PU substrates, this indicated that the antibacterial activity depended, not on photo-irradiation of the surfaces, but rather, direct contact of the QDs with bacteria on the surface. The lack of photo-activity was inconsistent with solution phase experimental results which showed that QDs produce ROS upon visible light illumination.

Therefore, the uptake of QDs by the polymer was quantified using UV-vis absorption spectroscopy. Absorption spectra of the swelling solutions before and after swell-encapsulation treatments revealed that each treatment (which produced four modified polyurethane squares) took up ~15% QD material, meaning that QD uptake per polyurethane square was ~4%. This equated to 0.4 mg of QD material per polyurethane square in a typical swell-encapsulation where 1 mg/mL QD concentration was used. Similar estimates of nanomaterial uptake were recently reported in a study that used fluorescence lifetime imaging, water contact angle measurement and energy-dispersive X-ray analysis to quantify nanomaterial concentration when CdSe QDs and TiO<sub>2</sub> NPs were embedded into a polydimethylsiloxane host matrix via swell encapsulation.<sup>411</sup> Quantification studies therefore revealed limited QD uptake by polyurethane and the low antibacterial effect induced by QD PU substrates was attributed to this. It is believed that the final QD concentration with the rQD PU and gQD PU surfaces itself was not sufficient to induce cytotoxic effects via *photochemical*

means i.e. the QD concentrations were too low to produce enough ROS to induce bacterial death.

Based on the efficiency of indium-based QDs and CV dye as FRET donor/acceptor pairs in solution as demonstrated in Chapter 2, CHAPTER 4 explores the ability of polyurethane embedded with QDs and CV to act as functional antibacterial surfaces based on aPDT. Initially, the antibacterial surfaces were fabricated using a two-step swell-encapsulation technique which saw the QDs incorporated first after 24 h, followed by the CV after 72 h (QD/CV PU). Two different QD concentrations – 0.1 mg/mL and 0.5 mg/mL – were used in the swelling solutions to produce the QD/CV PU substrates, keeping CV concentration constant (at 1 mM). For green QD/CV PU (gQD/CV PU) against laboratory strain *E. coli*, there was a positive correlation between the concentration of QDs in the polymer (swelling solution) and the reduction of *E. coli* numbers. gQD/CV PU achieved 2.4 log<sub>10</sub> and 3.3 log<sub>10</sub> kill of *E. coli* (6600lux, 3 h) when the green QDs swelling solution were 0.1 mg/mL and 0.5 mg/mL respectively, implying a synergistic effect between the PS and the NPs. In contrast, no improvement of antibacterial activity was seen with the increase of red QD swelling solution concentrations. Rather, the antibacterial effect stayed the same at ~2.2 log<sub>10</sub> (6600lux, 3 h), similar to the activity achieved by CV-only substrates.

Based on the ability of red QDs and CV to engage in FRET interactions, it was then inferred that controlling conditions to better enable more efficient FRET should improve ROS yields and therefore antibacterial activity. Spectral overlap was already significant and could not be changed. However, close proximity between the donor and acceptor could be enhanced by altering the experimental set-up. A novel one-step swell-encapsulation process was designed to improve co-localisation of the QD and CV in the polymer - the QDs and CV were mixed in a miscible 1:1 cyclohexane/dichloromethane solvent system prior to the addition of the polyurethane. This new method was advantageous as it allowed electrostatic complex formation between the donor and acceptor before polymer impregnation. Also, in practical terms, the method drastically reduced the fabrication time from 96 h to 24 h in total. Red QD and CV containing polymers produced by the 1-step method (rQD + CV PU) indeed showed more potent antibacterial activity compared to the two-step method, inducing a 4.3 log<sub>10</sub> kill of laboratory strain *E. coli*. Similarly, the antibacterial activity of green QD and CV containing polymers produced by the 1-step method (gQD + CV PU) was potentiated. gQD + CV PU

achieved a 3.9 log<sub>10</sub> kill against laboratory strain *E. coli*. The increase in antibacterial activity upon adjustment of the QD-CV encapsulation technique strongly indicated the occurrence of synergistic interactions between QDs and CV via FRET in the polymer. This improvement in activity was noteworthy in light of the fact that CV concentration was halved in the 1-step swelling solutions thus activity was more dependent on synergistic interactions than in 2-step experiments. The success of the new method meant that moving forward, all functional surfaces were fabricated via this technique.

Following the efficacious results against laboratory strain *E. coli*, rQD + CV PU and gQD + CV PU were tested against clinical strains of bacteria. It was expected that similarly potent antibacterial effects would be observed against multi-drug resistant bacterial strains because FRET was involved in antibacterial activity, meaning that the effectiveness of the surfaces was at least partly reliant on ROS generation, a mechanism that is independent of antibiotic resistance routes. Indeed, rQD + CV PU and gQD + CV PU surfaces induced ~4 log<sub>10</sub> destruction of Gram-positive clinical strains such as EMRSA 4742 and MRSA NCTC 13413 after 1 h white light irradiation. Against Gram-negative clinical strain *E. coli* 1030, rQD + CV PU and gQD + CV PU displayed ~3.5 log<sub>10</sub> and ~4 log<sub>10</sub> reduction respectively after 4 h white light irradiation at 6000 lux.

Beyond nosocomial pathogens, foodborne bacterial infections affect millions each year and are a rising problem even in countries with strict food safety measures. In the food industry, high levels of foodborne bacterial pathogens such as *S. typhimurium* and *L. monocytogenes* are present. Because QD + CV PU are made from cadmium-free QDs of low toxicity<sup>476</sup> and an FDA-approved PS,<sup>481</sup> they are an acceptable means for the prevention of foodborne bacterial infections in the food industry. Studies to test the efficacy of gQD + CV PU surfaces against Gram-negative *S. typhimurium* and Gram-positive *L. monocytogenes* were carried out. After 4 h 6600 lux white light irradiation of gQD + CV PU, *S. typhimurium* levels were reduced by 2.2 log<sub>10</sub>, a remarkable result since *Salmonella* is intrinsically very resistant and has a higher survival rate than *E. coli*. The bacterium's resistance was clearly demonstrated as CV PU had no significant antibacterial effect on *S. typhimurium*. On the other hand, Gram-positive *Listeria* was more susceptible to CV PU than typically seen for *S. aureus*. Thus, when green QDs were added to CV in the polymer, 100% elimination was achieved after 4 h irradiation at 6600 lux. Based on the results, QD-CV combinations in polymer are effective antimicrobial

surfaces against susceptible and resistant nosocomial and foodborne bacterial Gram-positive and Gram-negative pathogens at high light intensities. In order to achieve potent activity, the presence of the PS in the surfaces was crucial. However, more than that, it was important to ensure that QDs and CV sat in close proximity with in the polymer to encourage close-range interactions to boost light-activated bactericidal effects. From this chapter and the previous one, it was clear that enhancement of the antibacterial effect of QD + CV PU substrates was not a result of additive but rather synergistic effects as QDs alone in polyurethane do not yield any significant bactericidal effect.

Next in CHAPTER 5, to determine if the QD + CV PU surfaces are functional at low light intensities, antibacterial tests were carried out at 500 lux, more than 13 times lower than the light intensity previously employed. This was motivated by the desire to replicate a more realistic clinical setting where general lighting criteria (e.g. in wards, reception areas and treatment rooms) to which hospitals must conform often require light intensities less than 1000 lux.<sup>511</sup> *E. coli* and *P. aeruginosa* were selected as they are hard-to-treat Gram-negative pathogens that often colonise moist hospital environment and are the most common causative agents in catheter-associated UTIs and ventilator-associated pneumonia. gQD + CV PU induced significant reductions ( $> 3 \log_{10}$ ) in the numbers of an environmental isolate of *P. aeruginosa* (recovered from a hospital sink) as well as a clinical isolate of *P. aeruginosa* (derived from a cystic fibrosis patient) after 24 h of low level white light irradiation. The levels of multi drug resistant *E. coli* was also reduced by similar levels after an 18 h low light irradiation. Thus by reducing the white intensity and increasing the irradiation, it was possible to achieve antimicrobial efficiencies comparable to strong light intensities in short time bursts. This was an important outcome as it demonstrated that in cases where specialised lighting or high intensity lighting for photokilling was unavailable, QD + CV PU surfaces were still effective. Additionally, because bacteria can persist on inanimate surfaces for several months, comparatively slower killing over a lower light intensities may prove more useful and applicable in clinical settings.<sup>530</sup>

Finally, CHAPTER 6 described the processes employed to explore the mechanism at work in QD + CV PU substrates. Previously, in Chapter 2, it was determined that Type II and Type I mechanism were at work in solution-phase QD-CV complexes. In the polymer, various direct and indirect methods were employed to distinguish Type I and Type II mechanisms. Using

fluorescence measurements in polymer, some effects caused by CV could be observed in 'polymer phase'. In solution, CV's intramolecular charge transfer (TICT) states meant that no features of CV fluorescence could be observed with increasing dye concentration. However when rotation is restricted in a viscous microenvironment, CV fluorescence is evident, though still of low yield compared to QDs. With red QDs, bathochromic shifts are observed in the emission spectra with increasing CV concentration in the polymer. In polymer, time-resolved photoluminescence measurement using the TCSPC method showed that QDs embedded in polymer had shorter lifetimes compared to QDs in polymer, due to the new microenvironment. However, the lifetimes were still long compared to CV fluorescence lifetime which is  $< 5$  ns in viscous solvents or when bound to protein.<sup>430, 535</sup> The derived putative FRET efficiencies appeared to be generally higher in the polymer environment than in solution, however since not all the NPs and PS was taken up in polyurethane during swell-encapsulation-shrink, we were wary of making comparisons from this observation. As with QD-CV solution mixtures, singlet oxygen phosphorescence was considered to confirm the occurrence of FRET in the polymer. Indeed, red and green QD + CV PU surfaces were shown to produce  $^1\text{O}_2$ . CV embedded in polymer has been shown to produce  $^1\text{O}_2$  and the observed decay kinetics and derived  $^1\text{O}_2$  lifetimes for CV PU were in good agreement with the literature.<sup>536</sup> Subsequently, the decay curves for rQD + CV PU and gQD + CV PU closely matched that observed for CV PU with a congruent  $^1\text{O}_2$  lifetime. Superoxide release from the polymer was investigated using chemical detection assays and also with microbiological ROS inhibitor assays. Chemical detection of  $\text{O}_2^{\bullet-}$  release from the modified substrates was carried out with XTT, a colorimetric assay for probing total  $\text{O}_2^{\bullet-}$  capacity using an experimental set-up adapted from literature.<sup>537</sup> However, due to issues with reproducibility, this approach was abandoned. On the other hand, carrying out a normal antibacterial test and introducing ROS scavengers that inhibited  $\text{O}_2^{\bullet-}$  proved to be a reliable means of verifying the release of superoxide from the functional surfaces. The addition of excess superoxide dismutase scavenged  $\text{O}_2^{\bullet-}$  and consequently, CV PU and QD + CV PU activities were attenuated by  $\sim 2.5 \log_{10}$  and  $\sim 3 \log_{10}$  respectively. This microbiology assay route was adopted for other ROS identification as it was straightforward, reliable and offered the opportunity to evaluate and compare the importance of different ROS to QD + CV PU activity. Catalase, mannitol and L-histidine scavengers verified the release of  $\text{H}_2\text{O}_2$ ,  $\bullet\text{OH}$  and  $^1\text{O}_2$  from the QD + CV PU surfaces, therefore light-activated antibacterial activities were mediated through both Type I and II photochemical pathways. Comparing the effect of the ROS inhibitors on QD + CV PU, the L-histidine scavenger caused the strongest attenuation of QD + CV activity proving though Type I mechanisms were

significant, Type II mechanisms were dominant. Between CV PU and QD + CV PU, results showed that CV PU generated minimal levels of  $H_2O_2$  and  $\bullet OH$  and  $^1O_2$  production was significantly lower than QD + CV PU. As lethal activity was ROS-dependent, these mechanistic studies explained why CV PU displayed lower antibacterial activity throughout and likewise, the superior performance of QD + CV PU.

QD + CV PU surfaces performed better than CdTe QDs in aqueous solutions. After 8 h irradiation of 100 nM CdTe in aqueous suspension with bacteria, 29% and 59% reductions of patient isolates of MRSA and *K. pneumoniae* were observed respectively. For a clinical isolate of MDR *Salmonella typhimurium*, growth was inhibited by 56% and for two MDR *E. coli* isolates, 83% and 64% reductions in bacterial levels were noted respectively.<sup>377</sup> QD + CV PU surfaces demonstrated antibacterial activities of well over 99.9% ( $>3 \log_{10}$ ) for almost all lab and MDR bacteria (*E. coli*, *S. aureus*, MRSA, *S. typhimurium*, *L. monocytogenes*) strains tested within 4 h of light irradiation at 6000 lux (*K. pneumoniae* not tested in this thesis). Activity was superior despite the fact that QDs and CV were embedded in polyurethane and thus had no direct contact with bacteria.

Other reported polymer surfaces incorporated with NPs and PS showed similar levels of activity as QD + CV PU. For example, Perni *et al.* showed that methylene blue (MB), in addition to 2 nm gold (Au) NPs, incorporated into polysiloxane demonstrated up to  $3.5 \log_{10}$  in the viable count of *E. coli* and MRSA.<sup>402</sup> Similarly, against *S. aureus*, Naik *et al.* found that when 2 nm Au NPs were added, the activity of MB-incorporated polyurethane increased from  $2.8 \log_{10}$  kill to  $3.8 \log_{10}$  and the activity of toluidine blue O (TBO)-incorporated polyurethane increased from  $4.3 \log_{10}$  kill to  $4.8 \log_{10}$  kill.<sup>412</sup> This study highlights the inherent light-activated activities of MB and TBO dye molecules – trialling these PS into new QD-PS surfaces may yield antibacterial surfaces that are more potent.

Sehmi *et al.* studied the effect of the addition of ZnO and MgO NPs to the photo-antibacterial activity of CV-incorporated polyurethane. Both NPs when combined with CV enhanced antibacterial activity against both MRSA and *E. coli*, with polymers embedded with a combination of ZnO and CV showing the strongest photo-bactericidal activity against MRSA and *E. coli*.<sup>407</sup> This study showed that NPs capped with oleic acid ligands gave the best results

therefore in the future, it may be worth considering the QD capping ligand as it may have a critical role in the bactericidal activity of the QD + CV PU surfaces.

Therefore QD + CV PU substrates compare favourably with other substrates containing NPs and PS. Crucially though, with QD + CV PU, more mechanistic insight could be gleaned as the QDs are photoluminescent which enabled detailed photophysical studies of their properties when inside the polymer.

## **7.2. Implications & Importance of Findings**

The key finding in this thesis is that cadmium-free quantum dots can be combined with conventional PS to develop powerful antibacterial surfaces. In the presence of CV dye molecule, QDs can engage in Type I and Type II reactions, acting as an electron donor and energy donor correspondingly. Our success in simultaneously incorporating QDs and PS into commercially obtained medical grade polyurethane via a simplified swell-encapsulation-shrink technique means that ordinary surfaces offers an easy, straightforward means of transforming ordinary polymer substrates into potent antimicrobial surfaces. Industrialisation to enable mass production of antibacterial surfaces is also realisable due to the uncomplicated nature of this one-step procedure.

Since polyurethane is a clinically approved polymer widely used in medical applications, it is fitting that this thesis demonstrates potent photo-bactericidal activity with this polymer. Polyurethane is commonly used in general purpose tubing, surgical drains, dialysis devices, medical garments, hospital bedding, wound dressings and more.<sup>555</sup> Antimicrobial function can be added to these various applications via swell-encapsulation-shrink. In addition to polyurethane, swell-encapsulation-shrink was been employed to endow other medically relevant polymers such as silicone with antibacterial properties, furthering the applications. Generally, the biocompatibility, flexibility, and inexpensiveness of polymers makes them preferable to other surfaces such as glass and titania. Polyurethane is also exceptionally resistant to tear and abrasion, making it an ideal polymer to endow with antimicrobial functions. Flexible antimicrobial polyurethanes can be moulded to fit any high-touch surface e.g. bed rails, supply carts, over-bed tables, doorknobs and intravenous infusion pumps, reducing transmission of bacteria form these surfaces.

The QD + CV PU functional surfaces are also made from non-toxic materials: cadmium-free indium-based QDs shown to be non-toxic in rat toxicological and biodistribution studies<sup>141, 476</sup> and crystal violet, which has been FDA approved for various medical applications.<sup>481</sup> Considering the biocompatibility of polyurethane, QD + CV PU may potentially be utilised with short-term implants to prevent infection such as catheter tubing, endotracheal tubes, feeding tubes and chemotherapy ports. Biofilm formation leading to infections such as UTIs, and pneumonia are prevalent with tubing; incorporating QDs and CV can prevent planktonic bacteria colonisation and thus prevent biofilm formation in the first place. In this thesis, it has been shown that activation of QD + CV requires minimal light levels so light-activated disinfection can take place at ambient light. In addition, various broad-band or narrow band light sources can activate these materials. These findings are important as it means QD and CV-incorporated surfaces can perform well under normal hospital lighting conditions. Also, *in situ* sterilisation of indwelling devices such as catheters and endotracheal tubes can be carried out using fibre-optic light delivery of a laser or LED.

Finally, as the photoactivity of QD + CV PU functional surfaces depends not on release of QDs or PS from the polymer but rather depends on ROS generation, these surfaces are safer as any adverse effect or damage to the host tissue as a result of ion release is severely restricted. Secondly, as the materials are photo-active, there is low toxicity in the absence of light activation. Finally, the material exhibit specificity when used internally as generated ROS do not travel far beyond the target area (due to their short diffusion pathway) and when used externally on inanimate surfaces, ROS are cytotoxic to bacteria, attacking multiple intracellular sites however, ROS cannot penetrate the skin.

In this thesis, the focus has primarily been on the application of QD + CV PU surfaces in hospitals, however, other healthcare facilities such as nursing homes, GP surgeries, clinics, outpatient centres and even ambulances would benefit from the installation of these non-toxic surfaces. Another area where QD + CV PU surfaces could be applied is in the food sector.

### **7.3. Future Work**

In this thesis, the potent antibacterial activity of QD + CV PU surfaces has been demonstrated against a number of common Gram-negative and Gram-positive bacteria. The results have shown that antibacterial activity is dependent on factors such as QD uptake into polymer,

irradiation time and light intensity. For future application in the clinical setting and other sectors, a number of issues must be addressed.

Firstly, it is important to determine the efficacy of these substrates against other microorganisms such as *S. epidermis*, *C. difficile*, *Acinetobacter* spp., *Candida albicans* and norovirus which are common colonisers of surfaces in healthcare facilities.<sup>556</sup> In light of the recent pandemic caused by the novel coronavirus (SARS-CoV-2), which studies have shown can persist on a variety of surfaces from hours to days, a very relevant and potentially highly impactful study would be to test the ability of QD + CV PU surfaces to kill SARS-CoV-2.<sup>557</sup>

Secondly, future studies could also look at the effect of using other common PS such as methylene blue and rose Bengal combined with QDs carefully selected to enable FRET mechanistic interactions. Also, regarding mechanism, recent studies have identified another mechanism could be involved that directly populates the CV triplet state - Dexter energy transfer (DET), triplet energy transfer from the QD to the acceptor without populating the singlet excited state or charge transfer intermediates. To investigate the possibility of DET, ultrafast transient absorption spectroscopy can be performed to monitor triplet-to-triplet absorptions in QD-CV nanocomposites over different timescales, as has been done in recent studies.<sup>441, 442</sup>

Finally, although the presence of QDs alone in the polymer failed to induce photo-antibacterial activity, in the presence of CV, synergistic potentiation of the antibacterial activity of CV was observed. This highlighted an important issue – optimising the uptake of the QDs into the polymer. Future studies should focus on improving swell-encapsulation-shrink by varying parameters such as swelling time and solvent ratios. Any improvement in the concentration of NPs in the polymer would prevent waste of nanomaterial thus making production of the QD + CV PU more attractively commercially. Also, more NPs in the polymer would increase PET and FRET efficiency, boosting ROS production and potentially augmenting antibacterial activity towards the level of 'disinfection' as defined by the CDC ( $\geq 6 \log_{10}$  kill).<sup>313</sup>

# Publications & Presentations

## Publications

Owusu, E. G. A.; Yaghini, E.; Naasani, I.; Parkin, I. P.; Allan, E.; MacRobert, A. J., Synergistic interactions of cadmium-free quantum dots embedded in a photosensitised polymer surface: efficient killing of multidrug-resistant strains at low ambient light levels. *Nanoscale* 2020, 12 (19), 10609-10622.

Owusu, E. G. A.; MacRobert, A. J.; Naasani, I.; Parkin, I. P.; Allan, E.; Yaghini, E., Photoactivable Polymers Embedded with Cadmium-Free Quantum Dots and Crystal Violet: Efficient Bactericidal Activity against Clinical Strains of Antibiotic-Resistant Bacteria. *ACS Appl. Mater. Inter.* 2019, 11 (13), 12367-12378.

## Conference Presentations

Koranteng, E. G. A.; Yaghini, E.; Naasani, I.; Parkin, I. P.; Allan, E.; MacRobert, A. J., Light-Activated Surfaces for Reducing Hospital-Acquired Infections. 2018 Materials Research Society Spring Meeting & Exhibit, Arizona, USA, April 2018

Koranteng, E. G. A., 'How do we refresh the antibiotic pipeline? Challenges and considerations' Medical Research Foundation National PhD Training Programme in AMR Research, University of Bristol, August 2018

Koranteng, E. G. A.; Yaghini, E.; Naasani, I.; Parkin, I. P.; Allan, E.; MacRobert, A. J., Antimicrobial Surfaces Containing Quantum Dots for Reducing Hospital Acquired Infections. British Society of Nanomedicine Early Career Researcher Meeting, London, August 2018

Koranteng, E. G. A., Nanoparticles for Antimicrobial & Antimicrobial Resistance Applications. Point-of-Care Diagnostics Workshop Programme, University College London, October 2017

Koranteng, E. G. A., Smart Surfaces. UCL AMR Network Research Showcase Event, University College London, July 2017

### **Poster Presentations**

Koranteng, E. G. A.; Yaghini, E.; Naasani, I.; Parkin, I. P.; Allan, E.; MacRobert, A. J., Light-Activated Polymer Quantum Dot-Photosensitiser Systems for Application in Antimicrobial Hospital Surfaces. MRF National PhD Training Programme in AMR Research, University of Bristol, August 2018

## References

1. Smith, A. M.; Gao, X.; Nie, S., Quantum Dot Nanocrystals for *In Vivo* Molecular and Cellular Imaging. *Photochem. Photobiol.* **2004**, *80*, 377-385.
2. Paul, A., The Use of Nanocrystals in Biological Detection. *Nat. Biotechnol.* **2003**, *22* (1), 47.
3. Igor, L. M.; Uyeda, H. T.; Ellen, R. G.; Hedi, M., Quantum Dot Bioconjugates for Imaging, Labelling and Sensing. *Nat. Mater.* **2005**, *4* (6), 435.
4. Ishikawa, M.; Biju, V., Luminescent Quantum Dots, Making Invisibles Visible in Bioimaging. In *Nanoparticles in Translational Science and Medicine*, Academic Press: **2011**; Vol. 104, pp 53-99.
5. Algar, W. R.; Massey, M.; Krull, U. J., Semiconductor Quantum Dots and FRET. In *FRET – Förster Resonance Energy Transfer*, Weinheim : Wiley-VCH Verlag GmbH & Co. KGaA: **2013**; pp 475-605.
6. Xu, G.; Zeng, S.; Zhang, B.; Swihart, M. T.; Yong, K.-T.; Prasad, P. N., New Generation Cadmium-Free Quantum Dots for Biophotonics and Nanomedicine. *Chem. Rev.* **2016**, *116* (19), 12234.
7. Talapin, D. V.; Haubold, S.; Rogach, A. L.; Kornowski, A.; Haase, M.; Weller, H., A Novel Organometallic Synthesis of Highly Luminescent CdTe Nanocrystals. *J Phys Chem B* **2001**, *105* (12), 2260-2263.
8. Peng, X.; Schlamp, M. C.; Kadavanich, A. V.; Alivisatos, A. P., Epitaxial Growth of Highly Luminescent CdSe/CdS Core/shell Nanocrystals with Photostability and Electronic Accessibility. *J. Am. Chem. Soc.* **1997**, *119* (30), 7019-7029.
9. Dabbousi, B.; Rodriguezviejo, J.; Mikulec, F.; Heine, Jr.; Mattoussi, H.; Ober, R.; Jensen, K.; Bawendi, M. G., (CdSe)ZnS Core-shell Quantum Dots: Synthesis and Characterization of a Size Series of Highly Luminescent Nanocrystallites. *J. Phys. Chem. B* **1997**, *101* (46), 9463-9475.
10. Chen, H. S.; Lo, B.; Hwang, J. Y.; Chang, G. Y.; Chen, C. M.; Tasi, S. J.; Wang, S. J. J., Colloidal ZnSe, ZnSe/ZnS, and ZnSe/ZnSeS Quantum Dots Synthesized from ZnO. *J Phys Chem B* **2004**, *108* (44), 17119-17123.
11. Battaglia, D.; Peng, X., Formation of High Quality InP and InAs Nanocrystals in a Noncoordinating Solvent. *Nano Lett.* **2002**, *2* (9), 1027-1030.
12. Lucey, D. W.; MacRae, D. J.; Furis, M.; Sahoo, Y.; Cartwright, A. N.; Prasad, P. N., Monodispersed InP Quantum Dots Prepared by Colloidal Chemistry in a Noncoordinating Solvent. *Chem. Mater.* **2005**, *17* (14), 3754-3762.
13. Steven, A. M.; Gerasimos, K.; Shiguo, Z.; Paul, W. C.; Ethan, J. D. K.; Larissa, L.; Edward, H. S., Solution-processed PbS Quantum Dot Infrared Photodetectors and Photovoltaics. *Nat. Mater.* **2005**, *4* (2), 138.

14. La Porta, F. A.; Ferrer, M. M.; de Santana, Y. V. B.; Raubach, C. W.; Longo, V. M.; Sambrano, J. R.; Longo, E.; Andrés, J.; Li, M. S.; Varela, J. A., Synthesis of Wurtzite ZnS Nanoparticles using the Microwave Assisted Solvothermal Method. *J. Alloys Compd.* **2013**, *556* (C), 153-159.
15. Brus, L. E., Electron–electron and Electron-hole Interactions in Small Semiconductor Crystallites: The Size Dependence of the Lowest Excited Electronic State. *J. Chem. Phys.* **1984**, *80* (9), 4403-4409.
16. Rossetti, R.; Nakahara, S.; Brus, L. E., Quantum Size Effects in the Redox Potentials, Resonance Raman Spectra, and Electronic Spectra of CdS Crystallites in Aqueous Solution. *J. Chem. Phys.* **1983**, *79* (2), 1086-1088.
17. Steigerwald, M. L.; Alivisatos, A. P.; Gibson, J. M.; Harris, T. D.; Kortan, R.; Muller, A. J.; Thayer, A. M.; Duncan, T. M.; Douglass, D. C.; Brus, L. E., Surface Derivatization and Isolation of Semiconductor Cluster Molecules. *J. Am. Chem. Soc.* **1988**, *110* (10), 3046-3050.
18. Murray, C. B.; Norris, D. J.; Bawendi, M. G., Synthesis and Characterization of Nearly Monodisperse CdE (E = S, Se, Te) Semiconductor Nanocrystallites. *J. Am. Chem. Soc.* **1993**, *115* (19), 8706-8715.
19. Hines, M. A.; Guyot-Sionnest, P., Synthesis and Characterization of Strongly Luminescing ZnS-Capped CdSe Nanocrystals. *J. Phys. Chem.* **1996**, *100* (2), 468-471.
20. Bruchez, M.; Moronne, M.; Gin, P.; Weiss, S.; Alivisatos, A. P., Semiconductor nanocrystals as fluorescent biological labels. *Science* **1998**, *281* (5385), 2013-2016.
21. Chan, W. C.; Nie, S., Quantum Dot Bioconjugates for Ultrasensitive Nonisotopic Detection. *Science* **1998**, *281* (5385), 2016.
22. Fox, M., *Optical Properties of Solids* 2nd ed.; Oxford, England : Oxford University Press: **2010**.
23. Norris, D.; Bawendi, M., Measurement and Assignment of the Size-Dependent Optical Spectrum in CdSe Quantum Dots. *Phys. Rev. B* **1996**, *53* (24), 16338-16346.
24. Villaverde, A., *Nanoparticles in Translational Science and Medicine*. London : Academic Press: **2011**.
25. Vo-Dinh, T., *Biomedical Photonics Handbook. Therapeutics and Advanced Biophotonics*. 2nd ed.; Boca Raton, Florida : CRC Press: **2015**.
26. Zhu, L.; Ang, S.; Liu, W. T., Quantum Dots as a Novel Immunofluorescent Detection system for *Cryptosporidium parvum* and *Giardia lamblia*. *Appl. Environ. Microbiol.* **2004**, *70* (1), 597-598.
27. Jamieson, T.; Bakhshi, R.; Petrova, D.; Pocock, R.; Imani, M.; Seifalian, A. M., Biological applications of quantum dots. *Biomaterials* **2007**, *28* (31), 4717-32.
28. Walling, M. A.; Novak, J. A.; Shepard, J. R., Quantum dots for live cell and in vivo imaging. *Int. J. Mol. Sci.* **2009**, *10* (2), 441-91.

29. Gao, X.; Yang, L.; Petros, J. A.; Marshall, F. F.; Simons, J. W.; Nie, S., *In vivo* Molecular and Cellular Imaging with Quantum Dots. *Curr. Opin. Biotechnol.* **2005**, *16* (1), 63-72.
30. Berlier, J. E.; Rothe, A.; Buller, G.; Bradford, J.; Gray, D. R.; Filanoski, B. J.; Telford, W. G.; Yue, S.; Liu, J.; Cheung, C. Y.; Chang, W.; Hirsch, J. D.; Beechem, J. M.; Haugland, R. P.; Haugland, R. P., Quantitative comparison of long-wavelength Alexa Fluor dyes to Cy dyes: fluorescence of the dyes and their bioconjugates. *J. Histochem. Cytochem.* **2003**, *51* (12), 1699-712.
31. Panchuk-Voloshina, N.; Haugland, R. P.; Bishop-Stewart, J.; Bhargat, M. K.; Millard, P. J.; Mao, F.; Leung, W. Y.; Haugland, R. P., Alexa dyes, a series of new fluorescent dyes that yield exceptionally bright, photostable conjugates. *J. Histochem. Cytochem.* **1999**, *47* (9), 1179-1188.
32. Resch-Genger, U.; Grabolle, M.; Cavaliere-Jaricot, S.; Nitschke, R.; Nann, T., Quantum Dots versus Organic Dyes as Fluorescent Labels. *Nat. Methods* **2008**, *5* (9), 763-775.
33. Chan, W. C. W.; Nie, S. M., Quantum dot bioconjugates for ultrasensitive nonisotopic detection. *Science* **1998**, *281* (5385), 2016-2018.
34. Dahan, M.; Laurence, T.; Pinaud, F.; Chemla, D. S.; Alivisatos, A. P.; Sauer, M.; Weiss, S., Time-gated biological imaging by use of colloidal quantum dots. *Opt. Lett.* **2001**, *26* (11), 825-827.
35. Grecco, H. E.; Lidke, K. A.; Heintzmann, R.; Lidke, D. S.; Spagnuolo, C.; Martinez, O. E.; Jares-Erijman, E. A.; Jovin, T. M., Ensemble and single particle photophysical properties (two-photon excitation, anisotropy, FRET, lifetime, spectral conversion) of commercial quantum dots in solution and in live cells. *Microsc Res Tech* **2004**, *65* (4-5), 169-79.
36. Derfus, A. M.; Chan, W. C. W.; Bhatia, S. N., Probing the Cytotoxicity Of Semiconductor Quantum Dots. *Nano Lett.* **2004**, *4* (1), 11-18.
37. Hoshino, A.; Fujioka, K.; Oku, T.; Suga, M.; Sasaki, Y. F.; Ohta, T.; Yasuhara, M.; Suzuki, K.; Yamamoto, K., Physicochemical properties and cellular toxicity of nanocrystal quantum dots depend on their surface modification. *Nano Lett.* **2004**, *4* (11), 2163-2169.
38. Cho, S. J.; Maysinger, D.; Jain, M.; Roder, B.; Hackbarth, S.; Winnik, F. M., Long-Term Exposure to CdTe Quantum Dots Causes Functional Impairments in Live Cells. *Langmuir* **2007**, *23* (4), 1974-1980.
39. Ma, J.; Chen, J. Y.; Guo, J.; Wang, C. C.; Yang, W. L.; Xu, L.; Wang, P. N., Photostability of thiol-capped CdTe quantum dots in living cells: the effect of photo-oxidation. *Nanotechnology* **2006**, *17* (9), 2083-2089.
40. Lewinski, N.; Colvin, V.; Drezek, R., Cytotoxicity of nanoparticles. *Small* **2008**, *4* (1), 26-49.
41. Selvan, S. T.; Tan, T. T.; Ying, J. Y., Robust, non-cytotoxic, silica-coated CdSe quantum dots with efficient photoluminescence. *Adv. Mater.* **2005**, *17* (13), 1620-+.
42. Chen, F. Q.; Gerion, D., Fluorescent CdSe/ZnS nanocrystal-peptide conjugates for long-term, nontoxic imaging and nuclear targeting in living cells. *Nano Lett.* **2004**, *4* (10), 1827-1832.

43. Jaiswal, J. K.; Mattoussi, H.; Mauro, J. M.; Simon, S. M., Long-term multiple color imaging of live cells using quantum dot bioconjugates. *Nat. Biotechnol.* **2003**, *21* (1), 47-51.
44. Empedocles, S.; Bawendi, M., Spectroscopy of single CdSe nanocrystallites. *Accounts Chem Res* **1999**, *32* (5), 389-396.
45. Nirmal, M.; Dabbousi, B. O.; Bawendi, M. G.; Macklin, J. J.; Trautman, J. K.; Harris, T. D.; Brus, L. E., Fluorescence intermittency in single cadmium selenide nanocrystals. *Nature* **1996**, *383* (6603), 802-804.
46. Galland, C.; Ghosh, Y.; Steinbruck, A.; Sykora, M.; Hollingsworth, J. A.; Klimov, V. I.; Htoon, H., Two Types of Luminescence Blinking Revealed by Spectroelectrochemistry of Single Quantum Dots. *Nature* **2011**, *479* (7372), 203-U75.
47. Lidke, K. A.; Rieger, B.; Jovin, T. M.; Heintzmann, R., Superresolution by localization of quantum dots using blinking statistics. *Opt. Express* **2005**, *13* (18), 7052-7062.
48. Deng, Y.; Sun, M. Z.; Lin, P. H.; Ma, J. J.; Shaevitz, J. W., Spatial Covariance Reconstructive (SCORE) Super-Resolution Fluorescence Microscopy. *PLoS One* **2014**, *9* (4).
49. Wang, Y.; Fruhwirth, G.; Cai, E.; Ng, T.; Selvin, P. R., 3D Super-Resolution Imaging with Blinking Quantum Dots. *Nano Lett.* **2013**, *13* (11), 5233-5241.
50. Zong, S. F.; Zong, J. Z.; Chen, C.; Jiang, X. Y.; Zhang, Y. Z.; Wang, Z. Y.; Cui, Y. P., Single molecule localization imaging of exosomes using blinking silicon quantum dots. *Nanotechnology* **2018**, *29* (6).
51. Chien, F. C.; Kuo, C. W.; Chen, P. L., Localization imaging using blinking quantum dots. *Analyst* **2011**, *136* (8), 1608-1613.
52. Chen, Y.; Vela, J.; Htoon, H.; Casson, J. L.; Werder, D. J.; Bussian, D. A.; Klimov, V. I.; Hollingsworth, J. A., "Giant" Multishell CdSe Nanocrystal Quantum Dots with Suppressed Blinking. *J. Am. Chem. Soc.* **2008**, *130* (15), 5026.
53. Hohng, S.; Ha, T., Near-complete suppression of quantum dot blinking in ambient conditions. *J. Am. Chem. Soc.* **2004**, *126* (5), 1324.
54. Zhang, A. D.; Dong, C.; Li, L.; Yin, J.; Liu, H.; Huang, X.; Ren, J., Non-blinking (Zn)CuInS/ZnS Quantum Dots Prepared by In Situ Interfacial Alloying Approach. *Sci. Rep.* **2015**, *5* (1).
55. Ekimov, A. I.; Onushchenko, A. A., Quantum size effect in three-dimensional microscopic semiconductor crystals. *JETP Lett.* **1981**, *34* (6), 345-349.
56. Ekimov, A. I.; Efros, A. L.; Onushchenko, A. A., Quantum Size Effect in Semiconductor Microcrystals. *Solid State Commun.* **1985**, *56* (11), 921-924.

57. Murray, C. B.; Norris, D. J.; Bawendi, M. G., Synthesis and Characterization of nearly Monodisperse CdE (E = sulfur, selenium, tellurium) Semiconductor Nanocrystallites. *J. Am. Chem. Soc.* **1993**, *115* (19), 8706-8715.
58. Alivisatos, A. P., Perspectives on the Physical Chemistry of Semiconductor Nanocrystals. *J. Phys. Chem.* **1996**, *100* (31), 13226-13239.
59. Peng, Z. A.; Peng, X., Formation of High-Quality CdTe, CdSe, and CdS Nanocrystals using CdO as Precursor. *J. Am. Chem. Soc.* **2001**, *123* (1), 183-184.
60. Qu, L.; Peng, Z. A.; Peng, X., Alternative Routes toward High Quality CdSe Nanocrystals. *Nano Lett.* **2001**, *1* (6), 333-337.
61. Yu, W. W.; Peng, X., Formation of High-Quality CdS and Other II-VI Semiconductor Nanocrystals in Noncoordinating Solvents: Tunable Reactivity of Monomers. *Angew. Chem. Int. Ed.* **2002**, *41* (13), 2368-2371.
62. Bailey, R. E.; Smith, A. M.; Nie, S., Quantum Dots in Biology and Medicine. *Physica E Low Dimens. Syst. Nanostruct.* **2004**, *25* (1), 1-12.
63. Micic, O. I.; Sprague, J. R.; Curtis, C. J.; Jones, K. M.; Machol, J. L.; Nozik, A. J., Synthesis and Characterization of InP, GaP, and GaInP<sub>2</sub> Quantum Dots. *J. Phys. Chem.* **1995**, *99* (19), 7754-7759.
64. Micić, O. I.; Curtis, C. J.; Jones, K. M.; Sprague, J. R.; Nozik, A. J., Synthesis and Characterization of InP Quantum Dots. *J. Phys. Chem.* **1994**, *98* (19), 4966-4969.
65. Xu, S.; Kumar, S.; Nann, T., Rapid Synthesis of High-Quality InP Nanocrystals. *J. Am. Chem. Soc.* **2006**, *128* (4), 1054.
66. Lee, J. C.; Jang, E.-P.; Jang, D. S.; Choi, Y.; Choi, M.; Yang, H., Solvothermal Preparation and Fluorescent Properties of Color-Tunable InP/ZnS Quantum Dots. *J. Lumin.* **2013**, *134*, 798-805.
67. Anc, M.; Pickett, N.; Gresty, N. C.; Harris, J.; Mishra, K., Progress in Non-Cd Quantum Dot Development for Lighting Applications. *ECS J. Solid State Sci. Technol.* **2013**, *2* (2), R3071-R3082.
68. Song, W.-S.; Lee, H.-S.; Lee, J.; Jang, D.; Choi, Y.; Choi, M.; Yang, H., Amine-Derived Synthetic Approach to Color-Tunable InP/ZnS Quantum Dots with High Fluorescent Qualities. *J. Nanopart. Res.* **2013**, *15* (6), 1-10.
69. Kim, S.; Wolters, R. H.; Heath, J. R., Photophysics of Size-Selected InP Nanocrystals: Exciton Recombination Kinetics. *J. Chem. Phys.* **1996**, *105* (18), 7957-7963.
70. Heath, J. R., Covalency in Semiconductor Quantum Dots. *Chem. Soc. Rev.* **1998**, *27* (1), 65-71.

71. Xie, R.; Battaglia, D.; Peng, X., Colloidal InP nanocrystals as efficient emitters covering blue to near-infrared. *J. Am. Chem. Soc.* **2007**, *129* (50), 15432.
72. Haubold, S.; Haase, M.; Kornowski, A.; Weller, H., Strongly Luminescent InP/ZnS Core–Shell Nanoparticles. *ChemPhysChem* **2001**, *2* (5), 331-334.
73. Micic, O. I.; Sprague, J.; Lu, Z.; Nozik, A. J., Highly efficient band-edge emission from InP quantum dots. *Appl. Phys. Lett.* **1996**, *68* (22), 3150-3152.
74. Talapin, D. V.; Gaponik, N.; Borchert, H.; Rogach, A. L.; Haase, M.; Weller, H., Etching of colloidal InP nanocrystals with fluorides: Photochemical nature of the process resulting in high photoluminescence efficiency. *J. Phys. Chem. B* **2002**, *106* (49), 12659-12663.
75. Byun, H.-J.; Lee, J. C.; Yang, H., Solvothermal synthesis of InP quantum dots and their enhanced luminescent efficiency by post-synthetic treatments. *J. Colloid Interface Sci.* **2011**, *355* (1), 35-41.
76. Pradhan, N.; Efrima, S., Single-precursor, one-pot versatile synthesis under near ambient conditions of tunable, single and dual band fluorescing metal sulfide nanoparticles. *J. Am. Chem. Soc.* **2003**, *125* (8), 2050.
77. Ouyang, J.; Zaman, M. B.; Yan, F. J.; Johnston, D.; Li, G.; Leek, D.; Ratcliffe, C. I.; Ripmeester, J. A.; Yu, K.; Wu, X., Multiple families of magic-sized CdSe nanocrystals with strong bandgap photoluminescence via noninjection one-pot syntheses. *J Phys Chem C* **2008**, *112* (36), 13805-13811.
78. Jiang, P.; Wang, R.; Chen, Z., Thiol-based non-injection synthesis of near-infrared Ag<sub>2</sub>S/ZnS core/shell quantum dots. *RSC Adv.* **2015**, *5* (70), 56789-56793.
79. Liu, T.-Y.; Li, M.; Ouyang, J.; Zaman, M. B.; Wang, R.; Wu, X.; Yeh, C.-S.; Lin, Q.; Yang, B.; Yu, K., Non-Injection and Low-Temperature Approach to Colloidal Photoluminescent PbS Nanocrystals with Narrow Bandwidth. *J. Phys. Chem. C* **2009**, *113* (6), 2301-2308.
80. Wang, J.; Zhai, J.; Han, S., Non-injection one-pot preparation strategy for multiple families of magic-sized CdTe quantum dots with bright bandgap photoemission. *Chem. Eng. J.* **2013**, *215-216*, 23-28.
81. Kanehara, M.; Arakawa, H.; Honda, T.; Saruyama, M.; Teranishi, T., Large-Scale Synthesis of High-Quality Metal Sulfide Semiconductor Quantum Dots with Tunable Surface-Plasmon Resonance Frequencies. *Chem. Eur. J.* **2012**, *18* (30), 9230-9238.
82. Bawendi, M.; Stott, N. E. Continuous flow process for production of semiconductor nanocrystals. US6576291B2, 2000.
83. Michalet, X.; Pinaud, F. F.; Bentolila, L. A.; Tsay, J. M.; Doose, S.; Li, J. J.; Sundaresan, G.; Wu, A. M.; Gambhir, S. S.; Weiss, S., Quantum dots for live cells, in vivo imaging, and diagnostics. *Science* **2005**, *307* (5709), 538.

84. Mussa Farkhani, S.; Valizadeh, A., Review: three synthesis methods of CdX (X = Se, S or Te) quantum dots. *IET Nanobiotechnol.* **2014**, *8* (2), 59-76.
85. Yu, W. W., Water-soluble quantum dots for biomedical applications. *Biochem. Biophys. Res. Commun.* **2006**, *348* (3).
86. Koneswaran, M.; Narayanaswamy, R., RETRACTED: Mercaptoacetic acid capped CdS quantum dots as fluorescence single shot probe for mercury(II). *Sens. Actuators B Chem.* **2009**, *139* (1), 91-96.
87. Andrade, J. J.; Brasil, A. G.; Farias, P. M. A.; Fontes, A.; Santos, B. S., Synthesis and characterization of blue emitting ZnSe quantum dots. *Microelectron. J.* **2009**, *40* (3), 641-643.
88. Qian, H.; Qiu, X.; Li, L.; Ren, J., Microwave-assisted aqueous synthesis: a rapid approach to prepare highly luminescent ZnSe(S) alloyed quantum dots. *J. Phys. Chem. B* **2006**, *110* (18), 9034.
89. Fang, Z.; Liu, L.; Xu, L.; Yin, X.; Zhong, X., Synthesis of highly stable dihydrolipoic acid capped water-soluble cdte nanocrystals. *Nanotechnology* **2008**, *19* (23), 235603.
90. Cao, J.; Xue, B.; Li, H.; Deng, D.; Gu, Y., Facile synthesis of high-quality water-soluble N-acetyl- l-cysteine-capped Zn 1- x Cd x Se/ZnS core/shell quantum dots emitting in the violet-green spectral range. *J. Colloid Interface Sci.* **2010**, *348* (2), 369-376.
91. Zhou, D.; Lin, M.; Chen, Z.; Sun, H.; Zhang, H.; Sun, H.; Yang, B., Simple Synthesis of Highly Luminescent Water-Soluble CdTe Quantum Dots with Controllable Surface Functionality. *Chem. Mater.* **2011**, *23* (21), 4857-4862.
92. Zhang, Y.; Clapp, A., Overview of Stabilizing Ligands for Biocompatible Quantum Dot Nanocrystals. *Sensors* **2011**, *11* (12), 11036-11055.
93. Brichkin, S.; Chernykh, E., Hydrophilic semiconductor quantum dots. *High Energy Chem.* **2011**, *45* (1), 1-12.
94. Dong, C.; Huang, X.; Ren, J., Characterization of Water-soluble Luminescent Quantum Dots by Fluorescence Correlation Spectroscopy. *Ann. N. Y. Acad. Sci.* **2008**, *1130* (1), 253-261.
95. Zhang, H.; Wang, L.; Xiong, H.; Hu, L.; Yang, B.; Li, W., Hydrothermal Synthesis for High-Quality CdTe Nanocrystals. *Adv. Mater.* **2003**, *15* (20), 1712-1715.
96. Sukanya, D.; Sagayaraj, P., A simple and facile synthesis of MPA capped CdSe and CdSe/CdS core/shell nanoparticles. *AIP Conf. Proc.* **2015**, *1665* (050028).
97. Aboulaich, A.; Billaud, D.; Abyan, M.; Balan, L.; Gaumet, J.-J.; Medjadhi, G.; Ghanbaja, J.; Schneider, R., One-pot noninjection route to CdS quantum dots via hydrothermal synthesis. *ACS Appl. Mater. Inter.* **2012**, *4* (5), 2561.

98. Liu, C.; Ji, Y.; Tan, T., One-pot hydrothermal synthesis of water-dispersible ZnS quantum dots modified with mercaptoacetic acid. *J. Alloys Compd.* **2013**, *570*, 23-27.
99. Gaponik, N.; Talapin, D. V.; Rogach, A. L.; Hoppe, K.; Shevchenko, E. V.; Kornowski, A.; Eychmüller, A.; Weller, H., Thiol-Capping of CdTe Nanocrystals: An Alternative to Organometallic Synthetic Routes. *J. Phys. Chem. B* **2002**, *106* (29), 7177-7185.
100. Xuan, T.; Wang, X.; Zhu, G.; Li, H.; Pan, L.; Sun, Z., One-step microwave-assisted synthesis of water soluble CdSe quantum dots for white light-emitting diodes with excellent color rendering. *J. Alloys Compd.* **2013**, *558*, 105-108.
101. Molaei, M.; Iranizad, E. S.; Marandi, M.; Taghavinia, N.; Amrollahi, R., Synthesis of CdS nanocrystals by a microwave activated method and investigation of the photoluminescence and electroluminescence properties. *Appl. Surf. Sci.* **2011**, *257* (23), 9796-9801.
102. Huang, L.; Han, H., One-step synthesis of water-soluble ZnSe quantum dots via microwave irradiation. *Mater. Lett.* **2010**, *64* (9), 1099-1101.
103. Qian, H.; Dong, C.; Weng, J.; Ren, J., Facile One-Pot Synthesis of Luminescent, Water-Soluble, and Biocompatible Glutathione-Coated CdTe Nanocrystals. *Small* **2006**, *2* (6), 747-751.
104. Du, J.; Li, X.; Wang, S.; Wu, Y.; Hao, X.; Xu, C.; Zhao, X., Microwave-assisted synthesis of highly luminescent glutathione-capped Zn<sub>1-x</sub>Cd<sub>x</sub>Te alloyed quantum dots with excellent biocompatibility. *J. Mater. Chem.* **2012**, *22* (22), 11390-11395.
105. Sai, L.-M.; Kong, X., Microwave-assisted synthesis of water-dispersed CdTe/CdSe core/shell type II quantum dots. *Nanoscale Res. Lett.* **2011**, *6* (1), 1-7.
106. Zhan, H. J.; Zhou, P. J.; He, Z. Y.; Tian, Y., Microwave-Assisted Aqueous Synthesis of Small-Sized, Highly Luminescent CdSeS/ZnS Core/Shell Quantum Dots for Live Cell Imaging. *Eur. J. Inorg. Chem.* **2012**, *2012* (15), 2487-2493.
107. Chen, X.; Li, L.; Lai, Y.; Yan, J.; Tang, Y.; Wang, X., Microwave-Assisted Synthesis of Glutathione-Capped CdTe/CdSe Near-Infrared Quantum Dots for Cell Imaging. *Int. J. Mol. Sci.* **2015**, *16* (5), 11500-11508.
108. Zhu, M.-Q.; Gu, Z.; Fan, J.-B.; Xu, X.-B.; Cui, J.; Liu, J.-H.; Long, F., Microwave-mediated nonaqueous synthesis of quantum dots at moderate temperature. *Langmuir* **2009**, *25* (17), 10189.
109. Washington, A. L.; Strouse, G. F., Microwave synthesis of CdSe and CdTe nanocrystals in nonabsorbing alkanes. *J. Am. Chem. Soc.* **2008**, *130* (28), 8916.
110. Moghaddam, M. M.; Baghbanzadeh, M.; Keilbach, A.; Kappe, C. O., Microwave-assisted synthesis of CdSe quantum dots: can the electromagnetic field influence the formation and quality of the resulting nanocrystals? *Nanoscale* **2012**, *4* (23), 7435-7442.

111. Shakir, M.; Kushwaha, S. K.; Maurya, K. K.; Bhagavannarayana, G.; Wahab, M. A., Characterization of ZnSe nanoparticles synthesized by microwave heating process. *Solid State Commun.* **2009**, *149* (45-46), 2047-2049.
112. Dahl, J. A.; Maddux, B. L. S.; Hutchison, J. E., Toward greener nanosynthesis. *Chem. Rev.* **2007**, *107* (6), 2228.
113. Kim, K.; Jeong, S.; Woo, J. Y.; Han, C.-S., Successive and large-scale synthesis of InP/ZnS quantum dots in a hybrid reactor and their application to white LEDs. *Nanotechnology* **2012**, *23* (6), 065602.
114. O'Brien, P.; Pickett, N. Preparation of Nanoparticle Materials. Patent WO/2005/106082, **2005**.
115. N. Pickett, S. D., I. Mushtaq Preparation of Nanoparticle Materials. Patent US-7588828-B2, **2009**.
116. O'Brien, P.; Pickett, N. Preparation of Nanoparticle Materials. Patent US-8062703-B2, **2011**.
117. Steckel, J. S.; Ho, J.; Hamilton, C.; Xi, J.; Breen, C.; Liu, W.; Allen, P.; Coe-Sullivan, S., Quantum dots: The ultimate down-conversion material for LCD displays. *J. Soc. Inf. Disp.* **2015**, *23* (7), 294-305.
118. Zhenyue, L.; Daming, X.; Shin-Tson, W., Emerging Quantum-Dots-Enhanced LCDs. *J. Disp. Technol.* **2014**, *10* (7), 526-539.
119. Haiwei, C.; Juan, H.; Shin-Tson, W., Recent Advances on Quantum-Dot-Enhanced Liquid-Crystal Displays. *IEEE J. Sel. Top. Quantum Electron.* **2017**, *23* (5), 1-11.
120. Coe-Sullivan, S., The Quantum Dot Revolution: Marching Towards the Mainstream. *Dig. Tech. Pap.* **2016**, *47* (1), 239-240.
121. Hong, Q.; Lee, K.-C.; Luo, Z.; Wu, S.-T., High-efficiency quantum dot remote phosphor film. *Appl. Opt.* **2015**, *54* (15), 4617.
122. Kitai, A., *Materials for Solid State Lighting and Displays*. Hoboken, NJ, USA : John Wiley & Sons Inc.: **2017**.
123. Thielen, J.; Hillis, J.; Derlofske, J. V.; Lamb, D.; Lathrop, A. In *Quantum Dots and Rec. 2020: Bringing the Color of Tomorrow Closer to Reality Today*, SMPTE 2014 Annual Technical Conference & Exhibition, **2014**; pp 1-11.
124. Zhu, R.; Luo, Z.; Chen, H.; Dong, Y.; Wu, S.-T., Realizing Rec. 2020 color gamut with quantum dot displays. *Opt. Express* **2015**, *23* (18), 23680.
125. Directive 2011/65/EU of the European Parliament and of the Council on the Restriction of the Use of Certain Hazardous Substances in Electrical and Electronic Equipment. *OJEU* **2011**, *174*, 88-110.

126. Forrest, S. R.; Bradley, D. D. C.; Thompson, M. E., Measuring the Efficiency of Organic Light-Emitting Devices. *Adv. Mater.* **2003**, *15* (13), 1043-1048.
127. Colvin, V. L.; Schlamp, M. C.; Alivisatos, A. P., Light-emitting diodes made from cadmium selenide nanocrystals and a semiconducting polymer. *Nature* **1994**, *370* (6488), 354.
128. Dabbousi, B. O.; Bawendi, M. G.; Onitsuka, O.; Rubner, M. F., Electroluminescence from CdSe quantum-dot/polymer composites. *Appl. Phys. Lett.* **1995**, *66* (11), 1316-1318.
129. Yixing, Y.; Ying, Z.; Weiran, C.; Alexandre, T.; Jake, H.; Jesse, R. M.; Jiangeng, X.; Paul, H. H.; Lei, Q., High-efficiency light-emitting devices based on quantum dots with tailored nanostructures. *Nat. Photonics* **2015**, *9* (4), 259.
130. Manders, J. R.; Qian, L.; Titov, A.; Hyvonen, J.; Tokarz-Scott, J.; Acharya, K. P.; Yang, Y.; Cao, W.; Zheng, Y.; Xue, J.; Holloway, P. H., High efficiency and ultra-wide color gamut quantum dot LEDs for next generation displays. *J. Soc. Inf. Disp.* **2015**, *23* (11), 523-528.
131. Zhang, H.; Chen, S.; Sun, X. W., Efficient Red/Green/Blue Tandem Quantum-Dot Light-Emitting Diodes with External Quantum Efficiency Exceeding 21%. *ACS Nano* **2018**, *12* (1), 697.
132. Moon Kee, C.; Jiwoong, Y.; Taeghwan, H.; Dae-Hyeong, K., Flexible quantum dot light-emitting diodes for next-generation displays. *npj Flex. Electron.* **2018**, *2* (1), 1-14.
133. Harris, J.; Glarvey, P.; Masala, O.; Pickett, N.; N., G. Quantum Dot Light-Emitting Diodes for Phototherapy. Patent WO2014177943A2, **2014**.
134. Pickett, N.; Nasaani, I.; Harris, J.; Gresty, N. Quantum Dot LEDs to Enhance Growth in Photosynthetic Organism Patent US-20130326941-A1, **2013**.
135. Gerischer, H.; Michel-Beyerle, M. E.; Reberstrost, F.; Tributsch, H., Sensitization of charge injection into semiconductors with large band gap. *Electrochim. Acta* **1968**, *13* (6), 1509-1515.
136. Kamat, P. V., Quantum Dot Solar Cells. Semiconductor Nanocrystals as Light Harvesters. *J. Phys. Chem. C* **2008**, *112* (48), 18737-18753.
137. Pan, Z.; Rao, H.; Mora-Ser, I.; Bisquert, J.; Zhong, X., Quantum dot-sensitized solar cells. *Chem. Soc. Rev.* **2018**, *47* (20), 7659-7702.
138. Du, J.; Du, Z.; Hu, J.-S.; Pan, Z.; Shen, Q.; Sun, J.; Long, D.; Dong, H.; Sun, L.; Zhong, X.; Wan, L.-J., Zn-Cu-In-Se Quantum Dot Solar Cells with a Certified Power Conversion Efficiency of 11.6%. *J. Am. Chem. Soc.* **2016**, *138* (12), 4201.
139. Zhang, L.; Pan, Z.; Wang, W.; Du, J.; Ren, Z.; Shen, Q.; Zhong, X., Copper deficient ZnCuInSe quantum dot sensitized solar cells for high efficiency. *J. Mater. Chem. A* **2017**, *5* (40), 21442-21451.

140. Xiaohu, G.; Yuanyuan, C.; Richard, M. L.; Leland, W. K. C.; Shuming, N., In vivo cancer targeting and imaging with semiconductor quantum dots. *Nat. Biotechnol.* **2004**, *22* (8), 969.
141. Yaghini, E.; Turner, H. D.; Le Marois, A. M.; Suhling, K.; Naasani, I.; MacRobert, A. J., In vivo Biodistribution Studies and ex vivo Lymph Node Imaging using Heavy Metal-free Quantum Dots. *Biomaterials* **2016**, *104*, 182-191.
142. Dong, B.; Li, C.; Chen, G.; Zhang, Y.; Zhang, Y.; Deng, M.; Wang, Q., Facile Synthesis of Highly Photoluminescent Ag<sub>2</sub>Se Quantum Dots as a New Fluorescent Probe in the Second Near-Infrared Window for in Vivo Imaging. *Chem. Mater.* **2013**, *25* (12), 2503-2509.
143. Cai, X.; Luo, Y.; Zhang, W.; Du, D.; Lin, Y., pH-Sensitive ZnO Quantum Dots-Doxorubicin Nanoparticles for Lung Cancer Targeted Drug Delivery. *ACS Appl. Mater. Inter.* **2016**, *8* (34), 22442.
144. Yang, X.; Zhang, W.; Zhao, Z.; Li, N.; Mou, Z.; Sun, D.; Cai, Y.; Wang, W.; Lin, Y., Quercetin loading CdSe/ZnS nanoparticles as efficient antibacterial and anticancer materials. *J. Inorg. Biochem.* **2017**, *167*, 36-48.
145. Xiong, W.-w.; Yang, G.-h.; Wu, X.-c.; Zhu, J.-j., Microwave-assisted synthesis of highly luminescent AgInS<sub>2</sub>/ZnS nanocrystals for dynamic intracellular Cu(II) detection. *J. Mater. Chem. B* **2013**, *1* (33), 4160-4165.
146. Liu, S.; Shi, F.; Zhao, X.; Chen, L.; Su, X., 3-Aminophenyl boronic acid-functionalized CuInS<sub>2</sub> quantum dots as a near-infrared fluorescence probe for the determination of dopamine. *Biosens. Bioelectron.* **2013**, *47*, 379.
147. Pelley, J. L.; Daar, A. S.; Saner, M. A., State of academic knowledge on toxicity and biological fate of quantum dots. *Toxicol. Sci.* **2009**, *112* (2), 276-96.
148. Lovric, J.; Bazzi, H. S.; Cuie, Y.; Fortin, G. R.; Winnik, F. M.; Maysinger, D., Differences in subcellular distribution and toxicity of green and red emitting CdTe quantum dots. *J. Mol. Med. (Berl)* **2005**, *83* (5), 377-85.
149. Lovric, J.; Cho, S. J.; Winnik, F. M.; Maysinger, D., Unmodified cadmium telluride quantum dots induce reactive oxygen species formation leading to multiple organelle damage and cell death. *Chem. Biol.* **2005**, *12* (11), 1227-34.
150. Chen, N.; He, Y.; Su, Y.; Li, X.; Huang, Q.; Wang, H.; Zhang, X.; Tai, R.; Fan, C., The cytotoxicity of cadmium-based quantum dots. *Biomaterials* **2012**, *33* (5), 1238-44.
151. Ipe, B. I.; Lehnig, M.; Niemeyer, C. M., On the Generation of Free Radical Species from Quantum Dots. *Small* **2005**, *1* (7), 706-709.
152. Brunetti, V.; Chibli, H.; Fiammengo, R.; Galeone, A.; Malvindi, M. A.; Vecchio, G.; Cingolani, R.; Nadeau, J. L.; Pompa, P. P., InP/ZnS as a safer alternative to CdSe/ZnS core/shell quantum dots: in vitro and in vivo toxicity assessment. *Nanoscale* **2013**, *5* (1), 307-17.

153. Chibli, H.; Carlini, L.; Park, S.; Dimitrijevic, N. M.; Nadeau, J. L., Cytotoxicity of InP/ZnS Quantum Dots Related to Reactive Oxygen Species Generation. *Nanoscale* **2011**, *3* (6), 2552-2559.
154. Su, Y.; He, Y.; Lu, H.; Sai, L.; Li, Q.; Li, W.; Wang, L.; Shen, P.; Huang, Q.; Fan, C., The cytotoxicity of cadmium based, aqueous phase - synthesized, quantum dots and its modulation by surface coating. *Biomaterials* **2009**, *30* (1), 19-25.
155. Peng, L.; He, M.; Chen, B.; Wu, Q.; Zhang, Z.; Pang, D.; Zhu, Y.; Hu, B., Cellular uptake, elimination and toxicity of CdSe/ZnS quantum dots in HepG2 cells. *Biomaterials* **2013**, *34* (37), 9545-58.
156. Chang, E.; Thekkekk, N.; Yu, W. W.; Colvin, V. L.; Drezek, R., Evaluation of quantum dot cytotoxicity based on intracellular uptake. *Small* **2006**, *2* (12), 1412-7.
157. Ryman-Rasmussen, J. P.; Riviere, J. E.; Monteiro-Riviere, N. A., Surface coatings determine cytotoxicity and irritation potential of quantum dot nanoparticles in epidermal keratinocytes. *J. Invest. Dermatol.* **2007**, *127* (1), 143-53.
158. Chang, S. Q.; Dai, Y. D.; Kang, B.; Han, W.; Chen, D., Gamma-radiation synthesis of silk fibroin coated CdSe quantum dots and their biocompatibility and photostability in living cells. *J. Nanosci. Nanotechnol.* **2009**, *9* (10), 5693-700.
159. Chang, S.; Kang, B.; Liu, X.; Dai, Y.; Chen, D., The combined influence of surface modification, size distribution, and interaction time on the cytotoxicity of CdTe quantum dots in PANC-1 cells. *Acta Biochim Biophys Sin (Shanghai)* **2012**, *44* (3), 241-8.
160. Dobrovolskaia, M. A.; McNeil, S. E., *Handbook of Immunological Properties of Engineered Nanomaterials* Hackensack, N.J. : World Scientific Pub. Co.: **2013**.
161. Geys, J.; Nemmar, A.; Verbeken, E.; Smolders, E.; Ratoi, M.; Hoylaerts, M. F.; Nemery, B.; Hoet, P. H. M., Acute Toxicity and Prothrombotic Effects of Quantum Dots: Impact of Surface Charge. *Environ. Health Perspect.* **2008**, *116* (12), 1607-1613.
162. Hoshino, A.; Hanada, S.; Yamamoto, K., Toxicity of nanocrystal quantum dots: the relevance of surface modifications. *Arch. Toxicol.* **2011**, *85* (7), 707-720.
163. Pelley, J. L.; Daar, A. S.; Saner, M. A., State of Academic Knowledge on Toxicity and Biological Fate of Quantum Dots. *Toxicol. Sci.* **2009**, *112* (2), 276-296.
164. Lin, G.; Ouyang, Q.; Hu, R.; Ding, Z.; Tian, J.; Yin, F.; Xu, G.; Chen, Q.; Wang, X.; Yong, K. T., In vivo toxicity assessment of non-cadmium quantum dots in BALB/c mice. *Nanomedicine-Uk* **2015**, *11* (2), 341-50.
165. Chen, T.; Li, L.; Xu, G.; Wang, X.; Wang, J.; Chen, Y.; Jiang, W.; Yang, Z.; Lin, G., Cytotoxicity of InP/ZnS Quantum Dots With Different Surface Functional Groups Toward Two Lung-Derived Cell Lines. *Front. Pharmacol.* **2018**, *9*, 763.

166. Zheng, W.; Xu, Y. M.; Wu, D. D.; Yao, Y.; Liang, Z. L.; Tan, H. W.; Lau, A. T. Y., Acute and chronic cadmium telluride quantum dots-exposed human bronchial epithelial cells: The effects of particle sizes on their cytotoxicity and carcinogenicity. *Biochem Biophys Res Commun* **2018**, *495* (1), 899-903.
167. Tang, S.; Allagadda, V.; Chibli, H.; Nadeau, J. L.; Mayer, G. D., Comparison of cytotoxicity and expression of metal regulatory genes in zebrafish (*Danio rerio*) liver cells exposed to cadmium sulfate, zinc sulfate and quantum dots. *Metallomics* **2013**, *5* (10), 1411-22.
168. Zhang, Y.; Chen, W.; Zhang, J.; Liu, J.; Chen, G.; Pope, C., In vitro and in vivo toxicity of CdTe nanoparticles. *J. Nanosci. Nanotechnol.* **2007**, *7* (2), 497-503.
169. Liu, Q.; Li, H.; Xia, Q.; Liu, Y.; Xiao, K., Role of surface charge in determining the biological effects of CdSe/ZnS quantum dots. *Int. J. Nanomedicine* **2015**, *10*, 7073-88.
170. Raab, O., Ueber die Wirkung fluorizierender Stoffe auf Infusorien. *Ztg. Biol.* **1900**, *39*, 524–526.
171. Tappeiner, H. v., Zur Kenntnis der lichtwirkenden (fluoreszierenden) stoffe. *Dtsch. Med. Wochenschr.* **1904**, *16*, 579-580.
172. Tappeiner, H. v.; Jesionek, A., Therapeutische Versuche mit fluoreszierenden Stoffen. *Münchener. Med. Wochenschr.* **1903**, *50*, 2042-2044.
173. Lipson, R. L.; Baldes, E. J., The Photodynamic Properties of a Particular Hematoporphyrin Derivative. *Arch. Dermatol.* **1960**, *82*, 508-16.
174. Lipson, R. L.; Baldes, E. J., Photosensitivity and Heat. *Arch. Dermatol.* **1960**, *82*, 517-20.
175. Dougherty, T. J., Activated Dyes as Antitumor Agents. *J. Natl. Cancer Inst.* **1974**, *52* (4), 1333.
176. Dougherty, T. J., Photodynamic Therapy (PDT) of Malignant Tumors. *Crit. Rev. Oncol. Hematol.* **1984**, *2* (2), 83-116.
177. Dougherty, T. J.; Potter, W. R.; Weishaupt, K. R., The structure of the active component of hematoporphyrin derivative. *Prog. Clin. Biol. Res.* **1984**, *170*, 301-14.
178. O'connor, A. E.; Gallagher, W. M.; Byrne, A. T., Porphyrin and Nonporphyrin Photosensitizers in Oncology: Preclinical and Clinical Advances in Photodynamic Therapy. *Photochem. Photobiol.* **2009**, *85*, 1053-1074.
179. Agostinis, P.; Berg, K.; Cengel, K.; Foster, T.; Girotti, A.; Gollnick, S.; Hahn, S.; Hamblin, M.; Juzeniene, A.; Kessel, D.; Korblik, M.; Moan, J.; Mroz, P.; Nowis, D.; Piette, J.; Wilson, B.; Golab, J., Photodynamic Therapy of Aancer: An Update. *CA Cancer J. Clin.* **2011**, *61* (4), 250.
180. Sharman, W. M.; Allen, C. M.; van Lier, J. E., Photodynamic Therapeutics: Basic Principles and Vlinical Applications. *Drug Discov. Today* **1999**, *4*, 507-517.

181. Weishaupt, K. R.; Gomer, C. J.; Dougherty, T. J., Identification of Singlet Oxygen as the Cytotoxic Agent in Photoinactivation of a Murine Tumor. *Cancer Res.* **1976**, 36 (7), 2326.
182. Marcon, N. E., Photodynamic Therapy and Cancer of the Esophagus. *Semin. Oncol.* **1994**, 21 (6 Suppl 15), 20-3.
183. Ost, D., Photodynamic Therapy in Lung Cancer. *Oncology (Williston Park, N.Y.)* **2000**, 14 (3), 379-86, 391; discussion 391-2, 395.
184. Huang, Z.; Xu, H.; Meyers, A. D.; Musani, A. I.; Wang, L.; Tagg, R.; Barqawi, A. B.; Chen, Y. K., Photodynamic Therapy for Treatment of Solid Tumors — Potential and Technical Challenges. *Technol. Cancer Res. T.* **2008**, 7 (4), 309-320.
185. Allison, R.; Moghissi, K.; Downie, G.; Dixon, K., Photodynamic Therapy (PDT) for Lung Cancer. *Photodiagnosis Photodyn. Ther.* **2011**, 8 (3), 231-239.
186. Nelke, K. H.; Pawlak, W.; Leszczyszyn, J.; Gerber, H., Photodynamic Therapy in Head and Neck Cancer. *Postepy. Hig. Med. Dosw.* **2014**, 68, 119-28.
187. Lucena, S. R.; Salazar, N.; Gracia-Cazana, T.; Zamarron, A.; Gonzalez, S.; Juarranz, A.; Gilaberte, Y., Combined Treatments with Photodynamic Therapy for Non-Melanoma Skin Cancer. *Int J Mol Sci* **2015**, 16 (10), 25912-33.
188. Hodgkinson, N.; Kruger, C. A.; Abrahamse, H., Targeted Photodynamic Therapy as Potential Treatment Modality for the Eradication of Colon Cancer and Colon Cancer Stem Cells. *Tumour Biol.* **2017**, 39 (10), 1010428317734691.
189. Railkar, R.; Agarwal, P. K., Photodynamic Therapy in the Treatment of Bladder Cancer: Past Challenges and Current Innovations. *Eur Urol Focus* **2018**, 4 (4), 509-511.
190. Macmillan, J. D.; Maxwell, W. A.; Chichester, C. O., Lethal photosensitization of microorganisms with light from a continuous-wave gas laser. *Photochem. Photobiol.* **1966**, 5 (7), 555-65.
191. Bellin, J. S.; Lutwick, L.; Jonas, B., Effects of photodynamic action on *E. coli*. *Arch. Biochem. Biophys.* **1969**, 132 (1), 157-164.
192. Ghorbani, J.; Rahban, D.; Aghamiri, S.; Teymouri, A.; Bahador, A., Photosensitizers in antibacterial photodynamic therapy: an overview. *Laser therapy* **2018**, 27 (4), 293.
193. Wainwright, M., Photodynamic antimicrobial chemotherapy (PACT). *J. Antimicrob. Chemother.* **1998**, 42 (1), 13-28.
194. Cieplik, F.; Deng, D.; Crielaard, W.; Buchalla, W.; Hellwig, E.; Al-Ahmad, A.; Maisch, T., Antimicrobial photodynamic therapy - what we know and what we don't. *Crit Rev Microbiol* **2018**, 44 (5), 571-589.

195. Gollmer, A.; Felgentrger, A.; Bumler, W.; Maisch, T.; Spth, A., A novel set of symmetric methylene blue derivatives exhibits effective bacteria photokilling a structureresponse study. *Photochem. Photobiol. Sci.* **2015**, *14* (2), 335-351.
196. Dovigo, L. N.; Carmello, J. C.; Carvalho, M. T.; Mima, E. G.; Vergani, C. E.; Bagnato, V. S.; Pavarina, A. C., Photodynamic inactivation of clinical isolates of *Candida* using Photodithazine®. *Biofouling* **2013**, *29* (9), 1057-1067.
197. Huang, L.; Krayner, M.; Roubil, J. G. S.; Huang, Y.-Y.; Holten, D.; Lindsey, J. S.; Hamblin, M. R., Stable synthetic mono-substituted cationic bacteriochlorins mediate selective broad-spectrum photoinactivation of drug-resistant pathogens at nanomolar concentrations. *J. Photochem. Photobiol. B* **2014**, *141*, 119-127.
198. Abrahamse, H.; Hamblin, M., New photosensitizers for photodynamic therapy. *Biochem. J.* **2016**, *473* (4), 347-364.
199. Henderson, B. W.; Dougherty, T. J., How Does Photodynamic Therapy Work. *Photochem. Photobiol.* **1992**, *55* (1), 145-157.
200. Wainwright, M.; Crossley, K. B., Photosensitising Agents - Circumventing Resistance and Breaking Down Biofilms: A Review. *Int. Biodeterior. Biodegrad.* **2004**, *53* (2), 119-126.
201. Josefsen, L. B.; Boyle, R. W., Photodynamic Therapy and the Development of Metal-Based Photosensitisers. *Met Based Drugs* **2008**, *2008*, 276109.
202. Plaetzer, K.; Krammer, B.; Berlanda, J.; Berr, F.; Kiesslich, T., Photophysics and Photochemistry of Photodynamic Therapy: Fundamental Aspects. *Lasers Med. Sci.* **2009**, *24* (2), 259-268.
203. Vatansever, F.; de Melo, W. C.; Avci, P.; Vecchio, D.; Sadasivam, M.; Gupta, A.; Chandran, R.; Karimi, M.; Parizotto, N. A.; Yin, R.; Tegos, G. P.; Hamblin, M. R., Antimicrobial Strategies Centered around Reactive Oxygen Species - Bactericidal Antibiotics, Photodynamic Therapy, and Beyond. *FEMS Microbiol. Rev.* **2013**, *37* (6), 955-89.
204. Flora, S. J., Structural, Chemical and Biological Aspects of Antioxidants for Strategies against Metal and Metalloid Exposure. *Oxid. Med. Cell. Longev.* **2009**, *2* (4), 191-206.
205. Sharma, P.; Jha, A. B.; Dubey, R. S.; Pessarakli, M., Reactive Oxygen Species, Oxidative Damage, and Antioxidative Defense Mechanism in Plants under Stressful Conditions. *J. Bot.* **2012**.
206. Moan, J.; Berg, K., The Photodegradation of Porphyrins in Cells can be used to Estimate the Lifetime of Singlet Oxygen. *Photochem. Photobiol.* **1991**, *53* (4), 549-553.
207. Dennis, E. J. G. J. D.; Dai, F.; Rakesh, K. J., Photodynamic Therapy for Cancer. *Nat. Rev. Cancer* **2003**, *3* (5), 380.
208. Yoon, I.; Li, J. Z.; Shim, Y. K., Advance in photosensitizers and light delivery for photodynamic therapy. *Clin Endosc.* **2013**, *46* (1), 7.

209. Brigger, I.; Dubernet, C.; Couvreur, P., Nanoparticles in Cancer Therapy and Diagnosis. *Adv. Drug Deliv. Rev* **2012**, *64*, 24-36.
210. Yaghini, E.; Seifalian, A. M.; MacRobert, A. J., Quantum Dots and their Potential Biomedical Applications in Photosensitization for Photodynamic Therapy. *Nanomedicine-Uk* **2009**, *4* (3), 353-363.
211. Villaverde, A., *Nanoparticles in Translational Science*. London : Academic Press: **2011**.
212. Yaghini, E.; Pirker, K. F.; Kay, C. W. M.; Seifalian, A. M.; MacRobert, A. J., Quantification of Reactive Oxygen Species Generation by Photoexcitation of PEGylated Quantum Dots. *Small* **2014**, *10* (24), 5106-5115.
213. Tsay, J. M.; Trzoss, M.; Shi, L.; Kong, X.; Selke, M.; Jung, M. E.; Weiss, S., Singlet oxygen production by Peptide-coated quantum dot-photosensitizer conjugates. *J. Am. Chem. Soc.* **2007**, *129* (21), 6865-71.
214. Förster, T., Transfer Mechanisms of Electronic Excitation Energy. *Radiat. Res. Suppl.* **1960**, *2*, 326-339.
215. Lakowicz, J. R., *Principles of Fluorescence Spectroscopy*. 3rd ed.; New York : Springer: **2006**.
216. Medintz, I. L.; Mattoussi, H., Quantum Dot-based Resonance Energy Transfer and its Growing Application in Biology. *Phys. Chem. Chem. Phys.* **2008**, *11* (1), 17-45.
217. Elizabeth, A. J.-E.; Thomas, M. J., FRET Imaging. *Nat. Biotechnol.* **2003**, *21* (11), 1387.
218. Miyawaki, A., Visualization of the Spatial and Temporal Dynamics of Intracellular Signaling. *Dev. Cell* **2003**, *4* (3), 295-305.
219. Wu, P. G.; Brand, L., Resonance Energy Transfer: Methods and Applications. *Anal. Biochem.* **1994**, *218* (1), 1-13.
220. Didenko, V., DNA probes using fluorescence resonance energy transfer (FRET): Designs and Applications. *Biotechniques* **2001**, *31* (5), 1106.
221. Turro, N. J., *Modern Molecular Photochemistry*. University Science Books: Mill Valley, Calif, **1991**.
222. Clapp, A. R.; Medintz, I. L.; Mattoussi, H., Förster Resonance Energy Transfer Investigations Using Quantum-Dot Fluorophores. *ChemPhysChem* **2006**, *7* (1), 47-57.
223. Kagan, C. R.; Murray, C.; Nirmal, M.; Bawendi, M. G., Electronic energy transfer in CdSe quantum dot solids. *Phys. Rev. Lett.* **1996**, *76* (9), 1517-1520.
224. Willard, D. M.; Carillo, L. L.; Jung, J.; Van Orden, A., CdSe-ZnS Quantum Dots as Resonance Energy Transfer Donors in a Model Protein-Protein Binding Assay. *Nano Lett.* **2001**, *1* (9), 469-474.

225. Samia, A. C. S.; Chen, X.; Burda, C., Semiconductor quantum dots for photodynamic therapy. *J. Am. Chem. Soc.* **2003**, *125* (51), 15736.
226. Medintz, I. L.; Trammell, S. A.; Mattoussi, H.; Mauro, J. M., Reversible modulation of quantum dot photoluminescence using a protein-bound photochromic fluorescence resonance energy transfer acceptor. *J. Am. Chem. Soc.* **2004**, *126* (1), 30.
227. Medintz, I. L.; Clapp, A. R.; Hedi, M.; Goldman, E. R.; Fisher, B.; Mauro, M. J., Self-assembled nanoscale biosensors based on quantum dot FRET donors. *Nat. Mater.* **2003**, *2* (9), 630.
228. Medintz, I. L.; Pons, T.; Susumu, K.; Boeneman, K.; Dennis, A.; Farrell, D.; Deschamps, J. R.; Melinger, J. S.; Bao, G.; Mattoussi, H., Resonance Energy Transfer Between Luminescent Quantum Dots and Diverse Fluorescent Protein Acceptors. *J. Phys. Chem. C* **2009**, *113* (43), 18552.
229. Tran, P.; Goldman, E.; Anderson, G. P.; Mauro, J.; Mattoussi, H., Use of luminescent CdSe-ZnS nanocrystal bioconjugates in quantum dot-based nanosensors. *Phys. Status Solidi B* **2002**, *229* (1), 427-432.
230. Sapsford, K.; Pons, T.; Medintz, I.; Higashiya, S.; Brunel, F.; Dawson, P.; Mattoussi, H., Kinetics of metal-affinity driven self-assembly between proteins or peptides and CdSe-ZnS quantum dots. *J. Phys. Chem. C* **2007**, *111* (31), 11528-11538.
231. Clapp, A. R.; Medintz, I. L.; Mauro, J. M.; Fisher, B. R.; Bawendi, M. G.; Mattoussi, H., Fluorescence resonance energy transfer between quantum dot donors and dye-labeled protein acceptors. *J. Am. Chem. Soc.* **2004**, *126* (1), 301.
232. Medintz, I. L.; Konnert, J. H.; Clapp, A. R.; Stanish, I.; Twigg, M. E.; Mattoussi, H.; Mauro, J. M.; Deschamps, J. R., A fluorescence resonance energy transfer-derived structure of a quantum dot-protein bioconjugate nanoassembly. *Proc. Natl. Acad. Sci. USA* **2004**, *101* (26), 9612.
233. Snee, P. T.; Somers, R. C.; Nair, G.; Zimmer, J. P.; Bawendi, M. G.; Nocera, D. G., A ratiometric CdSe/ZnS nanocrystal pH sensor. *J. Am. Chem. Soc.* **2006**, *128* (41), 13320.
234. Dennis, A. M.; Rhee, W. J.; Sotto, D.; Dublin, S. N.; Bao, G., Quantum dot-fluorescent protein FRET probes for sensing intracellular pH. *ACS Nano* **2012**, *6* (4), 2917.
235. Krooswyk, J. D.; Tyrakowski, C. M.; Snee, P., Multivariable Response of Semiconductor Nanocrystal-Dye Sensors: The Case of pH. *J. Phys. Chem. C* **2010**, *114* (49), 21348-21352.
236. Page, L.; Zhang, X.; Jawaid, A.; Snee, P., Detection of toxic mercury ions using a ratiometric CdSe/ZnS nanocrystal sensor. *Chem. Commun.* **2011**, *47* (27), 7773-7775.
237. Li, J.; Mei, F.; Li, W.-Y.; He, X.-W.; Zhang, Y.-K., Study on the fluorescence resonance energy transfer between CdTe QDs and butyl-rhodamine B in the presence of CTMAB and its application on the detection of Hg(II). *Spectrochim. Acta A Mol. Biomol. Spectrosc.* **2008**, *70* (4), 811-817.
238. Xu, C.; Xing, B.; Rao, J., A self-assembled quantum dot probe for detecting  $\beta$ -lactamase activity. *Biochem. Biophys. Res. Commun.* **2006**, *344* (3), 931-935.

239. Shi, L.; De Paoli, V.; Rosenzweig, N.; Rosenzweig, Z., Synthesis and application of quantum dots FRET-based protease sensors. *J. Am. Chem. Soc.* **2006**, *128* (32), 10378.
240. Shi, L.; Rosenzweig, N.; Rosenzweig, Z., Luminescent quantum dots fluorescence resonance energy transfer-based probes for enzymatic activity and enzyme inhibitors. *Anal. Chem.* **2007**, *79* (1), 208-214.
241. Igor, L. M.; Aaron, R. C.; Florence, M. B.; Theresa, T.; Uyeda, H. T.; Eddie, L. C.; Jeffrey, R. D.; Philip, E. D.; Hedi, M., Proteolytic activity monitored by fluorescence resonance energy transfer through quantum-dot-peptide conjugates. *Nat. Mater.* **2006**, *5* (7), 581.
242. Tsay, J. M.; Trzoss, M.; Shi, L.; Kong, X.; Selke, M.; Jung, M. E.; Weiss, S., Singlet oxygen production by Peptide-coated quantum dot-photosensitizer conjugates. *J. Am. Chem. Soc.* **2007**, *129* (21), 6865.
243. Patolsky, F.; Gill, R.; Weizmann, Y.; Mokari, T.; Banin, U.; Willner, I., Lighting-up the dynamics of telomerization and DNA replication by CdSe-ZnS quantum dots. *J. Am. Chem. Soc.* **2003**, *125* (46), 13918-13919.
244. Pons, T.; Medintz, I. L.; Sapsford, K. E.; Higashiya, S.; Grimes, A. F.; English, D. S.; Mattoussi, H., On the quenching of semiconductor quantum dot photoluminescence by proximal gold nanoparticles. *Nano Lett.* **2007**, *7* (10), 3157.
245. Chun-Yang, Z.; Hsin-Chih, Y.; Marcos, T. K.; Tza-Huei, W., Single-quantum-dot-based DNA nanosensor. *Nat. Mater.* **2005**, *4* (11), 826.
246. Algar, W.; Krull, U., Adsorption and hybridization of oligonucleotides on mercaptoacetic acid-capped CdSe/ZnS quantum dots and quantum dot-oligonucleotide conjugates. *Langmuir* **2006**, *22* (26), 11346-11352.
247. Algar, W. R.; Krull, U. J., Interfacial transduction of nucleic acid hybridization using immobilized quantum dots as donors in fluorescence resonance energy transfer. *Langmuir* **2009**, *25* (1), 633.
248. Algar, W. R.; Krull, U. J., Toward a multiplexed solid-phase nucleic acid hybridization assay using quantum dots as donors in fluorescence resonance energy transfer. *Anal. Chem.* **2009**, *81* (10), 4113.
249. Shahmuradyan, A.; Krull, U. J., Intrinsically Labeled Fluorescent Oligonucleotide Probes on Quantum Dots for Transduction of Nucleic Acid Hybridization. *Anal. Chem.* **2016**, *88* (6), 3186.
250. Suzuki, M.; Husimi, Y.; Komatsu, H.; Suzuki, K.; Douglas, K. T., Quantum dot FRET biosensors that respond to pH, to proteolytic or nucleolytic cleavage, to DNA synthesis, or to a multiplexing combination. *J. Am. Chem. Soc.* **2008**, *130* (17), 5720.
251. Huang, X.; Li, L.; Qian, H.; Dong, C.; Ren, J., A Resonance Energy Transfer between Chemiluminescent Donors and Luminescent Quantum-Dots as Acceptors (CRET). *Angew. Chem. Int. Ed.* **2006**, *45* (31), 5140-5143.

252. Li, Z.; Wang, Y.; Zhang, G.; Xu, W.; Han, Y., Chemiluminescence resonance energy transfer in the luminol–CdTe quantum dots conjugates. *J. Lumin.* **2010**, *130* (6), 995-999.
253. Wang, H.-Q.; Li, Y.-Q.; Wang, J.-H.; Xu, Q.; Li, X.-Q.; Zhao, Y.-D., Influence of quantum dot's quantum yield to chemiluminescent resonance energy transfer. *Anal. Chim. Acta* **2008**, *610* (1), 68-73.
254. Freeman, R.; Liu, X.; Willner, I., Chemiluminescent and chemiluminescence resonance energy transfer (CRET) detection of DNA, metal ions, and aptamer-substrate complexes using hemin/G-quadruplexes and CdSe/ZnS quantum dots. *J. Am. Chem. Soc.* **2011**, *133* (30), 11597.
255. Min-Kyung, S.; Chenjie, X.; Andreas, M. L.; Sanjiv, S. G.; Jianghong, R., Self-illuminating quantum dot conjugates for in vivo imaging. *Nat. Biotechnol.* **2006**, *24* (3), 339.
256. Kosaka, N.; Mitsunaga, M.; Bhattacharyya, S.; Miller, S. C.; Choyke, P. L.; Kobayashi, H., Self-illuminating in vivo lymphatic imaging using a bioluminescence resonance energy transfer quantum dot nano-particle. *Contrast Media Mol. Imaging* **2011**, *6* (1), 55-59.
257. Yao, H.; Zhang, Y.; Xiao, F.; Xia, Z.; Rao, J., Quantum Dot/Bioluminescence Resonance Energy Transfer Based Highly Sensitive Detection of Proteases. *Angew. Chem. Int. Ed.* **2007**, *46* (23), 4346-4349.
258. Zhang, Y.; So, M. K.; Loening, A. M.; Yao, H.; Gambhir, S. S.; Rao, J., HaloTag Protein-Mediated Site-Specific Conjugation of Bioluminescent Proteins to Quantum Dots. *Angew. Chem. Int. Ed.* **2006**, *45* (30), 4936-4940.
259. Charbonniere, L.; Hildebrandt, N.; Ziessel, R.; Loehmannsroeben, H., Lanthanides to quantum dots resonance energy transfer in time-resolved fluoro-immunoassays and luminescence microscopy. *J. Am. Chem. Soc.* **2006**, *128* (39), 12800-12809.
260. Hildebrandt, N.; Charbonnière, L. J.; Beck, M.; Ziessel, R. F.; Löhmannsröben, H.-G., Quantum dots as efficient energy acceptors in a time-resolved fluoroimmunoassay. *Angew. Chem. Int. Ed.* **2005**, *44* (46), 7612.
261. Hildebrandt, N.; Charbonnière, L. J.; Löhmannsröben, H.-G., Time-Resolved Analysis of a Highly Sensitive Förster Resonance Energy Transfer Immunoassay Using Terbium Complexes as Donors and Quantum Dots as Acceptors. *J. Biomed. Biotechnol.* **2007**, *2007* (7).
262. Xu, J.; Corneillie, T. M.; Moore, E. G.; Law, G.-L.; Butlin, N. G.; Raymond, K. N., Octadentate cages of Tb(III) 2-hydroxyisophthalamides: a new standard for luminescent lanthanide labels. *J. Am. Chem. Soc.* **2011**, *133* (49), 19900.
263. Li, Y.-Q.; Wang, J.-H.; Zhang, H.-L.; Yang, J.; Guan, L.-Y.; Chen, H.; Luo, Q.-M.; Zhao, Y.-D., High-sensitivity quantum dot-based fluorescence resonance energy transfer bioanalysis by capillary electrophoresis. *Biosens. Bioelectron.* **2010**, *25* (6), 1283-1289.
264. Hu, B.; Zhang, L.-P.; Chen, M.-L.; Chen, M.-L.; Wang, J.-H., The inhibition of fluorescence resonance energy transfer between quantum dots for glucose assay. *Biosens. Bioelectron.* **2012**, *32* (1), 82-88.

265. Kagan, C. R.; Murray, C.; Bawendi, M. G., Long-range resonance transfer of electronic excitations in close-packed CdSe quantum-dot solids. *Phys. Rev. B* **1996**, *54* (12), 8633-8643.
266. Liu, T.-C.; Zhang, H.-L.; Wang, J.-H.; Wang, H.-Q.; Zhang, Z.-H.; Hua, X.-F.; Cao, Y.-C.; Luo, Q.-M.; Zhao, Y.-D., Study on molecular interactions between proteins on live cell membranes using quantum dot-based fluorescence resonance energy transfer. *Anal. Bioanal. Chem.* **2008**, *391* (8), 2819-2824.
267. Seker, U. O. S.; Ozel, T.; Demir, H. V., Peptide-mediated constructs of quantum dot nanocomposites for enzymatic control of nonradiative energy transfer. *Nano Lett.* **2011**, *11* (4), 1530.
268. Medintz, I.; Hildebrandt, N., *FRET - Förster Resonance Energy Transfer: from Theory to Applications*. Weinheim : Wiley-VCH Verlag GmbH & Co. KGaA: **2014**.
269. Ma, Q.; Su, X., Recent advances and applications in QDs-based sensors. *Analyst* **2011**, *136* (23), 4883-4893.
270. Jones, M.; Lo, S. S.; Scholes, G. D., Quantitative modeling of the role of surface traps in CdSe/CdS/ZnS nanocrystal photoluminescence decay dynamics. *Proc. Natl. Acad. Sci. USA* **2009**, *106* (9), 3011-3016.
271. Algar, W. R.; Tavares, A. J.; Krull, U. J., Beyond labels: A review of the application of quantum dots as integrated components of assays, bioprobes, and biosensors utilizing optical transduction. *Anal. Chim. Acta* **2010**, *673* (1), 1-25.
272. Jeong, S.; Song, J.; Lee, W.; Ryu, Y. M.; Jung, Y.; Kim, S.-Y.; Kim, K.; Hong, S. C.; Myung, S. J.; Kim, S., Cancer-Microenvironment-Sensitive Activatable Quantum Dot Probe in the Second Near-Infrared Window. *Nano Lett.* **2017**, *17* (3), 1378-1386.
273. Horan, T. C.; Andrus, M.; Dudeck, M. A., CDC/NHSN surveillance definition of health care-associated infection and criteria for specific types of infections in the acute care setting. *Am. J. Infect. Control* **2008**, *36* (5), 309-332.
274. Plowman, R., The Socioeconomic Burden of Hospital Acquired Infection. *Euro Surveill.* **2000**, *5* (4), 49.
275. Plowman, R.; Graves, N.; Griffin, M. A. S.; Roberts, J. A.; Swan, A. V.; Cookson, B.; Taylor, L., The rate and cost of hospital-acquired infections occurring in patients admitted to selected specialties of a district general hospital in England and the national burden imposed. *J. Hosp. Infect.* **2001**, *47* (3), 198-209.
276. Foley, S. L., *Molecular Techniques for the Study of Hospital-Acquired Infection* Hoboken, N.J. : Wiley-Blackwell: **2011**.
277. European Centre for Disease Prevention and Control (ECDC), *Point Prevalence Survey of Healthcare-Associated Infections and Antimicrobial Use in European Acute Care Hospitals 2011-2012*. <https://www.ecdc.europa.eu/sites/portal/files/media/en/publications/Publications/healthcare-associated-infections-antimicrobial-use-PPS.pdf>.

278. National Institute for Health and Care Excellence (NICE), *Healthcare-Associated Infections: Prevention and Control in Primary and Community Care*. <https://www.nice.org.uk/guidance/cg139>.
279. Nuffield Trust, *Healthcare-associated Infections*. <https://www.nuffieldtrust.org.uk/resource/healthcare-associated-infections>.
280. World Health Organization (WHO), *Hospital Hygiene and Infection Control*. [https://www.who.int/water\\_sanitation\\_health/medicalwaste/148to158.pdf](https://www.who.int/water_sanitation_health/medicalwaste/148to158.pdf).
281. Kampf, G.; Kramer, A., Epidemiologic Background of Hand Hygiene and Evaluation of the Most Important Agents for Scrubs and Rubs. *Clin Microbiol Rev* **2004**, *17* (4), 863.
282. Denton, M.; Wilcox, M. H.; Parnell, P.; Green, D.; Keer, V.; Hawkey, P. M.; Evans, I.; Murphy, P., Role of environmental cleaning in controlling an outbreak of *Acinetobacter baumannii* on a neurosurgical intensive care unit. *J. Hosp. Infect.* **2004**, *56* (2), 106-110.
283. Boyce, J. M.; Potter-Bynoe, G.; Chenevert, C.; King, T., Environmental contamination due to methicillin-resistant *Staphylococcus aureus*: Possible infection control implications. *Infect. Control Hosp. Epidemiol.* **1997**, *18* (9), 622-627.
284. Hayden, M. K.; Bonten, M. J. M.; Blom, D. W.; Lyle, E. A.; van de Vijver, D. A. M. C.; Weinstein, R. A., Reduction in acquisition of vancomycin-resistant enterococcus after enforcement of routine environmental cleaning measures. *Clin. Infect. Dis.* **2006**, *42* (11), 1552.
285. Wilks, M.; Wilson, A.; Warwick, S.; Price, E.; Kennedy, D.; Ely, A.; Millar, Michael R., Control of an Outbreak of Multidrug-Resistant *Acinetobacter baumannii-calcoaceticus* Colonization and Infection in an Intensive Care Unit (ICU) Without Closing the ICU or Placing Patients in Isolation. *Infect. Control Hosp. Epidemiol.* **2006**, *27* (7), 654-658.
286. Kramer, A.; Schwebke, I.; Kampf, G., How Long do Nosocomial Pathogens Persist on Inanimate Surfaces? A Systematic Review. *BMC Infect. Dis.* **2006**, *6* (1).
287. Neely, A. N.; Maley, M. P., Survival of Enterococci and Staphylococci on Hospital Fabrics and Plastic. *J. Clin. Microbiol.* **2000**, *38* (2), 724.
288. Panagea, S.; Winstanley, C.; Walshaw, M. J.; Ledson, M. J.; Hart, C. A., Environmental contamination with an epidemic strain of *Pseudomonas aeruginosa* in a Liverpool cystic fibrosis centre, and study of its survival on dry surfaces. *J. Hosp. Infect.* **2005**, *59* (2), 102-107.
289. Chambers, R., Prolonged Colonization with Vancomycin-Resistant *Enterococcus faecium* in Long-Term Care Patients and the Significance of "Clearance". *Clin. Infect. Dis.* **2001**, *33* (10), 1654-1660.
290. Hota, B., Contamination, disinfection, and cross-colonization: Are hospital surfaces reservoirs for nosocomial infection? *Clin. Infect. Dis.* **2004**, *39* (8), 1182-1189.
291. Pelgrift, R. Y.; Friedman, A. J., Nanotechnology as a therapeutic tool to combat microbial resistance. *Adv. Drug Deliv. Rev* **2013**, *65* (13-14), 1803-1815.

292. Riley, M. A.; Robinson, S. M.; Roy, C. M.; Dennis, M.; Liu, V.; Dorit, R. L., Resistance is futile: The bacteriocin model for addressing the antibiotic resistance challenge. *Biochem. Soc. Trans.* **2012**, *40* (6), 1438-1442.
293. Mitchell, L. C., Changing patterns of infectious disease. *Nature* **2000**, *406* (6797), 762.
294. Nordberg, P.; Monnet, D. L.; Cars, O. *Antibacterial Drug Resistance [Background document for the WHO project: Priority Medicines for Europe and the World. 'A Public Health Approach to Innovation']*; 2004.
295. World Health Organization, *The World Health Report 2003 – Shaping the Future*. <http://www.who.int/whr/2003/en/>.
296. O'Neill, J. *Tackling Drug-Resistant Infections Globally: Final Report and Recommendations*; **2016**.
297. Davies, M., Superbugs Killing Twice as Many People as Government Says. *The Bureau of Investigative Journalism* 2016.
298. Davies, M.; Adams, C.; Newell, C., The True Cost of Antibiotic Resistance in Britain and around the World. *The Telegraph* 2018.
299. Bisen, P. S., *Emerging epidemics : Management and Control*. Hoboken, N.J. : Wiley Blackwell: **2013**.
300. David, L., Can better prescribing turn the tide of resistance? *Nat. Rev. Microbiol.* **2004**, *2* (1), 73.
301. Livermore, D. M., Bacterial resistance: Origins, epidemiology, and impact. *Clin. Infect. Dis.* **2003**, *36* (1), S11-S23.
302. Neu, H. C., The crisis in antibiotic resistance. *Science* **1992**, *257* (5073), 1064-1073.
303. Smith, R. D.; Coast, J., Antimicrobial resistance: a global response. *Bull. World Health Organ.* **2002**, *80* (2), 126-133.
304. Robin, A. H.; Alastair, M.; Mandy, W.; Timothy, R. W.; Mark, C. E., Vancomycin Susceptibility within Methicillin-resistant Staphylococcus aureus Lineages. *Emerg. Infect. Dis.* **2004**, *10* (5), 855-857.
305. *Surveillance of Antimicrobial Resistance in Europe – Annual Report of the European Antimicrobial Resistance Surveillance Network (EARS-Net) 2017*; European Centre for Disease Prevention and Control (ECDC): Stockholm, **2018**.
306. Sadikot, R.; Blackwell, T.; Christman, J. W.; Prince, A., Pathogen-host interactions in Pseudomonas aeruginosa pneumonia. *Am. J. Respir. Crit. Care Med.* **2005**, *171* (11), 1209-1223.

307. Barbier, F.; Andremont, A.; Wolff, M.; Bouadma, L., Hospital-acquired pneumonia and ventilator-associated pneumonia: recent advances in epidemiology and management. *Curr. Opin. Pulm. Med.* **2013**, *19* (3), 216-228.
308. *Antimicrobial Resistance Surveillance in Europe 2015. Annual Report of the European Antimicrobial Resistance Surveillance Network (EARS-Net)*. European Centre for Disease Prevention and Control (ECDC): Stockholm, **2017**.
309. Ellingson, K.; Haas, J. P.; Aiello, A. E.; Kusek, L.; Maragakis, L. L.; Olmsted, R. N.; Perencevich, E.; Polgreen, P. M.; Schweizer, M. L.; Trexler, P.; VanAmringe, M.; Yokoe, D. S., Strategies to Prevent Healthcare-Associated Infections through Hand Hygiene. *Infect. Control Hosp. Epidemiol.* **2014**, *35* (8), 937-960.
310. Mathur, P., Hand hygiene: Back to the basics of infection control. *Indian J. Med. Res.* **2011**, *134* (11), 611-620.
311. Andreas, F. W., Replace Hand Washing with Use of a Waterless Alcohol Hand Rub? *Clin. Infect. Dis.* **2000**, *31* (1), 136-143.
312. Hardy, Katherine J.; Oppenheim, Beryl A.; Gossain, S.; Gao, F.; Hawkey, Peter M., A Study of the Relationship Between Environmental Contamination with Methicillin-Resistant Staphylococcus Aureus (MRSA) and Patients' Acquisition of MRSA. *Infect. Control Hosp. Epidemiol.* **2006**, *27* (2), 127-132.
313. Rutala, W. A., Weber, D. J., Healthcare Infection Control Practices Advisory Committee (HICPAC). *Guideline for Disinfection and Sterilization in Healthcare Facilities (2008). Update : May 2019.* <https://www.cdc.gov/infectioncontrol/guidelines/disinfection/>.
314. Block, S. S., *Disinfection, Sterilization, and Preservation*. 5th ed.; London : Lippincott Williams & Wilkins: **2001**.
315. Bean, H. S., Types and characteristics of disinfectants. *J. Appl. Microbiol.* **1967**, *30* (1), 6.
316. Russell, A. D.; Hugo, W. B.; Ayliffe, G. A. J.; Fraiese, A. P.; Lambert, P. A.; Maillard, J. Y., *Russell, Hugo & Ayliffe's Principles and Practice of Disinfection, Preservation and Sterilization*. 4th ed.; Oxford : Blackwell Pub.: **2004**.
317. McDonnell, G.; Russell, A. D., Antiseptics and disinfectants: Activity, action, and resistance. *Clin. Microbiol. Rev.* **1999**, *12* (1), 147.
318. Russell, A. D., Factors Influencing the Efficacy of Antimicrobial Agents. In *Russell, Hugo & Ayliffe's Principles and Practice of Disinfection, Preservation & Sterilization*, 4th ed.; **2004**; pp 98-127.
319. Larson, E. L.; Liverman, C. T., *Preventing Transmission of Pandemic Influenza and Other Viral Respiratory Diseases: Personal Protective Equipment for Healthcare Personnel: Update 2010*. National Academies Press: **2011**.

320. Hayden, M. K.; Bonten, M. J. M.; Blom, D. W.; Lyle, E. A.; van de Vijver, D. A. M. C.; Weinstein, R. A., Reduction in Acquisition of Vancomycin-Resistant Enterococcus after Enforcement of Routine Environmental Cleaning Measures. *Clin. Infect. Dis.* **2006**, *42* (11), 1552-1560.
321. Bernstein, D. A.; Salsgiver, E.; Simon, M. S.; Greendyke, W.; Eiras, D. P.; Ito, M.; Caruso, D. A.; Woodward, T. M.; Perriel, O. T.; Saiman, L.; Furuya, E. Y.; Calfee, D. P., Understanding Barriers to Optimal Cleaning and Disinfection in Hospitals: A Knowledge, Attitudes, and Practices Survey of Environmental Services Workers. *Infect. Control Hosp. Epidemiol.* **2016**, *37* (12), 1492-1495.
322. Gershon, R. R. M.; Vlahov, D.; Felknor, S. A.; Vesley, D.; Johnson, P. C.; Delcios, G. L.; Murphy, L. R., Compliance with Universal Precautions among Health Care Workers at three Regional Hospitals. *Am. J. Infect* **1995**, *23* (4), 225-236.
323. Lemire, J. A.; Harrison, J. J.; Turner, R. J., Antimicrobial Activity of Metals: Mechanisms, Molecular Targets and Applications. *Nat. Rev. Microbiol.* **2013**, *11* (6), 371-384.
324. Seil, J.; Webster, T., Antimicrobial Applications of Nanotechnology: Methods and Literature. *Int. J. Nanomedicine* **2012**, *7*, 2767-2781.
325. Dizaj, S. M.; Lotfipour, F.; Barzegar-Jalali, M.; Zarrintan, M. H.; Adibkia, K., Antimicrobial Activity of the Metals and Metal Oxide Nanoparticles. *Mater. Sci. Eng. C* **2014**, *44*, 278-284.
326. Ssn, F.; Tdcp, G.; Holton, J., Antimicrobial Nanoparticles: Applications and Mechanisms of Action. *Sri Lankan J. Infect. Dis.* **2018**, *8* (1), 2-11.
327. Pal, S.; Tak, Y. K.; Song, J. M., Does the Antibacterial Activity of Silver Nanoparticles Depend on the Shape of the Nanoparticle? A Study of the Gram-Negative Bacterium Escherichia coli. *Appl. Environ. Microbiol.* **2007**, *73* (6), 1712.
328. Bera, R. K.; Mandal, S. M.; Raj, C. R., Antimicrobial Activity of Fluorescent Ag Nanoparticles. *Lett. Appl. Microbiol.* **2014**, *58* (6), 520-526.
329. Zewde, B. M.; Ambaye, A. B.; Stubbs, J. T.; Raghavan, R., A Review of Stabilized Silver Nanoparticles – Synthesis, Biological Properties, Characterization, and Potential Areas of Applications. *JSM Nanotechnol. Nanomed.* **2016**, *4* (2), 1043.
330. Prabhu, S.; Poulouse, E., Silver Nanoparticles: Mechanism of Antimicrobial Action, Synthesis, Medical Applications, and Toxicity Effects. *Int. Nano Lett.* **2012**, *2* (1), 1-10.
331. Sondi, I.; Salopek-Sondi, B., Silver Nanoparticles as Antimicrobial Agent: a Case Study on *E. coli* as a Model for Gram-Negative Bacteria. *J. Colloid Interface Sci.* **2004**, *275* (1), 177-182.
332. Danilczuk, M.; Lund, A.; Sadlo, J.; Yamada, H.; Michalik, J., Conduction Electron Spin Resonance of Small Silver Particles. *Spectrochim. Acta A Mol. Biomol. Spectrosc.* **2006**, *63* (1), 189-191.

333. Kim, J. S.; Kuk, E.; Yu, K. N.; Kim, J.-H.; Park, S. J.; Lee, H. J.; Kim, S. H.; Park, Y. K.; Park, Y. H.; Hwang, C.-Y.; Kim, Y.-K.; Lee, Y.-S.; Jeong, D. H.; Cho, M.-H., Antimicrobial Effects of Silver Nanoparticles. *Nanomedicine* **2007**, *3* (1), 95.
334. Egger, S.; Lehmann, R. P.; Height, M. J.; Loessner, M. J.; Schuppler, M., Antimicrobial Properties of a Novel Silver-Silica Nanocomposite Material. *Appl. Environ. Microbiol.* **2009**, *75* (9), 2973.
335. Sirelkhatim, A.; Mahmud, S.; Seeni, A.; Kaus, N.; Ann, L.; Bakhori, S.; Hasan, H.; Mohamad, D., Review on Zinc Oxide Nanoparticles: Antibacterial Activity and Toxicity Mechanism. *Nano-Micro Lett.* **2015**, *7* (3), 219-242.
336. Jiang, W.; Mashayekhi, H.; Xing, B., Bacterial Toxicity Comparison between Nano- and Micro-Scaled Oxide Particles. *Environ. Pollut.* **2009**, *157* (5), 1619-1625.
337. Nair, S.; Sasidharan, A.; Divya Rani, V.; Menon, D.; Nair, S.; Manzoor, K.; Raina, S., Role of Size Scale of ZnO Nanoparticles and Microparticles on Toxicity toward Bacteria and Osteoblast Cancer Cells. *J. Mater. Sci, Mater, Med.* **2009**, *20* (1), 235-241.
338. Azam, A.; Ahmed, A. S.; Oves, M.; Khan, M. S.; Habib, S. S.; Memic, A., Antimicrobial Activity of Metal Oxide Nanoparticles against Gram-Positive and Gram-Negative Bacteria: a Comparative Study. *Int. J. Nanomedicine* **2012**, *7*, 6003-6009.
339. Jones, N.; Ray, B.; Ranjit, K. T.; Manna, A. C., Antibacterial Activity of ZnO Nanoparticle Suspensions on a Broad Spectrum of Microorganisms. *FEMS Microbiol. Lett.* **2008**, *279* (1), 71-76.
340. Reddy, K. M.; Feris, K.; Bell, J.; Wingett, D. G.; Hanley, C.; Punnoose, A., Selective Toxicity of Zinc Oxide Nanoparticles to Prokaryotic and Eukaryotic Systems. *Appl. Phys. Lett.* **2007**, *90* (21).
341. Xie, Y.; He, Y.; Irwin, P. L.; Jin, T.; Shi, X., Antibacterial Activity and Mechanism of Action of Zinc Oxide Nanoparticles against *Campylobacter jejuni*. *Appl. Environ. Microbiol.* **2011**, *77* (7), 2325.
342. Hosseinkhani, P.; Zand, A.; Imani, S.; Rezayi, M.; Zarchi, S., Determining the Antibacterial Effect of ZnO Nanoparticle against the Pathogenic Bacterium, *Shigella dysenteriae* (type 1). *Int. J. Nano Dimens.* **2011**, *1* (4), 279-285.
343. Jin, T.; Sun, D.; Su, J.; Zhang, H.; Sue, H., Antimicrobial Efficacy of Zinc Oxide Quantum Dots against *Listeria monocytogenes*, *Salmonella Enteritidis*, and *Escherichia coli* O157:H7. *J. Food Sci.* **2009**, *74* (1), M46-M52.
344. Brayner, R.; Ferrari-Iliou, R.; Brivois, N.; Djediat, S.; Benedetti, M. F.; Fiévet, F., Toxicological Impact Studies based on *Escherichia coli* Bacteria in Ultrafine ZnO Nanoparticles Colloidal Medium. *Nano Lett.* **2006**, *6* (4), 866.
345. Zhang, L.; Jiang, Y.; Ding, Y.; Povey, M.; York, D., Investigation into the Antibacterial Behaviour of Suspensions of ZnO Nanoparticles (ZnO Nanofluids). *J. Nanopart. Res.* **2007**, *9* (3), 479-489.

346. Adams, L. K.; Lyon, D. Y.; Alvarez, P. J. J., Comparative Eco-Toxicity of Nanoscale TiO<sub>2</sub>, SiO<sub>2</sub>, and ZnO Water Suspensions. *Water Res.* **2006**, *40* (19), 3527-3532.
347. Kasemets, K.; Ivask, A.; Dubourguier, H.-C.; Kahru, A., Toxicity of Nanoparticles of ZnO, CuO and TiO<sub>2</sub> to Yeast *Saccharomyces cerevisiae*. *Toxicol. Vitro* **2009**, *23* (6), 1116-1122.
348. Brunner, T. J.; Wick, P.; Manser, P.; Spohn, P.; Grass, R. N.; Limbach, L. K.; Bruinink, A.; Stark, W. J., *In vitro* cytotoxicity of oxide Nanoparticles: Comparison to Asbestos, Silica, and the Effect of Particle Solubility. *Environ. Sci. Technol.* **2006**, *40* (14), 4374.
349. Sawai, J.; Shoji, S.; Igarashi, H.; Hashimoto, A.; Kokugan, T.; Shimizu, M.; Kojima, H., Hydrogen Peroxide as an Antibacterial Factor in Zinc Oxide Powder Slurry. *J. Ferment. Bioeng.* **1998**, *86* (5), 521-522.
350. Lipovsky, A.; Nitzan, Y.; Gedanken, A.; Lubart, R., Antifungal Activity of ZnO Nanoparticles- the Role of ROS Mediated Cell Injury. *Nanotechnology* **2011**, *22* (10).
351. Zhang, L.; Ding, Y.; Povey, M.; York, D., ZnO nanofluids – A Potential Antibacterial Agent. *Prog. Nat. Sci.* **2008**, *18* (8), 939-944.
352. Gupta, K.; Singh, R. P.; Pandey, A.; Pandey, A.; Schneider, J. J., Photocatalytic Antibacterial Performance of TiO<sub>2</sub> and Ag-doped TiO<sub>2</sub> against *S. aureus*, *P. aeruginosa* and *E. coli*. *Bellstein J. Nanotechnol.* **2013**, *4* (1), 345-351.
353. Sun, T.; Hao, H.; Hao, W.-t.; Yi, S.-m.; Li, X.-p.; Li, J.-r., Preparation and Antibacterial Properties of Titanium-Doped ZnO from Different Zinc Salts. *Nanoscale Res. Lett.* **2014**, *9* (1), 1-11.
354. Carre, G.; Hamon, E.; Ennahar, S.; Estner, M.; Lett, M.-C.; Horvatovich, P.; Gies, J.-P.; Keller, V.; Keller, N.; Andre, P., TiO<sub>2</sub> Photocatalysis Damages Lipids and Proteins in *Escherichia coli*. *Appl. Environ. Microbiol.* **2014**, *80* (8), 2573.
355. Haghighi, F.; Mohammadi, S. R.; Mohammadi, P. K.; Hosseinkhani, S.; Shipour, R., Antifungal Activity of TiO<sub>2</sub> Nanoparticles and EDTA on *Candida albicans* Biofilms. *Infection Epidemiology & Medicine* **2013**, *1* (1), 33-38.
356. Roy, A. S.; Parveen, A.; Koppalkar, A. R.; Prasad, M., Effect of Nano - Titanium Dioxide with Different Antibiotics against Methicillin-Resistant Staphylococcus Aureus. *J. Biomater. Nanobiotechnol.* **2010**, *1*, 37-41
357. Allahverdiyev, A.; Abamor, E.; Bagirova, M.; Rafailovich, M., Antimicrobial Effects of TiO<sub>2</sub> and Ag<sub>2</sub>O Nanoparticles against Drug-Resistant Bacteria and *leishmania* parasites. *Future Microbiol.* **2011**, *6*, 933-940.
358. Adriana, Z., Doped-TiO<sub>2</sub>: A Review. *Recent Pat. Eng.* **2008**, *2* (3), 157-164.
359. Usman, M. S.; El Zowalaty, M. E.; Shamel, K.; Zainuddin, N.; Salama, M.; Ibrahim, N. A., Synthesis, Characterization, and Antimicrobial Properties of Copper Nanoparticles. *Int. J. Nanomedicine* **2013**, *8* (1), 4467.

360. Ahamed, M.; Alhadlaq, H. A.; Khan, M. A. M.; Karuppiah, P.; Al-Dhabi, N. A., Synthesis, Characterization, and Antimicrobial Activity of Copper Oxide Nanoparticles. *J. Nanomater.* **2014**, 2014 (2014).
361. Ren, G.; Hu, D.; Cheng, E. W. C.; Vargas-Reus, M. A.; Reip, P.; Allaker, R. P., Characterisation of Copper Oxide Nanoparticles for Antimicrobial Applications. *Int. J. Antimicrob. Agents* **2009**, 33 (6), 587-590.
362. Mahapatra, O.; Bhagat, M.; Gopalakrishnan, C.; Arunachalam, K. D., Ultrafine Dispersed CuO Nanoparticles and their Antibacterial Activity. *J. Exp. Nanosci.* **2008**, 3 (3), 185-193.
363. Chatterjee, A. K.; Chakraborty, R.; Basu, T., Mechanism of Antibacterial Activity of Copper Nanoparticles. *Nanotechnology* **2014**, 25 (13), 135101.
364. Azam, A.; Ahmed, A.; Oves, M.; Khan, M. S.; Memic, A., Size-Dependent Antimicrobial Properties of CuO Nanoparticles against Gram-Positive and -Negative Bacterial Strains. *Int. J. Nanomedicine* **2012**, 7, 3527-3535.
365. Lima, E.; Guerra, R.; Lara, V.; Guzmán, A., Gold Nanoparticles as Efficient Antimicrobial Agents for *Escherichia coli* and *Salmonella typhi*. *Chem. Cent. J.* **2013**, 7 (1), 11.
366. Tiwari, P.; Vig, K.; Dennis, V. A.; Singh, Sr., Functionalized Gold Nanoparticles and Their Biomedical Applications. *Nanomaterials* **2011**, 1 (1), 31-63.
367. Zhou, Y.; Kong, Y.; Kundu, S.; Cirillo, J. D.; Liang, H., Antibacterial Activities of Gold and Silver Nanoparticles against *Escherichia coli* and *bacillus Calmette-Guerin*. *J. Nanobiotechnol.* **2012**, 10.
368. Zheng, K.; Setyawati, M. I.; Leong, D. T.; Xie, J., Antimicrobial Gold Nanoclusters. *ACS Nano* **2017**, 11 (7), 6904.
369. Cui, Y.; Zhao, Y.; Tian, Y.; Zhang, W.; Lü, X.; Jiang, X., The Molecular Mechanism of Action of Bactericidal Gold Nanoparticles on *Escherichia coli*. *Biomaterials* **2012**, 33 (7), 2327.
370. Cousins, B. G.; Allison, H. E.; Doherty, P. J.; Edwards, C.; Garvey, M. J.; Martin, D. S.; Williams, R. L., Effects of a Nanoparticulate Silica Substrate on Cell Attachment of *Candida albicans*. *J. Appl. Microbiol.* **2007**, 102 (3), 757-765.
371. I., M.; A., E.; G., K.; A., M., Antibacterial Action and Physicochemical Properties of Stabilized Silver and Gold Nanostructures on the Surface of Disperse Silica *J. Water Resour. Prot.* **2010**, 2, 131-136.
372. Yamamoto, O.; Ohira, T.; Alvarez, K.; Fukuda, M., Antibacterial Characteristics of CaCO<sub>3</sub>-MgO Composites. *Mater. Sci. Eng. B* **2010**, 173 (1-3), 208-212.
373. Hewitt, C.; Bellara, S.; Andreani, A.; Nebe-von-Caron, G.; McFarlane, C., An Evaluation of the Anti-Bacterial Action of Ceramic Powder Slurries using Multi-Parameter Flow Cytometry. *Biotechnol. Lett.* **2001**, 23 (9), 667-675.

374. Jin, T.; He, Y., Antibacterial Activities of Magnesium Oxide (MgO) Nanoparticles against Foodborne Pathogens. *J. Nanopart. Res.* **2011**, *13* (12), 6877-6885.
375. Leung, Y. H.; Ng, A. M. C.; Xu, X.; Shen, Z.; Gethings, L. A.; Wong, M. T.; Chan, C. M. N.; Guo, M. Y.; Ng, Y. H.; Djurišić, A. B.; Lee, P. K. H.; Chan, W. K.; Yu, L. H.; Phillips, D. L.; Ma, A. P. Y.; Leung, F. C. C., Mechanisms of Antibacterial Activity of MgO: Non-ROS Mediated Toxicity of MgO Nanoparticles Towards *Escherichia coli*. *Small* **2014**, *10* (6), 1171-1183.
376. Vidic, J.; Stankic, S.; Haque, F.; Ciric, D.; Goffic, R.; Vidy, A.; Jupille, J.; Delmas, B., Selective Antibacterial Effects of Mixed ZnMgO Nanoparticles. *J. Nanopart. Res.* **2013**, *15* (5), 1-10.
377. Courtney, C. M.; Goodman, S. M.; McDaniel, J. A.; Madinger, N. E.; Chatterjee, A.; Nagpal, P., Photoexcited Quantum Dots for Killing Multidrug-Resistant Bacteria. *Nat. Mater.* **2016**, *15* (5), 529-534.
378. Ristic, B. Z.; Milenkovic, M. M.; Dakic, I. R.; Todorovic-Markovic, B. M.; Milosavljevic, M. S.; Budimir, M. D.; Paunovic, V. G.; Dramicanin, M. D.; Markovic, Z. M.; Trajkovic, V. S., Photodynamic Antibacterial Effect of Graphene Quantum Dots. *Biomaterials* **2014**, *35* (15), 4428-4435.
379. Kuo, W.-S.; Shao, Y.-T.; Huang, K.-S.; Chou, T.-M.; Yang, C.-H., Antimicrobial Amino-Functionalized Nitrogen-Doped Graphene Quantum Dots for Eliminating Multidrug-Resistant Species in Dual-Modality Photodynamic Therapy and Bioimaging under Two-Photon Excitation. *ACS Appl. Mater. Inter.* **2018**, *10* (17), 14438.
380. Samuel, M. G.; Max, L.; Fei-Fei, L.; Yuchen, D.; Colleen, M. C.; Partha, P. C.; Annette, E.; Anushree, C.; Prashant, N., Designing Superoxide-Generating Quantum Dots for Selective Light-Activated Nanotherapy. *Front. Chem.* **2018**, *6*.
381. Gomes, S.; Vieira, C.; Almeida, D.; Santos-Mallet, J.; Menna-Barreto, R.; Cesar, C.; Feder, D., CdTe and CdSe Quantum Dots Cytotoxicity: A Comparative Study on Microorganisms. *Sensors* **2011**, *11* (12), 11664-11678.
382. Luo, Z.; Wu, Q.; Zhang, M.; Li, P.; Ding, Y., Cooperative antimicrobial activity of CdTe quantum dots with rocephin and fluorescence monitoring for *Escherichia coli*. *J. Colloid Interface Sci.* **2011**, *362* (1), 100-106.
383. Courtney, C. M.; Goodman, S. M.; Nagy, T. A.; Levy, M.; Bhusal, P.; Madinger, N. E.; Detweiler, C. S.; Nagpal, P.; Chatterjee, A., Potentiating antibiotics in drug-resistant clinical isolates via stimuli-activated superoxide generation. *Sci. Adv.* **2017**, *3* (10), e1701776.
384. Galdiero, E.; Siciliano, A.; Maselli, V.; Gesuele, R.; Guida, M.; Fulgione, D.; Galdiero, S.; Lombardi, L.; Falanga, A., An integrated study on antimicrobial activity and ecotoxicity of quantum dots and quantum dots coated with the antimicrobial peptide indolicidin. *Int. J. Nanomedicine* **2016**, *11*, 4199.
385. Ananth, D. A.; Rameshkumar, A.; Jeyadevi, R.; Jagadeeswari, S.; Nagarajan, N.; Renganathan, R.; Sivasudha, T., Antibacterial potential of rutin conjugated with thioglycolic acid capped cadmium telluride quantum dots (TGA-CdTe QDs). *Spectrochim. Acta A Mol. Biomol. Spectrosc.* **2015**, *138*, 684-692.

386. Page, K.; Wilson, M.; Parkin, I. P., Antimicrobial surfaces and their potential in reducing the role of the inanimate environment in the incidence of hospital-acquired infections. *J. Mater. Chem.* **2009**, *19* (23), 3819-3831.
387. Bures, S.; Fishbain, J. T.; Uyehara, C. F. T.; Parker, J. M.; Berg, B. W., Computer keyboards and faucet handles as reservoirs of nosocomial pathogens in the intensive care unit. *Am. J. Infect. Control* **2000**, *28* (6), 465-471.
388. Ciragil, P.; Gul, M.; Aral, M., Bacterial contamination of computers and telephones in a university hospital in Turkey. *J. Hosp. Infect.* **2006**, *62* (2), 247-248.
389. Oie, S.; Hosokawa, I.; Kamiya, A., Contamination of room door handles by methicillin-sensitive/methicillin-resistant *Staphylococcus aureus*. *J. Hosp. Infect.* **2002**, *51* (2), 140-143.
390. Evans, P.; Sheel, D. W., Photoactive and antibacterial TiO<sub>2</sub> thin films on stainless steel. *Surf. Coat. Tech.* **2007**, *201* (22-23), 9319-9324.
391. Page, K.; Palgrave, R. G.; Parkin, I. P.; Wilson, M.; Savin, S. L. P.; Chadwick, A. V., Titania and Silver-Titania Composite Films on Glass—Potent Antimicrobial Coatings. *J. Mater. Chem.* **2006**, *17* (1), 95-104.
392. Dunnill, C. W.; Aiken, Z. A.; Kafizas, A.; Pratten, J.; Wilson, M.; Morgan, D. J.; Parkin, I. P., White light induced photocatalytic activity of sulfur-doped TiO<sub>2</sub> thin films and their potential for antibacterial application. *J. Mater. Chem.* **2009**, *19* (46).
393. Hamblin, M. R.; Hasan, T., Photodynamic therapy: a new antimicrobial approach to infectious disease&quest. *Photochem. Photobiol. Sci.* **2004**, *3* (5), 436-450.
394. Wainwright, M., Photoantimicrobials—So what's stopping us? *Photodiagnosis Photodyn. Ther.* **2009**, *6* (3-4), 167-169.
395. Wainwright, M.; Byrne, M. N.; Gattrell, M. A., Phenothiazinium-based photobactericidal materials. *J. Photochem. Photobiol. B* **2006**, *84* (3), 227-230.
396. Wilson, M., Light-activated antimicrobial coating for the continuous disinfection of surfaces. *Infection Control & Hospital Epidemiology* **2003**, *24* (10), 782-784.
397. Decraene, V.; Pratten, J.; Wilson, M., Cellulose Acetate Containing Toluidine Blue and Rose Bengal Is an Effective Antimicrobial Coating when Exposed to White Light. *Appl. Environ. Microbiol.* **2006**, *72* (6), 4436.
398. Raad, I.; Hanna, H.; Nabulsi, K. Novel Antiseptic Derivatives with Broad Spectrum Antimicrobial Activity for the Impregnation of Surfaces. Patent WO2002082907A1, **2003**.
399. Chaiban, G.; Hanna, H.; Dvorak, T.; Raad, I., A rapid method of impregnating endotracheal tubes and urinary catheters with gendine: a novel antiseptic agent. *J. Antimicrob. Chemother.* **2005**, *55* (1), 51-56.

400. Raad, I. I.; Mohamed, J. A.; Reitzel, R. A.; Jiang, Y.; Dvorak, T. L.; Ghannoum, M. A.; Hachem, R. Y.; Chaftari, A.-M., The prevention of biofilm colonization by multidrug-resistant pathogens that cause ventilator-associated pneumonia with antimicrobial-coated endotracheal tubes. *Biomaterials* **2011**, *32* (11), 2689-2694.
401. Saji, M.; Taguchi, S.; Uchiyama, K.; Osono, E.; Hayama, N.; Ohkuni, H., Efficacy of Gentian-Violet in the Eradication of Methicillin-Resistant Staphylococcus-Aureus from Skin-Lesions. *J. Hosp. Infect.* **1995**, *31* (3), 225-228.
402. Perni, S.; Piccirillo, C.; Pratten, J.; Prokopovich, P.; Chrzanowski, W.; Parkin, I. P.; Wilson, M., The Antimicrobial Properties of Light-Activated Polymers Containing Methylene Blue and Gold Nanoparticles. *Biomaterials* **2009**, *30* (1), 89-93.
403. Perni, S.; Prokopovich, P.; Piccirillo, C.; Pratten, J.; Parkin, I. P.; Wilson, M., Toluidine Blue-Containing Polymers Exhibit Potent Bactericidal Activity when Irradiated with Red Laser Light. *J. Mater. Chem.* **2009**, *19* (18), 2715-2723.
404. Noimark, S.; Dunnill, C. W.; Kay, C. W. M.; Perni, S.; Prokopovich, P.; Ismail, S.; Wilson, M.; Parkin, I. P., Incorporation of Methylene Blue and Nanogold into Polyvinyl Chloride Catheters; A New Approach for Light-Activated Disinfection of Surfaces. *J. Mater. Chem.* **2012**, *22* (30), 15388-15396.
405. Noimark, S.; Bovis, M.; MacRobert, A. J.; Correia, A.; Allan, E.; Wilson, M.; Parkin, I. P., Photobactericidal Polymers; The Incorporation of Crystal Violet and Nanogold into Medical Grade Silicone. *RSC Adv.* **2013**, *3* (40), 18383-18394.
406. Sehmi, S. K.; Noimark, S.; Bear, J. C.; Peveler, W. J.; Bovis, M.; Allan, E.; MacRobert, A. J.; Parkin, I. P., Lethal Photosensitisation of Staphylococcus aureus and Escherichia coli Using Crystal Violet and Zinc Oxide-Encapsulated Polyurethane. *J Mater Chem B* **2015**, *3* (31), 6490-6500.
407. Sehmi, S. K.; Noimark, S.; Pike, S. D.; Bear, J. C.; Peveler, W. J.; Williams, C. K.; Shaffer, M. S. P.; Allan, E.; Parkin, I. P.; MacRobert, A. J., Enhancing the Antibacterial Activity of Light-Activated Surfaces Containing Crystal Violet and ZnO Nanoparticles: Investigation of Nanoparticle Size, Capping Ligand, and Dopants. *ACS Omega* **2016**, *1* (3), 334-343.
408. Sehmi, S. K.; Noimark, S.; Weiner, J.; Allan, E.; MacRobert, A. J.; Parkin, I. P., Potent Antibacterial Activity of Copper Embedded into Silicone and Polyurethane. *ACS Appl. Mater. Inter.* **2015**, *7* (41), 22807-22813.
409. Owusu, E. G. A.; MacRobert, A. J.; Naasani, I.; Parkin, I. P.; Allan, E.; Yaghini, E., Photoactivable Polymers Embedded with Cadmium-Free Quantum Dots and Crystal Violet: Efficient Bactericidal Activity against Clinical Strains of Antibiotic-Resistant Bacteria. *ACS Appl. Mater. Inter.* **2019**, *11* (13), 12367-12378.
410. Ozkan, E.; Allan, E.; Parkin, I. P., The antibacterial properties of light-activated polydimethylsiloxane containing crystal violet. *RSC Adv.* **2014**, *4* (93), 51711-51715.

411. Crick, C. R.; Noimark, S.; Peveler, W. J.; Bear, J. C.; Ivanov, A. P.; Edel, J. B.; Parkin, I. P., Advanced Analysis of Nanoparticle Composites - A Means toward Increasing the Efficiency of Functional Materials. *RSC Adv.* **2015**, 5 (66), 53789-53795.
412. Naik, A.; Ismail, S.; Kay, C.; Wilson, M.; Parkin, I., Antimicrobial activity of polyurethane embedded with methylene blue, toluidene blue and gold nanoparticles against *Staphylococcus aureus*; illuminated with white light. *Mater. Chem. Phys.* **2011**, 129 (1-2), 446-450.
413. Dąbrowski, J. M., Reactive Oxygen Species in Photodynamic Therapy: Mechanisms of Their Generation and Potentiation. *Adv. Inorg. Chem.* **2017**, 70, 343-394.
414. Vatansever, F.; Melo, W. C. M. A.; Avci, P.; Vecchio, D.; Sadasivam, M.; Gupta, A.; Chandran, R.; Karimi, M.; Parizotto, N. A.; Yin, R.; Tegos, G. P.; Hamblin, M. R., Antimicrobial strategies centered around reactive oxygen species – bactericidal antibiotics, photodynamic therapy, and beyond. *FEMS Microbiol. Rev.* **2013**, 37, 955-989.
415. Striolo, A.; Ward, J.; Prausnitz, J. M.; Parak, W. J.; Zanchet, D.; Gerion, D.; Milliron, D.; Alivisatos, A. P., Molecular Weight, Osmotic Second Virial Coefficient, and Extinction Coefficient of Colloidal CdSe Nanocrystals. *J. Phys. Chem. B* **2002**, 106 (21), 5500-5505.
416. Qu, L.; Peng, X., Control of Photoluminescence Properties of CdSe Nanocrystals in Growth. *J. Am. Chem. Soc.* **2002**, 124 (9), 2049.
417. Sapsford, K.; Pons, T.; Medintz, I.; Mattoussi, H., Biosensing with Luminescent Semiconductor Quantum Dots. *Sensors* **2006**, 6 (8), 925-953.
418. Igor, L. M.; Aaron, R. C.; Hedi, M.; Ellen, R. G.; Brent, F.; Mauro, J. M., Self-Assembled Nanoscale Biosensors Based on Quantum Dot FRET Donors. *Nat. Mater.* **2003**, 2 (9), 630.
419. Dennis, A. M.; Bao, G., Quantum Dot-Fluorescent Protein pairs as Novel Fluorescence Resonance Energy Transfer Probes. *Nano Lett.* **2008**, 8 (5), 1439.
420. Medintz, I. L.; Mattoussi, H., Quantum Dot-Based Resonance Energy Transfer and its Growing Application in Biology. *Phys. Chem. Chem. Phys.* **2009**, 11 (1), 17-45.
421. Fischer, V.; Harrelson, W. G.; Chignell, C. F.; Mason, R. P., Spectroscopic Studies of Cutaneous Photosensitizing Agents 5. Spin Trapping and Direct Electron-Spin Resonance Investigations of the Photoreduction of Gentian (Crystal) Violet. *Photobioch. Photobiop.* **1984**, 7 (2), 111-119.
422. Maley, A. M.; Arbiser, J. L., Gentian Violet: A 19th Century Drug Re-Emerges in the 21st Century. *Exp. Dermatol.* **2013**, 22 (12), 775-780.
423. Choudhary, K. N.; Soni, P. P.; Sao, D. K.; Murthy, R.; Deshkar, A. M.; Nanda, B. R., Role of gentian violet paint in burn wound management: a prospective randomised control trial. *J. Indian Med. Assoc.* **2013**, 111 (4), 248-50.

424. Heller, M. M.; Fullerton-Stone, H.; Murase, J. E., Caring for New Mothers: Diagnosis, Management and Treatment of Nipple Dermatitis in Breastfeeding Mothers. *Int. J. Dermatol.* **2012**, *51*, 1149-1161.
425. Zupan, J.; Garner, P.; Omari, A. A., Topical umbilical cord care at birth. *Cochrane Database Syst. Rev.* **2004**, (3), CD001057.
426. Pienaar, E. D.; Young, T.; Holmes, H., Interventions for the prevention and management of oropharyngeal candidiasis associated with HIV infection in adults and children. *Cochrane Database Syst. Rev.* **2010**, *11*, CD003940.
427. Valeur, B., *Molecular Fluorescence: Principles and Applications*. Weinheim, Germany : Wiley VCH Imprint: **2012**.
428. Brey, L. A.; Schuster, G. B.; Drickamer, H. G., High-Pressure Studies of Effect of Viscosity on Fluorescence Efficiency in Crystal Violet and Auramine O. *J. Chem. Phys.* **1977**, *67* (6), 2648-2650.
429. Cremers, D. A.; Windsor, M. W., A Study of the Viscosity-Dependent Electronic Relaxation of Some Triphenylmethane Dyes Using Picosecond Flash-Photolysis. *Chem. Phys. Lett.* **1980**, *71* (1), 27-32.
430. Baptista, M. S.; Indig, G. L., Effect of BSA Binding on Photophysical and Photochemical Properties of Triarylmethane Dyes. *J Phys Chem B* **1998**, *102* (23), 4678-4688.
431. Arbisser, J. L., Gentian Violet is Safe. *J. Am. Acad. Dermatol.* **2009**, *61* (2), 359-359.
432. Stoll, S.; Schweiger, A., EasySpin, a comprehensive software package for spectral simulation and analysis in EPR. *J. Magn. Reson.* **2006**, *178* (1), 42-55.
433. Sillen, A.; Engelborghs, Y., The Correct Use of "Average" Fluorescence Parameters. *Photochem. Photobiol.* **1998**, *67* (5), 475-486.
434. Issac, A.; Jin, S. Y.; Lian, T. Q., Intermittent Electron Transfer Activity from Single CdSe/ZnS Quantum Dots. *J. Am. Chem. Soc.* **2008**, *130* (34), 11280-11281.
435. Muir Wood, P., The Redox Potential of the System Oxygen-Superoxide. *FEBS Lett.* **1974**, *44* (1), 22-24.
436. Rao, P. S.; Hayon, E., Reduction of Dyes by Free-Radicals in Solution - Correlation between Reaction-Rate Constants and Redox Potentials. *J. Phys. Chem.* **1973**, *77* (23), 2753-2756.
437. Blackburn, J. L.; Selmarten, D. C.; Ellingson, R. J.; Jones, M.; Micic, O.; Nozik, A. J., Electron and Hole Transfer from Indium Phosphide Quantum Dots. *J Phys Chem B* **2005**, *109* (7), 2625-2631.
438. Devatha, G.; Roy, S.; Rao, A.; Mallick, A.; Basu, S.; Pillai, P. P., Electrostatically Driven Resonance Energy Transfer in "Cationic" Biocompatible Indium Phosphide Quantum Dots. *Chem. Sci.* **2017**, *8* (5), 3879-3884.

439. Oliveira, C. S.; Branco, K. P.; Baptista, M. S.; Indig, G. L., Solvent and Concentration Effects on the Visible Spectra of Tri-Para-Dialkylamino-Substituted Triarylmethane Dyes in Liquid Solutions. *Spectrochim. Acta A Mol. Biomol. Spectrosc.* **2002**, *58* (13), 2971-2982.
440. Leaver, I. H., Photoreduction of Crystal Violet in Solution and in Poly(Vinyl Alcohol) Films. *Photochem. Photobiol.* **1972**, *16* (3), 189-196.
441. Xu, Z.; Jin, T.; Huang, Y.; Mulla, K.; Evangelista, F. A.; Egap, E.; Lian, T., Direct triplet sensitization of oligothiophene by quantum dots. *Chem. Sci.* **2019**, *10* (24), 6120-6124.
442. Mongin, C.; Garakyaraghi, S.; Razgoniaeva, N.; Zamkov, M.; Castellano, F. N., Direct observation of triplet energy transfer from semiconductor nanocrystals. *Science* **2016**, *351* (6271), 369-372.
443. Sadhu, S.; Haldar, K. K.; Patra, A., Size Dependent Resonance Energy Transfer between Semiconductor Quantum Dots and Dye using FRET and Kinetic Model. *J Phys Chem C* **2010**, *114* (9), 3891-3897.
444. Murphy, C. B.; Zhang, Y.; Troxler, T.; Ferry, V.; Martin, J. J.; Jones, W. E., Probing Forster and Dexter Energy-Transfer Mechanisms in Fluorescent Conjugated Polymer Chemosensors. *J Phys Chem B* **2004**, *108* (5), 1537-1543.
445. Naguib, Y. M. A.; Steel, C.; Cohen, S. G.; Young, M. A., Triplet-Sensitized Photobleaching of Crystal Violet. *J. Photochem. Photobiol. A-Chem.* **1996**, *96* (1-3), 149-154.
446. Cantau, C.; Pigot, T.; Manoj, N.; Oliveros, E.; Lacombe, S., Singlet Oxygen in Microporous Silica Xerogel: Quantum Yield and Oxidation at the Gas-Solid Interface. *ChemPhysChem* **2007**, *8* (16), 2344-53.
447. Miyoshi, N.; Ueda, M.; Fuke, K.; Tanimoto, Y.; Itoh, M.; Tomita, G., Lifetime Of Singlet Oxygen and Quenching by  $\text{NaN}_3$  in Mixed Solvents. *Z. Naturforsch. B* **1982**, *37* (5), 649-652.
448. Kristiansen, M.; Scurlock, R. D.; Iu, K. K.; Ogilby, P. R., Charge-Transfer State and Singlet Oxygen ( $1\text{-}\Delta\text{-G O}_2$ ) Production in Photoexcited Organic-Molecule Molecular-Oxygen Complexes. *J. Phys. Chem.* **1991**, *95* (13), 5190-5197.
449. Schmidt, R.; Afshari, E., Collisional Deactivation of  $\text{O}_2(^1\Delta_g)$  by Solvent Molecules. Comparative Experiments with  $^{16}\text{O}_2$  and  $^{18}\text{O}_2$ . *Ber. Bunsen-Ges. Phys. Chem* **1992**, *96* (6), 788-794.
450. Oliveira, C. S.; Turchiello, R.; Kowaltowski, A. J.; Indig, G. L.; Baptista, M. S., Major Determinants of Photoinduced Cell Death: Subcellular Localization versus Photosensitization Efficiency. *Free Radic. Biol. Med.* **2011**, *51* (4), 824-833.
451. Brustolon, M.; Giamello, G., *Electron Paramagnetic Resonance: A Practitioner's Toolkit*. Wiley: Hoboken, N.J., **2009**.
452. Bruker What is EPR? <https://www.bruker.com/products/mr/epr/what-is-epr.html> (accessed March 2020).

453. Buettner, G. R., Spin Trapping: ESR Parameters of Spin Adducts. *Free Radic. Biol. Med.* **1987**, *3* (4), 259-303.
454. Cooper, D. R.; Dimitrijevic, N. M.; Nadeau, J. L., Photosensitization of CdSe/ZnS QDs and reliability of assays for reactive oxygen species production. *Nanoscale* **2010**, *2* (1), 114-121.
455. Nardi, G.; Manet, I.; Monti, S.; Miranda, M. A.; Lhiaubet-Vallet, V., Scope and limitations of the TEMPO/EPR method for singlet oxygen detection: the misleading role of electron transfer. *Free Radic. Biol. Med.* **2014**, *77* (C), 64-70.
456. Brezova, V.; Pigosova, J.; Havlinova, B.; Dvoranova, D.; Durovic, M., EPR Study of Photochemical Transformations of Triarylmethane Dyes. *Dyes Pigment.* **2004**, *61* (2), 177-198.
457. Chamulitrat, W.; Takahashi, N.; Mason, R., Peroxyl, Alkoxy, And Carbon-Centered Radical Formation From Organic Hydroperoxides By Chloroperoxidase. *J. Biol. Chem.* **1989**, *264* (14), 7889-7899.
458. Guo, Q.; Qian, S. Y.; Mason, R. P., Separation and Identification of DMPO Adducts of Oxygen-Centered Radicals formed from Organic Hydroperoxides by HPLC-ESR, ESI-MS and MS/MS. *J. Am. Soc. Mass Spectrom.* **2003**, *14* (8), 862-871.
459. Muller, P.-A.; Vauthey, E., Charge Recombination Dynamics of Geminate Ion Pairs Formed by Electron Transfer Quenching of Molecules in an Upper Excited State. *J. Phys. Chem. A* **2001**, *105* (25), 5994-6000.
460. Sekiguchi, Y.; Yao, Y.; Ohko, Y.; Tanaka, K.; Ishido, T.; Fujishima, A.; Kubota, Y., Self-sterilizing catheters with titanium dioxide photocatalyst thin films for clean intermittent catheterization: Basis and study of clinical use. *Int. J. Urol.* **2007**, *14* (5), 426-430.
461. Aiken, Z. A.; Hyett, G.; Dunnill, C. W.; Wilson, M.; Pratten, J.; Parkin, I. P., Antimicrobial Activity in Thin Films of Pseudobrookite-Structured Titanium Oxynitride under UV Irradiation Observed for Escherichia coli. *Chem. Vap. Depos.* **2010**, *16* (1-3), 19-22.
462. Dunnill, C. W.; Page, K.; Aiken, Z. A.; Noimark, S.; Hyett, G.; Kafizas, A.; Pratten, J.; Wilson, M.; Parkin, I. P., Nanoparticulate silver coated-titania thin films—Photo-oxidative destruction of stearic acid under different light sources and antimicrobial effects under hospital lighting conditions. *J. Photochem. Photobiol. A* **2011**, *220* (2-3), 113-123.
463. Ohko, Y.; Utsumi, Y.; Niwa, C.; Tatsuma, T.; Kobayakawa, K.; Satoh, Y.; Kubota, Y.; Fujishima, A., Self-sterilizing and self-cleaning of silicone catheters coated with TiO<sub>2</sub> photocatalyst thin films: A preclinical work. *J. Biomed. Mater. Res.* **2001**, *58* (1), 97-101.
464. Palza, H., Antimicrobial polymers with metal nanoparticles. *Int J Mol Sci* **2015**, *16* (1), 2099-116.
465. Pomogailo, A. D.; Kestelman, V. N., Physical Methods of Incorporating Nanoparticles into Polymers. In *Metallopolymer Nanocomposites*, Springer, Berlin, Heidelberg: **2005**.

466. Dumas, E.; Gao, C.; Suffern, D.; Bradforth, S. E.; Dimitrijevic, N. M.; Nadeau, J. L., Interfacial charge transfer between CdTe quantum dots and gram negative vs gram positive bacteria. *Environ. Sci. Technol.* **2010**, *44* (4), 1464.
467. Kumari, A.; Khare, S. K.; Kundu, J., Adverse effect of CdTe quantum dots on the cell membrane of *Bacillus subtilis* : Insight from microscopy. *Nano-Struct. Nano-Objects* **2017**, *12*, 19-26.
468. Patra, P.; Roy, S.; Sarkar, S.; Mitra, S.; Pradhan, S.; Debnath, N.; Goswami, A., Damage of lipopolysaccharides in outer cell membrane and production of ROS-mediated stress within bacteria makes nano zinc oxide a bactericidal agent. *Appl. Nanosci.* **2015**, *5* (7), 857-866.
469. Lu, Z.; Li, C. M.; Bao, H.; Qiao, Y.; Toh, Y.; Yang, X., Mechanism of antimicrobial activity of CdTe quantum dots. *Langmuir* **2008**, *24* (10), 5445.
470. Fang, T.-T.; Li, X.; Wang, Q.-S.; Zhang, Z.-J.; Liu, P.; Zhang, C.-C., Toxicity evaluation of CdTe quantum dots with different size on *Escherichia coli*. *Toxicol. Vitro* **2012**, *26* (7), 1233-1239.
471. Rajendiran, K.; Zhao, Z.; Pei, D.; Fu, A. L., Antimicrobial Activity and Mechanism of Functionalized Quantum Dots. *Polymers* **2019**, *11* (10).
472. Cho, S. J.; Maysinger, D.; Jain, M.; Röder, B.; Hackbarth, S.; Winnik, F. M., Long-term exposure to CdTe quantum dots causes functional impairments in live cells. *Langmuir* **2007**, *23* (4), 1974-1980.
473. Lucky, S. S.; Soo, K. C.; Zhang, Y., Nanoparticles in Photodynamic Therapy. *Chem. Rev.* **2015**, *115* (4), 1990-2042.
474. Popp, J.; Chiou, A.; Tuchin, V. V.; Heinemann, S., *Handbook of Biophotonics - Vol. 2: Photonics for Health Care*. Ringgold Inc: Portland, **2012**.
475. Samia, A. C. S.; Dayal, S.; Burda, C., Quantum Dot-based Energy Transfer: Perspectives and Potential for Applications in Photodynamic Therapy. *Photochem. Photobiol.* **2006**, *82*, 617-625.
476. Yaghini, E.; Turner, H.; Pilling, A.; Naasani, I.; MacRobert, A. J., In Vivo Biodistribution and Toxicology Studies of Cadmium-Free Indium-Based Quantum Dot Nanoparticles in a Rat Model. *Nanomedicine-Uk* **2018**, *14* (8), 2644-2655.
477. Jones, G. S.; D'Orazio, S. E. F., *Listeria monocytogenes*: Cultivation and Laboratory Maintenance. *Curr. Protoc. Microbiol.* **2013**, *31* (1), 9B.2.1-9B.2.7.
478. Berrios, R. L.; Arbiser, J. L., Effectiveness of Gentian Violet and Similar Products Commonly Used to Treat Pyodermas. *Dermatol. Clin.* **2011**, *29* (1), 69-73.
479. Jurevic, R.; Traboulsi, R.; Mukherjee, P.; Salata, R.; Ghannoum, M., Identification of gentian violet concentration that does not stain oral mucosa, possesses anti-candidal activity and is well tolerated. *Eur. J. Clin. Microbiol. Infect. Dis.* **2011**, *30* (5), 629-33.

480. Nyst, M. J.; Perriens, J. H.; Kimputu, L.; Lumbila, M.; Nelson, A. M.; Piot, P., Gentian violet, ketoconazole and nystatin in oropharyngeal and esophageal candidiasis in Zairian AIDS patients. *Ann. Soc. Belg. Med. Trop.* **1992**, 72 (1), 45-52.
481. Edwards, K., New Twist on an Old Favorite: Gentian Violet and Methylene Blue Antibacterial Foams. *Adv. Wound Care* **2016**, 5 (1), 11-18.
482. Dimitrijevic, N. M.; Takahashi, K.; Jonah, C. D., Visible Absorption Spectra of Crystal Violet in Supercritical Ethane-Methanol Solution. *J. Supercrit. Fluid.* **2002**, 24 (2), 153-159.
483. Haidekker, M. A.; Theodorakis, E. A., Environment-sensitive behavior of fluorescent molecular rotors. *J Biol Eng* **2010**, 4, 11.
484. EFSA Scientific Committee, Statistical Significance and Biological Relevance. *EFSA Journal* **2011**, 9 (9), 2372.
485. Fux, C. A.; Shirliff, M.; Stoodley, P.; Costerton, J. W., Can laboratory reference strains mirror 'real-world' pathogenesis? *Trends Microbiol.* **2005**, 13 (2), 58-63.
486. Castano, A. P.; Demidova, T. N.; Hamblin, M. R., Mechanisms in photodynamic therapy: part one—photosensitizers, photochemistry and cellular localization. *Photodiagnosis Photodyn. Ther.* **2004**, 1 (4), 279-293.
487. Grumezescu, A.; Oprea, A. E., *Nanotechnology Applications in Food: Flavor, Stability, Nutrition and Safety*. Elsevier Science: **2017**.
488. Centers for Disease Control and Prevention (CDC), *Estimates of Foodborne Illness in the United States*. <https://www.cdc.gov/foodborneburden/2011-foodborne-estimates.html>.
489. World Health Organisation (WHO), *The burden of foodborne diseases in the WHO European Region* (2017). <http://www.euro.who.int/en/health-topics/disease-prevention/food-safety/publications/2017/the-burden-of-foodborne-diseases-in-the-who-european-region-2017>.
490. Food Standards Agency, *Update on Investigation into Food Supply Chain Linked to Listeria*. 2019.
491. Bower, C. K.; McGuire, J.; Daeschel, M. A., The adhesion and detachment of bacteria and spores on food-contact surfaces. *Trends Food Sci. Technol.* **1996**, 7 (5), 152-157.
492. Moore, G.; Blair, I. S.; McDowell, D. A., Recovery and Transfer of Salmonella Typhimurium from Four Different Domestic Food Contact Surfaces. *J. Food Prot.* **2007**, 70 (10), 2273-2280.
493. European Centre for Disease Prevention and Control (ECDC), *Facts about salmonellosis*. <https://www.ecdc.europa.eu/en/infectious-diseases-and-public-health/salmonellosis/facts>.
494. Mayo Clinic, *Salmonella infection*. <https://www.mayoclinic.org/diseases-conditions/salmonella/symptoms-causes/syc-20355329>.

495. Centers for Disease Control and Prevention (CDC), *Salmonella*. <https://www.cdc.gov/salmonella/index.html>.
496. European Centre for Disease Prevention and Control (ECDC), *The European Union Summary report on antimicrobial resistance in zoonotic and indicator bacteria from humans, animals and food in 2017*. <https://www.ecdc.europa.eu/en/publications-data/european-union-summary-report-antimicrobial-resistance-zoonotic-and-indicator-5>.
497. Michael, M.; Kenneth, E. S.; John, S.; Sandra, W. C.; Phil, L.; Laura, C.; Steffen, P.; Johar, A.; Mike, D.; Feiyu, D.; Shunfang, H.; Dan, L.; Shawn, L.; Christine, N.; Kelsi, S.; Andrea, H.; Neenu, G.; Elizabeth, M.; Ellen, R.; Hui, S.; Liliana, F.; Webb, M.; Tamberlyn, S.; Michael, N.; Robert, W.; Richard, K. W., Complete genome sequence of *Salmonella enterica* serovar *Typhimurium* LT2. *Nature* **2001**, 413 (6858), 852.
498. Winfield, M. D.; Groisman, E. A., Role of Nonhost Environments in the Lifestyles of *Salmonella* and *Escherichia coli*. *Appl. Environ. Microbiol.* **2003**, 69 (7), 3687-3694.
499. European Centre for Disease Prevention and Control (ECDC), *Listeriosis - Annual Epidemiological Report for 2017*. <https://www.ecdc.europa.eu/en/publications-data/listeriosis-annual-epidemiological-report-2017>.
500. Centers for Disease Control and Prevention (CDC), *Preliminary Incidence and Trends of Infections with Pathogens Transmitted Commonly Through Food — Foodborne Diseases Active Surveillance Network, 10 U.S. Sites, 2015–2018*. [https://www.cdc.gov/mmwr/volumes/68/wr/mm6816a2.htm?s\\_cid=mm6816a2\\_w#T1\\_down](https://www.cdc.gov/mmwr/volumes/68/wr/mm6816a2.htm?s_cid=mm6816a2_w#T1_down).
501. European Centre for Disease Prevention and Control (ECDC), *Listeriosis - Annual Epidemiological Report for 2016*. <https://www.ecdc.europa.eu/en/publications-data/listeriosis-annual-epidemiological-report-2016>.
502. Drewinko, B.; Loo, T. L.; Brown, B.; Gottlieb, J. A.; Freireich, E. J., Combination chemotherapy in vitro with adriamycin. Observations of additive, antagonistic, and synergistic effects when used in two-drug combinations on cultured human lymphoma cells. *Cancer Biochem Biophys* **1976**, 1 (4), 187-95.
503. Mathews, M.; Shih, E.-C.; Zamora, G.; Sun, C.-H.; Hirschberg, H.; Blickenstaff, J.; Vo, V.; Madsen, S., Photochemical internalization of bleomycin for glioma treatment. *J. Biomed. Opt.* **2012**, 17 (5), 058001.
504. Yaghini, E.; Dondi, R.; Tewari, K. M.; Loizidou, M.; Eggleston, I. M.; MacRobert, A. J., Endolysosomal targeting of a clinical chlorin photosensitiser for light-triggered delivery of nano-sized medicines. *Sci. Rep.* **2017**, 7.
505. Walker, T.; Canales, M.; Noimark, S.; Page, K.; Parkin, I.; Faull, J.; Bhatti, M.; Ciric, L., A Light-Activated Antimicrobial Surface Is Active Against Bacterial, Viral and Fungal Organisms. *Sci. Rep.* **2017**, 7.
506. Raghunath, D., New metallo  $\beta$ -lactamase NDM-1. *Indian J. Med. Res.* **2010**, 132 (5), 478-481.

507. Khan, A. U.; Maryam, L.; Zarrilli, R., Structure, Genetics and Worldwide Spread of New Delhi Metallo- $\beta$ -lactamase (NDM): a threat to public health. *BMC Microbiol.* **2017**, *17* (1), 101-12.
508. Sperandio, F. F.; Huang, Y. Y.; Hamblin, M. R., Antimicrobial photodynamic therapy to kill Gram-negative bacteria. *Recent Pat. Antiinfect. Drug Discov.* **2013**, *8* (2), 108-20.
509. Pfeifer, G. P.; You, Y. H.; Besaratinia, A., Mutations induced by ultraviolet light. *Mutat. Res.* **2005**, *571* (1-2), 19-31.
510. Wilson, B. C.; Patterson, M. S., The physics, biophysics and technology of photodynamic therapy. *Phys. Med. Biol.* **2008**, *53* (9), R61-109.
511. Bukorović, N., *Lighting Guide 2: Hospitals and Health Care Buildings*. Chartered Institution of Building Services Engineers: London, **2008**.
512. Kang, C.-I.; Kim, S.-H.; Park, W. B.; Lee, K.-D.; Kim, H.-B.; Kim, E.-C.; Oh, M.-d.; Choe, K.-W., Bloodstream Infections Caused by Antibiotic-Resistant Gram- Negative Bacilli: Risk Factors for Mortality and Impact of Inappropriate Initial Antimicrobial Therapy on Outcome. *Antimicrob. Agents Chemother.* **2005**, *49* (2), 760.
513. Wise, J., Three babies die in pseudomonas outbreak at Belfast neonatal unit. *Brit. Med. J.* **2012**, *344*, e592.
514. Breathnach, A. S.; Cubbon, M. D.; Karunaharan, R. N.; Pope, C. F.; Planche, T. D., Multidrug-resistant *Pseudomonas aeruginosa* outbreaks in two hospitals: association with contaminated hospital waste-water systems. *J. Hosp. Infect.* **2012**, *82* (1), 19-24.
515. Lyczak, J. B.; Cannon, C. L.; Pier, G. B., Establishment of *Pseudomonas aeruginosa* infection: lessons from a versatile opportunist. *Microbes Infect.* **2000**, *2*, 1051-1060.
516. Taylor, P. K.; Yeung, A. T.; Hancock, R. E., Antibiotic Resistance in *Pseudomonas Aeruginosa* Biofilms: Towards the Development of Novel Anti-Biofilm Therapies. *J Biotechnol* **2014**, *191*, 121-30.
517. Rybtke, M.; Hultqvist, L. D.; Givskov, M.; Tolker-Nielsen, T., *Pseudomonas aeruginosa* Biofilm Infections: Community Structure, Antimicrobial Tolerance and Immune Response. *J. Mol. Biol.* **2015**, *427* (23), 3628-45.
518. Doring, G.; Hoiby, N.; Consensus Study, G., Early intervention and prevention of lung disease in cystic fibrosis: a European consensus. *J. Cyst. Fibros.* **2004**, *3* (2), 67-91.
519. Decraene, V.; Phan, H. T. T.; George, R.; Wyllie, D. H.; Akinremi, O.; Aiken, Z.; Cleary, P.; Dodgson, A.; Pankhurst, L.; Crook, D. W.; Lenney, C.; Walker, A. S.; Woodford, N.; Sebra, R.; Fath-Ordoubadi, F.; Mathers, A. J.; Seale, A. C.; Guiver, M.; McEwan, A.; Watts, V.; Welfare, W.; Stoesser, N.; Cawthorne, J.; Group, T. I., A Large, Refractory Nosocomial Outbreak of *Klebsiella pneumoniae* Carbapenemase-Producing *Escherichia coli* Demonstrates Carbapenemase Gene Outbreaks Involving Sink Sites Require Novel Approaches to Infection Control. *Antimicrob. Agents Chemother.* **2018**, *62* (12), e01689-18.

520. Roux, D.; Aubier, B.; Cochard, H.; Quentin, R.; van der Mee-Marquet, N.; Centre, H. A. I. P. G. o. t. R. d. H. d., Contaminated sinks in intensive care units: an underestimated source of extended-spectrum beta-lactamase-producing Enterobacteriaceae in the patient environment. *J Hosp Infect* **2013**, *85* (2), 106-111.
521. Kizny Gordon, A. E.; Mathers, A. J.; Cheong, E. Y. L.; Gottlieb, T.; Kotay, S.; Walker, A. S.; Peto, T. E. A.; Crook, D. W.; Stoesser, N., The Hospital Water Environment as a Reservoir for Carbapenem-Resistant Organisms Causing Hospital-Acquired Infections—A Systematic Review of the Literature. *Clin. Infect. Dis.* **2017**, *64* (10), 1435-1444.
522. Hans-Curt, F.; Jost, W., The biofilm matrix. *Nat. Rev. Microbiol.* **2010**, *8* (9), 623.
523. Costerton, J. W.; Stewart, P. S.; Greenberg, E., Bacterial biofilms: A common cause of persistent infections. *Science* **1999**, *284* (5418), 1318-1322.
524. Ramsay, K. A.; Wardell, S. J. T.; Patrick, W. M.; Brockway, B.; Reid, D. W.; Winstanley, C.; Bell, S. C.; Lamont, I. L., Genomic and Phenotypic Comparison of Environmental and Patient-Derived Isolates of *Pseudomonas aeruginosa* suggest that Antimicrobial Resistance is Rare within the Environment. *BioRxiv* **2019**, 663674.
525. Chevalier, S.; Bouffartigues, E.; Bodilis, J.; Maillot, O.; Lesouhaitier, O.; Feuilloley, M. G. J.; Orange, N.; Dufour, A.; Cornelis, P., Structure, Function and Regulation of *Pseudomonas aeruginosa* porins. *FEMS Microbiol. Rev.* **2017**, *41* (5), 698-722.
526. Yoshimura, F.; Nikaido, H., Permeability of *Pseudomonas aeruginosa* Outer Membrane to Hydrophilic Solutes. *J. Bacteriol.* **1982**, *152* (2), 636-42.
527. Kashef, N.; Hamblin, M. R., Can Microbial Cells Develop Resistance to Oxidative Stress in Antimicrobial Photodynamic Inactivation? *Drug Resist. Updat.* **2017**, *31*, 31-42.
528. Orlandi, V. T.; Bolognese, F.; Chiodaroli, L.; Tolker-Nielsen, T.; Barbieri, P., Pigments Influence the Tolerance of *Pseudomonas aeruginosa* PAO1 to Photodynamically Induced Oxidative Stress. *Microbiology* **2015**, *161* (12), 2298-309.
529. Adams, E., The antibacterial action of crystal violet. *J. Pharm. Pharmacol.* **1967**, *19* (12), 821-6.
530. Kramer, A.; Schwebke, I.; Kampf, G., How long do nosocomial pathogens persist on inanimate surfaces? A systematic review. *BMC infectious diseases* **2006**, *6*, 130.
531. Abdal Dayem, A.; Hossain, M. K.; Lee, S. B.; Kim, K.; Saha, S. K.; Yang, G. M.; Choi, H. Y.; Cho, S. G., The Role of Reactive Oxygen Species (ROS) in the Biological Activities of Metallic Nanoparticles. *Int. J. Mol. Sci.* **2017**, *18* (1), 120.
532. Lumb, A. B., *Nunn's Applied Respiratory Physiology*. 7th ed.; Churchill Livingstone: Edinburgh, **2010**.

533. Paravicini, T. M.; Touyz, R. M., NADPH oxidases, reactive oxygen species, and hypertension: clinical implications and therapeutic possibilities. *Diabetes Care* **2008**, *31 Suppl 2*, S170-80.
534. Narband, N.; Mubarak, M.; Ready, D.; Parkin, I. P.; Nair, S. P.; Green, M. A.; Beeby, A.; Wilson, M., Quantum Dots as Enhancers of the Efficacy of Bacterial Lethal Photosensitization. *Nanotechnology* **2008**, *19* (44).
535. Huston, A. L.; Justus, B. L.; Campillo, A. J., Direct Measurement of the Viscosity of Glycerol under Laser Driven Shock Compression - Fluorescence Lifetime Changes in Crystal Violet. *Chem. Phys. Lett.* **1985**, *122* (6), 617-621.
536. Noimark, S.; Salvadori, E.; Gomez-Bombarelli, R.; MacRobert, A. J.; Parkin, I. P.; Kay, C. W. M., Comparative Study of Singlet Oxygen Production by Photosensitiser Dyes Encapsulated in Silicone: Towards Rational Design of Anti-Microbial Surfaces. *Phys. Chem. Chem. Phys.* **2016**, *18* (40), 28101-28109.
537. Bovis, M. J.; Noimark, S.; Woodhams, J. H.; Kay, C. W. M.; Weiner, J.; Peveler, W. J.; Correia, A.; Wilson, M.; Allan, E.; Parkin, I. P.; MacRobert, A. J., Photosensitisation Studies of Silicone Polymer Doped with Methylene Blue and Nanogold for Antimicrobial Applications. *RSC Adv.* **2015**, *5* (68), 54830-54842.
538. Yaghini, E.; Giuntini, F.; Eggleston, I. M.; Suhling, K.; Seifalian, A. M.; MacRobert, A. J., Fluorescence Lifetime Imaging and FRET-Induced Intracellular Redistribution of Tat-Conjugated Quantum Dot Nanoparticles through Interaction with a Phthalocyanine Photosensitiser. *Small* **2014**, *10* (4), 782-792.
539. Reszka, K.; Cruz, F. S.; Docampo, R., Photosensitization by the Trypanocidal Agent Crystal Violet - Type-I versus Type-II Reactions. *Chem.-Biol. Interact.* **1986**, *58* (2), 161-172.
540. DasGupta, A., Methods for Measuring Oxidative Stress in the Laboratory. In *Antioxidants in Food, Vitamins and Supplements*, Elsevier Inc.: **2014**; pp 19-40.
541. Kuete, V.; Karaosmanoğlu, O.; Sivas, H., Anticancer Activities of African Medicinal Spices and Vegetables. In *Medicinal Spices and Vegetables from Africa: Therapeutic Potential Against Metabolic, Inflammatory, Infectious and Systemic Diseases*, **2017**; pp 271-297.
542. Scudiero, D. A.; Shoemaker, R. H.; Paull, K. D.; Monks, A.; Tierney, S.; Nofziger, T. H.; Currens, M. J.; Seniff, D.; Boyd, M. R., Evaluation of a soluble tetrazolium/formazan assay for cell growth and drug sensitivity in culture using human and other tumor cell lines. *Cancer Res.* **1988**, *48* (17), 4827.
543. Okado-Matsumoto, A.; Fridovich, I., Assay of superoxide dismutase: cautions relevant to the use of cytochrome c, a sulfonated tetrazolium, and cyanide. *Anal. Biochem.* **2001**, *298* (2), 337.
544. Sutherland, M. W.; Learmonth, B. A., The Tetrazolium Dyes MTS and XTT Provide New Quantitative Assays for Superoxide and Superoxide Dismutase. *Free Radic. Res.* **1997**, *27* (3), 283-289.

545. Bielski, B. H. J., Reevaluation of the Spectral and Kinetic Properties of HO<sub>2</sub> AND O<sub>2</sub><sup>-</sup> Free Radicals. *Photochem. Photobiol.* **1978**, 28 (4-5), 645-649.
546. AlNashef, I. M.; Leonard, M. L.; Matthews, M. A.; Weidner, J. W., Superoxide electrochemistry in an ionic liquid. *Ind. Eng. Chem. Res.* **2002**, 41 (18), 4475-4478.
547. Kumar, G.; Degheidy, H.; Casey, B. J.; Goering, P. L., Flow cytometry evaluation of in vitro cellular necrosis and apoptosis induced by silver nanoparticles. *Food Chem. Toxicol.* **2015**, 85 (C), 45-51.
548. Flohé, L.; Ötting, F., Superoxide Dismutase Assays. *Methods Enzymol.* **1984**, 105 (C), 93-104.
549. He, J.; Zhao, J.; Hidaka, H.; Serpone, N., EPR characteristics of a dye/colloidal TiO<sub>2</sub> system under visible light irradiation. *J. Chem. Soc. Faraday Trans.* **1998**, 94 (16), 2375-2378.
550. Shen, B.; Jensen, R. G.; Bohnert, H. J., Mannitol Protects against Oxidation by Hydroxyl Radicals. *Plant Physiol.* **1997**, 115 (2), 527.
551. Buettner, G. R.; Doherty, T. P.; Bannister, T. D., Hydrogen peroxide and hydroxyl radical formation by methylene blue in the presence of ascorbic acid. *Radiat. Environ. Biophys.* **1984**, 23 (4), 235-43.
552. Jennings, D. B.; Ehrenshaft, M.; Pharr, D. M.; Williamson, J. D., Roles for mannitol and mannitol dehydrogenase in active oxygen-mediated plant defense. *Proc. Natl. Acad. Sci. USA* **1998**, 95 (25), 15129-33.
553. Michaeli, A.; Feitelson, J., Reactivity of singlet oxygen toward amino acids and peptides. *Photochem. Photobiol.* **1994**, 59 (3), 284-9.
554. Tauber, A. I.; Babior, B. M., Evidence for hydroxyl radical production by human neutrophils. *J. Clin. Invest.* **1977**, 60 (2), 374-9.
555. American Chemistry Council, *Polyurethanes and Medical Applications*. <https://polyurethane.americanchemistry.com/Polyurethanes-and-Medical-Applications>.
556. Otter, J. A.; Yezli, S.; French, G. L., The Role Played by Contaminated Surfaces in the Transmission of Nosocomial Pathogens. *Infect. Control Hosp. Epidemiol.* **2015**, 32 (7), 687-699.
557. Kampf, G.; Todt, D.; Pfaender, S.; Steinmann, E., Persistence of coronaviruses on inanimate surfaces and their inactivation with biocidal agents. *J. Hosp. Infect.* **2020**, 104 (3), 246-251.